WOMEN IN BIOFILMS 2021

EDITED BY: Lauren O. Bakaletz and Carina Almeida
PUBLISHED IN: Frontiers in Cellular and Infection Microbiology

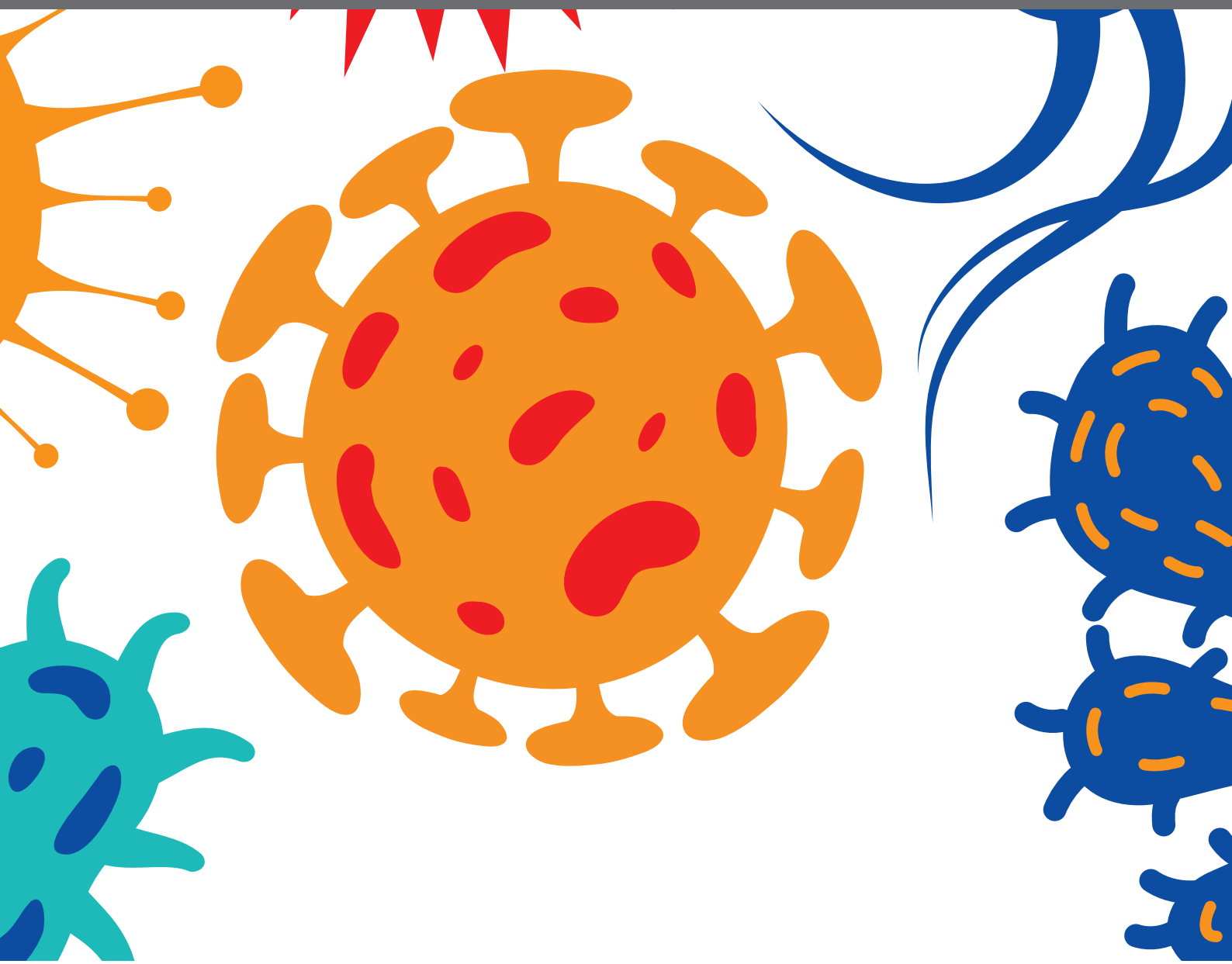

frontiers Research Topics

ISSN 1664-8714
ISBN 978-2-83250-779-7
DOI 10.3389/978-2-83250-779-7

About Frontiers

Frontiers is more than just an open-access publisher of scholarly articles: it is a pioneering approach to the world of academia, radically improving the way scholarly research is managed. The grand vision of Frontiers is a world where all people have an equal opportunity to seek, share and generate knowledge. Frontiers provides immediate and permanent online open access to all its publications, but this alone is not enough to realize our grand goals.

Frontiers Journal Series

The Frontiers Journal Series is a multi-tier and interdisciplinary set of open-access, online journals, promising a paradigm shift from the current review, selection and dissemination processes in academic publishing. All Frontiers journals are driven by researchers for researchers; therefore, they constitute a service to the scholarly community. At the same time, the Frontiers Journal Series operates on a revolutionary invention, the tiered publishing system, initially addressing specific communities of scholars, and gradually climbing up to broader public understanding, thus serving the interests of the lay society, too.

Dedication to Quality

Each Frontiers article is a landmark of the highest quality, thanks to genuinely collaborative interactions between authors and review editors, who include some of the world's best academicians. Research must be certified by peers before entering a stream of knowledge that may eventually reach the public - and shape society; therefore, Frontiers only applies the most rigorous and unbiased reviews.
Frontiers revolutionizes research publishing by freely delivering the most outstanding research, evaluated with no bias from both the academic and social point of view. By applying the most advanced information technologies, Frontiers is catapulting scholarly publishing into a new generation.

What are Frontiers Research Topics?

Frontiers Research Topics are very popular trademarks of the Frontiers Journals Series: they are collections of at least ten articles, all centered on a particular subject. With their unique mix of varied contributions from Original Research to Review Articles, Frontiers Research Topics unify the most influential researchers, the latest key findings and historical advances in a hot research area! Find out more on how to host your own Frontiers Research Topic or contribute to one as an author by contacting the Frontiers Editorial Office: frontiersin.org/about/contact

WOMEN IN BIOFILMS 2021

Topic Editors:
Lauren O. Bakaletz, Abigail Wexner Research Institute, Nationwide Children's Hospital, United States
Carina Almeida, Instituto Nacional Investigaciao Agraria e Veterinaria (INIAV), Portugal

Citation: Bakaletz, L. O., Almeida, C., eds. (2022). Women in Biofilms 2021. Lausanne: Frontiers Media SA. doi: 10.3389/978-2-83250-779-7

Table of Contents

frontiers | Frontiers in Cellular and Infection Microbiology

TYPE Editorial
PUBLISHED 28 October 2022
DOI 10.3389/fcimb.2022.1035280

OPEN ACCESS

EDITED AND REVIEWED BY
Diane McDougald,
University of Technology Sydney,
Australia

*CORRESPONDENCE
Carina Almeida
carina.almeida@iniav.pt

SPECIALTY SECTION
This article was submitted to Biofilms, a section of the journal Frontiers in Cellular and Infection Microbiology

RECEIVED 02 September 2022
ACCEPTED 20 September 2022
PUBLISHED 28 October 2022

CITATION
Almeida C and Bakaletz LO (2022) Editorial: Women in biofilms 2021. *Front. Cell. Infect. Microbiol.* 12:1035280. doi: 10.3389/fcimb.2022.1035280

Editorial: Women in biofilms 2021

Carina Almeida[1,2,3]* and Lauren O. Bakaletz[4,5]

[1]INIAV - National Institute for Agrarian and Veterinary Research, Food Safety Unit, Vila do Conde, Portugal, [2]LEPABE - Laboratory for Process Engineering, Environment, Biotechnology and Energy, Faculty of Engineering, University of Porto, Porto, Portugal, [3]Centre of Biological Engineering, Universidade do Minho, Campus de Gualtar, Braga, Portugal, [4]Abigail Wexner Research Institute, Center for Microbial Pathogenesis, Nationwide Children's Hospital, Columbus, OH, United States, [5]College of Medicine, Department of Pediatrics, The Ohio State University, Columbus, OH, United States

KEYWORDS

women in science, biofilms, biofilm control strategies, biofilm formation, clinical biofilms

Editorial on the Research Topic
Women in biofilms 2021

Female scientists lead ground-breaking research across the world, however, to date women represent only 33% of researchers worldwide. For instance in Europe, only 11% of senior research roles are held by women (UNESCO, 2021). Female representation decreases with the level of seniority, and this vertical segregation can be encountered in almost every country. A recent study evaluated articles in the medical field and found that those written by women in high-impact medical journals had fewer citations than those written by men, particularly when women wrote together as primary and senior authors (Chatterjee and Werner, 2021). This data clearly demonstrates that long-standing biases and gender stereotypes may have important consequences for the professional success of women and for achieving gender equity in science-related fields. This collection of innovative works can help empower more female scientists to achieve recognition for their scientific work, while participating equally in solving the major challenges in the field of microbial biofilms.

Biofilms are complex three-dimensional structures, corresponding to the sessile mode of microbial life (Flemming et al., 2021). These structures have been progressively recognized as the predominant form of life for microbes on Earth. In this sessile form, microorganisms live in close proximity to one another within a matrix of extracellular polymeric substances (EPS), providing an extra layer of protection against external and/or environmental stresses (Karygianni et al., 2020). In addition to EPS production, these sessile populations usually exhibit slow growth rates and high tolerances to antibiotics, chemical treatments, and host-immune effectors. Collectively, these properties make biofilm control a challenge that has yet to be tackled.

Women play a prominent role in the field of microbial biofilms, taking the lead on several innovative works that contribute to our understanding of these complex and diverse structures and set the basis for important findings. The works presented in this Research Topic boast women as the first or last authors, which indicates their prominent

role in leading this research. In particular, this collection advances our understating of biofilm dynamics and properties, effective control strategies, and even biofilm association with diseases previously thought to be unrelated to these structures.

Beginning with a study on biofilm formation mechanisms, Leggett et al. apply a metabolomics approach to biofilm-forming *Pseudomonas aeruginosa* in order to identify factors that trigger the transition from free/planktonic cells to adherence and static growth. The authors demonstrate that cadaverine can decrease biofilm accumulation; this information can eventually be used to design new interventional strategies. Moving on to the virulence traits of biofilms, Fleming et al. explore the contribution of two specific EPS in *P. aeruginosa* pathogenesis based on a wound infection model. The data suggest that the EPS do not affect the severity of wound infection in terms of bacteria load and wound closure rates; however, they may have important implications for bacterial persistence. The metabolic state is also particularly relevant and is addressed in an interesting study by Gaio et al.. The authors explore the relevance of the viable but non-culturable (VBNC) cells in *Staphylococcus epidermidis*, grown in either planktonic or biofilm conditions. Despite the identification of genes possibly associated with the VBNC state, there is no significant difference between the proportion of VBNC cells in sessile or biofilm populations. In a similar way, the same research group attempts to decipher the role played by a putative toxin-antitoxin system in the virulence traits of *S. epidermidis* (Gaio et al.). Despite the previously identified potential role of this system, the results suggest a minor role played in the different virulence factors evaluated. While not all hypotheses are verified, other have been corroborated by resorting to large-scale studies involving a high number of isolates. Thoming and Haussler confirm the high tolerance of *P. aeruginosa* biofilms to antimicrobials in a large study involving 352 clinical isolates. A broad distribution of biofilm-induced tolerance phenotypes is observed; however, these phenotypes are also affected by the antibiotic utilized.

Regarding the development of pioneering assessment strategies, this collection includes an important contribution by Gloag et al. The authors present an innovative method, originally applied to quantify marine biofilm fouling, to accurately detect and quantify the presence and/or detachment of biofilms as a function of shear stress. This rotating-disc rheometry method is used to investigate the effect of arginine on dental plaque-biofilms, corroborating previous observations on its ability to disrupt *Streptococcus gordonii* biofilms.

Regarding control strategies, natural compounds exhibiting anti-biofilm properties can be extremely valuable. The study by Priya et al. provides a good example of bioactive compounds, namely, piperine and thymol (present in pepper and thyme, respectively) that, when combined, display a strong synergistic effect against *Candida albicans* biofilms. This combination of therapies is frequently regarded as an excellent way to overcome biofilms' tolerance to antimicrobials. As such, Hawas et al. provide a comprehensive overview of combination therapies, primarily based on biofilm dispersing agents and antibiotics, highlighting various synergistic treatments that show outstanding potential.

Finally, exciting findings related to human diseases with little (or unknown) connection to biofilms are also presented. Mateus et al. explore the pathogenesis of pediatric obstructive sleep disordered breathing (SDB) and its potential link to biofilms associated with recurrent tonsillitis. The results suggest that persistent bacterial infection may be related to SDB since the microbial phenotypes are remarkably similar. Thus, the authors argue that anti-biofilm approaches may be relevant in the treatment of SDB. In the same way, Grando et al. explore the role of amyloid proteins; bacterial fibers that are a common component of bacterial biofilm matrixes, in the development of autoimmune diseases. A hypothesis that rests on the fact that autoimmune reactions are often developed after an infectious disease episode and that amyloid proteins have proved to be able to activate a pro-inflammatory response. The results obtained from a mouse model that is implanted with mesh-associated *S. aureus* biofilms (either producing, or defective in the production of, amyloids) provide compelling evidence for the involvement of these amyloid proteins in infection-associated autoimmunity. Last but not least, Ragan et al. describe the use of a probiotic strain, in its biofilm state, to modulate the human gut, preventing gut infections and preserving the natural gut functions.

These works clearly open new avenues in the study and understanding of biofilm structures. They demonstrate how these communities can be modulated not only to control biofilm-associated problems and infections, but also to improve health conditions that are not directly associated with biofilms. This collection of articles showcases women's contribution to this field of knowledge. Many more examples could be presented here to highlight the diversity of research performed by women across the full breadth of biofilm research.

Author contributions

CA and LB: drafting and critical revision of the manuscript. Both authors contributed to the article and approved the submitted version.

Conflict of interest

The authors declare that the research was conducted in the absence of any commercial or financial relationships that could be construed as a potential conflict of interest.

Publisher's note

References

Chatterjee, P., and Werner, R. M. (2021). Gender disparity in citations in high-impact journal articles. *JAMA Netw. Open* 4, e2114509. doi: 10.1001/jamanetworkopen.2021.14509

Flemming, H. C., Baveye, P., Neu, T. R., Stoodley, P., Szewzyk, U., Wingender, J., et al. (2021). Who put the film in biofilm? the migration of a term from wastewater engineering to medicine and beyond. *NPJ Biofilms Microbiomes* 7, 10. doi: 10.1038/s41522-020-00183-3

Karygianni, L., Ren, Z., Koo, H., and Thurnheer, T. (2020). Biofilm matrixome: Extracellular components in structured microbial communities. *Trends Microbiol.* 28, 668–681. doi: 10.1016/j.tim.2020.03.016

UNESCO 2021. *UNESCO Science report: the race against time for smarter development*. (Paris: UNESCO Publishing).

frontiers in Cellular and Infection Microbiology

ORIGINAL RESEARCH
published: 05 November 2021
doi: 10.3389/fcimb.2021.784388

Arginine Induced *Streptococcus gordonii* Biofilm Detachment Using a Novel Rotating-Disc Rheometry Method

Erin S. Gloag[1*], *Daniel J. Wozniak*[1,2], *Kevin L. Wolf*[3], *James G. Masters*[4], *Carlo Amorin Daep*[4] *and Paul Stoodley*[1,5,6]

[1] Department of Microbial Infection and Immunity, The Ohio State University, Columbus, OH, United States, [2] Department of Microbiology, The Ohio State University, Columbus, OH, United States, [3] Department of Mechanical and Aerospace Engineering, The Ohio State University, Columbus, OH, United States, [4] Colgate-Palmolive Technology Center, Piscataway, NJ, United States, [5] Department of Orthopedics, The Ohio State University, Columbus, OH, United States, [6] National Biofilm Innovation Centre (NBIC) and National Centre for Advanced Tribology at Southampton (nCATS), University of Southampton, Southampton, United Kingdom

OPEN ACCESS

Edited by:
Carina Almeida,
Instituto Nacional Investigaciao Agraria e Veterinaria (INIAV), Portugal

Reviewed by:
Eoin Casey,
University College Dublin, Ireland
Robert Palmer,
National Institute of Dental and Craniofacial Research (NIDCR), United States

***Correspondence:**
Erin S. Gloag
Erin.Gloag@osumc.edu

Specialty section:
This article was submitted to Biofilms, a section of the journal Frontiers in Cellular and Infection Microbiology

Received: 27 September 2021
Accepted: 21 October 2021
Published: 05 November 2021

Citation:
Gloag ES, Wozniak DJ, Wolf KL, Masters JG, Daep CA and Stoodley P (2021) Arginine Induced Streptococcus gordonii Biofilm Detachment Using a Novel Rotating-Disc Rheometry Method. Front. Cell. Infect. Microbiol. 11:784388. doi: 10.3389/fcimb.2021.784388

Oral diseases are one of the most common pathologies affecting human health. These diseases are typically associated with dental plaque-biofilms, through either build-up of the biofilm or dysbiosis of the microbial community. Arginine can disrupt dental plaque-biofilms, and maintain plaque homeostasis, making it an ideal therapeutic to combat the development of oral disease. Despite our understanding of the actions of arginine towards dental plaque-biofilms, it is still unclear how or if arginine effects the mechanical integrity of the dental plaque-biofilm. Here we adapted a rotating-disc rheometry assay, a method used to quantify marine biofilm fouling, to study how arginine treatment of *Streptococcus gordonii* biofilms influences biofilm detachment from surfaces. We demonstrate that the assay is highly sensitive at quantifying the presence of biofilm and the detachment or rearrangement of the biofilm structure as a function of shear stress. We demonstrate that arginine treatment leads to earlier detachment of the biofilm, indicating that arginine treatment weakens the biofilm, making it more susceptible to removal by shear stresses. Finally, we demonstrate that the biofilm disrupting affect is specific to arginine, and not a general property of amino acids, as *S. gordonii* biofilms treated with either glycine or lysine had mechanical properties similar to untreated biofilms. Our results add to the understanding that arginine targets biofilms by multifaceted mechanisms, both metabolic and physical, further promoting the potential of arginine as an active compound in dentifrices to maintain oral health.

Keywords: viscoelasticity, biophysical, mechanics, *Streptococcus gordonii*, arginine, dental plaque

INTRODUCTION

Biofilms are communities of microorganisms, encased in an extracellular polymeric slime (EPS). These communities adhere at either surface interfaces or to neighboring microorganisms (Bjarnsholt et al., 2013). Biofilms are responsible for a number of infectious diseases, where these communities are highly recalcitrant to traditional therapies, promoting the persistence of these

infections (Hall-Stoodley et al., 2004). Dental plaque is perhaps one of the most widely understood biofilms affecting human health. Oral pathologies typically arise due to poor oral hygiene and diet, that lead to dental plaque build-up or dysbiosis of the plaque microbial community. Together these factors can lead to oral diseases including dental caries, gingivitis and periodontitis (Mosaddad et al., 2019). Oral hygiene, including combinations of mechanical dental plaque removal and antimicrobial agents in dentifrices, continues to be the most effective method at preventing the development of these pathologies.

Exogenous arginine has emerged as a novel therapy to combat dental plaque. This mechanism has been chiefly attributed to the buffering capacity of arginine metabolism by arginolytic organisms, including *Streptococcus gordonii*. These organisms encode an arginine deiminase system (ADS), which metabolizes arginine, producing ammonia (Wijeyeweera and Kleinberg, 1989a; Wijeyeweera and Kleinberg, 1989b; Jakubovics et al., 2015). This in turn neutralizes acid produced by acidogenic organisms, maintaining a neutral pH within the dental plaque-biofilm (Wijeyeweera and Kleinberg, 1989a; Wijeyeweera and Kleinberg, 1989b). Exogenous arginine treatment also promotes *S. gordonii* growth and prevents the out-growth of cariogenic species, including *Streptococcus mutans*, in mixed species biofilm models (He et al., 2016; Bijle et al., 2019).

Exogenous arginine treatment can also reduce microbial coaggregation (Ellen et al., 1992; Kamaguch et al., 2001; Levesque et al., 2003), and alters the EPS biochemical composition, by preventing the out-growth of *S. mutans*, and subsequently reducing the amount of insoluble glycans produced by this organism (Kolderman et al., 2015; He et al., 2016). Interestingly, treatment with low concentrations of arginine promotes the growth of *S. gordonii* biofilms, however, high concentrations of the amino acid reduces biofilm biomass (Jakubovics et al., 2015). It was predicted that arginine treatment inhibited cell-cell interactions within the biofilm (Jakubovics et al., 2015). Taken together these data suggest that exogenous arginine treatment can disrupt dental plaque-biofilm, preventing its build-up (Kolderman et al., 2015; Manus et al., 2018; Wolff and Schenkel, 2018).

Despite the above observations, there is little understanding of how arginine treatment impacts the mechanical integrity of dental plaque-biofilms, an important factor in understanding how antimicrobials may penetrate the biofilm or how mechanical disruption may physically remove the biofilm. Atomic force microscopy (AFM) showed that *S. mutans* biofilms, grown in the presence of arginine, had reduced adhesion forces to the AFM tip (Sharma et al., 2014). This was predicted to be due to reduced glycan production or hydrogen bonds within the EPS (Sharma et al., 2014). However, effects of arginine treatment on the bulk biofilm properties and biofilm removal have yet to be considered. Furthermore, most studies have focused on how arginine impacts *S. mutans* biofilms, or caries-active plaque (Wolff and Schenkel, 2018). Few have focused on understanding how arginine impacts non-cariogenic plaque, or the biofilms of early plaque colonizers, such as *S. gordonii* (Jakubovics et al., 2015).

Rotating discs have long been used to analyze how biofilm fouling effects the hydrodynamics and drag associated with marine biofouling (Granville, 1982). The disc is rotated at increasing angular velocity, and the resulting torque (resistance to imparted rotary motion) is measured. Increases in torque is related to biomass, roughness and deformability of the biofilm (Dennington et al., 2015; Dennington et al., 2021). Conventionally, such discs are large [i.e. between 0.2 - 1 m diameter (Nelka, 1973; Schultz and Myers, 2003)], and hence cumbersome to manage. However, recently non-contact rotating-disc rheometry has been used to analyze drag associated with marine biofouling on discs 2.5 - 4 cm in diameter (Dennington et al., 2015; Dennington et al., 2021). In this method a rheometer is used as a highly sensitive torque monitor, allowing precise measurements of torque, even that generated by small discs compatible with the scale of routine laboratory biofilm growth systems (Dennington et al., 2015; Dennington et al., 2021). As such, it represents a novel method for direct quantification of biofilms outside of traditional assays, such as microscopic examination, viable counts and crystal violet staining. In addition, it allows real time correlation between imposed shear stress and changes in torque when biofilm is detached, informing how much shear is required to disrupt the biofilm. Here we adapted rotating-disc rheometry to study *S. gordonii* biofilm detachment after arginine treatment.

RESULTS

Adapted Rotating-Disc Rheometry Is Sensitive at Detecting Biofilm Rearrangement and Detachment Events

Mechanical analysis of biofilms is becoming more widespread in the field (Gloag et al., 2019). However, analyses of biofilm mechanics in the context of biofilm removal is currently lacking in the field. To meet this need we adapted rotating-disc rheology to analyze biofilm detachment from surfaces.

S. gordonii biofilms were grown on 3D printed coupons for 7 days. Biofilm coated coupons were connected to the rheometer and immersed in reverse osmosis water (**Figure 1A**). Coupons were spun across an angular velocity range of 0.1 – 300 rad·s^{-1} over 360 s, and the resulting torque, a measurement of resistance to rotation, was measured (**Movie S1**; https://doi.org/10.5061/dryad.p8cz8w9q2). Across this velocity range, detachment of biofilm aggregates was observed, particularly at the higher velocity regimes. These detachment events appeared to correlate to reductions in torque (**Movie S1**), with both small (**Figure 2A**) and larger (**Figure 2B**) aggregate detachments detected. After analysis there remained biofilm still attached to the coupon surface (**Figure 1B**). The remaining biofilm was not removed with repeated analysis (**Figure S1**).

To more easily observe the changes in torque associated with biofilm detachment, the torque – angular velocity data was first linearized and then transformed by determining the running slope of 5 consecutive data points (**Figure S2**). Using this transformed analysis, the reductions in torque were emphasized by being visualized as large peaks (**Figure 2** and **Movie S2**; https://doi.org/10.5061/dryad.p8cz8w9q2).

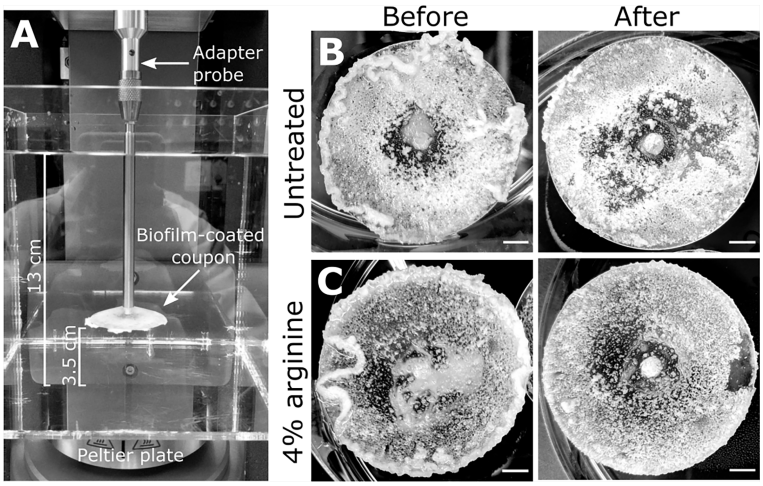

FIGURE 1 | *S. gordonii* biofilms before and after analysis. **(A)** Experimental design for the adapted rotating-disc rheometry analysis. Biofilm-coated coupons were attached to an adaptor probe on the rheometer using a threaded tap that was printed onto the back of the coupon. This was immersed in a container filled with reverse osmosis water. A gap thickness of 3.5 cm was set between the coupon and the bottom of the container. Prior to analysis 7 day *S. gordonii* biofilms, grown on the coupons, were treated with either **(B)** PBS (untreated control) or with **(C)** 4% arginine (labeled). Images depict biofilms before and after rheometry analysis (labeled). Scale bar indicates 5mm.

Furthermore, changes in torque not associated with macroscopic aggregate detachment were observed, particularly at the lower velocity regimes (**Movie S2**). This suggested that the adapted rotating-disc rheometry analysis was capable of detecting microscopic detachment events, or rearrangement of the biofilm structure in response to external shear stress.

Arginine-Treated Biofilms Are More Sensitive to Removal by Shear Stresses

Having validated the sensitivity of the adapted rotating-disc rheometry, we used this assay to determine how arginine treatment influenced biofilm mechanics, in regards to biofilm removal. Seven day *S. gordonii* biofilms were treated with either PBS (untreated control), 4% arginine, or equal molar concentrations of glycine or lysine (0.23M) for 2 min. This short treatment time was selected to mimic the time that a person would typically carry out their routine oral hygiene regimen. Glycine and lysine were selected as control amino acids, to determine if any biofilm disrupting effects were a general property of amino acids, or specific to arginine.

Macroscopically, arginine treatment did not appear to affect biofilm morphology, or the amount of remaining biofilm

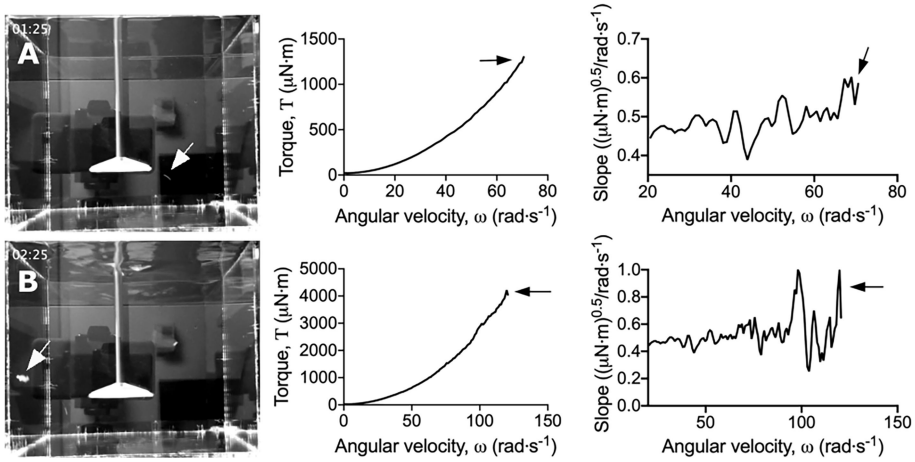

FIGURE 2 | Dips in the torque – angular velocity curve correlate to biofilm detachment events from the coupon. Stills taken from **Movies S1** and **S2** (left panel) depicting **(A)** small and **(B)** large biofilm detachment events. The torque – angular velocity curve (middle panel) and transformed linearized analysis (right panel) at each time is depicted. White arrows indicate detached biofilm and black arrows indicate the corresponding changes in the curve.

attached to the coupon after rheometry analysis (**Figures 1B, C**). However, arginine-treated biofilms displayed reduced torque, compared to untreated biofilms. In contrast glycine- and lysine-treated biofilms had similar torque – displacement profiles compared to untreated biofilms. These trends were true when considering the torque – displacement curves of individual biofilm replicates (**Figures 3A–D**) and combined data (**Figures 3E–H** and **Figure S3**). This indicates that coupons with arginine-treated biofilms could rotate more easily across the assayed angular velocity range. This is further highlighted by the transformed data (**Figure 4**) which amplified changes in torque that were occurring at lower angular velocity ranges that were not readily apparent in the torque – displacement curves (**Figure 3**). Visual inspection of this analysis revealed that changes in torque, indicated by negative slope values, were observed at lower angular velocity ranges for arginine-treated biofilms, compared to untreated and, glycine- and lysine-treated biofilms (**Figure 4**; green brackets and arrows, **Figure S4**). This suggests that biofilm detachment or rearrangement events were occurring at these lower angular velocity ranges for arginine-treated biofilms. Both treated and untreated biofilms had increased torque values compared to the coupon alone (**Figure 3**). The reduced torque of arginine-treated *S. gordonii* biofilms was not due to a reduction in biofilm biomass (**Figure 5**), suggesting that arginine treatment altered the mechanical properties of the biofilm.

To quantify the mechanical differences between treated and untreated *S. gordonii* biofilms, the biofilm momentum coefficient across the turbulent regimes of 200 – 300 rad·s^{-1}, was determined according the equation 1. The biofilm momentum coefficient is a dimensionless unit that is an indication of the drag caused by the biofilm, which in turn is related to the thickness and roughness of biofilm. Therefore, a higher coefficient is associated with more drag on the coupon, due to increased amount of adhered biofilm (Granville, 1982; Dennington et al., 2015). Glycine- and lysine-treated *S. gordonii* biofilms had biofilm momentum coefficients similar to untreated biofilms (**Figure 6A**). However, arginine-treated *S. gordonii* biofilms had a significantly lower biofilm momentum coefficient, compared to untreated biofilms (**Figure 6A**). This indicates that there was less drag caused by arginine-treated biofilms compared to either untreated or glycine- and lysine-treated biofilms.

To look into these differences further, the area under the curve (AUC) of the torque – angular velocity curves (**Figures 3A–D**) was determined (**Figure 6B**). Unlike the biofilm momentum coefficient, which only takes into consideration coupon rotation between 200 – 300 rad·s^{-1}, AUC considers the rotation across the whole analyzed range. Consistent with the biofilm momentum coefficient analysis, there were no significant differences between the AUC of both untreated and glycine- and lysine-treated biofilms (**Figure 6B**). However, arginine-treated biofilms had significantly reduced AUC, compared to untreated biofilms (**Figure 6B**). This suggests that, when also considering the lower velocity ranges, less work was required for rotation of the coupon of arginine-treated *S. gordonii* biofilms, compared to both untreated biofilms and glycine- and lysine-treated biofilms.

As previously mentioned, visual inspection of the transformed analysis, suggested that for arginine-treated biofilms, reductions in torque, associated with biofilm detachment events, occurred at lower angular velocity ranges, compared to untreated biofilms (**Figure 4**; green brackets and arrows, **Figure S4**). However, interpretation of this transformed analysis is subjective. To therefore quantify these differences, the angular velocity where the first reduction in torque occurred was converted to the shear stress acting on the outer edge of the coupon, according to equ 3, providing an initiation of detachment shear stress quantification (**Figure 6C**). This analysis revealed that there was no significant difference in the detachment shear stress of glycine- or lysine-treated *S. gordonii* biofilms compared to untreated. However, reductions in torque occurred at significantly lower shear stresses for arginine-treated biofilms, compared to untreated (**Figure 6C**). This indicates that arginine-treated biofilms were detaching from coupons at lower shear stresses, suggesting that they were more easily removed by external shear forces, compared to untreated or glycine- and lysine-treated *S. gordonii* biofilms.

DISCUSSION

Arginine is emerging as a potential therapeutic to prevent oral diseases, due to its ability to maintain dental plaque-biofilm homeostasis and disrupt biofilm formation (Kolderman et al., 2015; Manus et al., 2018; Wolff and Schenkel, 2018). However, there remains little understanding of how arginine treatment impacts biofilm mechanics or detachment. Here we adapted rotating-disc rheometry from the field of biofouling (Granville, 1982; Dennington et al., 2015; Dennington et al., 2021), to study how shear induced removal of *S. gordonii* biofilms was affected by arginine treatment.

Our data suggest that *S. gordonii* biofilms appear to consist of two layers. An upper layer that was readily removed, and a base layer that was more adherent, and resistant to removal (**Figure S1**). This was true for both arginine-treated and untreated *S. gordonii* biofilms (**Figures 1B, C**). Similarly, a remaining biofilm layer that was resistant to removal when exposed to increasing shear stresses was observed for *S. mutans* biofilms (Hwang et al., 2014), and biofilms grown from river (Desmond et al., 2018) and drinking (Abe et al., 2012) waters (refer to **Supplementary Table 1** for a summary of biofilm growth and testing conditions). Mechanical heterogeneity across the biofilm *z*-plane architecture has also been quantified for *Pseudomonas fluorescens* (Cao et al., 2016) and *Escherichia coli* (Galy et al., 2012) biofilms using micro-rheology methods. Together, this suggests that a stratified mechanical architecture may occur in biofilms, resulting in a cohesion/adhesion gradient, with the base of the biofilm being rigid and highly resistant to external forces. This could have important implications when considering the mechanical and chemical removal of biofilms from surfaces.

Our analysis also revealed that arginine-treated *S. gordonii* biofilms had both reduced drag on the coupon during rotation (**Figures 6A, B**), and detached from the coupon at lower shear

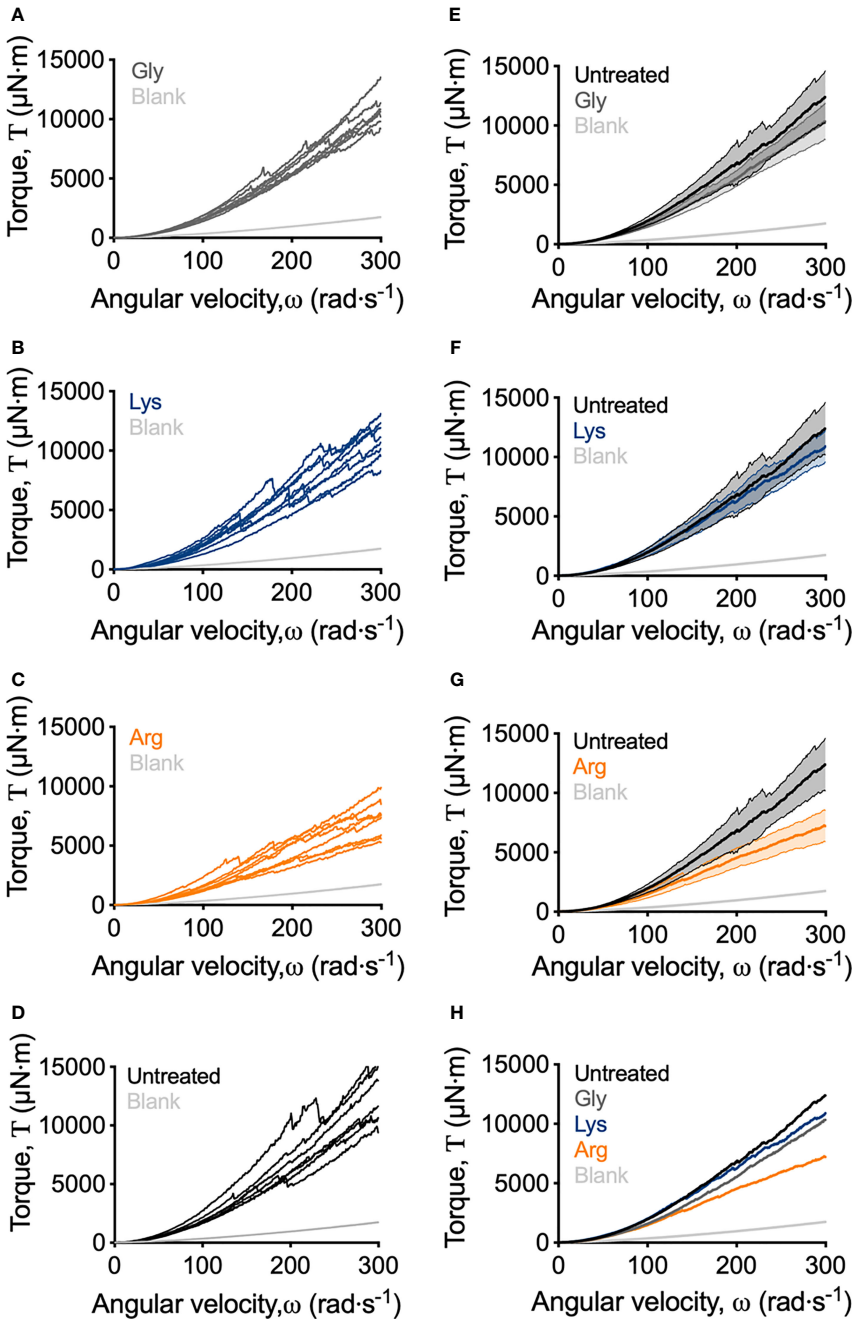

FIGURE 3 | Adapted rotating-disc measurements of untreated and amino acid treated *S. gordonii* biofilms. **(A–D)** Torque – displacement curves of individual replicates of glycine-, lysine-, arginine-treated and untreated (labelled) *S. gordonii* biofilms. **(E–G)** Comparison of the torque – displacement profiles of glycine-, lysine- and arginine-treated biofilms to untreated biofilms (labelled). Data is presented as mean ± 95% confidence interval. **(H)** Data from **(A–D)** expressed as mean. Replicate graph with data presented as mean ± 95% confidence interval is depicted in **Figure S3**. In each panel, blank indicates analysis for coupon alone, with no biofilm. 4 biological replicates were performed, with 2 biofilms analyzed for each replicate (total N = 8).

stresses (**Figure 6C**), compared to untreated biofilms. This suggests that arginine treatment weakened the structure of *S. gordonii* biofilms and that they were more easily removed from surfaces by external mechanical forces. Interestingly, previous observations of the biofilm disrupting effects of arginine either grew the biofilms in the presence of arginine, or treated the biofilms at multiple time points (Jakubovics et al., 2015; Kolderman et al., 2015; He et al., 2016). When mixed species biofilms were treated with arginine,

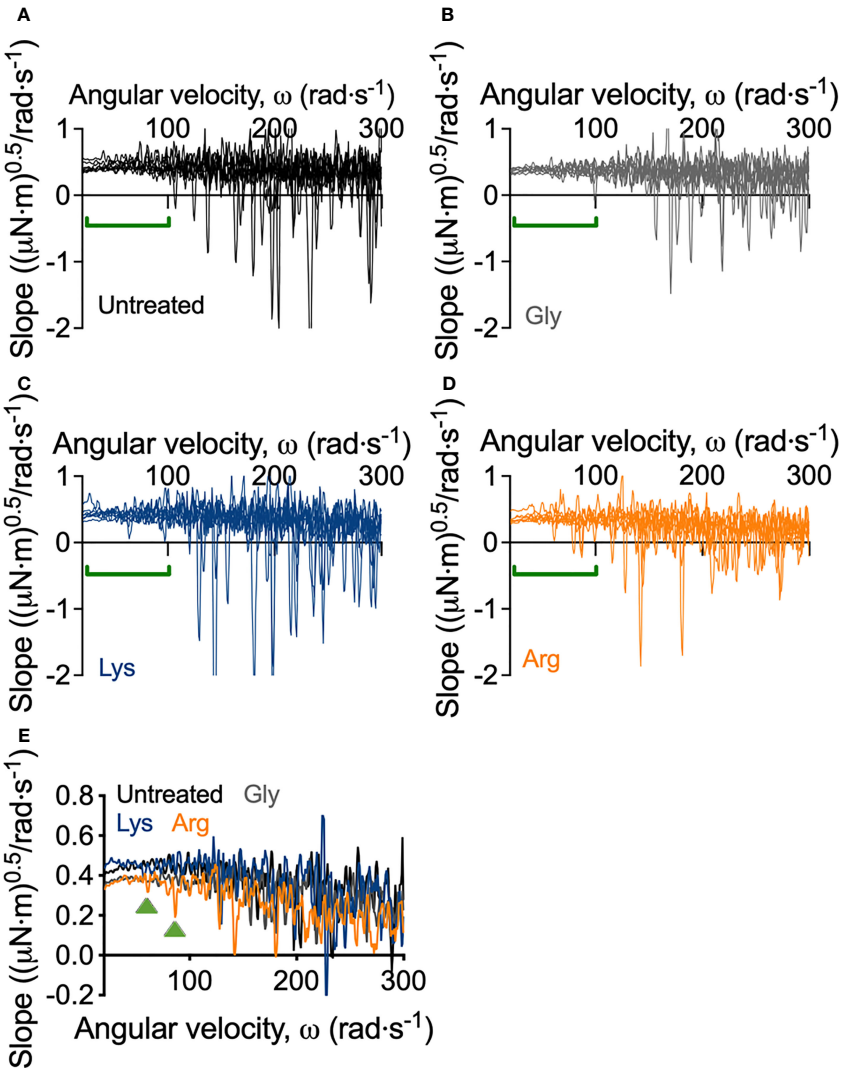

FIGURE 4 | Transformed linearized analysis of untreated and amino acid treated *S. gordonii* biofilms. Curves of individual replicates of **(A)** untreated *S. gordonii* biofilms and biofilms treated with **(B)** glycine, **(C)** lysine, and **(D)** arginine. Data presented as mean ± 95% confidence interval is depicted in **Figure S4**. **(E)** Data from **(A–D)** presented as mean. Green brackets **(A–D)** and arrows **(E)** highlights regions where changes in torque, depicted here as negative slope values, were observed for arginine-treated biofilms, but not for glycine- or lysine-treated or untreated biofilms. 4 biological replicates were performed, with 2 biofilms analyzed for each replicate (total N = 8).

three times a day over approximately 2 days, arginine effects to both microbial populations and biofilm structure were observed after 53 h (He et al., 2016). It was determined that arginine treatment takes time to exert effects on the biofilm, suggesting that arginine metabolism by arginolytic bacteria is required (He et al., 2016). However, here we observed arginine weakening *S. gordonii* biofilms after only 2 min of treatment. This suggests that mechanical destabilization of the biofilm can occur within a rapid time frame, compared to those that visually impact the biofilm architecture. These immediate mechanical effects are likely due to physical interactions, rather than metabolic. However, the biofilms analyzed here were thick (order of mm scale). As such there is the possibility that the exogenous arginine did not penetrate throughout the biofilm, particularly into the proposed rigid bottom biofilm layer, which was still attached to the coupon after analysis (**Figure 1C**).

AFM analysis of *S. mutans* biofilms, grown in the presence of arginine, identified that arginine reduced biofilm adhesion. *S. mutans* cannot metabolize arginine, and it was predicted that arginine prevented hydrogen bond interactions across glycan polymers within the EPS (Sharma et al., 2014). Furthermore, disruption of *S. gordonii* biofilms, when grown in the presence of high arginine concentrations, was predicted to be independent of arginine metabolism. Rather, it was predicted to be due to inhibition of cell-cell interactions within the biofilm (Jakubovics et al., 2015). We therefore predict that the

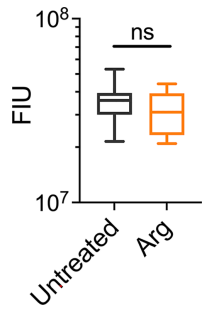

FIGURE 5 | Arginine treatment does not lead to reduced biofilm biomass. 7 day *S. gordonii* biofilms were treated with either PBS (untreated control) or with 4% arginine for 2min. Biofilm biomass was removed from the coupon surface and labelled with Syto 9. Syto 9 signal is presented as fluorescence intensity units (FIU). N = 4; ns indicates no significant difference.

weakening of arginine-treated *S. gordonii* biofilms observed here, may be due to disruption of chemical interactions between EPS components, or cell-cell or cell-EPS interactions within the biofilm. Similarly, *S. mutans* biofilms treated with a hydrolase that degrades EPS, were more easily removed from surfaces by exposure to external shear forces (Hwang et al., 2014). However, these biofilm destabilizing properties appear to be specific to arginine, and not a general action attributed to exogenous amino acids, as glycine or lysine treatment did not significantly alter *S. gordonii* biofilm mechanics compared to untreated biofilms (**Figures 3**, **6**).

Interestingly, *Pseudomonas aeruginosa* biofilms were more susceptible to tobramycin and ciprofloxacin treatment when the growth media was supplemented with arginine (Borriello et al., 2006). It was postulated that arginine was fermented in anoxic pockets of the mature biofilm, increasing the metabolic activity in these typically dormant regions and subsequently increasing the susceptibility to the antibiotic (Borriello et al., 2006). Our results suggest that arginine may also weaken the mechanical structure of the biofilm, allowing increased entry of the antibiotic into the biofilm. Together these results suggest that exogenous arginine can be used across multiple infection settings and has the potential to be used as an antimicrobial adjuvant.

Here we have adapted rotating-disc rheometry from the field of biofouling, as a novel methodology to analyze biofilm detachment from surfaces. We demonstrated that this assay is highly sensitive at detecting biofilm detachment, and possible structural rearrangements, with increasing shear forces. This methodology is also sensitive at detecting mechanical changes to the biofilm architecture that are not visually apparent. However, this method is destructive to the biofilm, and therefore, limits the sensitivity of assessing drag of the original structure at higher shears. Finally, we also identified, for the first time, that arginine treatment can weaken the mechanical structure of *S. gordonii* biofilms, resulting in detachment at lower shear stresses, compared to untreated biofilms. These effects were observed after only 2 min of treatment. Our results add to the multifaceted action of arginine at disrupting dental plaque-biofilms, and further promotes the potential use of arginine as an active compound in dentifrices to combat dental plaque and help improve oral health.

MATERIALS AND METHODS

3D Printing Coupons

The model for the coupons was designed in SolidWorks (Dassault Systèmes). The model is available through Dryad [https://doi.org/10.5061/dryad.jdfn2z3b2]. Coupons were 3D printed using a Prime 30 PolyJet 3D printer (Objet, Stratasys) using RGD720 photopolymer for the printing material (Stratasys). The coupon was printed at a resolution of 0.02 mm. The coupon surface was sanded used P300 sandpaper to create a rougher surface for bacteria to attach. Prior to inoculating, coupons were sterilized in 70% ethanol.

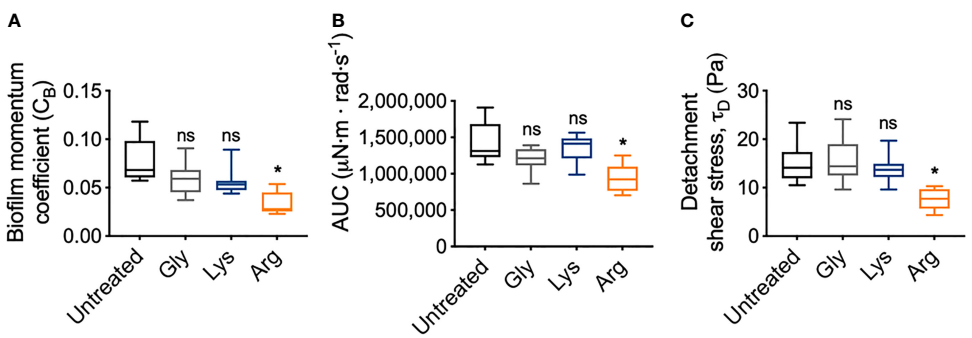

FIGURE 6 | Arginine treatment weakens *S. gordonii* biofilms. **(A)** Biofilm momentum coefficient (C_B), determined according to equation 1, at 200 – 300 rad.s^{-1} in **Figure 3** [Range; Untreated: 0.057 – 0.118; glycine: 0.037 – 0.091; lysine: 0.044 – 0.089; arginine: 0.023 – 0.054]. **(B)** Area under the curve (AUC) of torque – angular velocity curves depicted in **Figure 3** [Range; Untreated: 1,126,923 – 1,909,471; glycine: 863,187 – 1,390,189; lysine: 986,807 – 1,564,073; arginine: 702,523 – 1,250,791 μN·m · rad·s^{-1}]. **(C)** Initiation of detachment, indicated as the first reduction in torque in **Figures 3**, converted to shear stress according to equ 3 [Range; Untreated: 10.50 – 23.50; glycine: 9.61 – 24.10; lysine: 9.61 – 19.70; arginine: 4.34 – 10.30 Pa]. * p-value < 0.05, ns indicates no statistical difference.

S. gordonii Biofilm Growth and Treatment

S. gordonii wild type strain DL1 was used in this study. Overnight cultures were prepared by inoculating 10 mL of brain heart infusion broth (Oxoid; BHI) with a colony of *S. gordonii* and incubated statically overnight at 37°C with 5% CO_2.

Sterile 40 mm coupons were placed in a Petri dish containing 40 mL BHI, supplemented with 0.5% sucrose. Coupons were inoculated with 400 µL of overnight culture. Biofilms were incubated in a humidified chamber at 37°C with 5% CO_2, on an orbital shaker at 150 rpm. Every 24 h the media was replenished. Biofilms were grown for 7 days.

Biofilms were treated by transferring the coupons to a Petri dish containing either 40 mL PBS or 0.23M arginine, glycine, or lysine. This concentration was selected as it equated to 4% arginine, which has previously been shown to disrupt dental plaque-biofilms (Jakubovics et al., 2015). Amino acid solutions were normalized to pH 7. Biofilms were treated for 2 min at 37°C with 5% CO_2, shaking at 150 rpm. Biofilms were washed in PBS and transferred to 40 mL PBS until analysis. 4 biological replicates were performed, each with duplicate biofilms.

Adapted Rotating-Disc Rheometry Analysis

Biofilms were analyzed on a Discovery Hybrid Rheometer-2 (HD-2) (TA Instruments). A 15 x 15 cm square clear acrylic container filled with 2.8 L reverse osmosis water was transferred onto the Peltier plate. Biofilm-coated coupons were immersed and attached to the rheometer shaft using a custom-made adapter probe. The gap distance between the bottom of the container and the coupon was set to 3.5 cm (**Figure 1A**). Immersed coupons were spun at an angular velocity (ω) range of 0.1 – 300 rad·s^{-1}, incrementing the speed across 360 s. It is important to note that the geometry of the system will influence the motion of water in the reservoir. As such measurements should be considered system-specific.

Quantifying Biofilm Biomass

After treatment with either PBS (untreated control) or 4% arginine, *S. gordonii* biofilm biomass was scraped off the coupon using a cell scraper and resuspended in 5 mL PBS. Cellular aggregates were unable to be successfully disrupted by either sonication or syringe disruption. To therefore avoid these aggregates altering biomass quantification by colony forming units, biomass was quantified by labelling with Syto 9. Syto 9 is a green fluorescent membrane permeant nucleic acid stain, the signal of which increases when intercalated with nucleic acids. Therefore, Syto 9 will label all cells that contain DNA, and the presence of bacterial aggregates is predicted to have no impact on the fluorescent signal (Lebaron et al., 1998; Stocks, 2004). Styo 9 was diluted in PBS to a final concentration of 5 µM. 100 µL aliquots were transferred to the wells of a black 96-well plate. 100 µL aliquots of the treated or untreated biofilm suspension was added to the Styo 9 and incubated at room temperature for 15 min. Syto 9 fluorescence was measured on a SpectraMax i3 plate reader (Molecular Devices) as fluorescence intensity units (FIU) using an excitation of 485nm and emission of 535nm. 2 biological replicates, each with duplicate biofilms and four technical replicates were performed.

Data Analysis

Data was collected using TRIOS v5 software (TA instruments), with raw data exported in excel. Data was transformed, and calculations performed in excel. Data was visualized and statistical analysis performed in GraphPad Prism v8 (GraphPad Software). All statistical comparisons were performed using a one-way ANOVA with a Tukey's post-hoc test, with $p < 0.05$ indicating significance.

To more clearly observe the changes in torque, the torque – angular velocity curves were linearized and transformed (**Figure S2**). The data was linearized by taking the square root of the torque. The running slope of 5 data points of the linearized data was determined. This transformed data was linearized after 20 rad·s^{-1}. Therefore, final transformed data is presented as the running slope of the linearized data against angular velocity, starting at 20 rad·s^{-1} (**Figure S2**). An example excel spreadsheet of the transformed data has been included in the supplemental data files.

The biofilm momentum coefficient (C_B), also referred to as the momentum or torque coefficient, was determined as previously described (Dennington et al., 2015). The adapted rotating-disc rheology measurement is most sensitive at detecting changes in torque at the turbulent regime, between 200 – 300 rad·s^{-1}. Torque within this range has a linear relationship to ω^2, where the slope of this line ($T^{1/2}/\omega$) equates to $C_B \cdot k$. Therefore, C_B can be defined by equation 1:

$$C_B = \frac{slope}{k} \tag{1}$$

where k is a constant for the system, defined by:

$$k = \frac{\rho \cdot r^5}{2} \tag{2}$$

where ρ is the density of the fluid, in this case water (997 kg/m^3) and r is the radius of the coupon (0.02 m).

The angular velocity where the first decrease in torque was detected was converted to the shear stress acting at the outer edge of the coupon (τ), as previously described (Hunsucker et al., 2016), according to equation 3:

$$\tau = \sqrt{\tau_\varphi^2 + \tau_r^2} \tag{3}$$

where, τ_φ is the shear stress acting in the circumferential direction and τ_r is the shear stress acting radially. This is intended as a system specific comparator, and not an absolute value that can be applied across other experimental designs or applications.

The shear stress acting in the circumferential direction is described by equation 4:

$$\tau_\varphi = \frac{\omega^2 \cdot r^2}{(4.96 \cdot \log_{10} \mathrm{Re} - 5.74)^2} \cdot \rho \tag{4}$$

where Re is the Reynolds number acting at the outer edge of the coupon described by equation 5:

$$\mathrm{Re} = \frac{\omega \cdot r^2}{\nu} \quad (5)$$

where v is the kinematic viscosity (9 x 10^{-7} $m^2 \cdot s^{-1}$).

The shear stress acting in the radial direction is described by equation 6:

$$\tau_r = \alpha \cdot \tau_\varphi \quad (6)$$

where α is the skewness between the shear stress acting in both directions, and is described by equation 7:

$$\alpha = \frac{4.395}{4.96 \cdot \log_{10} \mathrm{Re} - 5.74)^2} - 0.0107 \quad (7)$$

Finally, the area under the curve (AUC) of the torque – angular velocity curves was determined using the analysis function in GraphPad Prism.

DATA AVAILABILITY STATEMENT

The raw data supporting the conclusions of this article will be made available by the authors, without undue reservation.

AUTHOR CONTRIBUTIONS

KW designed and printed the coupons. EG performed all experimental work. EG and PS analyzed and interpreted the experimental data. EG, DW, JM, CD, and PS wrote the manuscript. All authors gave their final approval and agree to be accountable for all aspects of the work.

FUNDING

This work was funded by Colgate-Palmolive. EG was funded by an American Heart Association Career Development Award (19CDA34630005). DW and PS were funded by the National Institute of Health (DJW: R01AI134895 and R01AI143916) (PS: R01GM124436).

SUPPLEMENTARY MATERIAL

The Supplementary Material for this article can be found online at: https://www.frontiersin.org/articles/10.3389/fcimb.2021.784388/full#supplementary-material

REFERENCES

Abe, Y., Skali-Lami, S., Block, J.-C., and Francius, G. (2012). Cohesiveness and Hydrodynamic Properties of Young Drinking Water Biofilms. *Water Res.* 46, 1155–1166. doi: 10.1016/j.watres.2011.12.013

Bijle, M. N. A., Ekambaram, M., Lo, E. C. M., and Yiu, C. K. Y. (2019). The Combined Antimicrobial Effect of Arginine and Fluoride Toothpaste. *Sci. Rep.* 9, 8405. doi: 10.1038/s41598-019-44612-6

Bjarnsholt, T., Alhede, M., Alhede, M., Eickhardt-Sørensen, S. R., Moser, C., Kühl, M., et al. (2013). The *In Vivo* Biofilm. *Trends Microbiol.* 21, 466–474. doi: 10.1016/j.tim.2013.06.002

Borriello, G., Richards, L., Ehrlich, G. D., and Stewart, P. S. (2006). Arginine or Nitrate Enhances Antibiotic Susceptibility of Pseudomonas Aeruginosa in Biofilms. *Antimicrob Agents Chemother* 50, 382–384. doi: 10.1128/AAC.50.1.382-384.2006

Cao, H., Habimana, O., Safari, A., Heffernan, R., Dai, Y., and Casey, E. (2016). Revealing Region-Specific Biofilm Viscoelastic Properties by Means of a Micro-Rheological Approach. *NPJ Biofilms Microbiomes* 2, 5. doi: 10.1038/s41522-016-0005-y

Dennington, S. P., Jackson, A., Finnie, A. A., Wharton, J. A., Longyear, J. E., and Stoodley, P. (2021). A Rapid Benchtop Method to Assess Biofilm on Marine Fouling Control Coatings. *Biofouling* 37, 1–13. doi: 10.1088/2051-672X/3/3/034004

Dennington, S., Mekkhunthod, P., Rides, M., Gibbs, D., Salta, M., Stoodley, V., et al. (2015). Miniaturized Rotating Disc Rheometer Test for Rapid Screening of Drag Reducing Marine Coatings. *Surface Topogr: Metrol. Prop.* 3, 034004. doi: 10.1080/08927014.2021.1929937

Desmond, P., Böni, L., Fischer, P., Morgenroth, E., and Derlon, N. (2018). Stratification in the Physical Structure and Cohesion of Membrane Biofilms —Implications for Hydraulic Resistance. *J. Membr Sci.* 564, 897–904. doi: 10.1016/j.memsci.2018.07.088

Ellen, R. P., Song, M., and Buivids, I. A. (1992). Inhibition of Actinomyces Viscosus–Porphyromonas Gingivalis Coadhesion by Trypsin and Other Proteins. *Oral. Microbiol. Immunol.* 7, 198–203. doi: 10.1111/j.1399-302X.1992.tb00025.x

Galy, O., Latour-Lambert, P., Zrelli, K., Ghigo, J.-M., Beloin, C., and Henry, N. (2012). Mapping of Bacterial Biofilm Local Mechanics by Magnetic Microparticle Actuation. *Biophys. J.* 103, 1400–1408. doi: 10.1016/j.bpj.2012.07.001

Gloag, E. S., Fabbri, S., Wozniak, D. J., and Stoodley, P. (2019). Biofilm Mechanics: Implications in Infection and Survival. *Biofilm.* 2, 100017. doi: 10.1016/j.bioflm.2019.100017:100017

Granville, P. (1982). Drag-Characterization Method for Arbitrarily Rough Surfaces by Means of Rotating Disks. *J. Fluids Eng.* 104, 373–377. doi: 10.1115/1.3241854

Hall-Stoodley, L., Costerton, J. W., and Stoodley, P. (2004). Bacterial Biofilms: From the Natural Environment to Infectious Diseases. *Nat. Rev. Microbiol.* 2, 95–108. doi: 10.1038/nrmicro821

He, J., Hwang, G., Liu, Y., Gao, L., Kilpatrick-Liverman, L., Santarpia, P., et al. (2016). L-Arginine Modifies the Exopolysaccharide Matrix and Thwarts Streptococcus Mutans Outgrowth Within Mixed-Species Oral Biofilms. *J. Bacteriol* 198, 2651–2661. doi: 10.1128/JB.00021-16

Hunsucker, J. T., Hunsucker, K. Z., Gardner, H., and Swain, G. (2016). Influence of Hydrodynamic Stress on the Frictional Drag of Biofouling Communities. *Biofouling* 32, 1209–1221. doi: 10.1080/08927014.2016.1242724

Hwang, G., Klein, M. I., and Koo, H. (2014). Analysis of the Mechanical Stability and Surface Detachment of Mature Streptococcus Mutans Biofilms by Applying a Range of External Shear Forces. *Biofouling* 30, 1079–1091. doi: 10.1080/08927014.2014.969249

Jakubovics, N. S., Robinson, J. C., Samarian, D. S., Kolderman, E., Yassin, S. A., Bettampadi, D., et al. (2015). Critical Roles of Arginine in Growth and Biofilm Development by Streptococcus Gordonii. *Mol. Microbiol.* 97, 281–300. doi: 10.1111/mmi.13023

Kamaguch, A., Nakayama, K., Ohyama, T., Watanabe, T., Okamoto, M., and Baba, H. (2001). Coaggregation of Porphyromonas Gingivalis and Prevotella Intermedia. *Microbiol. Immunol.* 45, 649–656. doi: 10.1111/j.1348-0421.2001.tb01298.x

Kolderman, E., Bettampadi, D., Samarian, D., Dowd, S. E., Foxman, B., et al. (2015) L-Arginine Destabilizes Oral Multi-Species Biofilm Communities Developed in Human Saliva. *PloS One* 10, e0121835. doi: 10.1371/journal.pone.0121835

Lebaron, P., Parthuisot, N., and Catala, P. (1998). Comparison of Blue Nucleic Acid Dyes for Flow Cytometric Enumeration of Bacteria in Aquatic Systems. *Appl. Environ. Microbiol.* 64, 1725–1730. doi: 10.1128/AEM.64.5.1725-1730.1998

Levesque, C., Lamothe, J., and Frenette, M. (2003). Coaggregation of Streptococcus Salivarius With Periodontopathogens: Evidence for Involvement of Fimbriae in the Interaction With Prevotella Intermedia. *Oral. Microbiol. Immunol.* 18, 333–337. doi: 10.1034/j.1399-302X.2003.00085.x

Manus, L. M., Daep, C., Begum-Gafur, R., Makwana, E., Won, B., Yang, Y., et al. (2018). Enhanced *In Vitro* Zinc Bioavailability Through Rational Design of a Dual Zinc Plus Arginine Dentifrice. *J. Clin. Dent.* 29, A10–A19.

Mosaddad, S. A., Tahmasebi, E., Yazdanian, A., Rezvani, M. B., and Seifalian, A. Yazdanian M and Tebyanian H. (2019). Oral Microbial Biofilms: An Update. *Eur. J. Clin. Microbiol. Infect. Dis.* 38, 2005–2019. doi: 10.1007/s10096-019-03641-9

Nelka, J. J. Evaluation of a Rotating Disk Apparatus: Drag of a Disk Rotating in a Viscous Fluid. David W Taylor Naval Ship Research And Development Center Bethesda Md Ship Performance Dept. (1973).

Schultz, M., and Myers, A. (2003). Comparison of Three Roughness Function Determination Methods. *Exp. Fluids* 35, 372–379. doi: 10.1007/s00348-003-0686-x

Sharma, S., Lavender, S., Woo, J., Guo, L., Shi, W., Kilpatrick-Liverman, L., et al. (2014). Nanoscale Characterization of Effect of L-Arginine on Streptococcus Mutans Biofilm Adhesion by Atomic Force Microscopy. *Microbiology* 160, 1466–1473. doi: 10.1099/mic.0.075267-0

Stocks, S. (2004). Mechanism and Use of the Commercially Available Viability Stain, BacLight. *Cytometry Part A: J. Int. Soc. Anal. Cytol.* 61, 189–195. doi: 10.1002/cyto.a.20069

Wijeyeweera, R., and Kleinberg, I. (1989a). Acid-Base pH Curves *In Vitro* With Mixtures of Pure Cultures of Human Oral Microorganisms. *Arch. Oral. Biol.* 34, 55–64. doi: 10.1016/0003-9969(89)90046-0

Wijeyeweera, R., and Kleinberg, I. (1989b). Arginolytic and Ureolytic Activities of Pure Cultures of Human Oral Bacteria and Their Effects on the pH Response of Salivary Sediment and Dental Plaque *In Vitro*. *Arch. Oral. Biol.* 34, 43–53. doi: 10.1016/0003-9969(89)90045-9

Wolff, M. S., and Schenkel, A. B. (2018). The Anticaries Efficacy of a 1.5% Arginine and Fluoride Toothpaste. *Adv. Dent. Res.* 29, 93–97. doi: 10.1177/0022034517735298

Conflict of Interest: Authors CD and JM are employees of Colgate-Palmolive.

The remaining authors declare that the research was conducted in the absence of any commercial or financial relationships that could be construed as a potential conflict of interest.

The study received funding from Colgate-Palmolive. The funder had the following involvement with the study: study design, decision to publish and preparation of the manuscript.

Publisher's Note: All claims expressed in this article are solely those of the authors and do not necessarily represent those of their affiliated organizations, or those of the publisher, the editors and the reviewers. Any product that may be evaluated in this article, or claim that may be made by its manufacturer, is not guaranteed or endorsed by the publisher.

frontiers in Cellular and Infection Microbiology

BRIEF RESEARCH REPORT
published: 15 November 2021
doi: 10.3389/fcimb.2021.771666

codY and *pdhA* Expression Is Induced in *Staphylococcus epidermidis* Biofilm and Planktonic Populations With Higher Proportions of Viable but Non-Culturable Cells

Vânia Gaio[†], *Nathalie Lopes*[†], *Nuno Cerca and Angela França*[*]

Laboratory of Research in Biofilms Rosário Oliveira (LIBRO), Centre of Biological Engineering (CEB), University of Minho, Braga, Portugal

OPEN ACCESS

Edited by:
Carolina Henritta Pohl, University of the Free State, South Africa

Reviewed by:
Claudia NH Marques, Binghamton University, United States
Ferdinand Xiankeng Choong, Karolinska Institutet (KI), Sweden

***Correspondence:**
Angela França
afranca@ceb.uminho.pt

[†]*These authors have contributed equally to this work*

Specialty section:
This article was submitted to Biofilms, a section of the journal Frontiers in Cellular and Infection Microbiology

Received: *06 September 2021*
Accepted: *27 October 2021*
Published: *15 November 2021*

Citation:
Gaio V, Lopes N, Cerca N and França A (2021) codY and pdhA Expression Is Induced in Staphylococcus epidermidis Biofilm and Planktonic Populations With Higher Proportions of Viable but Non-Culturable Cells. Front. Cell. Infect. Microbiol. 11:771666. doi: 10.3389/fcimb.2021.771666

Staphylococcus epidermidis biofilm cells can enter a physiological state known as viable but non-culturable (VBNC), where, despite being alive, they do not grow in conventional laboratory media. As such, the presence of VBNC cells impacts the diagnosis of *S. epidermidis* biofilm-associated infections. Previous transcriptomics analysis of *S. epidermidis* strain 9142 biofilms with higher proportions of VBNC cells suggested that the genes *pdhA, codY* and *mazEF* could be involved in the induction of the VBNC state. However, it was previously demonstrated that VBNC induction is strain-dependent. To properly assess the role of these genes in VBNC induction, the construction of mutant strains is necessary. Thus, herein, we assessed if VBNC cells could be induced in strain 1457, a strain amenable to genetic manipulation, and if the previously identified genes were involved in the modulation of the VBNC state in this strain. Furthermore, we evaluated the formation of VBNC cells on planktonic cultures. Our results showed that despite being commonly associated with biofilms, the proportion of VBNC cells can be modulated in both biofilm and planktonic cultures and that the expression of *codY* and *pdhA* was upregulated under VBNC inducing conditions in both phenotypes. Overall, our study revealed that the formation of VBNC cells in *S. epidermidis* is independent of the mode of growth and that the genes *codY* and *pdhA* seem to be relevant for the regulation of this physiological condition.

Keywords: *Staphylococcus epidermidis* infections, VBNC cells induction model, planktonic cells, biofilms, glucose, magnesium, gene expression

INTRODUCTION

Staphylococcus epidermidis is now considered an opportunistic pathogen responsible for many healthcare-associated infections, mainly those related to biofilm formation on indwelling medical devices (Mack et al., 2013). *S. epidermidis* biofilm-associated infections are often recurrent leading to high rates of morbidity (Otto, 2009). The failure of antibiotics to cure these types of infections is

primarily associated with the poor capacity to eradicate biofilms, which are known to have bacterial cells with distinct physiological states (Rani et al., 2007), including viable but non-culturable (VBNC) cells (Cerca et al., 2011a; Zhang et al., 2018; Li et al., 2020). Although VBNC cells cannot grow on standard growth media, these cells present a reduced metabolic activity, replication rate and gene transcription (Lleo et al., 2000; Zhang et al., 2018). For this reason, their detection with traditional culture-based methods and, consequently, the diagnosis of *S. epidermidis* biofilm-related infections is hindered (Zandri et al., 2012). Moreover, *S. epidermidis* VBNC cells can be more tolerant to antibiotics (Cerca et al., 2014), limiting the efficacy of current treatment options. As such, the study of the mechanisms underlying the development of this physiological state in *S. epidermidis* is of utmost importance.

An *in vitro* model aimed to induce the formation of VBNC cells in *S. epidermidis* biofilms, developed on strain 9142, demonstrated that the addition of a high concentration of glucose (1%) increased the proportion of VBNC cells, while the addition of magnesium chloride ($MgCl_2$, 20 mM) prevented the formation of VBNC cells. This modulation resulted in biofilms with approximately the same number of viable cells but about 1 log difference in the number of culturable cells (Cerca et al., 2011a; Carvalhais et al., 2014). Importantly, although glucose enrichment was associated with medium acidification, it was formerly demonstrated that the prevention of the VBNC state is a pH-independent phenomenon since the addition of $MgCl_2$ does not prevent acidification of the medium (Cerca et al., 2011a). The applicability of this model to induce the formation of VBNC cells in *S. epidermidis* biofilms was further analysed in 19 clinical and 24 commensal isolates (Carvalhais et al., 2018). Most of the clinical isolates tested (70%) showed at least a 0.5 $\log_{10}$ decrease in culturability, whereas only 33% of the commensal isolates presented a similar reduction, suggesting that VBNC cells induction by glucose and prevention by magnesium chloride is not a universal phenomenon amongst *S. epidermidis* isolates. A possible explanation for this isolate-specific response may be related to transcriptomic changes, for instance, in genes involved in metabolism and oxidative stress (Keren et al., 2011; Carvalhais et al., 2014; Postnikova et al., 2015). Therefore, the analysis of genes whose products could be associated with the regulation of this physiological state is crucial to underpin the mechanisms behind its emergence.

Previously, using an RNA-Sequencing (RNA-Seq) approach, we have detected changes in the transcription of the genes *codY*, *mazE*, *mazF* and *pdhA* in biofilms with a higher proportion of VBNC cells, suggesting that these genes could be linked to the emergence of the VBNC state in *S. epidermidis* strain 9142 (Carvalhais et al., 2014). To confirm this hypothesis, the study of strains lacking the genes of interest is essential. *S. epidermidis* is known to be difficult to be genetically manipulated, with only a few strains known to be amenable (Mack et al., 2001; Winstel et al., 2015; Winstel et al., 2016; Galac et al., 2017), being *S. epidermidis* strain 1457 the most frequently used for mutagenesis studies. Unfortunately, earlier studies aiming to modulate VBNC cells proportions in *S. epidermidis* biofilms did not include such strain. Therefore, to determine if *S. epidermidis* 1457 could be a suitable candidate for the study of the mechanisms behind the formation of VBNC cells, the ability of this strain to form VBNC cells needs to be investigated.

Thus, herein, we tested the induction of VBNC cells in biofilms formed by strain 1457, using the previously optimized *in vitro* VBNC cells induction model, and assessed the expression of the genes *codY*, *mazE*, *mazF* and *pdhA*. Additionally, we investigated the suitability of this model in planktonic cultures, further exploring the potential role of the previously identified genes in the VBNC state mediation in planktonic cells.

MATERIAL AND METHODS

Strains and Growth Media

S. epidermidis 1457, a strain isolated from a venous catheter-associated infection (Mack et al., 1992) was used for this study, together with the commensal isolate COM040A (skin sample from a healthy volunteer) and the clinical isolate PT11004 (isolated from a bloodstream infection), which were previously shown to accumulate high amounts of VBNC cells (Carvalhais et al., 2018). Additionally, to validate previous RNA-Seq data, strain 9142 was also included. For each experiment, all *S. epidermidis* strains were grown directly from the glycerol stocks (30% glycerol) in tryptic soy broth (TSB, Merck, Darmstadt, Germany) at 37°C and with shaking at 120 rpm (10 mm orbit shaker). The optical density (OD) of overnight suspensions was adjusted, at 640 nm, to 0.25 ± 0.05, corresponding to ≈ 2×10^8 colony-forming units/mL (CFU/mL) (Freitas et al., 2014), to be used as inoculum for all the experiments subsequently described.

Biofilm Cultures

Biofilms were formed, in 24-well plates (Orange Scientific, Braine-l'Alleud, Belgium), by inoculating 10 µL of overnight suspensions, previously adjusted to OD_{640nm}= 0.25 ± 0.05, into 1 mL of TSB supplemented with 0.4% glucose or 0.4% glucose plus 20 mM $MgCl_2$, for further induction and prevention of the VBNC state, respectively (Cerca et al., 2014). The plates were then incubated for 24 h at 37°C and 120 rpm. After that period, the spent media was removed and replaced by fresh TSB supplemented with either 1% glucose (induced VBNC state) or 1% glucose plus 20 mM $MgCl_2$ (prevented VBNC state), and grown under the same temperature and agitation conditions for additional 24 h. Thereafter, the biofilm bulk fluid was removed, and the biofilms washed twice with 500 µL of 0.9% NaCl. Finally, biofilms were scraped from the plate bottom and suspended in 1 mL of the same saline solution.

Planktonic Cultures

For the analysis of VBNC cells formation in planktonic cells, 24 h and 48 h cultures, grown in 10 mL erlenmeyers, were evaluated. In the case of 24 h planktonic assays, a 1:100 dilution of the overnight growth was performed in TSB supplemented with 1% glucose (induction of the VBNC state) or 1% glucose plus 20 mM of $MgCl_2$ (prevention of the VBNC state) and incubated at 37°C and 120 rpm for 24 h. The second approach (48 h growth) aimed

to mimic the conditions used for biofilms growth. This consisted of pre-growing bacteria with TSB supplemented with 0.4% glucose (plus 20 mM of $MgCl_2$ for prevented VBNC condition) for 24 h, followed by centrifugation of the cells (16.000 g, 10 min, 4°C) and replacement of the spent medium with fresh TSB supplemented with 1% glucose or 1% glucose plus 20 mM $MgCl_2$. The suspensions were then grown for additional 24 h under the same temperature and agitation conditions.

Assessment of VBNC State Induction in Both Biofilm and Planktonic Cultures

At the selected time points, bacterial cells from either biofilms or planktonic cultures were collected and sonicated for 10 s at 33% amplitude (Ultrasonic Processor Model CP750, Cole-Parmer, IL, USA) to dissociate cells clusters and create a homogeneous biofilms cells suspension. Importantly, the selected sonication cycle has no significant effect on cells viability, as previously determined by CFU counting and propidium iodide incorporation (Freitas et al., 2014). The quantification of the total amount of suspended cells was performed by OD_{640nm} measurements, as previously shown (Freitas et al., 2014). Viable cells were quantified by flow cytometry using SYBR Green (1:80000)/propidium iodide (20 μg/mL) staining as previously optimized (Cerca et al., 2011b). Samples were acquired in an EC800™ flow cytometer (Sony Biotech, CA, USA), with a flow rate of 10 μL/min and a total of 100000 events were acquired for each sample. Data analysis was performed using FCS Express 6 and considering the populations $SYBR^+/PI^-$ (live cells) and $SYBR^+/PI^+$ (live cells somewhat permeable to PI), and excluding $SYBR^-/PI^+$ (dead cells). Finally, the number of culturable cells was determined by CFU counting. Briefly, serial dilutions were performed in 0.9% NaCl and 5 μL of each dilution were plated on TSA plates. Plates were incubated at 37°C for at least 16 h. The analysis of the proportion of VBNC cells in both biofilm and planktonic cultures was determined as the ratio (%) between the values obtained for induced and prevented conditions (IND/PRE), in terms of culturability (CFU) or OD.

Gene Expression Quantification by Quantitative PCR (qPCR)

RNA Extraction

For total RNA isolation from biofilm cells, the bulk fluid of the biofilm culture was discarded, the biofilms washed twice with 0.9% NaCl and then suspended in the same solution by scraping the cells from the plate bottom. All the procedure was performed on ice. Three independent biofilms were pooled to reduce biological variability (Sousa et al., 2014) and immediately centrifuged at 16000 g for 10 min at 4°C. For RNA isolation from planktonic cultures, 1 mL of culture was collected and immediately centrifuged at 16000 g for 10 min at 4°C. Of note, bacterial cells were suspended in 0.9% NaCl before RNA isolation since we have previously determined that mRNA quantification was similar to when using RNA preserving solutions if processed immediately (**Supplementary Figure 1**). The extraction of RNA from both suspensions was then performed using the kit ExtractMe RNA Bacteria & Yeast (Blirt S.A., Gdansk, Poland) as previously optimized (França et al., 2012). In brief, bacterial pellets were suspended in 600 μL of RYBL buffer, transferred into 2 mL tubes containing 0.5 g of acid-washed silica beads (150–212 mm) (Sigma-Aldrich, USA) and the cells were lysed using a BeadBug 6 Microtube Homogenizer (Benchmark Scientific, NJ, USA) for 35 s at ~4.5 rpm. Subsequently, samples were incubated on ice for 5 min and the cell disruption and cooling steps repeated three more times. Afterwards, samples were centrifuged at 16000 g for 1 min at 4°C, the supernatants transferred into 2 mL RNase-free tubes and mixed with an equal volume of 70% ethanol. The subsequent steps were performed according to the manufacturer's instructions. RNA samples were then treated with DNase I (Thermo Fisher Scientific Inc, MA, USA) to degrade contaminating genomic DNA. RNA concentration and purity ($A_{260/A280}$ and $A_{260/A230}$) were determined by NanoDrop One (Thermo Fisher Scientific Inc) and RNA integrity was inferred by visualization of the 23S/16S rRNA banding pattern using a 1% non-denaturing agarose gel.

Complementary (c) DNA Synthesis

Total RNA concentration was adjusted to 250 ng in all samples and then reverse transcribed, in a 10 μL reaction volume, using RevertAid H minus Reverse Transcriptase enzyme (M-Mulv RT, Thermo Fisher Scientific, Inc.) and random primers (Bioron, Römerberg, Germany) as priming strategy. The synthesis was performed following the manufacturer's instructions. A control lacking the reverse transcriptase enzyme (no-RT control) was prepared to later determine the level of genomic DNA contamination.

qPCR

The primers used for qPCR were designed with the support of Primer3 software (Untergasser et al., 2012) and using *S. epidermidis* RP62A (for *16S* rRNA primers) or 1457 complete genome as a template (NCBI accession no. CP000029.1 and CP020463.1, respectively) (**Supplementary Table 1**). qPCR analysis was prepared in a 10 μL reaction containing 2 μL of diluted cDNA or no-RT control (1:400), 5 μL of Xpert Fast SYBR Mastermix (GRiSP, Lda., Porto, Portugal), 0.5 μL of each forward and reverse primers (0.5 μM per reaction), and 2 μL of water. qPCR run was performed in a CFX96 (Bio-Rad, CA, USA), with the following cycle parameters: 95°C for 2 min, and 40 cycles of 95°C for 5 s, 60°C for 30 s. A no-template control was included to assess reagent contamination and a melting curve analysis was performed to ensure the absence of unspecific products and primer dimers. Reaction efficiency was assessed at 60°C by performing 10-fold dilution series of the cDNA samples and determined from the slope of a standard curve. The expression of the genes tested was normalised to the expression of the reference genes *16S rRNA* and *gyrB* using a variation of the LivaK method, according to Eq. (1), where E stands for the reaction efficiency. To simplify the analysis between strains and conditions, the results are represented as the ratio of $TSB_{1\%+Mg}/TSB_{1\%G}$ (Fold-change IND/PRE).

$$E^{\Delta Ct} = E^{Ct_{geometric\ mean\ of\ 16S\ rRNA/gyrB} - Ct_{target\ gene}} \quad \text{Eq. (1)}$$

Statistical Analysis

Statistical differences between conditions were determined using either unpaired T-test with Welch's correction or One-way ANOVA with Tukey's multiple comparisons test, using

GraphPad Prism version 7 (Trial version, CA, USA). A *p*-value less than 0.05 was considered significant. At least three independent experiments were performed for each assay presented.

RESULTS

Validation of VBNC State Induction Model in *S. epidermidis* 1457 Biofilms

To assess if the previously described VBNC induction model could be used in strain 1457, we first compared the total amount of cells (assessed by optical density), the number of living cells (assessed by flow cytometry) and the number of culturable cells (assessed by CFU quantification). For biofilms with an equivalent amount of total and live cells, the induction of the VBNC state resulted in a significantly lower number of cultivable cells, confirming that the formation of VBNC cells in stain 1457 can be induced (**Figure 1**). Additionally, no differences were found regarding the pH of the media (data not shown), confirming that VBNC state prevention with $MgCl_2$ did not affect the pH of the culture, as previously shown (Cerca et al., 2011a).

To better correlate our data with previously published results, we compared the level of VBNC cells in strain 1457 with the reference strains COM040A and PT11004, whose significant ability to enter into a VBNC state was formerly confirmed (Carvalhais et al., 2018). As we showed above that flow

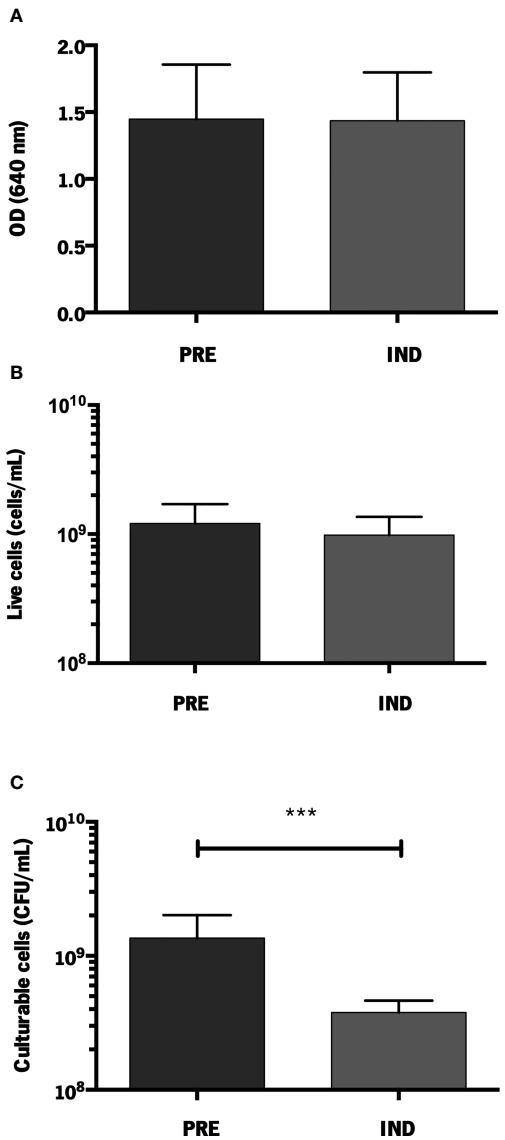

FIGURE 1 | Quantification of *S. epidermidis* 1457 biofilms formed under VBNC conditions. **(A)** Total amount of cells ($OD_{640\ nm}$); **(B)** Live cells (cells/mL) and **(C)** Culturable cells (CFU/mL). The results are displayed as the mean + standard deviation of at least six independent experiments. ***$p < 0.001$ (One-way ANOVA). PRE, prevented; IND, induced.

cytometry and OD measurements yielded similar results, VBNC quantification was further analysed by comparing the total amount of cells (OD) and total culturable cells (CFU). Although the 70% decrease in culturability in strain 1457 was lower than the one found in the reference isolates (≈ 90%) (**Supplementary Figure 2**), it is still within the range previously considered relevant in the context of VBNC state induction (Carvalhais et al., 2018).

Validation of RNA-Seq Results by qPCR

Aiming to determine possible candidates for future mutagenesis studies, the expression of the genes highlighted in a former RNA-Seq analysis of *S. epidermidis* 9142 biofilms under inducing VBNC conditions was validated by qPCR (**Figure 2**). The first step was to compare the results obtained by RNA-Seq and qPCR for biofilms of strain 9142. Although a higher fold-change was observed in qPCR results, the ratios were not significantly different from the ones obtained by RNA-Seq, confirming the results previously obtained (*codY*, 1.5 ± 0.4; *mazE*, not applicable; *mazF*, 1.0 ± 0.6 and *pdhA*, 1.7 ± 0.2) (Carvalhais et al., 2014). Secondly, we assessed the expression of the selected genes in biofilms of the reference isolates, as well as in strain 1457. Not surprisingly, strain-to-strain variability was observed. Nevertheless, qPCR data confirmed that all tested genes were upregulated under VBNC inducing conditions in the reference isolates. Interestingly, although in strain 1457 the expression of the genes *codY* and *pdhA* was significantly increased in the induced VBNC state, the expression of the *mazEF* complex was not significantly affected.

Applicability of the VBNC State Induction Model in Planktonic Populations

After validating the applicability of the VBNC state induction model in biofilms formed by strain 1457, we became interested in determining if this experimental model was also applicable to planktonic cultures, something yet undetermined. As observed in biofilms, a significant decrease in the number of culturable cells was

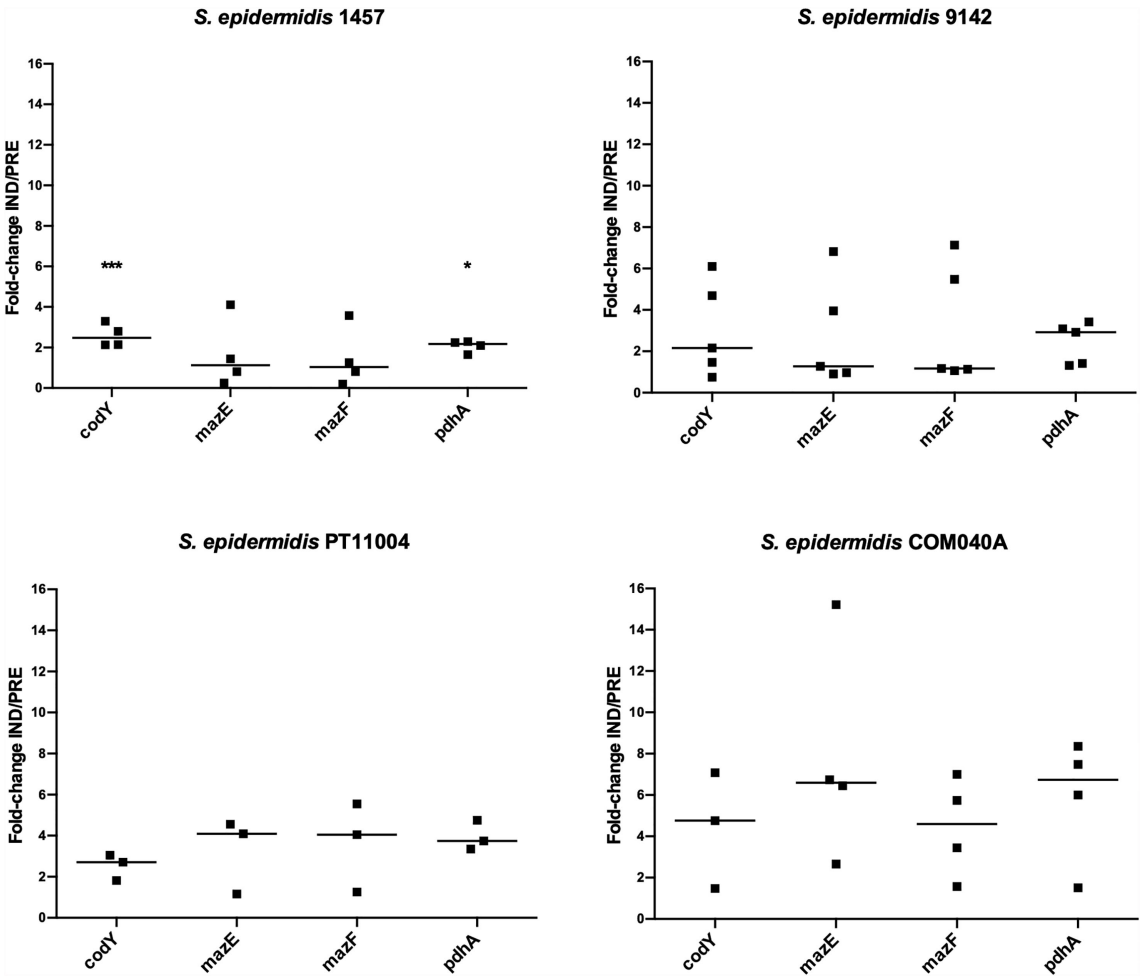

FIGURE 2 | Expression of the genes of interest in 48 h-old biofilms populations of *S. epidermidis* 1457 grown under induced (IND) and prevented (PRE) VBNC conditions. Data is presented as the fold-change between the IND and the PRE VBNC conditions (IND/PRE). Data is represented as the fold-change of the individual assays, where the horizontal lines represent the median of at least three independent experiments. $^{*}p < 0.05$, $^{***}p < 0.001$ (Unpaired Welch's T-test).

also found under VBNC inducing conditions for all isolates tested, whereas the total amount of planktonic cells was identical in both induced and prevented conditions (≈100%) (**Figure 3A**). Interestingly, for strain 1457, the induction of VBNC cells in planktonic cultures reached 48%, while in biofilms it reached 70%. However, these results are not directly comparable since growth conditions and incubation time differed: while VBNC cells induction in biofilms cultures was initiated in a pre-established 24 h-old biofilm, in planktonic cultures the VBNC state was induced from the start of the incubation period. Thus, to better mimic the biofilm experimental setup, another experiment was conducted, where planktonic cultures were first allowed to grow for 24 h, followed by another 24 h of growth in TSB with 1% glucose or 1% glucose plus 20 mM $MgCl_2$. Notably, with longer incubation periods the proportion of VBNC cells in planktonic cultures (**Figure 3B**) reached similar levels to what was previously observed in biofilms (**Supplementary Figure 2**).

Subsequently, we aimed to understand if the genes previously identified as potentially involved in the regulation of VBNC cells formation in biofilms could also play a role in planktonic cells. As can be seen in **Figure 4**, all genes were upregulated under the VBNC inducing conditions, with *codY* and *pdhA* reaching statistical significance. Interestingly, when comparing the fold-change IND/PREV between planktonic and biofilm cells (**Figures 2**, **4**), the fold-change IND/PRE of the *codY* and *pdhA* was higher in planktonic cells. Although the expression of both *mazE* and *mazF* genes seemed to be more pronounced when the VBNC state was induced in planktonic cultures, this difference was not statistically significant.

DISCUSSION

The induction of VBNC cells in *S. epidermidis* biofilms was previously reported in a wide range of clinical and commensal isolates, however, it was also found that not all strains formed VBNC cells under our *in vitro* VBNC state induction model (Cerca et al., 2011a; Carvalhais et al., 2018). Until now, the ability of *S. epidermidis* 1457, a strain widely used in genetic manipulation studies, to form VBNC cells using the previously developed model was unknown. Our results showed that the supplementation of the culture medium with 1% glucose induced a reduction in 1457 biofilm cells culturability of about 70% when compared to biofilms grown in media supplemented with 1% glucose plus 20 mM $MgCl_2$.

Earlier, it was shown that the induction of VBNC cells in *S. epidermidis* biofilms led to modifications in cells transcriptomic and proteomic profiles. Carvalhais et al. reported, using an RNA-Seq approach, the upregulation of the genes *codY*, *mazE*, *mazF* and *pdhA* in *S. epidermidis* 9142 biofilms with higher proportions of VBNC cells, which indicated a potential involvement of these genes in the emergence of the VBNC state (Carvalhais et al., 2014). Even though RNA-Seq is a powerful technique to assess gene transcription, it is important to validate the results through an alternative method, being qPCR still considered the gold standard for gene expression quantification assays. Therefore, using qPCR, we first validated, in biofilm cultures, the RNA-Seq data previously obtained with strain 9142, and then assessed the expression of the genes of interest in strain 1457, as well as in the reference strains PT11004 and COM040A. Interestingly, using qPCR we were able to detect the expression of the gene *mazE* in both induced and prevented VBNC conditions, while in RNA-Seq analysis *mazE* was only detected in one of the conditions (Carvalhais et al., 2014). Additionally, *mazE* and *mazF* expression in strains 9142 and PT11004 was notably upregulated when the VBNC state was induced, but not in the target strain 1457, suggesting that *mazEF* might not have a key impact on VBNC state induction in this strain. On the contrary, *codY* and *pdhA* expression was noticeably upregulated in all strains tested, including 1457, which supports the hypothesis that these genes may be involved in the induction of VBNC cells. Unlike PdhA, the

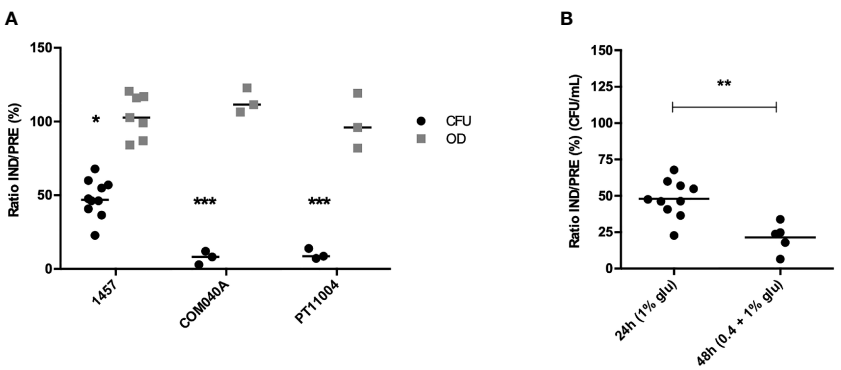

FIGURE 3 | Culturability (CFU/mL) and total amount of cells (OD_{640nm}) of **(A)** *S. epidermidis* 1457, COM040A and PT11004 24 h-old planktonic suspensions grown under induced (IND) and prevented (PRE) VBNC conditions. Data is represented as the ratio (%) of the culturability (CFU) or OD between cells in the IND or PRE VBNC state; and **(B)** *S. epidermidis* 1457 planktonic cells grown under IND and PRE VBNC conditions using two different growth strategies: (i) planktonic cells grown for 24 h in 1% glucose and (ii) planktonic cells grown for 24 h in 0.4% glucose + 24 h in 1% glucose; in both strategies 20 mM of $MgCl_2$ was added in the prevented condition. Data is represented as the result of the individual assays, where the horizontal lines represent the mean of at least three independent experiments. *$p < 0.05$, **$p < 0.01$, ***$p < 0.001$ (Unpaired Welch's T-test). Glu, glucose.

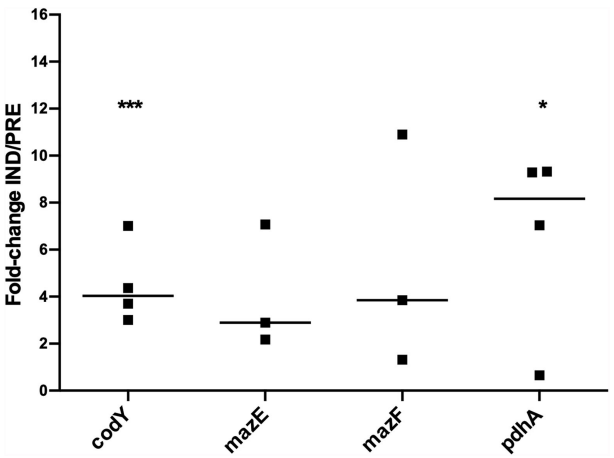

FIGURE 4 | Expression of the genes of interest in 48 h-old planktonic populations of *S. epidermidis* 1457 grown under induced and prevented VBNC conditions. Data is presented as the fold-change between the induced (IND) and the prevented (PRE) VBNC conditions (IND/PRE). Data is represented as the fold-change of the individual assays, where the horizontal lines represent the median of at least three independent experiments. $^{*}p < 0.05$, $^{***}p < 0.001$ (Unpaired Welch's T-test).

function of CodY has already been characterized in other strains. CodY is a repressor of hundreds of genes implicated in the transition from the exponential to the stationary growth phase, i.e., when nutrients become limited (Joseph et al., 2005; Barbieri et al., 2015). Additionally, it seems to regulate the *agr* quorum-sensing system, as well as genes associated with biofilm formation in *Staphylococcus aureus* (Majerczyk et al., 2008).

Although the onset of VBNC cells is commonly associated with the biofilm phenotype, non-culturable cells have also been reported in planktonic populations of several species, such as *S. aureus* and *Escherichia coli* (Xu et al., 2018). However, to our knowledge, no reports of VBNC cells in planktonic populations were found for *S. epidermidis.* As such, we aimed to understand if our VBNC state induction model could be applied to planktonic populations. As observed in biofilms, the decrease of culturability was more pronounced in the reference isolates, however, a significant proportion of VBNC cells was also obtained in planktonic populations of *S. epidermidis* 1457. Though, VBNC induction was significantly higher when planktonic populations were grown under biofilm-mimicking conditions (48 h of total growth), showing that the experimental setup with 24 h-old planktonic populations was not the most appropriate for the comparison with biofilms. Based on these results, we hypothesized that the lower proportion of VBNC cells in 24 h planktonic cultures may be, in part, related to the lower starting cell density, as in 24 h-old planktonic cultures the induction of the VBNC state started with $\approx 10^7$ CFU/mL, whereas in 48 h-old planktonic started with $\approx 10^9$ CFU/mL. The higher amount of VBNC cells attained in 48 h-old planktonic cultures raised our interest in understanding if the genes identified as playing a role in the emergence of VBNC cells in biofilms could also be involved in planktonic cultures. The analysis of gene expression showed that *codY* and *pdhA* were also upregulated in planktonic cultures under VBNC state inducing conditions. Although the exact function of *codY* and *pdhA* in the emergence of VBNC cells is still unknown, *codY* is responsible for the repression of genes when the cell is under unfavourable conditions, such as nutritional depletion and environmental stresses (Barbieri et al., 2015; Waters et al., 2016). This seems to be related to its upregulation when the VBNC condition is induced since the entrance of bacteria into a non-culturable state creates stress that leads to physiological and metabolic changes. On the other hand, although the role of *pdhA* has not yet been studied in *Staphylococcus* spp., the product of this gene – pyruvate dehydrogenase, has been related to the regulation of metabolism and perturbations on the cell membrane (Zhang et al., 2014; Singh et al., 2018).

Taken together, our data provide evidence that VBNC cells in *S. epidermidis* strain 1457 can be generated *in vitro*, both in biofilm and planktonic cultures. Additionally, this study reinforced the potential involvement of the genes *codY* and *pdhA* in VBNC cells formation in biofilm and revealed, for the first time, the potential involvement of these genes in VBNC cells formation in planktonic cultures. The role of both genes is now being assessed in our laboratory with knockout strains of *S. epidermidis* 1457.

DATA AVAILABILITY STATEMENT

The original contributions presented in the study are included in the article/**Supplementary Files**, further inquiries can be directed to the corresponding author/s.

AUTHOR CONTRIBUTIONS

Conceptualization, NC and AF. Investigation, VG and NL. Writing original draft, VG and NL. Writing—review and editing, NC and AF. Supervision, NC and AF. All authors contributed to the article and approved the submitted version.

FUNDING

This work was supported by the Portuguese Foundation for Science and Technology (FCT) by the funded project PTDC/BIA-MOL/29553/2017, under the scope of COMPETE2020 (POCI-01-0145-FEDER-029553) and by the strategic funding of unit UIDB/04469/2020. VG and NL acknowledge the support of FCT individual fellowships [SFRH/BD/131452/2017 and SFRH/BD/136998/2018], respectively.

SUPPLEMENTARY MATERIAL

The Supplementary Material for this article can be found online at: https://www.frontiersin.org/articles/10.3389/fcimb.2021.771666/full#supplementary-material

REFERENCES

Barbieri, G., Voigt, B., Albrecht, D., Hecker, M., Albertini, A. M., Sonenshein, A. L., et al. (2015). CodY Regulates Expression of the Bacillus Subtilis Extracellular Proteases Vpr and Mpr. *J. Bacteriol.* 197, 1423–1432. doi: 10.1128/JB.02588-14

Carvalhais, V., França, A., Cerca, F., Vitorino, R., Pier, G. B., Vilanova, M., et al. (2014). Dormancy Within Staphylococcus Epidermidis Biofilms: A Transcriptomic Analysis by RNA-Seq. *Appl. Microbiol. Biotechnol.* 98, 2585–2596. doi: 10.1007/s00253-014-5548-3

Carvalhais, V., Pérez-Cabezas, B., Oliveira, C., Vitorino, R., Vilanova, M., and Cerca, N. (2018). Tetracycline and Rifampicin Induced a Viable But Nonculturable State in Staphylococcus Epidermidis Biofilms. *Future Microbiol.* 13, 27–36. doi: 10.2217/fmb-2017-0107

Cerca, F., Andrade, F., França, A., Andrade, E. B., Ribeiro, A., Almeida, A. A., et al. (2011a). *Staphylococcus Epidermidis* Biofilms With Higher Proportions of Dormant Bacteria Induce a Lower Activation of Murine Macrophages. *J. Med. Microbiol.* 60, 1717–1724. doi: 10.1099/jmm.0.031922-0

Cerca, F., França, A., Perez-Cabezas, B., Carvalhais, V., Ribeiro, A., Azeredo, J., et al. (2014). Dormant Bacteria Within Staphylococcus Epidermidis Biofilms Have Low Inflammatory Properties and Maintain Tolerance to Vancomycin and Penicillin After Entering Planktonic Growth. *J. Med. Microbiol.* 63, 1274–1283. doi: 10.1099/jmm.0.073163-0

Cerca, F., Trigo, G., Correia, A., Cerca, N., Azeredo, J., and Vilanova, M. (2011b). SYBR Green as a Fluorescent Probe to Evaluate the Biofilm Physiological State of Staphylococcus Epidermidis, Using Flow Cytometry. *Can. J. Microbiol.* 57, 850–856. doi: 10.1139/W11-078

França, A., Freitas, A. I., Henriques, A. F., and Cerca, N. (2012). Optimizing a qPCR Gene Expression Quantification Assay for S. Epidermidis Biofilms: A Comparison Between Commercial Kits and a Customized Protocol. *PloS One* 7, e37480. doi: 10.1371/journal.pone.0037480

Freitas, A. I., Vasconcelos, C., Vilanova, M., and Cerca, N. (2014). Optimization of an Automatic Counting System for the Quantification of Staphylococcus Epidermidis Cells in Biofilms. *J. Basic Microbiol.* 54, 750–757. doi: 10.1002/jobm.201200603

Galac, M. R., Stam, J., Maybank, R., Hinkle, M., Mack, D., Rohde, H., et al. (2017). Complete Genome Sequence of Staphylococcus Epidermidis 1457. *Genome Announc*, 5, e00450–17. doi: 10.1128/genomeA.00450-17

Joseph, P., Ratnayake-Lecamwasam, M., and Sonenshein, A. L. (2005). A Region of *Bacillus Subtilis* CodY Protein Required for Interaction With DNA. *J. Bacteriol.* 187, 4127–4139. doi: 10.1128/JB.187.12.4127-4139.2005

Keren, I., Minami, S., Rubin, E., and Lewis, K. (2011). Characterization and Transcriptome Analysis of Mycobacterium Tuberculosis Persisters. *MBio* 2, 3–12. doi: 10.1128/mBio.00100-11

Li, Y., Huang, T. Y., Mao, Y., Chen, Y., Shi, F., Peng, R., et al. (2020). Study on the Viable But non-Culturable (VBNC) State Formation of *Staphylococcus Aureus* and its Control in Food System. *Front. Microbiol.* 11, 599739. doi: 10.3389/fmicb.2020.599739

Lleo, M. M., Pierobon, S., Tafi, M. C., Signoretto, C., and Canepari, P. (2000). mRNA Detection by Reverse Transcription-PCR for Monitoring Viability Over Time in an Enterococcus Faecalis Viable But Nonculturable Population Maintained in a Laboratory Microcosm. *Appl. Environ. Microbiol.* 66, 4564–4567. doi: 10.1128/AEM.66.10.4564-4567.2000

Mack, D., Bartscht, K., Fischer, C., Rohde, H., Grahl, C., Dobinsky, S., et al. (2001). Genetic and Biochemical Analysis of Staphylococcus Epidermidis Biofilm Accumulation. *Methods Enzymol.* 336, 215–239. doi: 10.1016/S0076-6879(01)36592-8

Mack, D., Davies, A. P., Harris, L. G., Jeeves, R., Pascoe, B., Knobloch, J. K., et al. (2013). "Staphylococcus Epidermidis in Biomaterial-Associated Infections," in *Biomaterials Associated Infection: Immunological Aspects and Antimicrobial Strategies*. Eds. F. Moriarty, S. A. J. Zaat and H. J. Busscher (New York: Springer-Verlag), 25–56. doi: 10.1007/978-1-4614-1031-7

Mack, D., Siemssen, N., and Laufs, R. (1992). Parallel Induction by Glucose of Adherence and a Polysaccharide Antigen Specific for Plastic-Adherent Staphylococcus Epidermidis: Evidence for Functional Relation to Intercellular Adhesion. *Infect. Immun.* 60, 2048–2057. doi: 10.1128/iai.60.5.2048-2057.1992

Majerczyk, C. D., Sadykov, M. R., Luong, T. T., Lee, C., Somerville, G. A., and Sonenshein, A. L. (2008). *Staphylococcus Aureus* CodY Negatively Regulates Virulence Gene Expression. *J. Bacteriol.* 190, 2257–2265. doi: 10.1128/JB.01545-07

Otto, M. (2009). *Staphylococcus Epidermidis* – The "Accidental" Pathogen. *Nat. Rev. Microbiol.* 7, 555–567. doi: 10.1038/nrmicro2182.Staphylococcus

Postnikova, O. A., Shao, J., Mock, N. M., Baker, C. J., and Nemchinov, L. G. (2015). Gene Expression Profiling in Viable But Nonculturable (VBNC) Cells of *Pseudomonas Syringae* Pv. *Syringae*. *Front. Microbiol.* 6, 1419. doi: 10.3389/fmicb.2015.01419

Rani, S. A., Pitts, B., Beyenal, H., Veluchamy, R. A., Lewandowski, Z., Davison, W. M., et al. (2007). Spatial Patterns of DNA Replication, Protein Synthesis, and Oxygen Concentration Within Bacterial Biofilms Reveal Diverse Physiological States. *J. Bacteriol.* 189, 4223–4233. doi: 10.1128/JB.00107-07

Singh, V. K., Sirobhushanam, S., Ring, R. P., Singh, S., Gatto, C., and Wilkinson, B. J. (2018). Roles of Pyruvate Dehydrogenase and Branched-Chain a-Keto Acid Dehydrogenase in Branched-Chain Membrane Fatty Acid Levels and Associated Functions in *Staphylococcus Aureus*. *J. Med. Microbiol.* 67, 570–578. doi: 10.1099/jmm.0.000707

Sousa, C., França, A., and Cerca, N. (2014). Assessing and Reducing Sources of Gene Expression Variability in Staphylococcus Epidermidis Biofilms. *Biotechniques* 57, 295–301. doi: 10.2144/000114238

Untergasser, A., Cutcutache, I., Koressaar, T., Ye, J., Faircloth, B. C., Remm, M., et al. (2012). Primer3 - New Capabilities and Interfaces. *Nucleic Acids Res* 40, e115. doi: 10.1093/nar/gks596

Waters, N. R., Samuels, D. J., Behera, R. K., Livny, J., Rhee, K. Y., Sadykov, M. R., et al. (2016). A Spectrum of CodY Activities Drives Metabolic Reorganization and Virulence Gene Expression in Staphylococcus Aureus. *Mol. Microbiol.* 101, 495–514. doi: 10.1111/mmi.13404

Winstel, V., Kühner, P., Krismer, B., Peschel, A., and Rohde, H. (2015). Transfer of Plasmid DNA to Clinical Coagulase-Negative Staphylococcal Pathogens by Using a Unique Bacteriophage. *Appl. Environ. Microbiol.* 81, 2481–2488. doi: 10.1128/AEM.04190-14

Winstel, V., Kühner, P., Rohde, H., and Peschel, A. (2016). Genetic Engineering of Untransformable Coagulase-Negative Staphylococcal Pathogens. *Nat. Protoc.* 11, 949–959. doi: 10.1038/nprot.2016.058

Xu, Z., Cheng, C., Shen, J., Lan, Y., Hu, S., Han, W., et al. (2018). *In Vitro* Antimicrobial Effects and Mechanisms of Direct Current Air-Liquid Discharge Plasma on Planktonic *Staphylococcus Aureus* and *Escherichia Coli* in Liquids. *Bioelectrochemistry* 121, 125–134. doi: 10.1016/j.bioelechem.2018.01.012

Zandri, G., Pasquaroli, S., Vignaroli, C., Talevi, S., Manso, E., Donelli, G., et al. (2012). Detection of Viable But non-Culturable Staphylococci in Biofilms From Central Venous Catheters Negative on Standard Microbiological Assays. *Clin. Microbiol. Infect.* 18, E259–E261. doi: 10.1111/j.1469-0691.2012.03893.x

Zhang, S., Guo, L., Yang, K., Zhang, Y., Ye, C., Chen, S., et al. (2018). Induction of Escherichia Coli Into a VBNC State by Continuous-Flow UVC and Subsequent Changes in Metabolic Activity at the Single-Cell Level. *Front. Microbiol.* 9, 2243. doi: 10.3389/fmicb.2018.02243

Zhang, S., Hulver, M. W., McMillan, R. P., Cline, M. A., and Gilbert, E. R. (2014). The Pivotal Role of Pyruvate Dehydrogenase Kinases in Metabolic Flexibility. *Nutr. Metab.* 11, 10. doi: 10.1186/1743-7075-11-10

Conflict of Interest: The authors declare that the research was conducted in the absence of any commercial or financial relationships that could be construed as a potential conflict of interest.

frontiers in Cellular and Infection Microbiology

BRIEF RESEARCH REPORT
published: 13 January 2022
doi: 10.3389/fcimb.2021.803134

mazEF Homologue Has a Minor Role in *Staphylococcus epidermidis* 1457 Virulence Potential

Vânia Gaio[1], *Tânia Lima*[2,3], *Manuel Vilanova*[2,3,4], *Nuno Cerca*[1] *and Angela França*[1]*

[1] Laboratory of Research in Biofilms Rosário Oliveira, Centre of Biological Engineering, University of Minho, Braga, Portugal, [2] Instituto de Investigação e Inovação em Saúde, Universidade do Porto, Porto, Portugal, [3] Instituto de Biologia Molecular e Celular, Universidade do Porto, Porto, Portugal, [4] Instituto de Ciências Biomédicas de Abel Salazar, Universidade do Porto, Porto, Portugal

Staphylococcus epidermidis biofilm cells are characterized by increased antimicrobial tolerance and improved ability to evade host immune system defenses. These features are, in part, due to the presence of viable but non-culturable (VBNC) cells. A previous study identified genes potentially involved in VBNC cells formation in *S. epidermidis* biofilms, among which *SERP1682/1681* raised special interest due to their putative role as a toxin–antitoxin system of the *mazEF* family. Herein, we constructed an *S. epidermidis* mutant lacking the *mazEF* genes homologues and determined their role in (i) VBNC state induction during biofilm formation, (ii) antimicrobial susceptibility, (iii) survival in human blood and plasma, and (iv) activation of immune cells. Our results revealed that *mazEF* homologue did not affect the proportion of VBNC cells in *S. epidermidis* 1457, refuting the previous hypothesis that *mazEF* homologue could be linked with the emergence of VBNC cells in *S. epidermidis* biofilms. Additionally, *mazEF* homologue did not seem to influence key virulence factors on this strain, since its deletion did not significantly affect the mutant biofilm formation capacity, antimicrobial tolerance or the response by immune cells. Surprisingly, our data suggest that *mazEF* does not behave as a toxin–antitoxin system in *S. epidermidis* strain 1457, since no decrease in the viability and culturability of bacteria was found when only the *mazF* toxin homologue was being expressed.

Keywords: *SERP1681*, *SERP1682*, antimicrobial tolerance, biofilms, human blood, human plasma, macrophages, dendritic cells

OPEN ACCESS

Edited by:
Lauren O Bakaletz, Nationwide Children's Hospital, United States

Reviewed by:
Fernanda Buzzola, CONICET Research Institute in Microbiology and Medical Parasitology (IMPaM), Argentina
Ferdinand Xiankeng Choong, Karolinska Institutet (KI), Sweden
Timothy J. Foster, Trinity College Dublin, Ireland

***Correspondence:**
Angela França
afranca@ceb.uminho.pt

Specialty section:
This article was submitted to Biofilms, a section of the journal Frontiers in Cellular and Infection Microbiology

Received: *27 October 2021*
Accepted: *06 December 2021*
Published: *13 January 2022*

Citation:
Gaio V, Lima T, Vilanova M, Cerca N and França A (2022) mazEF Homologue Has a Minor Role in Staphylococcus epidermidis 1457 Virulence Potential. Front. Cell. Infect. Microbiol. 11:803134. doi: 10.3389/fcimb.2021.803134

INTRODUCTION

Staphylococcus epidermidis, a commensal bacterium that is a common inhabitant of the skin and mucous membranes of humans and several mammals, is recognized by its ability to form thick and multi-layered biofilms, especially on the surface of indwelling medical devices (Fey and Olson, 2011). Although *S. epidermidis* generally presents a benign relationship with the host, this species has been considered an opportunistic pathogen particularly affecting preterm neonates and immunocompromised patients and is now considered one of the main causes of medical device-associated infections (Otto, 2009).

Previous *in vitro* studies have shown that *S. epidermidis* biofilms present an increased tolerance to antibiotics (Cerca et al., 2005; Anderson and O'Toole, 2008) and to the host immune response (Brescó et al., 2017; Nguyen et al., 2017), which may hinder the treatment of biofilm-associated infections. Moreover, *S. epidermidis* cells can enter a state of dormancy, either becoming persisters (Shapiro et al., 2011) or viable but non-culturable (VBNC) (Zandri et al., 2012). The presence of high amounts of VBNC cells can hamper the routine detection or interpretation of the actual status of the infection (Zandri et al., 2012). Furthermore, VBNC cells within *S. epidermidis* biofilms account for a greater ability to evade the host innate immune system (Cerca et al., 2011a) and decreased susceptibility to antibiotics (Cerca et al., 2014).

Following an *in vitro* model that induces VBNC cells in *S. epidermidis* biofilms (Cerca et al., 2011a), the transcriptome of biofilms with higher amounts of VBNC cells was characterized. Among the genes of interest identified, *SERP1682*, a *mazE* homologue, raised special interest since it was uniquely detected when the VBNC state was induced (Carvalhais et al., 2014). Importantly, the *mazEF* gene family has been described as a toxin–antitoxin (TA) system and is composed of genes that encode a stable toxin (*mazF*) and a labile antitoxin (*mazE*) (Van Melderen, 2010), which are involved in the regulation of essential cell processes (Karimi et al., 2015). These genes were first described as a TA system in *E. coli* (Metzger et al., 1988). Nevertheless, the function of this module as a TA system has been experimentally confirmed in other species such as *Streptococcus mutans* (Syed et al., 2011), *S. aureus* (Zhu et al., 2009), and *S. equorum* (Schuster et al., 2013). Furthermore, several homology studies indicate the presence of the putative *mazEF* TA complex in other species, such as *Pseudomonas aeruginosa* (Valadbeigi et al., 2017), *Mycobacterium tuberculosis* (Tiwari et al., 2015), and *S. epidermidis* (Behrooz et al., 2018). However, so far, the role of *mazEF* homologue in *S. epidermidis* virulence has not been determined. As such, herein, we constructed and characterized a *mazEF* homologue mutant strain.

MATERIAL AND METHODS

Strains and Growth Media

S. epidermidis 1457 (Mack et al., 1992) was used in this study. The wild type (WT) and constructs were grown overnight in Tryptic Soy Broth (TSB, Merck) at 37°C and with agitation at 120 rpm. In the case of strains harboring the plasmids pRB473 or pRMC2, TSB supplemented with 10 μg/ml chloramphenicol was used (TSB_{CM10}). For further experiments, the overnight cultures were diluted in TSB or TSB_{CM10} to an optical density (OD) of 0.250 ± 0.05 at 640 nm, corresponding to approximately 2×10^8 colony-forming units/ml (CFU/ml) (Freitas et al., 2014).

Mutant Construction

Genetic manipulations were based on previous protocols (Brückner, 1997; Monk et al., 2012). Briefly, the flanking regions of the *mazEF* homologue operon were amplified and linked together by an overlap PCR. The resulting fragment was ligated into the plasmid pIMAY and transformed into *E. coli* DC10B, where the correct sequence and orientation of the flanking regions were confirmed by sequencing. The knockout plasmid was then transformed into the WT strain by electroporation (Monk et al., 2012; Cui et al., 2015). The allelic replacement protocol was performed as described in Monk et al. (2012) and the confirmation of the deletion of the *mazEF* homologue operon was done by PCR. Then, the *ΔmazEF* mutant was transformed with two distinct plasmids: the pRB473 (Bruckner et al., 1993) and the pRMC2 inducible plasmid (Corrigan and Foster, 2009). In brief, the homologous sequences of the genes *mazE*, *mazF* or the operon *mazEF* were amplified and cloned into pRB473 (sequences cloned included the target genes and their natural promoter region) or pRMC2 (sequences cloned included a strong ribosomal binding site and start and stop codons). While the plasmid pRB473 was first transformed into *E. coli* DC10B, the inducible plasmid pRMC2 was first transformed into *S. aureus* RN4220. Finally, the expression plasmids were inserted into *ΔmazEF* mutant strain by electroporation. The successful restoration of *mazE*/*mazF*/*mazEF* homologues expression was performed by qPCR, as described below. The primers used herein were designed using Primer3 software (Untergasser et al., 2012) and are listed in **Supplementary Table 1**.

Induction of *mazEF* Expression

The optimal conditions to induce the pRMC2 plasmid were first assessed by evaluating the effect of different concentrations of anhydrotetracycline (ATC, 0.64 and 1.28 μg/ml) or tetracycline (TET, 0.08 and 0.16 μg/ml), both purchased from Sigma-Aldrich, in the culturability of *ΔmazEF* cells. Thereafter, the induction of the expression of the genes cloned into the inducible plasmid (*mazE, mazF* or *mazEF* homologues) was started by adjusting the overnight cultures of each construct to an OD_{640nm} = 0.5, followed by a 1:10 dilution in 10 ml of TSB_{CM10} and incubation for 3 h at 37°C and 120 rpm. Then, 0.64 μg/ml of ATC was added, and the tubes were incubated under the same temperature and agitation conditions for up to 24 h. A tube without ATC was used as a control. Aliquots were collected at the beginning of the induction (T = 0 h), after 30, 60, 90, 120, 180, and 240 min and at the end of the experiment (T = 24 h) to measure the OD and quantify the number of culturable cells.

Planktonic Growth and Biofilm Formation

A suspension with approximately 2×10^8 CFU/ml, prepared as described above, was used to start both planktonic cultures and biofilms. Planktonic cultures were started by inoculating 100 μl of this suspension into 10 ml of TSB/TSB_{CM10} and further incubated at 37°C and 120 rpm, for up to 24 h. Biofilms were formed as described before in either 24-well plates (for VBNC state assessment, confocal analysis and gene expression studies) (Cerca et al., 2011a; Carvalhais et al., 2014) or 96-well plates (for antimicrobial assays) (Oliveira et al., 2015). Of note, for confocal analysis, biofilms were formed on Nunc™ thermanox™ coverslips (Thermo Fisher Scientific) that were placed inside

the wells. After 48 h of growth, biofilms were washed twice and either stained (for confocal analysis) or scraped from the plate bottom, in 0.9% NaCl, and submitted to a pulse of sonication of 10 s at 33% amplitude (Cole-Parmer), to dissociate cells clusters but without interfering with cell viability (Freitas et al., 2014). The amount of planktonic and biofilm cells was then quantified by OD_{640nm} and CFU counting. Moreover, for VBNC state-modulated biofilms, the total number of viable cells was also assessed by flow cytometry as previously optimized (Cerca et al., 2011b). The gating strategy is represented in **Supplementary Figure 1A**. Additionally, their structure was analyzed by confocal laser scanning microscopy (CLSM) using wheat germ agglutinin (WGA), which binds PNAG and allows the detection of the matrix, and DAPI, which stains nucleic acids and allows cells visualization (Cerca et al., 2006).

Gene Expression

To quantify the expression levels of the genes cloned into the plasmid pRMC2, planktonic cultures induced for 4 h with 0.64 μg/ml ATC were used. For the quantification of gene expression in 48 hour-old biofilms, biofilm cells were collected as described above and, then, pooled together to decrease variability (Sousa et al., 2014). One milliliter of both planktonic or biofilm cells pool was used for RNA isolation with the kit ExtractMe RNA Bacteria & Yeast (Blirt S.A.) and as optimized before for *S. epidermidis* (França et al., 2012). RNA was treated with DNase and RNA concentration and purity were assessed using NanoDrop One (Thermo Fisher Scientific). Subsequently, RNA was reverse transcribed using the RevertAid H minus M-Mulv RT enzyme (Thermo Fisher Scientific) and quantitative PCR (qPCR) reactions prepared using Xpert Fast SYBR Mastermix (GRiSP). Finally, samples were run in a CFX96 thermal cycler (Bio-Rad) with the following cycle parameters: 95°C for 2 min, and 40 cycles of 95°C for 5 s, 60°C for 30 s. No-template and no-reverse transcriptase controls were included to evaluate, respectively, reagents and RNA contamination with genomic DNA. The absence of unspecific products and primer dimers was assessed by analysis of melting curves. Primers were designed with Primer3 (Untergasser et al., 2012) using *S. epidermidis* 1457 genome as the template (**Supplementary Table 2**).

Antimicrobial Tolerance

The susceptibility to antibiotics was evaluated upon 6 and 24 h of incubation through CFU counting and by the reduction of tetrazolium salt XTT, which estimates cells metabolic activity, as described before (Cerca et al., 2005). Briefly, 2 ml of TSB supplemented with the peak serum concentrations (PSC) of vancomycin (40 μg/ml) (VWR), tetracycline (16 μg/ml), and rifampicin (10 μg/ml) (all purchased from Sigma-Aldrich) were inoculated with 1×10^7 CFU/ml of bacteria in the stationary phase (24-hour growth). In the case of biofilms, 200 μl of TSB supplemented with PSC of the antibiotics under study were added to 48 hour-old biofilms grown in 96-well plates. Both planktonic and biofilm populations were incubated at 37°C and 120 rpm for up to 24 h.

Survival in Human Blood and Plasma

Plasma was separated by centrifugation of whole blood for 20 min at 1,440*g* and 4°C. The co-incubation of bacteria with either whole blood, plasma or TSB supplemented with heparin (TSB + heparin, control) was performed as described before (França et al., 2016; Brás et al., 2020). Briefly, 50 μl of bacterial suspensions with 2×10^5 CFU/ml were mixed with 450 μl of whole blood, plasma or TSB + heparin and incubated at 37°C and 80 rpm for up to 4 h. Cells culturability was assessed at the beginning of the assay (T = 0 h) and 1, 2, and 4 h after incubation.

Dendritic Cells and Macrophages Differentiation

Peripheral blood mononuclear cells (PBMC) were isolated from buffy coats through density gradient centrifugation (1,200g for 15 min), using Histopaque 1077 (Sigma-Aldrich) in SepMate PBMC isolation tubes (Stemcell Technologies). $CD14^+$ cells were isolated using anti-human CD14 MicroBeads (Miltenyi Biotec), according to manufacturer's instructions and, then, suspended in complete RPMI medium—RPMI 1640 (Sigma-Aldrich) supplemented with 10% Fetal Bovine Serum (Biowest), 4 mM L-glutamine (Sigma-Aldrich), 10 mM HEPES (Sigma-Aldrich), and 50 μM β-mercaptoethanol (Merck) and seeded on 6-well culture plates at a concentration of 1×10^6 cells/ml. Granulocyte–macrophage colony-stimulating factor (GM-CSF) (50 ng/ml) and macrophage colony-stimulating factor (M-CSF) (50 ng/ml) were used to differentiate monocytes into M1- and M2-like macrophages, respectively. To differentiate monocytes into dendritic cells (DC), GM-CSF (50 ng/ml) and interleukin-4 (50 ng/ml) were used. All cell cultures were incubated at 37°C with 5% CO_2 for 7 days. Every 3 days, half of the cell culture medium was replaced with fresh complete RPMI with the respective growth factors.

Infection of DC and M1/M2 Macrophages

On day 7, non-adherent and loosely adherent DC were harvested by gentle up and down pipetting movements. M1/M2-like macrophages were detached with 5 mM EDTA. Afterwards, cells were seeded in 96-well plates and infected with each strain using a multiplicity of infection (MOI) of 1:5 or 1:10 (human cell: bacteria) and incubated at 37°C and 5% CO_2. After 2 h of incubation, 50 μg/ml gentamicin (AppliChem) was added to stop bacterial growth and the plates were again incubated at 37°C and 5% CO_2 for 24 h. After the incubation period, the plates were centrifuged (300*g*, 10 min), the supernatants collected and stored at −80°C for cytokines quantification. In the case of DC, after supernatant collection, the cells were stained for flow cytometry cell surface activation detection.

Quantification of Cytokine Production

Cytokine levels in cell culture supernatants were evaluated by sandwich ELISA using commercial kits, according to the manufacturer's instructions (TNF-α, IL-6, IL-8, IL-10, and IL-12p70 DuoSet® ELISA Development System—R&D Systems).

Evaluation of DC Activation

To assess the expression of cell surface activation markers, DC were collected 24 h after infection with *S. epidermidis* strains, washed and incubated with fixable viability dye (eFluor 780) and with cell-surface antibodies, anti-human CD11c-APC conjugated (clone BU15), anti-human HLA-PECy7 conjugated (clone L243), anti-human CD83-FITC conjugated (clone HB15e), anti-human CD14-PE-conjugated (clone 61D3), anti-human CD80-BV510 conjugated (clone 2D10), and anti-human CD86-PECy5 conjugated (clone IT2.2), all purchased from eBiosciences. Cells were fixed with paraformaldehyde and resuspended in FACS buffer. Samples were analyzed by flow cytometry, using BD FACSCanto™ II and data analysis was performed using FlowJo™ 10.7.1 Software (BD Life Sciences), using the gating strategy represented in **Supplementary Figure 1B**.

Ethics Statement

Human blood was collected in heparin-coated tubes (Vacuette), from adult healthy volunteers under a protocol approved by the Institutional Review Board of the University of Minho [SECVS 002/2014 (ADENDA)]. Buffy coats from healthy adult blood donors, used for M1/M2 macrophages and DC differentiation, were acquired at the Immunohemoterapy Department of Centro Hospitalar de São João (Porto, Portugal), under ethical approval of the service (Protocol reference 260/11). All procedures were performed in agreement with the Helsinki declaration and Oviedo convention and all donors gave written consent before blood collection.

Statistical Analysis

Statistical analysis was performed using either unpaired T-test with Welch's correction or One-way ANOVA with Tukey's multiple comparisons test, using GraphPad Prism version 7 (Trial version, CA, USA). *P*-values below 0.05 were considered significant.

RESULTS

mazEF Homologue Mutation and Complementation

The deletion of *mazEF* homologue in *S. epidermidis* strain 1457 was successfully achieved as confirmed by PCR and qPCR (**Supplementary Figure 2**), originating the mutant strain *ΔmazEF*. We then complemented the mutant with *mazEF* homologue sequence using the plasmid pRB473. The presence of the plasmid was confirmed by PCR (**Supplementary Figure 3A**) and the expression of the genes was confirmed by qPCR (**Supplementary Figure 2**). In addition, qPCR analysis confirmed that *mazEF* homologue deletion did not significantly interfere with *rsbU* regulation (Donegan and Cheung, 2009; Schuster et al., 2015) and that the plasmid pRB473 + *mazEF* restored *mazEF* homologue expression (**Supplementary Figure 2**). Moreover, the mutant strain was also complemented with *mazE*, *mazF* or *mazEF* homologous sequences using the inducible plasmid pRMC2 (**Supplementary Figure 3B**) required for the toxin–antitoxin experiments, further described below.

Role of *mazEF* Homologue in VBNC State Induction in *S. epidermidis* 1457

Based on the previous hypothesis that *mazEF* could be involved in VBNC state modulation in *S. epidermidis* biofilms, the proportions of VBNC cells in biofilms formed by the WT, *ΔmazEF*, and *ΔmazEF*::pRB473 strains were characterized using three techniques: OD, to evaluate the amount of total cells (**Figure 1A**), flow cytometry, to quantify total live cells (**Figure 1B**), and CFU counting, to determine the number of culturable cells (**Figure 1C**). No differences were observed in all strains tested, suggesting that *mazEF* did not have a significant role in VBNC state induction. We then assessed if there was any structural difference in the biofilms formed by these strains. However, as shown by the CLSM analysis (**Figure 1D**), no differences in biofilms structure were found.

Role of *mazEF* Homologue in *S. epidermidis* 1457 Virulence Potential

Although our data do not support that *mazEF* homologue has an important role in VBNC state modulation in biofilms, we further explored the role of this operon in *S. epidermidis* 1457 general virulence. For that, the mutant strain complemented with the target genes and their natural promoter (*ΔmazEF*::pRB473+*mazEF*) was used to try to mimic the level of transcription in the WT strain.

As shown in **Figure 2A**, all strains presented a similar growth rate in the planktonic mode of growth. When analyzing the expression of genes putatively linked with VBNC cells formation (*pdhA*, *codY*, and *clpP*) (Carvalhais et al., 2014), and also related to biofilm formation (*icaA*) (Heilmann et al., 1996a; Heilmann et al., 1996b), we observed that the mutant had approximately a 3-fold increase in the expression of the gene *codY*, although some variability was observed among assays and no statistical significance was reached (**Figure 2B**). Regarding antimicrobial tolerance of biofilms (**Figure 2C**), minor differences in cells culturability were detected between the mutant and WT, but none were statistically significant. Interestingly, when evaluating biofilm cells metabolism, we observed that tetracycline was significantly more effective against the WT strain (**Supplementary Figure 4**). Furthermore, the same assays were repeated for planktonic cultures but, again, no substantial differences were found among strains (**Supplementary Figure 5**). Finally, when analyzing the ability to survive in human blood and plasma, similar results were obtained among strains at either earlier (1 and 2 h) (**Supplementary Figure 6**) or later (4 h) time points (**Figure 2D**).

Despite the lack of compelling differences in the ability of the strains to survive in human blood and plasma, we also assessed if the *mazEF* homologue could have an impact on the response of macrophages and DC when challenged with *S. epidermidis*. As shown in **Figure 3**, similar results were detected in the production of pro- (IL-12, IL-6, IL-8, and TNF) or anti-inflammatory (IL-10) cytokines by M1- and M2-like macrophages or DC when stimulated with different multiplicities of infection (MOI 1:5, **Figure 3** or MOI 1:10, **Supplementary Figure 7**).

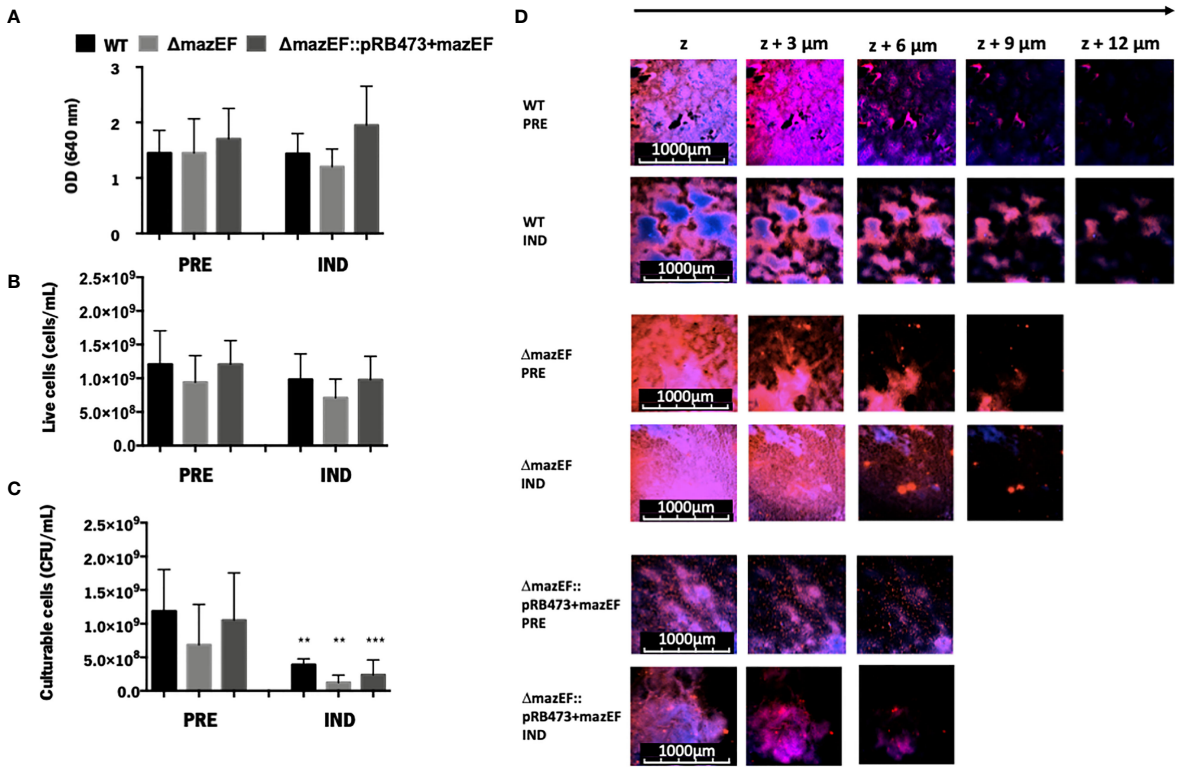

FIGURE 1 | The role of *mazEF* homologue on the regulation of the VBNC state in *S. epidermidis* 1457 48-hour old biofilms. Quantification of *S. epidermidis* biofilms grown under VBNC inducing conditions in terms of **(A)** Total amount of cells (OD); **(B)** Concentration of live cells (flow cytometry); and **(C)** Concentration of culturable cells (CFU/ml). Results are represented as the mean + standard deviation of at least 3 independent experiments. Statistical analysis was performed with One-way ANOVA with Tukey's multiple comparisons test, $^{**}p$ <0.01,$^{***}p$ <0.001. **(D)** Biofilm structure analysis assessed by CLSM. The images shown are representative of 2 independent experiments. PRE, Prevented VBNC; IND, Induced VBNC.

Role of *mazEF* Homologue as a Putative TA System

Since *mazEF* operon has been described, either experimentally or by homology, as a TA system in some staphylococcal species, we aimed to experimentally investigate if it has the same function in *S. epidermidis* 1457. After successful transformation of pRMC2 plasmids, the expression of the target genes was induced with either tetracycline (TET) or anhydrotetracycline (ATC), aiming to assess the best concentration to induce expression but without interfering with the culturability of *ΔmazEF* cells. While TET caused a slight reduction in the number of culturable cells compared to the control (no antibiotic), the ATC did not significantly affect cells culturability (**Figure 4A**). To ensure that *mazE/F/EF* homologues were being expressed under the selected inducing conditions (0.64 µg/ml of ATC), a qPCR analysis was performed and showed that *mazEF* homologous genes were being significantly expressed (**Figure 4B**). To analyze the putative role of *mazEF* as a TA system in *S. epidermidis*, the amount of total cells, as determined by OD, and the number of culturable cells, as determined by CFU counting, was assessed in the mutant and the complemented strains upon induction of *mazE/mazF/mazEF* homologues expression. However, in our conditions, no significant differences were observed in the OD (**Figures 4C, D**) or cells culturability (**Supplementary Table 3**).

DISCUSSION

The *mazEF* operon was initially identified as a TA system in *E. coli*, and then further confirmed in other gram-negative and gram-positive bacteria, with homology studies suggesting that this operon could have a TA function also in *S. epidermidis*. Importantly, although the homology between *S. epidermidis* 1457 *mazEF* homologue operon and *E. coli* is not very high (about 40% of nucleotide and 22 to 36% amino acid homology), greater homology was found with *S. aureus* strain Newman (**Supplementary Table 4**), where *mazEF* has been recently confirmed to function as a TA system (Ma et al., 2019). Interestingly, other biological roles have been linked with *mazEF*. Recently, *mazEF* increased expression was associated with *P. aeruginosa* and some staphylococcal species higher tolerance to gentamicin, ciprofloxacin, and clindamycin (Coskun et al., 2018). Furthermore, a role in biofilm formation and evasion from the host system was also described in *S. aureus* (Ma et al., 2019).

In *S. epidermidis*, preliminary evidence suggesting that *mazEF* homologue could play an important role in virulence came from previous transcriptomics studies, where it was suggested that the *mazEF* homologue could be involved in the regulation of the

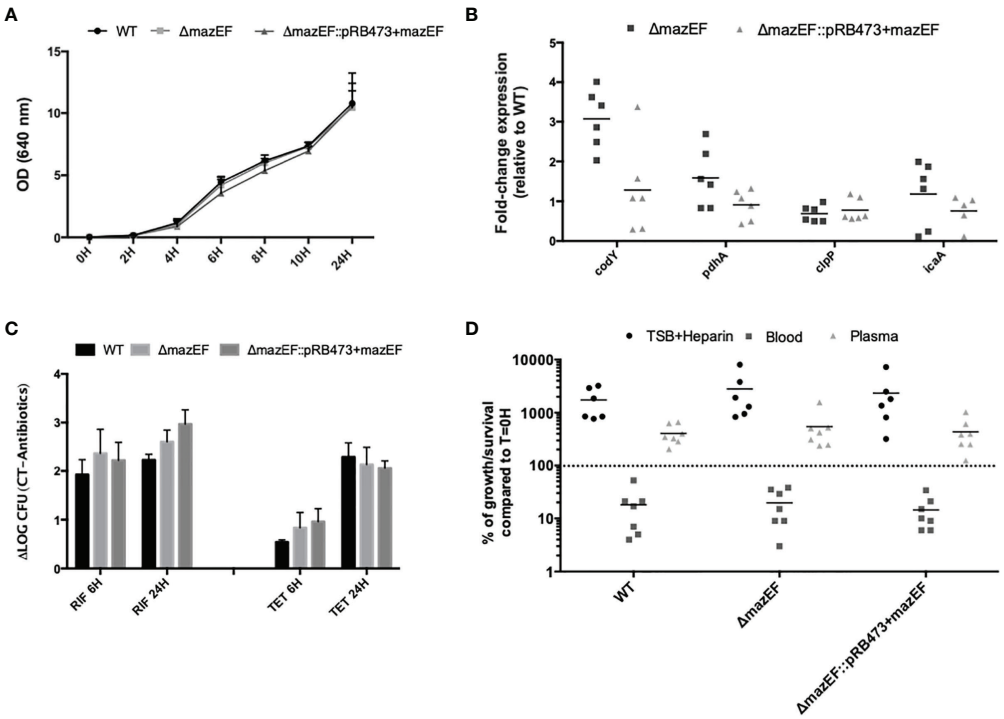

FIGURE 2 | Characterization of the role of *mazEF* homologue constructs in *S. epidermidis* 1457 phenotype and virulence potential. **(A)** Growth curve of *S. epidermidis* strains as determined by optical density (OD 640 nm); **(B)** Fold-change expression in 48 hour-old biofilms formed by all strains. The values obtained in the WT strain were used as control. Each point represents a single experiment and the horizontal lines the mean of at least 5 independent experiments; **(C)** Effect of rifampicin (RIF) and tetracycline (TET) on the culturability of 48-hour old biofilm cells. Results are presented as the LOG difference between the control samples (no antibiotic) and the antibiotic-treated samples (ΔLOG); **(D)** Survival of *S. epidermidis* strains in human blood and plasma upon 4 h of incubation. Each point is relative to a different donor/assay and the horizontal lines represent the median of 6 independent experiments performed with different donors (3 females and 3 males). TSB supplemented with heparin (TSB + Heparin) was used to evaluate the effect of heparin on bacterial growth. Results **(A, C)** are presented as the mean + standard deviation of at least 3 independent assays. Statistical analysis was performed using One-way ANOVA with Tukey's multiple comparisons test for all the assays.

VBNC state in biofilms (Carvalhais et al., 2014). As such, we started by evaluating if the *mazEF* homologue mutant could impact the proportion of VBNC cells. VBNC cell formation in *S. epidermidis* biofilms is not universal, showing high variability among strains (Carvalhais et al., 2018). We recently confirmed that strain 1457 can form VBNC cells (Gaio et al., 2021), however, at a lower extent than previously tested strains (Carvalhais et al., 2018). Moreover, we observed that the expression of *mazEF* genes in biofilms grown under VBNC state inducing conditions was lower in 1457 than in other strains (Gaio et al., 2021). As such, it was not surprising that the lack of *mazEF* homologue did not significantly affect VBNC cells formation in *S. epidermidis* 1457, but we can't exclude that in some clinical strains where the VBNC state is more pronounced, *mazEF* could play a role. Interestingly, the deletion of the *mazEF* homologue led to an increased expression of the gene *codY*, which has been also proposed to play a role in VBNC cells formation in *S. epidermidis* biofilms (Carvalhais et al., 2014). These results suggest that this gene may be compensating for the effect of the *mazEF* homologue absence, but this should be further explored. Other relevant genes, namely genes associated with biofilm formation, such as *icaA* and *rsbU* (Heilmann et al., 1996a; Heilmann et al., 1996b; Knobloch et al., 2004) were not affected by the *mazEF* homologue deletion.

We then further explored if the deletion of the *mazEF* homologue operon could influence other phenotypical traits in *S. epidermidis*. When assessing the response of planktonic and biofilm cells to vancomycin, rifampicin, and tetracycline, we observed that biofilm cells lacking *mazEF* homologue showed a significantly lower metabolic activity, after 6 h of treatment. This was an interesting result since it was previously shown that tetracycline might enhance the development of VBNC cells in *S. epidermidis* biofilms (Carvalhais et al., 2018). However, despite the change in metabolism, we did not observe any significant difference in bacterial culturability. Moreover, no differences in the bacterial survival in human blood or plasma were detected, as well as no relevant alterations in the levels of cytokines produced by M1- and M2-like macrophages or DC upon incubation with the distinct strains. This suggests that the deletion of *mazEF* homologue does not have a direct impact on the activation of the cells studied, which is usually driven by bacterial cell wall components.

Finally, considering the proximal relation and close homology to *S. aureus*, we also investigated the possible role of *mazEF*

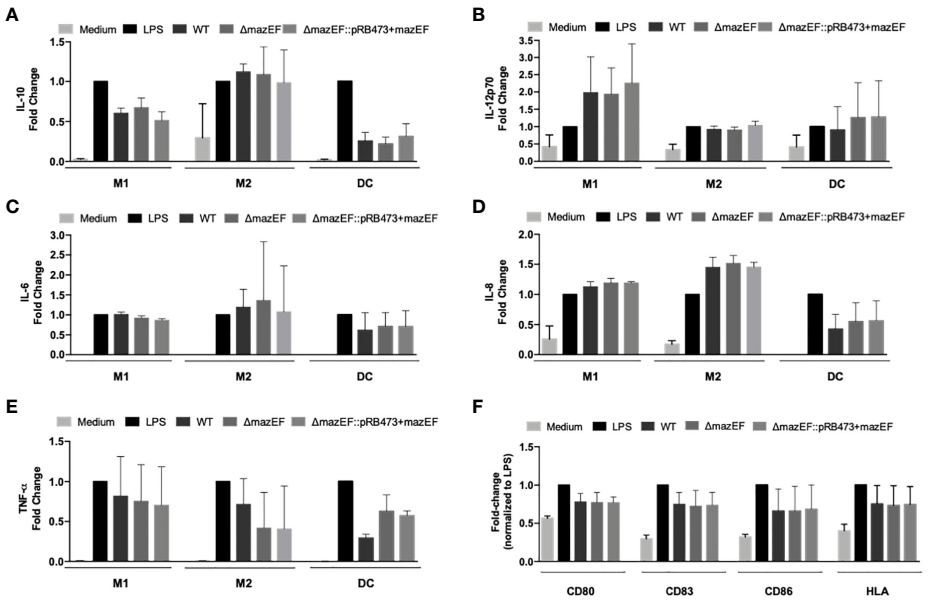

FIGURE 3 | Effect of *mazEF* homologue deletion in the response of mononuclear phagocytes. **(A–E)** Quantification of the cytokines secreted by human monocyte-derived M1- and M2-type macrophages (M1 and M2) and dendritic cells (DC) in cell-culture supernatants upon incubation with *S. epidermidis* cells at a MOI of 1 M1/M2/DC:5 bacteria. **(F)** Cell surface expression of activation/maturation markers detected by flow cytometry on DC upon incubation with *S. epidermidis* cells at a MOI of 1 DC:5 bacteria. Cytokine levels and activation marker expression are presented as fold-changes to the respective values of positive control (LPS) samples. Bars correspond to means + standard deviation of at least 3 independent experiments, where each condition was set in duplicate. Statistical analysis was performed using One-way ANOVA with Tukey's multiple comparison test. HLA, human leukocyte antigen.

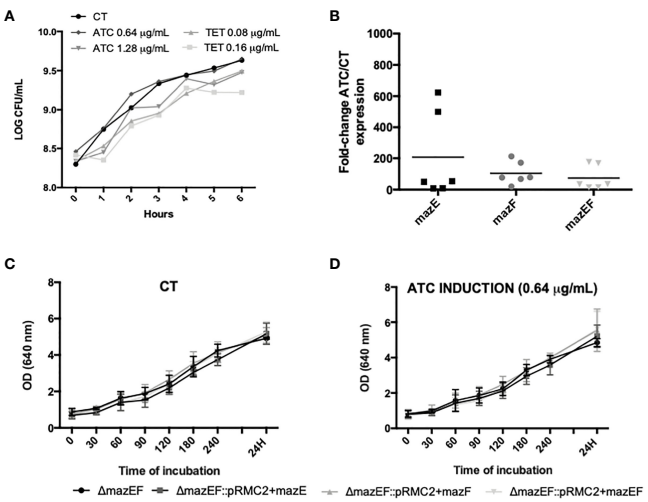

FIGURE 4 | Study of the putative TA action of *mazEF* homologue. **(A)** Growth curve of *ΔmazEF* planktonic cells upon incubation with different concentrations of anhydrotetracycline (ATC) and tetracycline (TET). The control (CT) data refers to non-induced cells. The data presented are relative to a single assay; **(B)** Fold-change expression of the *mazEF* homologue genes upon 4 h of induction with ATC 0.64 μg/ml. *ΔmazEF* cells harboring the inducible plasmids but without induction were used as control. Each point represents a single experiment and the horizontal lines represent the mean of 6 independent experiments; **(C)** Optical density (OD) of the control strains; and **(D)** strains induced with 0.64 μg/ml of ATC. Results are represented as the mean + standard deviation of at least 3 independent assays **(C, D)**. Statistical analysis was completed with One-way ANOVA with Tukey's multiple comparisons test **(B–D)**.

homologue operon as a TA module. In our experimental conditions, *mazEF* homologue did not seem to act as a TA system in *S. epidermidis* strain 1457. Despite the many similar traits between *S. aureus* and *S. epidermidis*, it was previously shown that the regulation of some important genes associated with biofilm formation is different, notwithstanding their significant homology (Cerca et al., 2008).

Altogether, in this brief report we performed the first characterization of a *mazEF* homologue mutant and demonstrated that, at least in strain 1457, the *mazEF* homologue does not seem to have a major role in *S. epidermidis* virulence potential.

DATA AVAILABILITY STATEMENT

The original contributions presented in the study are included in the article/**Supplementary Material**. Further inquiries can be directed to the corresponding author.

ETHICS STATEMENT

Human blood was collected in heparin-coated tubes (Vacuette), from adult healthy volunteers under a protocol approved by the Institutional Review Board of the University of Minho (SECVS 002/2014 (ADENDA)). Buffy coats from healthy adult blood donors, used for M1/M2 macrophages and DC differentiation, were acquired at the Immunohemoterapy Department of Centro Hospitalar de São João (Porto, Portugal), under ethical approval of the service (Protocol reference 260/11). All procedures were performed in agreement with the Helsinki declaration and Oviedo convention and all donors gave written consent before blood collection.

AUTHOR CONTRIBUTIONS

Conceptualization, MV, NC, and AF. Investigation, VG and TL. Writing original draft, VG and AF. Writing—review and editing, NC, TL, and MV. Supervision, MV, NC, and AF. All authors contributed to the article and approved the submitted version.

FUNDING

This work was supported by the Portuguese Foundation for Science and Technology (FCT) by the funder project PTDC/BIA-MOL/29553/2017, under the scope of COMPETE2020 (POCI-01-0145-FEDER-029553) and by the strategic funding unit UIDB/04469/2020. VG acknowledges the support of FCT individual fellowship [SFRH/BD/131452/2017].

ACKNOWLEDGMENTS

We thank Tim Foster for kindly providing the plasmid pRMC2.

SUPPLEMENTARY MATERIAL

The Supplementary Material for this article can be found online at: https://www.frontiersin.org/articles/10.3389/fcimb.2021.803134/full#supplementary-material

REFERENCES

Anderson, G. G., and O'Toole, G. A. (2008). Innate and Induced Resistance Mechanisms of Bacterial Biofilms. *Curr. Top. Microbiol. Immunol.* 322, 85–105. doi: 10.1007/978-3-540-75418-3_5

Behrooz, S. K., Lida, L., Ali, S., Mehdi, M., Rasoul, M., Elnaz, O., et al. (2018). Study of MazEF, Sam, and Phd-Doc Putative Toxin-Antitoxin Systems in Staphylococcus Epidermidis. *Acta Microbiol. Immunol. Hung.* 65, 1–11. doi: 10.1556/030.65.2018.003

Brás, S., França, A., and Cerca, N. (2020). Optimizing a Reliable Ex Vivo Human Blood Model to Analyze Expression of Staphylococcus Epidermidis Genes. *PeerJ* 8, e9295. doi: 10.7717/peerj.9295

Brescó, M. S., Harris, L. G., Thompson, K., Stanic, B., Morgenstern, M., O'Mahony, L., et al. (2017). Pathogenic Mechanisms and Host Interactions in Staphylococcus Epidermidis Device-Related Infection. *Front. Microbiol.* 8, 1401. doi: 10.3389/fmicb.2017.01401

Brückner, R. (1997). Gene Replacement in Staphylococcus Carnosus and *Staphylococcus Xylosus*. *FEMS Microbiol. Lett.* 151, 1–8. doi: 10.1016/S0378-1097(97)00116-X

Bruckner, R., Wagner, E., and Gotz, F. (1993). Characterization of a Sucrase Gene From *Staphylococcus Xylosus*. *J. Bacteriol.* 175 (3), 851–857. doi: 10.1128/jb.175.3.851-857.1993

Carvalhais, V., França, A., Cerca, F., Vitorino, R., Pier, G. B., Vilanova, M., et al. (2014). Dormancy Within Staphylococcus Epidermidis Biofilms: A Transcriptomic Analysis by RNA-Seq. *Appl. Microbiol. Biotechnol.* 98, 1–12. doi: 10.1007/s00253-014-5548-3

Carvalhais, V., Pérez-Cabezas, B., Oliveira, C., Vitorino, R., Vilanova, M., and Cerca, N. (2018). Tetracycline and Rifampicin Induced a Viable But Nonculturable State in Staphylococcus Epidermidis Biofilms. *Future Microbiol.* 13, 27–36. doi: 10.2217/fmb-2017-0107

Cerca, F., Andrade, F., França, A., Andrade, E. B., Ribeiro, A., Almeida, A. A., et al. (2011a). *Staphylococcus Epidermidis* Biofilms With Higher Proportions of Dormant Bacteria Induce a Lower Activation of Murine Macrophages. *J. Med. Microbiol.* 60, 1717–1724. doi: 10.1099/jmm.0.031922-0

Cerca, N., Brooks, J. L., and Jefferson, K. K. (2008). Regulation of the Intercellular Adhesin Locus Regulator (Icar) by SarA, σb, and IcaR in *Staphylococcus Aureus*. *J. Bacteriol.* 190 (19), 6530–6533. doi: 10.1128/JB.00482-08

Cerca, F., França, A., Perez-Cabezas, B., Carvalhais, V., Ribeiro, A., Azeredo, J., et al. (2014). Dormant Bacteria Within Staphylococcus Epidermidis Biofilms Have Low Inflammatory Properties and Maintain Tolerance to Vancomycin and Penicillin After Entering Planktonic Growth. *J. Med. Microbiol.* 63, 1274–1283. doi: 10.1099/jmm.0.073163-0

Cerca, N., Jefferson, K. K., Oliveira, R., Pier, G. B., and Azeredo, J. (2006). Comparative Antibody-Mediated Phagocytosis of Staphylococcus Epidermidis Cells Grown in a Biofilm or in the Planktonic State. *Infect. Immun.* 74, 4849–4855. doi: 10.1128/IAI.00230-06

Cerca, N., Martins, S., Cerca, F., Jefferson, K. K., Pier, G. B., Oliveira, R., et al. (2005). Comparative Assessment of Antibiotic Susceptibility of Coagulase-Negative Staphylococci in Biofilm Versus Planktonic Culture as Assessed by Bacterial Enumeration or Rapid XTT Colorimetry. *J. Antimicrob. Chemother.* 56, 331–336. doi: 10.1093/jac/dki217

Cerca, F., Trigo, G., Correia, A., Cerca, N., Azeredo, J., and Vilanova, M. (2011b). SYBR Green as a Fluorescent Probe to Evaluate the Biofilm Physiological State of Staphylococcus Epidermidis, Using Flow Cytometry. *Can. J. Microbiol.* 57, 850–856. doi: 10.1139/w11-078

Corrigan, R. M., and Foster, T. J. (2009). An Improved Tetracycline-Inducible Expression Vector for *Staphylococcus Aureus*. *Plasmid* 61 (2), 126–129. doi: 10.1016/j.plasmid.2008.10.001

Coskun, U. S. S., Cicek, A. C., Kilinc, C., Guckan, R., Dagcioglu, Y., Demir, O., et al. (2018). Effect of MazEF, HigBA and RelBE Toxin-Antitoxin Systems on Antibiotic Resistance in Pseudomonas Aeruginosa and *Staphylococcus* Isolates. *Malawi Med. J.* 30 (2), 67–72. doi: 10.4314/mmj.v30i2.3

Cui, B., Smooker, P. M., Rouch, D. A., and Deighton, M. A. (2015). Enhancing DNA Electro-Transformation Efficiency on a Clinical *Staphylococcus Capitis* Isolate. *J. Microbiol. Methods* 109, 25–30. doi: 10.1016/j.mimet.2014.11.012

Donegan, N. P., and Cheung, A. L. (2009). Regulation of the mazEF Toxin-Antitoxin Module in *Staphylococcus Aureus* and Its Impact on sigB Expression. *J. Bacteriol.* 191, 2795–2805. doi: 10.1128/JB.01713-08

Fey, P. D., and Olson, M. E. (2011). Current Concepts in Biofilm Formation of *Staphylococcus Epidermidis*. *Future Microbiol.* 5, 917–933. doi: 10.2217/fmb.10.56.Current

França, A., Freitas, A. I., Henriques, A. F., and Cerca, N. (2012). Optimizing a qPCR Gene Expression Quantification Assay for S. Epidermidis Biofilms: A Comparison Between Commercial Kits and a Customized Protocol. *PloS One* 7, e37480. doi: 10.1371/journal.pone.0037480

França, A., Pier, G. B., Vilanova, M., and Cerca, N. (2016). Transcriptomic Analysis of Staphylococcus Epidermidis Biofilm-Released Cells Upon Interaction With Human Blood Circulating Immune Cells and Soluble Factors. *Front. Microbiol.* 7, 1143. doi: 10.3389/fmicb.2016.01143

Freitas, A. I., Vasconcelos, C., Vilanova, M., and Cerca, N. (2014). Optimization of an Automatic Counting System for the Quantification of Staphylococcus Epidermidis Cells in Biofilms. *J. Basic Microbiol.* 54, 750–757. doi: 10.1002/jobm.201200603

Gaio, V., Lopes, N., Cerca, N., and França, A. (2021). codY and *pdhA* Expression is Induced in *Staphylococcus Epidermidis* Biofilm and Planktonic Populations With Higher Proportions of Viable But non-Culturable Cells. *Front. Cell. Infect. Microbiol.* 11, 771666. doi: 10.3389/fcimb.2021.771666

Heilmann, C., Gerke, C., Perdreau-Remington, F., and Götz, F. (1996a). Characterization of Tn917 Insertion Mutants of Staphylococcus Epidermidis Affected in Biofilm Formation. *Infect. Immun.* 64, 277–282. doi: 10.1128/iai.64.1.277-282.1996

Heilmann, C., Schweitzer, O., Gerke, C., Vanittanakom, N., Mack, D., and Götz, F. (1996b). Molecular Basis of Intercellular Adhesion in the Biofilm-Forming Staphylococcus Epidermidis. *Mol. Microbiol.* 20 (5), 1083–1091. doi: 10.1111/j.1365-2958.1996.tb02548.x

Karimi, S., Ghafourian, S., Kalani, M. T., Jalilian, F. A., Hemati, S., and Sadeghifard, N. (2015). Association Between Toxin-Antitoxin Systems and Biofilm Formation. *Jundishapur J. Microbiol.* 8, 1–6. doi: 10.5812/jjm.14540

Knobloch, J. K. M., Jäger, S., Horstkotte, M. A., Rohde, H., and Mack, D. (2004). RsbU-Dependent Regulation of Staphylococcus Epidermidis Biofilm Formation is Mediated via the Alternative Sigma Factor çb by Repression of the Negative Regulator Gene icaR. *Infect. Immun.* 72, 3838–3848. doi: 10.1128/IAI.72.7.3838-3848.2004

Mack, D., Siemssen, N., and Laufs, ,. R. (1992). Parallel Induction by Glucose of Adherence and a Polysaccharide Antigen Specific for Plastic-Adherent Staphylococcus Epidermidis: Evidence for Functional Relation to Intercellular Adhesion. *Infect. Immun.* 60, 2048–2057. doi: 10.1128/iai.60.5.2048-2057.1992

Ma, D., Mandell, J. B., Donegan, N. P., Cheung, A. L., Ma, W., Rothenberger, S., et al. (2019). The Toxin-Antitoxin mazEF Drives Staphylococcus Aureus Biofilm Formation, Antibiotic Tolerance, and Chronic Infection. *MBio* 10 (6), e01658–19. doi: 10.1128/mBio.01658-19

Metzger, S., Dror, I. B., Aizenman, E., Schreiber, G., Toone, M., Friesen, J. D., et al. (1988). The Nucleotide Sequence and Characterization of the relA Gene of Escherichia Coli. *J. Biol. Chem.* 263, 15699–15704. doi: 10.1111/j.1574-6968.1996.tb08317.x

Monk, I. R., Shah, I. M., and Xu, M. (2012). Transforming the Untransformable: Application of Direct Transformation to Manipulate Genetically Staphylococcus Aureus and Staphylococcus Epidermidis. *MBio* 3, e00277–e00211. doi: 10.1128/mBio.00277-11.Editor

Nguyen, T. H., Park, M. D., and Otto, M. (2017). Host Response to Staphylococcus Epidermidis Colonization and Infections. *Front. Cell. Infect. Microbiol* 7, 90. doi: 10.3389/fcimb.2017.00090

Oliveira, F., Lima, C. A., Bras, S., França, A., and Cerca, N. (2015). Evidence for Inter- and Intraspecies Biofilm Formation Variability Among a Small Group of Coagulase-Negative Staphylococci. *FEMS Microbiol. Lett.* 362, 1–20. doi: 10.1093/femsle/fnv175

Otto, M. (2009). *Staphylococcus Epidermidis* – the "Accidental" Pathogen. *Nat. Rev. Microbiol.* 7, 555–567. doi: 10.1038/nrmicro2182.Staphylococcus

Schuster, C. F., Mechler, L., Nolle, N., Krismer, B., Zelder, M. E., Götz, F., et al. (2015). The mazEF Toxin-Antitoxin System Alters the β-Lactam Susceptibility of Staphylococcus Aureus. *PloS One* 10, 1–22. doi: 10.1371/journal.pone.0126118

Schuster, C. F., Park, J. H., Prax, M., Herbig, A., Nieselt, K., Rosenstein, R., et al. (2013). Characterization of a MazEF Toxin-Antitoxin Homologue From Staphylococcus Equorum. *J. Bacteriol.* 195, 115–125. doi: 10.1128/JB.00400-12

Shapiro, J. A., Nguyen, V. L., and Chamberlain, N. R. (2011). Evidence for Persisters in *Staphylococcus Epidermidis* RP62A Planktonic Cultures and Biofilms. *J. Med. Microbiol.* 60, 950–960. doi: 10.1099/jmm.0.026013-0

Sousa, C., França, A., and Cerca, N. (2014). Assessing and Reducing Sources of Gene Expression Variability in Staphylococcus Epidermidis Biofilms. *Biotechniques* 57, 295–301. doi: 10.2144/000114238

Syed, M. A., Koyanagi, S., Sharma, E., Jobin, M. C., Yakunin, A. F., and Lévesque, C. M. (2011). The Chromosomal *mazEF* Locus of *Streptococcus Mutans* Encodes a Functional Type II Toxin-Antitoxin Addiction System. *J. Bacteriol.* 193 (5), 1122–1130. doi: 10.1128/JB.01114-10

Tiwari, P., Arora, G., Singh, M., Kidwai, S., Narayan, O. P., and Singh, R. (2015). MazF Ribonucleases Promote Mycobacterium Tuberculosis Drug Tolerance and Virulence in Guinea Pigs. *Nat. Commun.* 6, 6059. doi: 10.1038/ncomms7059

Untergasser, A., Cutcutache, I., Koressaar, T., Ye, J., Faircloth, B. C., Remm, M., et al. (2012). Primer3 - New Capabilities and Interfaces. *Nucleic Acids Res.* 40, e115. doi: 10.1093/nar/gks596

Valadbeigi, H., Sadeghifard, N., and Salehi, M. B. (2017). Assessment of Biofilm Formation in *Pseudomonas Aeruginosa* by Antisense *mazE*-PNA. *Microb. Pathog.* 104, 28–31. doi: 10.1016/j.micpath.2017.01.009

Van Melderen, L. (2010). Toxin-Antitoxin Systems: Why So Many, What for? *Curr. Opin. Microbiol.* 13, 781–785. doi: 10.1016/j.mib.2010.10.006

Zandri, G., Pasquaroli, S., Vignaroli, C., Talevi, S., Manso, E., Donelli, G., et al. (2012). Detection of Viable But non-Culturable Staphylococci in Biofilms From Central Venous Catheters Negative on Standard Microbiological Assays. *Clin. Microbiol. Infect.* 18, 259–261. doi: 10.1111/j.1469-0691.2012.03893.x

Zhu, L., Inoue, K., Yoshizumi, S., Kobayashi, H., Zhang, Y., Ouyang, M., et al. (2009). *Staphylococcus Aureus* MazF Specifically Cleaves a Pentad Sequence, UACAU, Which is Unusually Abundant in the mRNA for Pathogenic Adhesive Factor SraP. *J. Bacteriol.* 191, 3248–3255. doi: 10.1128/JB.01815-08

Conflict of Interest: The authors declare that the research was conducted in the absence of any commercial or financial relationships that could be construed as a potential conflict of interest.

Publisher's Note: All claims expressed in this article are solely those of the authors and do not necessarily represent those of their affiliated organizations, or those of the publisher, the editors and the reviewers. Any product that may be evaluated in this article, or claim that may be made by its manufacturer, is not guaranteed or endorsed by the publisher.

frontiers in Cellular and Infection Microbiology

ORIGINAL RESEARCH
published: 19 January 2022
doi: 10.3389/fcimb.2021.780545

Synergistic Interaction of Piperine and Thymol on Attenuation of the Biofilm Formation, Hyphal Morphogenesis and Phenotypic Switching in *Candida albicans*

Arumugam Priya, Srinivasan Nivetha and Shunmugiah Karutha Pandian *

Department of Biotechnology, Alagappa University, Karaikudi, India

OPEN ACCESS

Edited by:
Carina Almeida, Instituto Nacional Investigaciao Agraria e Veterinaria (INIAV), Portugal

Reviewed by:
David Williams, Cardiff University, United Kingdom
Sónia Silva, University of Minho, Portugal
Maria Elisa Rodrigues, University of Minho, Portugal

***Correspondence:**
Shunmugiah Karutha Pandian
pandiansk@gmail.com

Specialty section:
This article was submitted to Biofilms, a section of the journal Frontiers in Cellular and Infection Microbiology

Received: *21 September 2021*
Accepted: *21 December 2021*
Published: *19 January 2022*

Citation:
Priya A, Nivetha S and Pandian SK (2022) Synergistic Interaction of Piperine and Thymol on Attenuation of the Biofilm Formation, Hyphal Morphogenesis and Phenotypic Switching in Candida albicans. Front. Cell. Infect. Microbiol. 11:780545. doi: 10.3389/fcimb.2021.780545

The incidence of fungal infections has significantly increased in recent years due to the emergence of antifungal resistance. Biofilm formation is considered to be a major contributor to both the infectious diseases and to antimicrobial resistance. Consequently, biofilm-associated infections are often problematic to treat with existing therapeutics. Adhesion of *C. albicans* to the host surface or implanted materials followed by hyphal invasion and biofilm formation enhances *C. albicans* pathogenicity and virulence. Thus, developing a therapeutic agent that inhibits candidal adherence, biofilm development and morphological switching could improve clinical management of infections. The present investigation studied two emerging and alternatives strategies, namely antibiofilm and combinatorial approach, to attenuate biofilm formation and the expression of *Candida* virulence factors. Piperine and thymol are major bioactive components of pepper and thyme, respectively. These phytochemicals are known to possess numerous biological activities, including recently reported antibiofilm effects against *C. albicans*. The minimum biofilm inhibitory concentration (MBIC) of both phytochemicals was determined to be 32 µg/ml. The phytochemical treatment of *Candida* biofilms using piperine and thymol revealed synergistic effects at four different combinations of concentrations, i.e. 8 and 8, 8 and 4, 8 and 2 and 4 and 8 µg/ml. These synergistic combinations resulted in the significant reduction in adherence of *Candida*, hyphal extension and morphological transformation. Moreover, limited exposure of synergistic combinations controlled the hyphal elongation. Results were validated through the gene expression analysis. Results from the present investigation suggest that piperine and thymol can be synergistically employed for the treatment of biofilm-associated *C. albicans* infection.

Keywords: *C. albicans*, synergism, antibiofilm, combinatorial therapy, piperine, thymol, antihyphae

INTRODUCTION

The genus *Candida* is ubiquitously distributed and comprises more than 350 species of "yeast-like fungi" (Williams and Lewis, 2011; Williams et al., 2012). The majority of the *Candida* species are unable to grow at 37°C and thus not generally associated with colonization of humans (Schauer and Hanschke, 1999). Nevertheless, certain species such as *Candida albicans*, *C. glabrata*, *C. tropicalis*, *C. krusei*, *C. parapsilosis* and *C. dubliniensis* exist as a part of the human commensal microbiota that can transmute to opportunistic pathogens under favourable conditions (Fisher et al., 1987; Vanden Abbeele et al., 2008; Luque et al., 2009; Martins et al., 2010; Meurman et al., 2011). These yeast reside in an individual's oral cavity, gastrointestinal tract and vagina (Shao et al., 2007). Infections caused by *Candida* species are generally known as candidiasis, and *Candida* infections associated with the oral cavity are described as oral candidiasis. Of the *Candida* species isolated from humans, *C. albicans* is the most predominant species associated with both health and disease (LaFleur et al., 2010; de Oliveira Mima et al., 2010). Several mycological studies have shown that *C. albicans* represents more than 80% of isolates in all forms of candidiasis (Pfaller and Diekema, 2007). Of the various mucosal sites, colonization of *C. albicans* in the oral cavity is more significant, with 80% of healthy individuals carrying *C. albicans* in their mouth (Williams et al., 2012). Predisposing risk factors associated with oral candidiasis include decreased salivary production, immunocompromised status, smoking, diabetes, malnutrition, impaired oral flora and/or poor oral hygiene (Rautemaa and Ramage, 2011). The local breach in the mucosal surfaces caused by mucositis, radiation and trauma are also considered as predisposing factors. Colonization of *Candida* in the oral cavity may occur at several sites including biotic surfaces such as tongue, buccal mucosa, palate and abiotic surfaces such as denture (Nett et al., 2010). Denture stomatitis is considered one of the most prevalent forms of oral candidiasis, affecting up to 70% of denture wearers (Wilson, 1998; Senpuku et al., 2003). *C. albicans* can directly interact either with the denture acrylic surface or with plaque-forming bacteria (Chandra et al., 2001).

Pathogenesis and virulence of *C. albicans* rely on numerous factors which altogether support the organism to survive and proliferate in the healthy host surpassing the immune factors and attack of antibiotics (Nett et al., 2010). Among the various virulence factors, most imperative are those that support adherence to the host tissues and implanted devices, biofilm formation and secretion of hydrolytic enzymes such as phospholipase, lipase, proteases and haemolysins (Sardi et al., 2013). Additionally, the invasiveness of *C. albicans* is contributed by the proficiency for phenotypic switching between yeast and filamentous forms (Cullen and Sprague, 2012).

Biofilm formation by fungal species is defined as a major standard for pathogenesis (Martinez and Fries, 2010). Studies suggest that majority of the infections caused by *C. albicans* are associated with biofilm formation. Early biofilm formation initiates when *C. albicans* instigates an interaction with the host tissue or with the implant surfaces. Increased pathogenicity is observed in the biofilm form of infection as the biofilm matrix defends *Candida* cells from the host immunological responses and from antifungal therapy (Ramage et al., 2004). Biofilm-mediated drug resistance is emerging as a major contributor to numerous human ailments. *C. albicans* cells encased within the biofilm matrix are less susceptible to the antifungals compared to their planktonic counterparts (Kuhn and Ghannoum, 2004; Uppuluri et al., 2009; Rautemaa and Ramage, 2011). Numerous broad-spectrum antifungal drugs are available currently for the treatment of *Candida* infections, which include azole drugs (fluconazole, itraconazole, clotrimazole and ketoconazole), echinocandins (micafungin, caspofungin) and polyenes (amphotericin B). Adverse side effects and rising resistance development have made the usage of antifungals sceptical. Thus, research on the identification of therapeutic regimens has shifted the focus in targeting the biofilm and other virulence factors of the pathogen rather than affecting the survival (Bandara et al., 2017; Vila et al., 2017). With the traditional practice of medicinal plants for the cure of numerous ailments, studies have demonstrated the usage of plant-based active molecules to overcome biofilm-associated *Candida* infections (Priya and Pandian, 2020; Muthamil et al., 2020). Numerous bioactives with antibiofilm activity have been identified from various natural sources (Abraham et al., 2012). Yet, most of the bioactives fail to cross clinical trials due to high concentration and/or toxic effects. To overcome this, a recent approach, combinatorial drug therapy, has gained more attention due to the benefits of reduced toxicity, improved efficacy and being devoid of antibiotic resistance with increased potential than individual drug candidates (Chanda and Rakholiya, 2011).

With this backdrop, the present study aimed to evaluate the synergistic antivirulence potential of two phytochemicals, piperine and thymol, against *C. albicans*. Our earlier study has reported the antibiofilm potential of piperine, a major bioactive component of the pepper seeds against *C. albicans* (Priya and Pandian, 2020). Thymol is a major constituent in the essential oil of thyme plant (*Thymus vulgaris*) and was previously reported to possess antibiofilm and hyphal inhibitory activity against *C. albicans* (Braga et al., 2007; Braga et al., 2008). The present work is expected to pave way for the prevention of biofilm-associated *C. albicans* infection (antibiofilm activity) and invasive candidiasis (antihyphal activity).

MATERIALS AND METHODS

Ethical Statement

In the present study, human blood and buccal epithelial cells were collected from healthy individuals after procuring a written informed consent. The experimental protocol and the use of human blood and HBECs were assessed and approved by the Institutional Ethical Committee, Alagappa University, Karaikudi (IEC Ref No. IEC/AU/2018/5). All the methods were carried out in accordance with relevant guidelines.

FUNGAL STRAIN AND GROWTH CONDITIONS

Reference fungal strain *C. albicans* 90028 from the American Type Culture Collection (ATCC) was used in the present study. In addition to the reference strain, four different clinical isolates of *C. albicans*, namely CI-1 (GenBank accession no.: MF445114.1); CI-2 (GenBank accession no.: MF445113.1); CI-3 (GenBank accession no.: MF445115.1) and CI-4 (GenBank accession no.: MF445116.1), were included to evaluate the efficacy of phytocompounds and their combinatorial effects. Culture was maintained in YEPD (1% yeast extract, 2% peptone and 2% dextrose) agar plates at 4°C. Routine culturing was carried out in YEPD broth and incubated at 37°C with constant shaking at 160 rpm. Assays associated with biofilm formation and hyphal development were performed with spider medium (1% of mannitol, 0.2% of dipotassium hydrogen phosphate and 1% of nutrient broth). Hyphal induction for hyphal to yeast transition assay was carried out using RPMI medium (HiMedia, India).

Phytochemicals

Piperine (PubChem CID: 638024) and thymol (PubChem CID: l6989) were commercially procured from HiMedia and Alfa Aesar, respectively. Stock solutions of both the phytocompounds were prepared with the concentration of 50 mg/ml in methanol. The highest volume of compound used in the test group was taken as the volume of methanol for vehicle control in each assay.

Influence of Piperine and Thymol on Viability and Biofilm Formation of *C. albicans*

The impact of individual effects of piperine and thymol on the growth of *C. albicans* reference and clinical strains was determined by microbroth dilution assay as per the CLSI guideline (Wayne, 2008). The determination of the biofilm inhibitory concentration was performed as described earlier (Priya and Pandian, 2020). Briefly, in a 24-well microtiter plate (MTP), 1 ml of spider broth was added with increasing concentrations of individual phytochemicals in the range of 2–1,024 μg/ml. The medium added with methanol served as vehicle control. To this, 1% of overnight culture of *C. albicans* was inoculated. Wells containing medium alone served as blank. The plates were incubated at 37°C for 48 h at static conditions. Following incubation, the planktonic part was discarded and the loosely bound biofilm cells were detached by carefully rinsing the wells with sterile PBS. Plates were air dried. Biofilm cells bound to the surface of the MTP were stained with 0.4% crystal violet and incubated at room temperature for 5 min, and the excess unbound stain was decanted. Plates were then destained with 10% glacial acetic acid solution and read at 595 nm in a multifunctional spectrophotometer. Inhibition of biofilm formation was calculated in percentage using the following formula:

$$\%\ of\ biofilm\ inhibition = \frac{(\mathrm{ControlOD}_{570}\mathrm{nm} - \mathrm{TreatedOD}_{570}\ nm)}{\mathrm{ControlOD}_{570}\mathrm{nm}}$$

MBIC was considered as the minimum concentration required to inhibit a minimum of 85% or more of biofilm when compared to the control biofilm.

Checkerboard Assay to Identify the Combinatorial Efficacy of Piperine and Thymol Against *C. albicans* Biofilm

The interaction between two phytochemicals piperine and thymol in exhibiting increased antibiofilm activity at lesser concentrations than their individual effect was evaluated through two-dimensional checkerboard assay for *C. albicans* reference and clinical strains. A total of 25 different antibiofilm combinations were analysed between phytochemicals in a decreasing concentration ranging from biofilm inhibitory concentration (BIC) to 1/16 BIC. The assay was performed in a 48-well MTP. In the first column, piperine was added to the spider medium at the BIC concentration, and then 2-fold dilutions were made for the subsequent plate columns. In a similar way, BIC of thymol was added to the first row and 2-fold dilutions were made for the subsequent plate rows. The last drug concentration in the row and column of the plate was set to 0 μg/ml, to examine the activity of individual phytochemicals at various test concentrations in combination. Appropriate control, vehicle control and negative controls were maintained in parallel. Plates were incubated at 37°C for 48 h in static conditions. At the end of the incubation period, the plates were processed to analyse the antibiofilm activity with the similar procedure detailed in the previous methods section. The percentage of biofilm inhibition by individual and combinations of piperine and thymol was calculated, and a heatmap was generated. The fractional inhibitory concentration (FIC) was calculated individually, and the FIC index (FICI) was calculated by summing up the FIC of both the phytocompounds as the following:

$$\mathrm{FICI} = \mathrm{FIC_A} + \mathrm{FIC_B}$$

$\mathrm{FIC_A}$ =BIC of A in combination with B/BIC of A alone

$\mathrm{FIC_B}$ =BIC of B in combination with A/BIC of B alone

The combinations were said to be synergistic when the FICI is ≤ 0.5. Combinations with the FICI in the range of greater than 0.5 to less than or equal to 4 is said to be indifferent. When FICI is greater than 4, the phytochemicals in the combination were known to exhibit antagonistic effect.

Effect of Combinations of Piperine and Thymol on Viability of *C. albicans*

Checkerboard assay was performed with YEPD broth and incubated at 37°C for 24 h. Followed by incubation, culture was mixed well and 5 μl from each well was spotted on the agar plate which was incubated for 37°C for 24 h. Similarly, *C. albicans* grown in the absence and presence of the identified synergistic combinations were grown and CFU analysis was performed.

Analysis of Biofilm Cell Count Under the Influence of Individual and Combined Activity of Piperine and Thymol

C. albicans was allowed to form biofilm in the absence and presence of piperine, thymol and their synergistic combinations

in spider medium for 48 h at 37°C. Planktonic cells were removed, and loosely bound cells were removed by gentle wash with PBS. The adhered biofilm cells were resuspended in PBS. Serial dilutions were made and plated on YEPD agar plates. CFU/mL was calculated after incubation for 24 h at 37°C, and log reduction in biofilm cells compared to control was plotted as graph.

Microscopic Visualization of Biofilm Architecture

Biofilm architecture and filamentous morphology of *C. albicans* in the absence and presence of individual and synergistic combinations of piperine and thymol were microscopically evaluated. Briefly, *C. albicans* was allowed to form biofilm on a 1 × 1-cm glass surface for 48 h at 37°C. After incubation, the glass slides were carefully removed and processed as mentioned earlier. Crystal violet-stained glass slides were observed under the light microscope (Nikon Eclipse 80i, USA) at ×400 magnification.

Checkerboard Assay to Evaluate the Combinatorial Efficacy of Piperine and Thymol Against *C. albicans* Hyphae

Checkerboard assay was performed as mentioned previously. Instead of liquid medium, solid spider agar was prepared and 5% foetal bovine serum was supplemented after the agar reached ambient temperature to induce the filamentation. To this mixture, various concentrations of piperine and thymol were added, mixed well and poured on glass plates. After proper solidification, 5 µl of *C. albicans* overnight culture was spotted on the centre of the medium. Plates were incubated at 37°C for 5–7 days. Variation in the filamentous morphology was observed and documented using the gel documentation system (Bio-Rad Gel Doc™ XR+).

Influence of Individual and Synergistic Combinations of Piperine and Thymol on *C. albicans* Phenotypic Switching

The ability of the phytochemicals to control *C. albicans* phenotypic switching between yeast to hyphal and vice versa was appraised by the following methods.

(A) Yeast to Hyphal Morphogenesis

C. albicans was grown on YEPD medium supplemented with 10% FBS to facilitate hyphal induction. Individual and synergistic combinations of piperine and thymol were added separately and incubated at 37°C with constant shaking at 160 rpm for 4 h. Further, the transition in the morphology was observed under the microscope (Nikon Eclipse Ts2R, Japan).

(B) Hyphal to Yeast Transition

Reversal of hyphal to yeast form under the influence of individual and synergistic combinations of piperine and thymol was performed in hyphal-inducing conditions. Briefly, the cells were inoculated into the RPMI medium and allowed to develop hyphae for 4 h at 37°C. After ensuring the presence of hyphal forms, phytochemicals at their individual and synergistic combination concentrations were added and further incubated for 2 h. Subsequently, the morphology was microscopically evaluated.

Post Antihyphal Effect

C. albicans cells were briefly exposed to the phytochemicals for 1 h at 37°C with gentle shaking. After incubation, the compounds were removed by three rounds of centrifugation. Subsequently, phytochemical-exposed *C. albicans* cells were used as inoculum and introduced into RPMI medium which was further incubated for 2 h. Later, cells were observed under the microscope.

Antifungal Sensitivity Assay

Sensitivity of the *C. albicans* cells treated with individual and synergistic combinations of piperine and thymol to antifungals such as miconazole, itraconazole, ketoconazole and nystatin was evaluated by disc diffusion assay. Briefly, *C. albicans* cells were grown in the absence and presence of individual and combination of phytochemicals overnight in YEPD medium at 37°C. The cultures were inoculated on the YEPD agar plates, and antifungal discs were placed on the centre and incubated for 24 h at 37°C. The zone of clearance was noted.

Gene Expression Analysis

The dynamics in the expression of candidate genes responsible for biofilm formation, hyphal regulation, adhesion between the control and synergistic combinations of piperine and thymol-treated *C. albicans* was assessed through qPCR analysis. RNA from control and phytocompound-treated *C. albicans* was extracted by the TRIzol method using commercial TRI reagent (Sigma-Aldrich, India). Extracted RNA was converted to cDNA using the high-capacity cDNA Reverse Transcription Kit (Applied Biosystems, United States), and qPCR analysis was performed with SYBR Green Master Mix (Applied Biosystems, United States) with the Applied Biosystems® 7500 Real-Time PCR system. A list of candidate genes, primer details and functions is provided in **Table 1**. Alterations in the gene expression were calculated by the $^{\Delta\Delta}$CT method.

Analysis of Cytotoxic Effect of Piperine, Thymol and Their Synergistic Combinations

The toxic effect of phytocompounds and their combinations were analysed on human red blood cells and human buccal epithelial cells (HBECs).

(A) Haemolytic Activity

Human erythrocytes were collected from healthy volunteers in a tube containing EDTA as anticoagulant. Cells were harvested by centrifugation for 10 min at 2,000 rpm and subsequently washed in PBS thrice. Cells were diluted to get a suspension of 1:10 in PBS. Test compounds were added to 1 ml of this suspension and incubated for 1 h at 37°C. Positive control was maintained with 1% Triton X-100. After incubation period, the tubes were

TABLE 1 | Candidate genes, primer details and function in the virulence and pathogenicity of *C. albicans*.

S. no.	Gene	Primer sequence (5′–3′)		Function
		Forward	Reverse	
1	*nrg1*	CCAAGTACCTCCACCAGCAT	GGGAGTTGGCCAGTAAATCA	Negative regulator of filamentous growth. Repress *ece1* and *hwp1*
2	*ume6*	ACCACCACTACCACCACCAC	TATCCCCATTTCCAAGTCCA	Transcriptional activator of filamentous growth. Regulates hyphal elongation and germ tube formation
3	*tup1*	CTTGGAGTTGGCCCATAGAA	TGGTGCCACAATCTGTTGTT	Negative regulator of filamentation. Farnesol-mediated inhibition of filamentation, controls phenotypic switching
4	*efg1*	GCCTCGAGCACTTCCACTGT	TTTTTTCATCTTCCCACATGGTAGT	Regulates switch between white and opaque cells and cell wall dynamics. Essential for biofilm formation and filamentous growth
5	*cph1*	TATGACGCTTCTGGGTTTCC	ATCCCATGGCAATTTGTTGT	Transcription factor involved in pseudohyphal and hyphal formation and phenotypic switching
6	*eap1*	TGTGATGGCGGTTCTTGTTC	GGTAGTGACGGTGATGATAGTGACA	Associated with cell adhesion and filamentation. Instigates adhesion to polystyrene and epithelial cells
7	*ras1*	CCCAACTATTGAGGATTCTTATCGTAAA	TCTCATGGCCAGATATTCTTCTTG	Mediates cell adhesion, induces filamentous growth, regulates phenotypic switching
8	*als1*	CCTATCTGACTAAGACTGCACC	ACAGTTGGATTTGGCAGTGGA	Adhesin. Vital for adhesion to oral mucosa and epithelial cells. Mediates yeast aggregation, a first step in biofilm formation
9	*ece1*	CCAGAAATTGTTGCTCGTGTTGCCA	TCCAGGACGCCATCAAAAACGTTAG	Candidalysin. Regulates biofilm formation and filamentation
10	*hwp1*	GCTCCTGCTCCTGAAATGAC	CTGGAGCAATTGGTGAGGTT	Hyphal wall protein. Essential for hyphal elongation

centrifuged for 10 min at 2000 rpm. The supernatant was transferred to MTP, and the absorbance was measured spectroscopically at 450 nm. The percentage of haemolysis was calculated by the following formula (Ahmad et al., 2010)

$$\text{Percentage haemolysis} = \frac{(\text{Absorbance of treated sample} - \text{Absorbance of control sample})}{(\text{Absorbance of positive control} - \text{Absorbance of control sample})} \times 100$$

(B) Effect of Individual and Synergistic Combinations of Phytocompounds on HBECs

HBECs were collected from healthy individuals with good oral hygiene by gently rubbing the inner mucosal surface of the cheeks with a sterile swab which was subsequently swirled and suspended in sterile PBS. HBEC suspension was used immediately after collection. The cell suspension from different individuals was pooled together and centrifuged at 3,000 rpm for 10 min. The supernatant was discarded, and the pellet was resuspended in PBS. Cells were counted using the Automated Cell Counter (Countess II FL, Invitrogen, United States) and adjusted to 5×10^5 cells/ml. HBECs were then incubated with different concentrations of individual and combinations of piperine and thymol for 20 min at 37°C. Hydrogen peroxide was used as positive control; after incubation, cells were stained with crystal violet and observed under the microscope (Nikon Eclipse TsR2, Japan) (Priya and Pandian, 2020).

Statistical Analysis

All the experiments were carried out in at least three biological replicates with at least two technical replicates, and values are presented as mean ± standard deviation (SD). To analyse the significant difference between the value of control and treated samples, one-way analysis of variance (ANOVA) and Duncan's *post hoc* test were performed with the significant p-value of <0.05 by the SPSS statistical software package version 17.0 (Chicago, IL, United States).

RESULTS

Minimum Biofilm Inhibitory Concentration (MBIC) of Piperine and Thymol Against *C. albicans*

The biofilm inhibitory potential of piperine against *C. albicans* was reported in our previous study (Priya and Pandian, 2020). Piperine at 32 μg/ml inhibited the biofilm formation of the reference strain of *C. albicans* without affecting the viability (**Figure 1A**). From the present investigation, the antibiofilm potential of thymol was identified. At 32 μg/ml, thymol inhibited up to 90% of surface adherence and biofilm formation of the *C. albicans* reference strain without affecting the growth. A concentration higher than 32 μg/ml was found to be growth inhibitory in a dose-dependent manner (**Figure 1B**). Thus, 32 μg/ml was determined to be MBIC for both the phytochemicals piperine and thymol for the reference strain. MBIC was found to be slightly different for the clinical isolates. For CI-1, 128 μg/ml of piperine and thymol was determined as MBIC. For CI-2, 64 and 32 μg/ml of piperine and thymol, respectively, were identified as MBIC. The MBIC of piperine and thymol for CI-3 was identified as 32 μg/ml, whereas for CI-4, 32 and 64 μg/ml of piperine and thymol, respectively, was considered as MBIC (**Supplementary Figure 1**).

Synergistic Antibiofilm Efficacy of Piperine and Thymol Against Biofilm of *C. albicans*

The interaction between piperine and thymol in exerting antibiofilm activity against *C. albicans* was analysed through checkerboard assay. The interaction was found to be synergistic at the following four different combinations of piperine and thymol in μg/ml: 8 + 8, 8 + 4, 8 + 2 and 4 + 8. The antibiofilm activity was found in other combinations. However, the FICI was found to be higher than 0.5 (**Table 2**). Thus, the aforementioned four combinations of piperine and thymol were determined to the synergistic combinations with antibiofilm activity against *C. albicans* (**Figure 2A**). When compared to the individual concentrations of piperine and thymol in synergistic

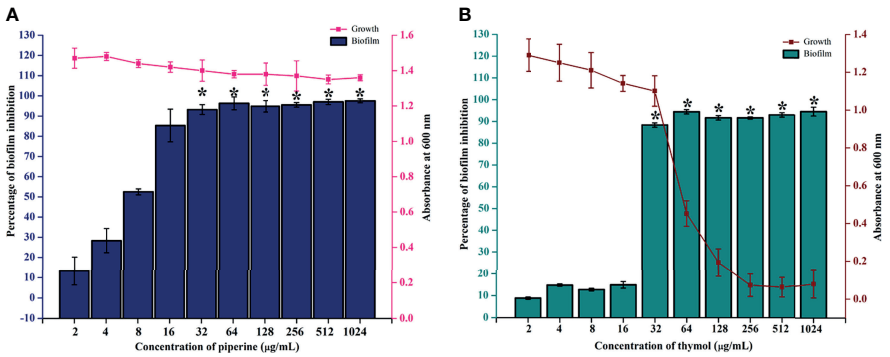

FIGURE 1 | Determination of MBIC of piperine and thymol against *C. albicans*. **(A)** Piperine and **(B)** thymol at the 32-µg/ml concentration significantly reduced the biofilm formation without affecting the growth. Error bars represent standard deviations from the mean, and * indicates significance $p < 0.05$.

combinations, the antibiofilm efficacy of the synergistic combinations was found to be higher (**Figure 2B**). The heatmap displaying the synergistic antibiofilm efficacy of piperine and thymol for clinical strains of *C. albicans* is provided in **Supplementary Figure 2**.

Non-Growth Inhibitory Effect of Combinations of Piperine and Thymol

The effect of combinations of piperine and thymol on the growth of *C. albicans* was assessed through spot assay and CFU analysis. Individual and combinations of piperine and thymol were not found to exhibit any growth inhibitory effect on *C. albicans* as observed through the spot assay (**Figure 3A**). Control and synergistic combinations of piperine and thymol-treated *C. albicans* were spread plated in order to identify alterations in the CFU, if any. No significant change in CFU/mL was observed between the control and synergistic combinations treated, which validates that the combinatorial antibiofilm effect of piperine and thymol is not due to growth inhibition but rather to the phytochemical target only of the biofilm formation and virulence of the pathogen (**Figure 3B**).

Piperine and Thymol Combination Influenced the Adhered Biofilm Cells of *C. albicans*

Biofilm cells of *C. albicans* in the absence and presence of individual and synergistic combinations of piperine and thymol were subjected to CFU analysis. It is observed that the phytocompounds reduced the number of adhered biofilm cells drastically. A log reduction of more than 2 in biofilm cells was observed in treatment with phytocompounds at MBIC and synergistic combinations (**Figure 4**).

Biofilm Architecture of *C. albicans* Under the Influence of Individual and Synergistic Combinations of Piperine and Thymol

Adhesion of *C. albicans* cells to the glass surface was impaired by the influence of phytochemicals. Yeast cells entangled within the hyphal mesh were observed in the control whereas scarcely dispersed yeast cells without hyphal extension were observed in the *C. albicans* treated with MBIC of piperine and thymol. The individual effect of the concentrations in synergistic combinations was also analysed. Piperine at 8-µg/ml concentration resulted in few hyphal elongations. Although the number of adhered cells was lesser than the control, other individual concentrations in synergistic combinations of piperine and thymol resulted in hyphal morphogenesis, whereas the synergistic combinations of piperine and thymol significantly impeded the biofilm formation and hyphal elongation (**Figure 5**).

Synergistic Antihyphal Efficacy of Piperine and Thymol

Since the filamentous morphology of *C. albicans* was inhibited by the synergistic combinations of piperine and thymol in the microscopic observation, synergistic antihyphal activity was appraised. Compared to the individual MBIC of phytochemicals,

TABLE 2 | FICI values of various combinations of piperine and thymol.

Concentration of thymol in µg/mL	Concentration of piperine in µg/mL					
	0	**2**	**4**	**8**	**16**	**32**
0	–	–	–	–	*	*
2	–	0.125	0.1875	**0.3125***	0.5625*	1.0625*
4	–	0.1875	0.25	**0.375***	0.625*	1.125*
8	–	0.3125	**0.375***	**0.5***	0.75*	1.25*
16	–	0.5625	0.625*	0.75*	1*	1.5*
32	*	1.0625*	1.125*	1.25*	1.5*	2*

*The FIC indices of piperine and thymol combinations at different concentrations are tabulated in **Table 1**. The sign "*" indicates the presence of antibiofilm activity in individual and combination of drugs, and "-" indicates the absence of antibiofilm activity. The inhibition of biofilm was observed at most of the combinations, but the synergistic effect of piperine and thymol was observed at combinations of 8 + 8 µg/ml; 8 + 4 µg/ml; 8 + 2 µg/ml and 4 + 8 µg/ml of piperine and thymol with FIC indices of 0.5, 0.375, 0.3125 and 0.375 respectively (highlighted).*

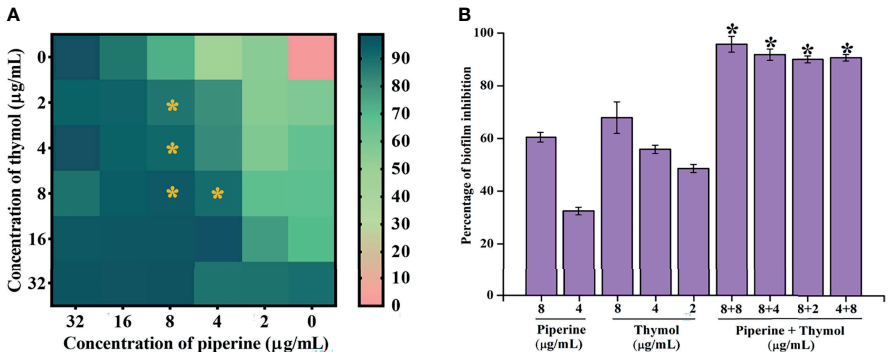

FIGURE 2 | Synergistic antibiofilm efficacy of piperine and thymol against *C. albicans*. **(A)** Interaction of piperine and thymol in exhibiting antibiofilm efficacy was appraised through checkerboard analysis. Heatmap displays the percentage of biofilm inhibition by various combinations of piperine and thymol. Four different synergistic antibiofilm combinations of piperine and thymol were identified—8 + 8, 8 + 4, 8 + 2, and 4 + 8 µg/ml. **(B)** Comparative analysis of individual and combinatorial efficacy of piperine and thymol at synergistic combination concentrations against biofilm of *C. albicans*. Error bars represent standard deviations from the mean, and * indicates significance $p < 0.05$.

a combination of piperine and thymol at a concentration of 8 + 8 µg/ml ensued in a synergistic antihyphal activity. The filamentous structure around the entire surface of the *C. albicans* colony was observed in control. Piperine at MBIC completely inhibited the hyphal growth. Synergistic antihyphal activity was observed at 8 + 8 µg/ml of piperine and thymol with an FIC index of 0.5. Certain other combinations were found to exhibit antihyphal activity, but the FICI was greater than 0.5 (**Figure 6**).

Impact of Piperine and Thymol on Phenotypic Switching Between Yeast and Hyphal Forms

Phenotypic switching in *C. albicans* is one of the major virulence determinants. Under hyphal-inducing conditions, the ability of the phytochemicals piperine and thymol in inhibiting the hyphal protrusion and relapsing the hyphal form to yeast morphology was assessed. FBS favourably enhanced the filamentous morphology in control, whereas the MBIC of piperine and thymol completely suppressed the filamentation. Similarly, only yeast cells were observed in the synergistic combinations (**Figure 7**). Contrarily, synergistic combinations of piperine and thymol limited and reversed the hyphal extension (**Figure 8**).

Post-Antihyphal Effect

A brief exposure of *C. albicans* to individual and synergistic combinations of piperine and thymol limited the extension of filamentous morphology in hyphal inducing conditions. Also, yeast cell morphology was observed which could be due to the reversal of extended hyphae to yeast cells (**Figure 9**).

Synergistic Combinations of Piperine and Thymol Enhanced the Susceptibility of *C. albicans* to Antifungals

The antifungal susceptibility of *C. albicans* treated with individual and synergistic combinations of piperine and thymol was found to be increased. The zone of inhibition in *C. albicans* exposed to

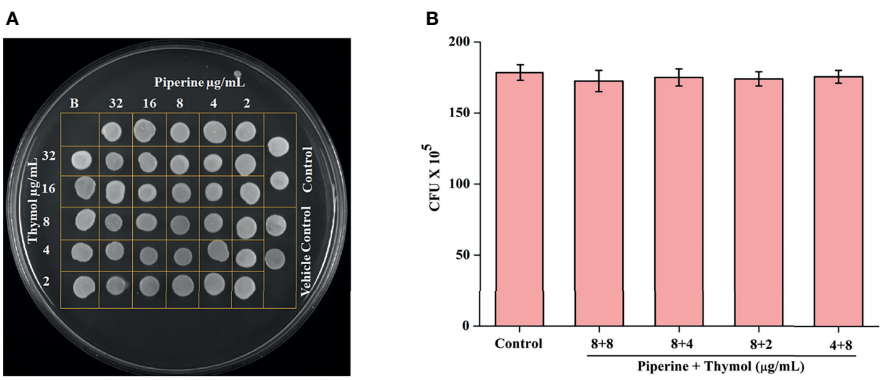

FIGURE 3 | Non-growth inhibitory effect of synergistic combinations of piperine and thymol. **(A)** Spot assay displaying the growth of *C. albicans* treated with the individual and combined activity of piperine and thymol as compared to the control. **(B)** Bar graph representing the number of CFU by *C. albicans* grown in the absence and presence of identified synergistic combinations. No significant reduction in the growth was observed.

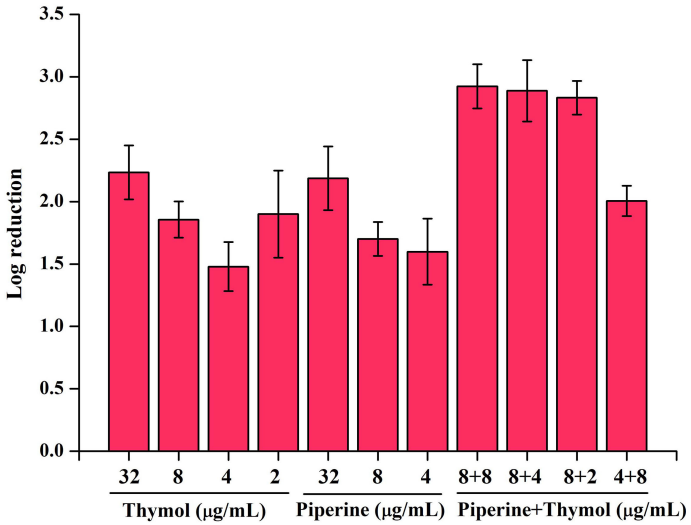

FIGURE 4 | Effect of individual and synergistic combinations of piperine and thymol on biofilm cells of *C. albicans*. Adhered biofilm cells were found to be reduced above 2 log in MBIC of individual phytocompounds and their synergistic combinations.

synergistic combinations of piperine and thymol was comparatively equal or higher than the inhibition in *C. albicans* exposed to MBIC of individual phytochemicals (**Table 3**).

Regulation in the Expression of Candidate Virulence Genes

Proficiency to inhibit biofilm formation and hyphal morphogenesis and to control the phenotypic switching between yeast and hyphal forms by the synergistic combination of piperine and thymol against *C. albicans* was validated through real-time PCR. Negative regulators of filamentation growth such as *nrg1* and *tup1* were upregulated whereas the transcriptional activator of filamentous growth, *ume6*, was downregulated. Filamentation and adhesion-related genes such as *efg1*, *cph1*, *eap1*, *ras1*, *als1* and *ece1* were found to be downregulated, which further corroborates the *in vitro* proficiency of piperine and thymol such as antibiofilm, antihyphal and control of phenotypic switch in *C. albicans* (**Figure 10**).

Non-Toxic Nature of Piperine, Thymol and Their Combinations

Phytocompounds piperine, thymol and their synergistic combinations were subjected to toxicity analysis on human red

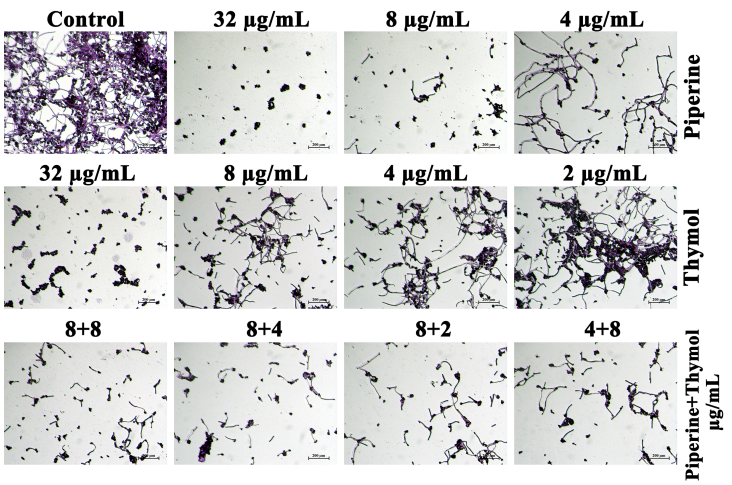

FIGURE 5 | Microscopic visualisation of *C. albicans* biofilm formed under the influence of the synergistic effect of piperine and thymol. Biofilm of *C. albicans* without any treatment is encased with the conglomeration of yeast cells and filaments. Scarcely distributed yeast cells alone were found in the piperine and thymol-treated *C. albicans*. Few hyphal elongations were observed in treatment with sub-BIC of the phytochemicals. Synergistic combinations of piperine and thymol reduced the adherence of cells and filamentous morphology.

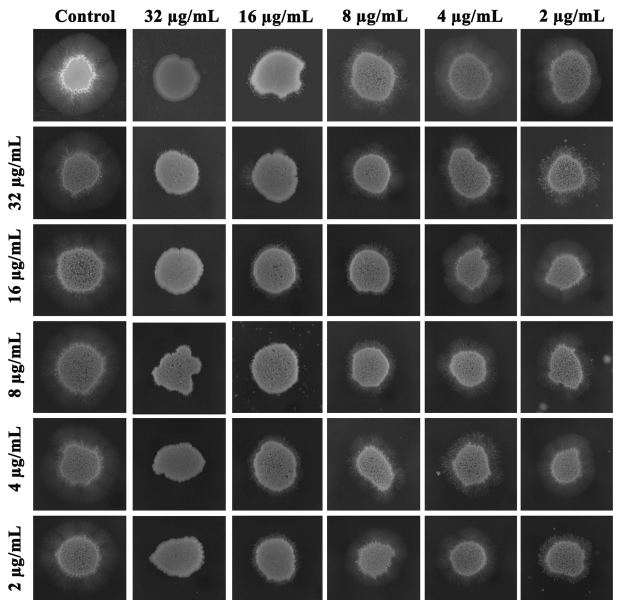

FIGURE 6 | Antihyphal activity of individual and combination of piperine and thymol. Supplementation of FBS, a filament-inducing component, resulted in increased hyphal elongation around the cell surface of untreated *C. albicans*, whereas piperine at MBIC resulted in complete inhibition of hyphal form. Thymol at MBIC slightly inhibited the filamentation. At the 8 + 8-µg/ml concentration, synergistic antihyphal activity was observed with a FICI of 0.5.

blood cells and HBECs. No toxic effect was observed at the tested concentrations in both erythrocytes and HBECs. In erythrocytes, the positive control Triton X-100 completely lysed the red blood cells as the treatment with phytocompounds did not lyse any detectable number of erythrocytes (**Figure 11A**). Similarly, no morphological alterations were observed in HBECs treated with phytocompounds whereas positive control hydrogen peroxide instigated alterations in the normal morphology of the cells (**Figure 11B**). These results demonstrate that the phytocompounds alone or in combination did not instigate any adverse effects to human erythrocytes or HBECs and thus can be considered safe for human application.

DISCUSSION

C. albicans being a eukaryotic organism shares several cellular mechanisms with humans. Thus, the identification and development of novel antifungal drugs without any adverse secondary effects on the human beings are a major confrontation. Conventional antifungal drugs target mechanisms or the end product that differs between fungi and humans. One such is the ergosterol biosynthetic pathway (Ksiezopolska and Gabaldón, 2018). Nevertheless, the emergence of resistance strains, including those with multidrug resistance are constantly being reported in recent years (Pfaller et al., 2013; Pfaller et al., 2014; Lockhart et al., 2017; Krishnasamy et al., 2020). To combat these challenges, the search for alternatives to antibiotics has been the recent theme of research. Numerous approaches such as antibiofilm therapy, use of antimicrobial peptides and phage therapy are recently being experimented for the treatment of infectious diseases to combat the persistent biofilm-associated infections. Among the various strategies that followed, the combinatorial approach is an emerging trend (León-Buitimea et al., 2020). The combination of drugs offers numerous advantages over monotherapy which includes reduced dosage, synergistic response, decreased possibility of resistance development and reduced toxicity (Lehár et al., 2009; Ahmed et al., 2014). To surmount these drawbacks, in the present investigation, the blended use of two emerging approaches such as antibiofilm

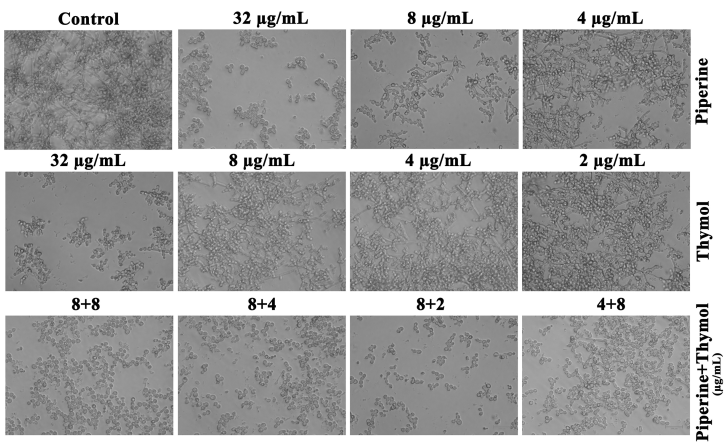

FIGURE 7 | Impediment of phenotypic switch between yeast to hyphal form. Extension of hyphae was completely arrested by piperine and thymol at individual MBIC as well the identified synergistic combinations. Few filamentous extensions were observed in *C. albicans* treated with individual phytochemicals at the concentration present in synergistic combinations.

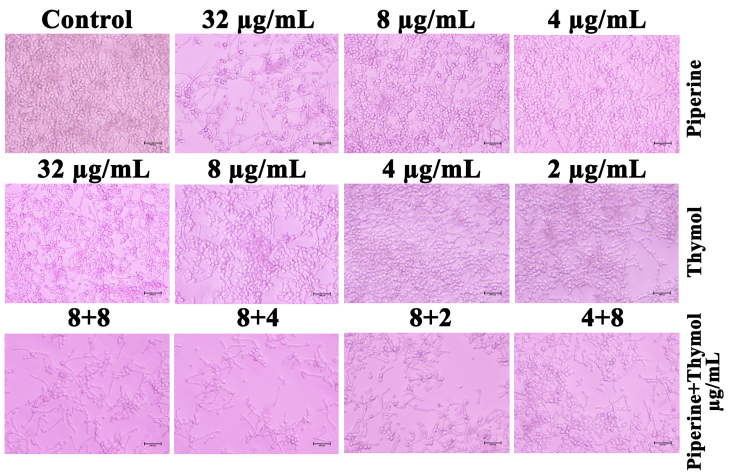

FIGURE 8 | Reversion of hyphal to yeast morphology. Synergistic combinations of piperine and thymol exhibited proficiency in limiting and reverting the hyphal extension to yeast form.

therapy and the combinatorial strategy has been employed to control the oral candidiasis, which is a biofilm-mediated *C. albicans* infection.

Initially, the antibiofilm potential of piperine and thymol was evaluated using the standard crystal violet procedure. Alongside, the effect of these phytochemicals on the growth of *C. albicans* was also assessed as a potential antibiofilm agent should not affect the growth and vitality of the organism. The results displayed that piperine has no detrimental effects on the viability of *C. albicans* even at the highest tested concentration (1,024 µg/ml) whereas at 32-µg/ml concentration, more than 90% of *C. albicans* biofilm was found to be inhibited. Thymol was found to be slightly antifungal at higher concentrations. Hence, for thymol, 32 µg/ml was considered as BIC where more than 87% of biofilm inhibition was observed. Both the phytochemicals were found to be active against the biofilm of clinical isolates also but at slightly varying concentrations. The synergistic interaction between piperine and thymol was assessed through checkerboard assay. The interaction between piperine and thymol was found to exhibit synergistic activity. Four synergistic combinations were identified for the interaction between phytochemicals piperine and thymol, namely piperine + thymol combinations: 8 + 4 µg/ml; 8 + 4 µg/ml; 8 + 2 µg/ml and 4 + 8 µg/ml for the reference strain. Similarly, different combinations of piperine and thymol were found to exhibit synergistic antibiofilm activity against clinical isolates. Augmented antibiofilm activity was displayed by the synergistic combinations than the individual drugs in the concentration included in combinations. The possible growth inhibitory effect of the identified synergistic combinations was assessed through spot and CFU assay. No detrimental changes in the viability or significant changes in the

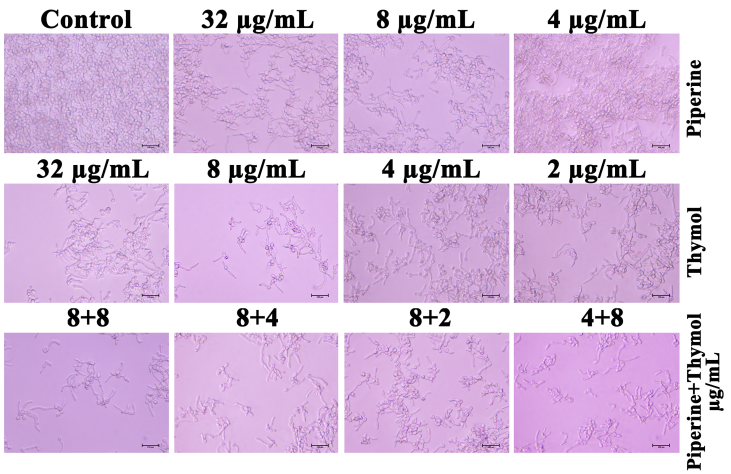

FIGURE 9 | Short-term exposure of *C. albicans* cells with individual and synergistic combinations of piperine and thymol reduced/delayed the hyphal elongation process.

TABLE 3 | Susceptibility of *C. albicans* to antifungals in the absence and presence of individual and synergistic combinations of piperine and thymol.

		Zone of inhibition in mm			
		Miconazole	**Itraconazole**	**Ketoconazole**	**Nystatin**
Control		26	16	26	17
Piperine (µg/mL)	**32**	27	17	28	18
	8	28	17	28	20
	4	30	18	29	18
Thymol (µg/mL)	**32**	29	20	30	19
	8	29	19	29	22
	4	28	18	28	19
	2	27	19	31	20
Piperine + thymol (µg/mL)	**8+8**	29	19	28	22
	8+4	29	21	29	21
	8+2	29	21	29	20
	4+8	29	18	26	17

number of cells were found between *C. albicans* grown in the absence and presence of synergistic combinations of piperine and thymol. Hence, it is evident that the identified synergistic combinations were found to exhibit antibiofilm activity without any effect on the growth of *C. albicans*. The *C. albicans* biofilm which is a conglomerate of yeast cells and hyphal forms along with the extracellular matrix is a major virulence attribute for persistent and recurrent infection. The effect of piperine and thymol combinations on the inhibition of biofilm formation was further validated through light microscopic analysis, and the results revealed that the synergistic combinations were effective in inhibiting the surface adherence of the cells as well as the hyphal elongation. Further, the combinatorial effect of piperine and thymol against the hyphal development, which is one of the major virulence factors of *C. albicans* required for the establishment of invasive infection, was assessed through solid agar assay. Various combinations of piperine and thymol were found to exhibit hyphal inhibitory activity, but only one synergistic combination with hyphal inhibitory activity was identified for piperine and thymol combinations. As the hyphal elongation was found to be suppressed, the effect of the synergistic combinations on the phenotypic switching ability of *C. albicans* was evaluated. Both yeast-to-hyphal transition and hyphal-to-yeast transition were significantly inhibited by the synergistic combinations which elucidate that the invading ability of *C. albicans* could be reduced when treated with piperine and thymol. Furthermore, the limited duration exposure of both the phytochemicals exhibited an antihyphal effect.

The *in vitro* results were validated through gene expressional analysis and found to be comparable. *nrg1* and *tup1* are negative transcriptional regulators of filamentous growth (Braun and Johnson, 1997; Braun et al., 2001). The expression of *nrg1* and *tup1* was found to be upregulated under the influence of piperine and thymol. In contrast, *ume6*, a positive regulator of the filamentation morphology, was found to be significantly downregulated. *efg*1 is reported as one of the filamentous

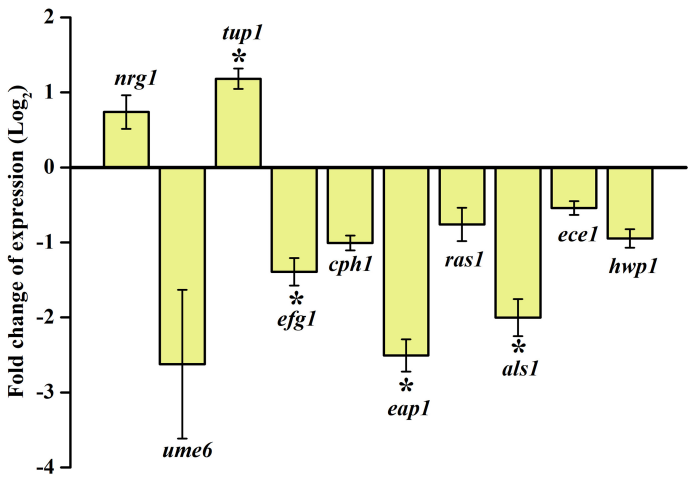

FIGURE 10 | Dynamics in the expression of candidate genes under the influence of synergistic combinations of piperine and thymol. Negative and positive regulators of filamentation, *nrg 1*, *tup1*, and *ume6* are upregulated and downregulated, respectively. Other genes responsible for adhesion, biofilm formation, and filamentous growth are found to be downregulated.

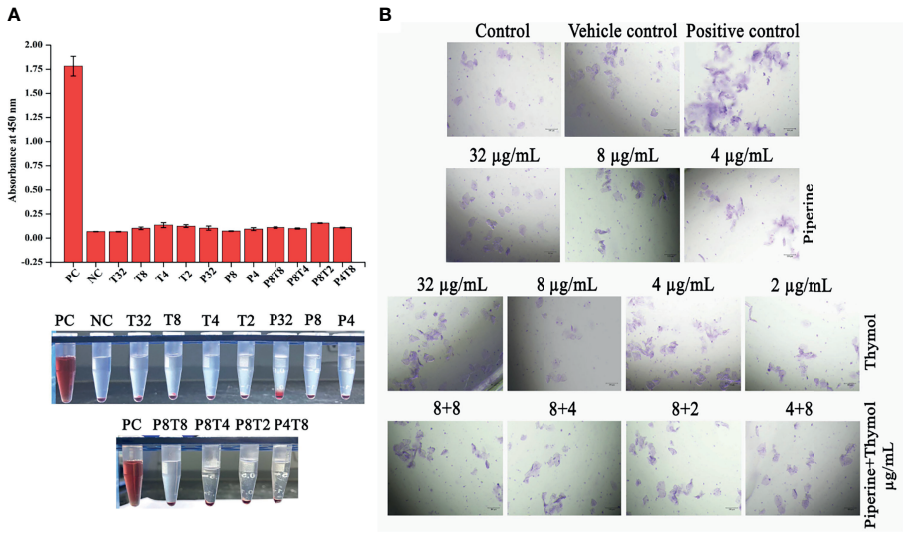

FIGURE 11 | Non-toxic nature of phytocompounds. **(A)** Effect of phytocompounds and their synergistic combinations on human erythrocytes. No haemolytic activity was observed. As no haemolysis was observed, the graph was plotted with absorbance. Positive control Triton X-100 completely lysed the erythrocytes. **(B)** No toxic effect was observed on HBECs when treated with individual and combination of phytochemicals. Hydrogen peroxide (positive control) instigated morphological alterations in HBECs.

morphogenetic regulators in *C. albicans* (Leng et al., 2001). Similarly, *cph1* also acts as an activator of filamentous growth (Braun and Johnson, 2000). *ras1* regulates the switch between yeast and hyphal forms (David, 2013). Whereas *als* and *eap1* encode for adhesins that facilitate the adherence of *C. albicans* to polystyrene and epithelial surfaces, *ece1* encodes for the candidalysin that regulates various virulence factors such as biofilm formation, adhesion and filamentation (Engku Nasrullah Satiman et al., 2020). All these virulence regulators were found to be downregulated by the influence of piperine and thymol. No toxic effects were observed on erythrocytes or HBECs by individual or combined effect of piperine and thymol.

Altogether, these results suggest that piperine and thymol, two major bioactive components with diverse activities, can interact synergistically in exerting antibiofilm and antihyphal activity against *C. albicans*. Hence, a synergistic combination of piperine and thymol can be possibly used in the formulation of dentifrices that are specifically recommended for the treatment of oral candidiasis.

DATA AVAILABILITY STATEMENT

The original contributions presented in the study are included in the article/**Supplementary Material**. Further inquiries can be directed to the corresponding author.

ETHICS STATEMENT

The studies involving human participants were reviewed and approved by the Institutional Ethical Committee, Alagappa University, Karaikudi (IEC Ref No. IEC/AU/2018/5). The patients/participants provided their written informed consent to participate in this study.

AUTHOR CONTRIBUTIONS

SKP and AP designed the study. AP and SN performed the experiments. AP analysed the data, prepared the figures and tables and wrote the manuscript. SKP revised the manuscript. All authors have read and approved the final version of the manuscript.

ACKNOWLEDGMENTS

The authors thankfully acknowledge DST-FIST [Grant No. SR/FST/LSI-639/2015 (C)], UGC-SAP [Grant No. F.5-1/2018/DRS-II (SAP-II)], and DST PURSE [Grant No. SR/PURSE Phase 2/38 (G)] for providing instrumentation facilities. SKP is thankful to UGC for Mid-Career Award [F.19-225/2018 (BSR)] and RUSA 2.0 [F.24-51/2014-U, Policy (TN Multi-Gen), Department of Education, Government of India]. The authors thankfully acknowledge Dr. A. Wilson, School of Medicine, CUSM, Loma Linda, CA, USA, for vetting the manuscript.

SUPPLEMENTARY MATERIAL

The Supplementary Material for this article can be found online at: https://www.frontiersin.org/articles/10.3389/fcimb.2021.780545/full#supplementary-material

REFERENCES

Abraham, K. P., Sreenivas, J. A., Venkateswarulu, T. C., Indira, M. I., Babu, D. J., Diwakar, T. E., et al. (2012). Investigation of the Potential Antibiofilm Activities of Plant Extracts. *Int. J. Pharm. Pharm. Sci.* 4 (4), 282–285.

Ahmad, A., Khan, A., Manzoor, N., and Khan, L. A. (2010). Evolution of Ergosterol Biosynthesis Inhibitors as Fungicidal Against Candida. *Microbial. Pathogenesis* 48 (1), 35–41. doi: 10.1016/j.micpath.2009.10.001

Ahmed, A., Azim, A., Gurjar, M., and Baronia, A. K. (2014). Current Concepts in Combination Antibiotic Therapy for Critically Ill Patients. *Indian J. Crit. Care Med: Peer-Reviewed Off. Publ. Indian Soc. Crit. Care Med.* 18 (5), p.310. doi: 10.4103/0972-5229.132495

Bandara, H. M. H. N., Matsubara, V. H., and Samaranayake, L. P. (2017). Future Therapies Targeted Towards Eliminating Candida Biofilms and Associated Infections. *Expert Rev. Anti. Infect. Ther.* 15 (3), pp.299–pp.318. doi: 10.1080/14787210.2017.1268530

Braga, P. C., Alfieri, M., Culici, M., and Dal Sasso, M. (2007). Inhibitory Activity of Thymol Against the Formation and Viability of Candida Albicans Hyphae. *Mycoses* 50 (6), 502–506. doi: 10.1111/j.1439-0507.2007.01412.x

Braga, P. C., Culici, M., Alfieri, M., and Dal Sasso, M. (2008). Thymol Inhibits Candida Albicans Biofilm Formation and Mature Biofilm. *Int. J.Antimicrob. Agents* 31 (5), pp.472–pp.477. doi: 10.1016/j.ijantimicag.2007.12.013

Braun, B. R., and Johnson, A. D. (1997). Control of Filament Formation in Candida Albicans by the Transcriptional Repressor TUP1. *Science* 277 (5322), 105–109. doi: 10.1126/science.277.5322.105

Braun, B. R., and Johnson, A. D. (2000). TUP1, CPH1 and EFG1 Make Independent Contributions to Filamentation in Candida Albicans. *Genetics* 155 (1), 57–67. doi: 10.1093/genetics/155.1.57

Braun, B. R., Kadosh, D., and Johnson, A. D. (2001). NRG1, a Repressor of Filamentous Growth in C. Albicans, Is Down-Regulated During Filament Induction. *EMBO J.* 20 (17), 4753–4761.

Chanda, S., and Rakholiya, K. (2011). Combination Therapy: Synergism Between Natural Plant Extracts and Antibiotics Against Infectious Diseases. *Microbiol. Book Ser.* 1, 520–529.

Chandra, J., Mukherjee, P. K., Leidich, S. D., Faddoul, F. F., Hoyer, L. L., Douglas, L. J., et al. (2001). Antifungal Resistance of Candidal Biofilms Formed on Denture Acrylic *In Vitro*. *J. Dental Res.* 80 (3), 903–908. doi: 10.1177/00220345010800031101

Cullen, P. J., and Sprague, G. F. Jr. (2012). The Regulation of Filamentous Growth in Yeast. *Genetics* 190 (1), pp.23–pp.49. doi: 10.1534/genetics.111.127456

David, R. (2013). Ras1 as a Switch for Candida Albicans. *Nat. Rev. Microbiol.* 11 (7), pp.431–pp.431. doi: 10.1038/nrmicro3061

de Oliveira Mima, E. G., Pavarina, A. C., Dovigo, L. N., Vergani, C. E., de Souza Costa, C. A., Kurachi, C., et al. (2010). Susceptibility of Candida Albicans to Photodynamic Therapy in a Murine Model of Oral Candidosis. *Oral. Surg. Oral. Med. Oral. Pathol. Oral. Radiol. Endodontol.* 109 (3), 392–401. doi: 10.1016/j.tripleo.2009.10.006

Engku Nasrullah Satiman, E. A. F., Ahmad, H., Ramzi, A. B., Abdul Wahab, R., Kaderi, M. A., Wan Harun, W. H. A., et al. (2020). The Role of Candida Albicans Candidalysin ECE1 Gene in Oral Carcinogenesis. *J. Oral. Pathol. Med.* 49 (9), pp.835–pp.841. doi: 10.1111/jop.13014

Fisher, B. M., Lamey, P. J., Samaranayake, L. P., MacFarlane, T. W., and Frier, B. M. (1987). Carriage of Candida Species in the Oral Cavity in Diabetic Patients: Relationship to Glycaemic Control. *J. Oral. Pathol. Med.* 16 (5), 282–284. doi: 10.1111/j.1600-0714.1987.tb01494.x

Krishnasamy, L., Rubini, D., Senthilganesh, J., Saikumar, C., Kumaramanickavel, G., Aruni, A. W., et al. (2020). Phylogenetic Characterization of Biofilm Forming Multidrug Resistant Candida Albicans and Non Albicans Candida Causing Vulvovaginal Candidiasis. *Gene Rep.* 19, 100644. doi: 10.1016/j.genrep.2020.100644

Ksiezopolska, E., and Gabaldón, T. (2018). Evolutionary Emergence of Drug Resistance in Candida Opportunistic Pathogens. *Genes* 9 (9), 461. doi: 10.3390/genes9090461

Kuhn, D. M., and Ghannoum, M. A. (2004). Candida Biofilms: Antifungal Resistance and Emerging Therapeutic Options. *Curr. Opin. Invest Drugs (London England: 2000)* 5 (2), pp.186–pp.197.

LaFleur, M. D., Qi, Q., and Lewis, K. (2010). Patients With Long-Term Oral Carriage Harbor High-Persister Mutants of Candida Albicans. *Antimicrob. Agents Chemother.* 54 (1), 39–44. doi: 10.1128/AAC.00860-09

Lehár, J., Krueger, A. S., Avery, W., Heilbut, A. M., Johansen, L. M., Price, E. R., et al. (2009). Synergistic Drug Combinations Tend to Improve Therapeutically Relevant Selectivity. *Nat. Biotechnol.* 27 (7), pp.659–pp.666. doi: 10.1038/nbt.1549

Leng, P., Lee, P. R., Wu, H., and Brown, A. J. (2001). Efg1, A Morphogenetic Regulator in Candida Albicans, Is a Sequence-Specific DNA Binding Protein. *J. Bacteriol.* 183 (13), pp.4090–4093. doi: 10.1128/JB.183.13.4090-4093.2001

León-Buitimea, A., Garza-Cárdenas, C. R., Garza-Cervantes, J. A., Lerma-Escalera, J. A., and Morones-Ramírez, J. R. (2020). The Demand for New Antibiotics: Antimicrobial Peptides, Nanoparticles, and Combinatorial Therapies as Future Strategies in Antibacterial Agent Design. *Front. Microbiol.* 11, 1669. doi: 10.3389/fmicb.2020.01669

Lockhart, S. R., Etienne, K. A., Vallabhaneni, S., Farooqi, J., Chowdhary, A., Govender, N. P., et al. (2017). Simultaneous Emergence of Multidrug-Resistant Candida Auris on 3 Continents Confirmed by Whole-Genome Sequencing and Epidemiological Analyses. *Clin. Infect. Dis.* 64 (2), pp.134–pp.140. doi: 10.1093/cid/ciw691

Luque, A. G., Biasoli, M. S., Tosello, M. E., Binolfi, A., Lupo, S., and Magaró, H. M. (2009). Oral Yeast Carriage in HIV-Infected and Non-Infected Populations in Rosario, Argentina. *Mycoses* 52 (1), 53–59. doi: 10.1111/j.1439-0507.2008.01542.x

Martinez, L. R., and Fries, B. C. (2010). Fungal Biofilms: Relevance in the Setting of Human Disease. *Curr. Fungal Infect. Rep.* 4 (4), pp.266–pp.275. doi: 10.1007/s12281-010-0035-5

Martins, M., Henriques, M., Ribeiro, A. P., Fernandes, R., Gonçalves, V., Seabra, Á., et al. (2010). Oral Candida Carriage of Patients Attending a Dental Clinic in Braga, Portugal. *Rev. Iberoam. Micologia* 27 (3), 119–124. doi: 10.1016/j.riam.2010.03.007

Meurman, J. H., Pärnänen, P., Seneviratne, C. J., Samaranayake, L. P., Saarinen, A. M., and Kari, K. (2011). Prevalence and Antifungal Drug Sensitivity of Non-Albicans Candida in Oral Rinse Samples of Self-Caring Elderly. *Gerodontology* 28 (4), 246–252. doi: 10.1111/j.1741-2358.2010.00407.x

Muthamil, S., Prasath, K. G., Priya, A., Precilla, P., and Pandian, S. K. (2020). Global Proteomic Analysis Deciphers the Mechanism of Action of Plant Derived Oleic Acid Against Candida Albicans Virulence and Biofilm Formation. *Sci. Rep.* 10 (1), pp.1–pp.17. doi: 10.1038/s41598-020-61918-y

Nett, J. E., Marchillo, K., Spiegel, C. A., and Andes, D. R. (2010). Development and Validation of an In Vivo Candida Albicans Biofilm Denture Model. *Infect. Immun.* 78 (9), 3650–3659. doi: 10.1128/IAI.00480-10

Pfaller, M. A., Andes, D. R., Diekema, D. J., Horn, D. L., Reboli, A. C., Rotstein, C., et al. (2014). Epidemiology and Outcomes of Invasive Candidiasis Due to non-Albicans Species of Candida in 2,496 Patients: Data From the Prospective Antifungal Therapy (PATH) Registry 2004–2008. *PloS One* 9 (7), p.e101510. doi: 10.1371/journal.pone.0101510

Pfaller, M. A., and Diekema, D. J. (2007). Epidemiology of Invasive Candidiasis: A Persistent Public Health Problem. *Clin. Microbiol. Rev.* 20 (1), 133–163. doi: 10.1128/CMR.00029-06

Pfaller, M. A., Messer, S. A., Woosley, L. N., Jones, R. N., and Castanheira, M. (2013). Echinocandin and Triazole Antifungal Susceptibility Profiles for Clinical Opportunistic Yeast and Mold Isolates Collected From 2010 to 2011: Application of New CLSI Clinical Breakpoints and Epidemiological Cutoff Values for Characterization of Geographic and Temporal Trends of Antifungal Resistance. *J. Clin. Microbiol.* 51 (8), 2571–2581. doi: 10.1128/JCM.00308-13

Priya, A., and Pandian, S. K. (2020). Piperine Impedes Biofilm Formation and Hyphal Morphogenesis of Candida Albicans. *Front. Microbiol.* 11, 756. doi: 10.3389/fmicb.2020.00756

Ramage, G., Tomsett, K., Wickes, B. L., López-Ribot, J. L., and Redding, S. W. (2004). Denture Stomatitis: A Role for Candida Biofilms. *Oral. Surg. Oral. Med. Oral. Pathol. Oral. Radiol. Endodontol.* 98 (1), 53–59. doi: 10.1016/j.tripleo.2003.04.002

Rautemaa, R., and Ramage, G. (2011). Oral Candidosis–Clinical Challenges of a Biofilm Disease. *Crit. Rev. Microbiol.* 37 (4), 328–336. doi: 10.3109/1040841X.2011.585606

Sardi, J. C. O., Scorzoni, L., Bernardi, T., Fusco-Almeida, A. M., and Giannini, M. M. (2013). Candida Species: Current Epidemiology, Pathogenicity, Biofilm Formation, Natural Antifungal Products and New Therapeutic Options. *J. Med. Microbiol.* 62 (1), pp.10–pp.24. doi: 10.1099/jmm.0.045054-0

Schauer, F., and Hanschke, R. (1999). Zur Taxonomie Und Ökologie Der Gattung Candida: Taxonomy and Ecology of the Genus Candida. *Mycoses* 42 (S1), 12–21. doi: 10.1111/j.1439-0507.1999.tb04521.x

Senpuku, H., Sogame, A., Inoshita, E., Tsuha, Y., Miyazaki, H., and Hanada, N. (2003). Systemic Diseases in Association With Microbial Species in Oral Biofilm From Elderly Requiring Care. *Gerontology* 49 (5), 301–309. doi: 10.1159/000071711

Shao, L. C., Sheng, C. Q., and Zhang, W. N. (2007). Recent Advances in the Study of Antifungal Lead Compounds With New Chemical Scaffolds. *Yao Xue Xue Bao= Acta Pharm. Sin.* 42 (11), 1129.

Uppuluri, P., Pierce, C. G., and López-Ribot, J. L. (2009). Candida Albicans Biofilm Formation and Its Clinical Consequences. *Future Microbiol.* 4 (10), pp.1235–1237. doi: 10.2217/fmb.09.85

Vanden Abbeele, A., De Meel, H., Ahariz, M., Perraudin, J. P., Beyer, I., and Courtois, P. (2008). Denture Contamination by Yeasts in the Elderly. *Gerodontology* 25 (4), 222–228. doi: 10.1111/j.1741-2358.2007.00247.x

Vila, T., Romo, J. A., Pierce, C. G., McHardy, S. F., Saville, S. P., and Lopez-Ribot, J. L. (2017). Targeting Candida Albicans Filamentation for Antifungal Drug Development. *Virulence* 8 (2), pp.150–pp.158. doi: 10.1080/21505594.2016.1197444

Wayne, P. A. (2008). *Reference Method for Broth Dilution Antifungal Susceptibility Testing of Filamentous Fungi; Approved Standard – Second Edition*. CLSI document M38-A2. Clinical and Laboratory Standards Institute (CLSI).

Williams, D., and Lewis, M. (2011). Pathogenesis and Treatment of Oral Candidosis. *J. Oral. Microbiol.* 3 (1), 5771. doi: 10.3402/jom.v3i0.5771

Williams, D., Silva, S. C., Malic, S., Kuriyama, T., and Lewis, M. A. (2012). Candida Biofilms and Oral Candidosis: Treatment and Prevention. *Periodontology 2000* 55 (1), 250–265.

Wilson, J. (1998). The Aetiology, Diagnosis and Management of Denture Stomatitis. *Br. Dental J.* 185 (8), 380–384. doi: 10.1038/sj.bdj.4809821

Conflict of Interest: The authors declare that the research was conducted in the absence of any commercial or financial relationships that could be construed as a potential conflict of interest.

frontiers in Cellular and Infection Microbiology

ORIGINAL RESEARCH
published: 14 February 2022
doi: 10.3389/fcimb.2022.833269

Cadaverine Is a Switch in the Lysine Degradation Pathway in *Pseudomonas aeruginosa* Biofilm Identified by Untargeted Metabolomics

Abigail Leggett[1,2,3], Da-Wei Li[4], Devin Sindeldecker[3,5], Amelia Staats[3,6], Nicholas Rigel[2], Lei Bruschweiler-Li[4], Rafael Brüschweiler[1,2,4,7] and Paul Stoodley[3,6,8,9]**

[1] Ohio State Biochemistry Program, The Ohio State University, Columbus, OH, United States, [2] Department of Chemistry and Biochemistry, The Ohio State University, Columbus, OH, United States, [3] Department of Microbial Infection and Immunity, The Ohio State University, Columbus, OH, United States, [4] Campus Chemical Instrument Center, The Ohio State University, Columbus, OH, United States, [5] Biomedical Sciences Graduate Program, The Ohio State University, Columbus, OH, United States, [6] Department of Microbiology, The Ohio State University, Columbus, OH, United States, [7] Department of Biological Chemistry and Pharmacology, The Ohio State University, Columbus, OH, United States, [8] Department of Orthopaedics, The Ohio State University, Columbus, OH, United States, [9] National Biofilm Innovation Centre (NBIC) and National Centre for Advanced Tribology at Southampton (nCATS), Mechanical Engineering, University of Southampton, Southampton, United Kingdom

OPEN ACCESS

Edited by:
Carina Almeida,
Instituto Nacional Investigaciao Agraria e Veterinaria (INIAV), Portugal

Reviewed by:
Sebastián A. Riquelme,
Columbia University Irving Medical Center, United States
Oana Ciofu,
University of Copenhagen, Denmark

***Correspondence:**
Rafael Brüschweiler
bruschweiler.1@osu.edu
Paul Stoodley
paul.stoodley@osumc.edu

Specialty section:
This article was submitted to Biofilms, a section of the journal Frontiers in Cellular and Infection Microbiology

Received: 11 December 2021
Accepted: 18 January 2022
Published: 14 February 2022

Citation:
Leggett A, Li D-W, Sindeldecker D, Staats A, Rigel N, Bruschweiler-Li L, Brüschweiler R and Stoodley P (2022) Cadaverine Is a Switch in the Lysine Degradation Pathway in Pseudomonas aeruginosa Biofilm Identified by Untargeted Metabolomics. Front. Cell. Infect. Microbiol. 12:833269. doi: 10.3389/fcimb.2022.833269

There is a critical need to accurately diagnose, prevent, and treat biofilms in humans. The biofilm forming *P. aeruginosa* bacteria can cause acute and chronic infections, which are difficult to treat due to their ability to evade host defenses along with an inherent antibiotic-tolerance. Using an untargeted NMR-based metabolomics approach, we identified statistically significant differences in 52 metabolites between *P. aeruginosa* grown in the planktonic and lawn biofilm states. Among them, the metabolites of the cadaverine branch of the lysine degradation pathway were systematically decreased in biofilm. Exogenous supplementation of cadaverine caused significantly increased planktonic growth, decreased biofilm accumulation by 49% and led to altered biofilm morphology, converting to a pellicle biofilm at the air-liquid interface. Our findings show how metabolic pathway differences directly affect the growth mode in *P. aeruginosa* and could support interventional strategies to control biofilm formation.

Keywords: biofilm, *Pseudomonas aeruginosa*, NMR-based metabolomics, cadaverine, bacterial metabolism, lysine degradation pathway

INTRODUCTION

Pseudomonas aeruginosa is a Gram-negative, opportunistic pathogen that exhibits resistance to many antibiotics, leading to acute and chronic infections in immunocompromised individuals (Hall-Stoodley et al., 2004). In 2017 the World Health Organization rated *P. aeruginosa* as a priority pathogen for research and development of new treatment strategies (Tacconelli et al., 2017). *P. aeruginosa's* persistence is in part attributed to its ability to form biofilms, in which the cells are

embedded in a gel-like matrix of self-produced extracellular polymeric substances (EPS), such as polysaccharides, proteins, and DNA. Biofilms have been shown to be up to 1,000 times more resistant to antibiotics than their planktonic counterparts and evade host immune responses (Lewis, 2001). *P. aeruginosa* biofilms are prevalent in respiratory illnesses such as cystic fibrosis, chronic wounds, and device related surgical site infections, among other conditions (Hall-Stoodley et al., 2004), yet there is a lack of effective strategies for diagnosis, prevention, and mitigation of biofilms.

Previous studies have begun to provide evidence for the vast physical and molecular differences between planktonic and biofilm growth modes, such as changes in motility (O'Toole and Kolter, 1998), quorum sensing (Wagner et al., 2007), and certain genomic (Whiteley et al., 2001), transcriptomic (Waite et al., 2005; Cornforth et al., 2018), and proteomic (Sauer et al., 2002) characteristics. Yet, these analyses identified many genes and proteins differentially expressed in biofilm that are not quorum-sensing related and some with no putative function (Whiteley et al., 2001; Sauer et al., 2002; Cornforth et al., 2018). This reflects that our understanding of signaling processes is still limited, and there likely exist unidentified regulons involved in biofilm formation. There is still much to uncover about the underlying biological mechanisms involved in the transition from planktonic to biofilm state along with a clear need for new experimental approaches and analysis methods (Toyofuku et al., 2016).

Complementary to other omics approaches, the comprehensive identification and quantification of small molecules involved in metabolic pathways (Sussulini, 2017) *via* metabolomics is particularly promising. Metabolites reflect the downstream changes of genes and enzymes, therefore, metabolomics will directly capture a snapshot of activity in the cells related to the growth mode (Sussulini, 2017). The power of nuclear magnetic resonance (NMR)-based metabolomics stems from its ability to highly reproducibly and non-destructively detect and quantify all abundant metabolites in a complex mixture in an untargeted manner (Gowda and Raftery, 2015; Markley et al., 2017).

Metabolomics has been used to gain insight into the molecular mechanism of biofilm formation in other bacterial pathogens (Yeom et al., 2013; Stipetic et al., 2016; Favre et al., 2018; Lu et al., 2019; Rieusset et al., 2020; Tang et al., 2021), but a comprehensive and quantitative analysis of metabolic changes involved in biofilm formation in *P. aeruginosa* is still missing (Gjersing et al., 2007; Zhang and Powers, 2012; Borgos et al., 2015). Detailed elucidation of major shifts in metabolic pathways in planktonic versus biofilm phenotypes has the potential to identify mechanisms of metabolic regulation, new targets for prevention and mitigation, and specific metabolic signatures for diagnosis of biofilms. Our study demonstrates NMR-based metabolomics as a viable approach to provide an unbiased, fully quantitative analysis to reveal metabolic pathway changes associated with the biofilm phenotype.

Here, we use 2D NMR spectroscopy to perform an untargeted metabolomics analysis of *P. aeruginosa* PAO1 grown planktonically and statically as a biofilm lawn for comparative analysis. Many metabolites identified show significant concentration changes between the two growth modes, including metabolites in the lysine degradation pathway (LDP). Using targeted metabolite supplementation with crystal violet (CV) staining and microscopy the differential role of this pathway could be unambiguously established suggesting new strategies toward biofilm monitoring and control.

MATERIALS AND METHODS

Bacterial Strains, Growth Media, and Culturing Methods

P. aeruginosa strain PAO1 (Wilson et al., 2004) cultures were grown in lysogeny broth (LB) (Sigma Aldrich) shaking at 220 rpm at 37°C for 24 hours (hrs) to $OD_{600} \approx 1.0$. Cultures were diluted in LB to $OD_{600} = 0.1$ then grown in LB culture or plated for metabolomics experiments. PAO1 was grown planktonically in 50 mL LB at 220 rpm at 37°C for 24 hrs (n = 9) and as a biofilm on LB plates (28.4 cm^2) containing 1.5% (w/v) agar, statically, at 37°C in 5% CO_2 for 48 hrs (n = 9). A red fluorescent PAO1 strain carrying a constitutively expressed Td-tomato producing plasmid pMQ400 (Locke et al., 2020), was cultured with 50 μg/mL gentamicin and utilized for visualization. PAO1 strain Xen41 (Xenogen Corp.), a luminescent strain carrying a constitutively expressed *lux*CDABE cassette, was utilized for visualization. CFU/mL (n = 6) and CFU/mL × cm^2 (n = 4) were measured for planktonic and biofilm cultures, respectively, for metabolomics measurements by the microdilution plating technique (Pfeltz et al., 2001).

Metabolomics Sample Preparation

Planktonic cultures were harvested by centrifugation at 4,300 × *g* for 20 min at 4°C. The pellet was washed by 1 mL phosphate-buffered saline (PBS) and transferred into a microcentrifuge tube (Eppendorf). Biofilm cultures were harvested by scraping with a sterile loop and transferring the biomass into two microcentrifuge tubes per sample due to the limited tube capacity. Samples were immediately re-suspended in 600 μL cold 1:1 methanol (Fisher)/double distilled H_2O (ddH_2O) for quenching. 300 μL of 1.4 mm stainless-steel beads (SSB14B) were added and cells were homogenized and lysed by a Bullet Blender (24 Gold BB24-AU by Next Advance) at a speed of 8 for 9 min at 4°C (Fuchs et al., 2016). An additional 500 μL 1:1 methanol/ddH_2O was added and the sample was centrifuged at 14,000 × *g* for 10 min at 4°C to remove beads and solid debris. The supernatant was transferred to a 50 mL conical tube and 1:1:1 methanol/ddH_2O/chloroform (Fisher) was added for a total volume of 24 mL (Bligh and Dyer, 1959; Leggett et al., 2019). The sample was vortexed and centrifuged at 4,300 × *g* for 20 min at 4°C for phase separation. The aqueous phase was collected, the methanol content was reduced using rotary evaporation, and lyophilized overnight. Before lyophilization 100 μL of each sample was saved for mass spectrometry (3.3% of total sample). For NMR measurements, the samples were re-suspended in 200 μL of NMR buffer (50 mM sodium phosphate buffer in D_2O at pH 7.2 with 0.1 mM DSS (4,4-dimethyl-4-silapentane-1-sulfonic

acid) for referencing) and centrifuged at 20,000 × *g* for 15 min at 4°C for removal of any residual protein content. The pellet was washed with 100 µL NMR buffer and the supernatants were combined and transferred to a 3 mm NMR tube with a Teflon cap and sealed with parafilm.

NMR Experiments and Processing

NMR spectra were collected at 298 K on a Bruker AVANCE III HD 850 MHz solution-state spectrometer equipped with a cryogenically cooled TCI probe. 2D ^{1}H-^{1}H TOCSY spectra were collected (Bruker pulse program "dipsi2ggpphpr") with 256 complex t_1 and 2048 complex t_2 points for a measurement time of 4 hrs. The spectral widths along the indirect and direct dimensions were 10,202.0 and 10,204.1 Hz and the number of scans per t_1 increment was 14. 2D ^{13}C-^{1}H HSQC spectra (Bruker pulse program "hsqcetgpsisp2.2") were collected with 512 complex t_1 and 2048 complex t_2 points for a measurement time of 16 hrs. The spectral widths along the indirect and direct dimensions were 34206.2 and 9375.0 Hz and the number of scans per t_1 increment was 32. The transmitter frequency offset values were 75 ppm in the ^{13}C dimension and 4.7 ppm in the ^{1}H dimension for all experiments. NMR data was zero-filled four-fold in both dimensions, apodized using a cosine squared window function, Fourier-transformed, and phase-corrected using NMRPipe (Delaglio et al., 1995).

NMR-Based Metabolomics Data Analysis

HSQC and TOCSY spectra were uploaded to the new COLMARq web server (**Supplementary Figure 2**) for peak picking, peak alignment, metabolite identification, metabolite quantification *via* Gaussian fitting, spectral normalization *via* a factor based on the average, median 30% peak volume ratios between an arbitrarily selected reference spectrum, and univariate statistical analysis between cohorts. Multivariate statistical analysis, hierarchical clustering analysis and heatmap visualization, and metabolite box plot analysis was performed *via* MetaboAnalyst (Xia et al., 2009). Metabolites were mapped to pathways *via* the KEGG PATHWAY database (Kanehisa et al., 2017).

Mass Spectrometry Experiments

Lyophilized sample was dissolved in 1:1 acetonitrile (ACN)/ddH_2O (v/v) with 0.1% formic acid and diluted 1×10^{8}-fold for direct injection into a Q Exactive Plus Orbitrap mass spectrometer by ThermoFisher Scientific (resolving power of 280,000 and mass accuracy of <1 ppm). The instrument was internally calibrated with Thermo Scientific Pierce LTQ Velos ESI positive ion calibration solution and run in positive ion mode. The ionization method was electrospray ionization of 3.5 V. The mass range was set to 50-500 m/z. The flow rate was 3 µL/min with 0.9 scans/sec. Peak picking was done by PyOpenMS using a Gaussian width of 0.5. Peaks with amplitudes larger than one order of magnitude above the background were included as true peaks.

Crystal Violet Staining Assays

Cadaverine (Sigma Aldrich) 5 or 10 mM stocks were prepared in LB and sterile filtered with a 0.2 µM filter. PAO1 overnight cultures were diluted to OD_{600} = 0.17 in LB with cadaverine in a concentration ranging from 0-3.30 mM. Cultures were plated in 96-well microtitre plates in at least triplicate, and incubated statically at 37°C in 5% CO_2 for 24 hrs. Outer edge wells were filled with PBS to avoid "edge effects" due to evaporation (Sudhir K. Shukla, 2017). OD_{600} was measured to quantify planktonic growth. Liquid media was gently aspirated and wells were washed three times with 150 µL PBS. Adhered biofilm was stained with 125 µL of 0.1% crystal violet (CV) in 20% ethanol in ddH_2O (v/v) for 30 min. CV was gently aspirated, wells were washed five times with 150 µL PBS, and CV was solubilized with 150 µL 33% glacial acetic acid in ddH_2O (v/v) by shaking gently at 100 rpm at room temperature for 25 min. CV was quantified at OD_{590} to report biofilm accumulation. LB blanks were averaged and subtracted from readings. Control PAO1 wells were averaged and all measurements were normalized to control measurements per plate and reported as percent change from control.

Confocal Laser Scanning Microscopy (CLSM)

PAO1 overnight cultures were diluted to OD_{600} = 0.17 in LB with 0 or 3.30 mM cadaverine in 35 × 10 mm confocal dishes and incubated statically at 37°C in 5% CO_2 for 24 hrs. Liquid media was aspirated and adhered biofilm was stained with SYTO 9 for 10 min and washed with PBS. CLSM stitched images were collected (n=5) with a laser power of 4.5% under 10X magnification using an Olympus FluoView FV10i CLSM. Mean gray scale value and surface area coverage were quantified using Fiji (Schindelin et al., 2012).

Culture Growth and Imaging By Photo, Dissecting Microscope, and IVIS

PAO1 Td-tomato or Xen41 cultures were grown similarly to CLSM cultures described above. iPhone 8 images were taken in a controlled well-lit environment. The air-liquid interface was imaged using an Amscope dissecting microscope with an MU500 camera. Xen41 light emission was detected with an IVIS Lumina II system (Caliper LifeSciences) as an indicator of biofilm activity.

Statistical Analysis

All assays were performed in at least three independent replicates. Two-tailed unpaired Student's t-tests were used for significant differences between groups. P-values below 0.05 were considered statistically significant. Metabolomics results were checked for multiple comparisons testing using the Benjamini-Hochberg false discovery rate (FDR) test (Benjamini and Hochberg, 1995). All error bars represent one standard error.

RESULTS

Untargeted Metabolomics Analysis of *P. aeruginosa* in Planktonic and Biofilm States

The metabolic differences between wild-type (WT) *P. aeruginosa* PAO1 grown in the free-floating planktonic and static lawn

biofilm phenotypes were identified by NMR-based metabolomics and further investigated following the workflow in **Figure 1**. Lawn biofilms are known to generate large amounts of biomass and have been used to mimic bacterial growth on soft surfaces such as mucosal surfaces and tissue (Dusane et al., 2019; Hoiby et al., 2019). After growth both planktonic and biofilm samples yielded cultures of similar cell numbers for processing for NMR measurements (**Supplementary Figure 1**). All 2D NMR spectra were semi-automatically analyzed using our newly developed in-house COLMARq web server (**Supplementary Figure 2**) Representative planktonic and biofilm 2D ^{13}C-^{1}H HSQC spectra are shown as color-coded overlays in **Figure 2A**, with 1,302 distinct cross-peaks reflecting the rich content of detectable metabolites in these samples. A large number of peaks were only present either in the planktonic or the biofilm cultures signifying the presence of metabolites unique to each phenotype (**Figure 2A**). Of all cross-peaks, 436 were matched to known metabolites in the COLMAR database (Bingol et al., 2016). The remaining 866 HSQC peaks belong to "unknown" metabolites (**Supplementary Table 1**).

Multivariate Analysis of Metabolomics Data by PCA and PLS-DA

Changes in quantitative metabolite concentrations were analyzed by both unsupervised and supervised multivariate statistical analysis methods, namely principal component analysis (PCA) and partial least squares discriminant analysis (PLS-DA) (**Figures 2B, C**). Both analyses organized the planktonic and biofilm samples into well-defined clusters and the groups did not show any overlap of the 95% confidence regions. The score plots of both analyses show a PC1 that comprises 75.2% of the variance in the entire data, which was dominated by the mean separation between the biofilm and planktonic sample cohorts. The PC2's comprise 13.8% and 6.0% of the data variance for PCA and PLS-DA, respectively, which mostly reflect intra-cohort variability.

Metabolites Differing Significantly Between Planktonic and Biofilm

All metabolites reported were identified with high confidence using the COLMARm method (Bingol et al., 2016) by querying ^{13}C-^{1}H HSQC spectra against the COLMAR database with subsequent confirmation by 2D ^{1}H-^{1}H TOCSY. A total of 66 unique metabolites, visualized in the heatmap in **Figure 2D**, were identified and quantified for comparison between planktonic and biofilm cohorts. Hierarchical clustering by Ward's method and Euclidean distance show biofilm and planktonic samples were distinctly clustered into two groups (**Figure 2D**). Among the 66 distinct metabolites detected, the majority showed significant differences between the planktonic and biofilm phenotypes. 26 metabolites had a fold change greater than two, 52 metabolites had a statistically significant difference with $p<0.05$, 44 metabolites with $p<0.01$, and 14 metabolites with $p<1.00\times10^{-7}$. An additional 14 metabolites showed no significant change (**Supplementary Table 2**) with many of them likely to be serving as housekeeping metabolites, including 11 amino acids and their conjugates or involvement in central metabolism, such as glycolysis and the TCA cycle.

For the comparative quantitative analysis, we treat the planktonic metabolite quantities as reference and report relative changes in the biofilm. Metabolites with the most notable differences, having a fold change greater than two and $p<0.05$, include 14 metabolites in biofilm that were significantly increased and 11 metabolites that were significantly decreased (**Supplementary Table 2**). Selected metabolites with interpreted potential roles are shown in **Figure 3**. A majority of metabolites

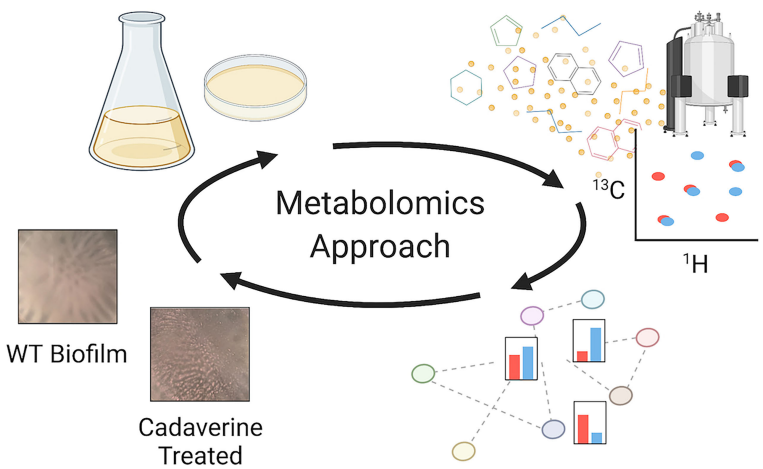

FIGURE 1 | Metabolomics workflow to perform untargeted NMR-based metabolomics measurements, identify major metabolite changes, and test the role of the metabolites of interest. From the top left following the arrows: planktonic and biofilm PAO1 samples are prepared, and metabolites are extracted and measured by NMR; metabolites are then quantified and mapped to pathways for a biological interpretation; differentially quantified metabolites are tested to interpret their role in mode of growth. For example, there are significant decreases in the cadaverine pathway metabolites in biofilm compared to planktonic. When cadaverine is supplemented to the culture, biofilm accumulation is significantly reduced and morphology is altered. Created with Biorender.com.

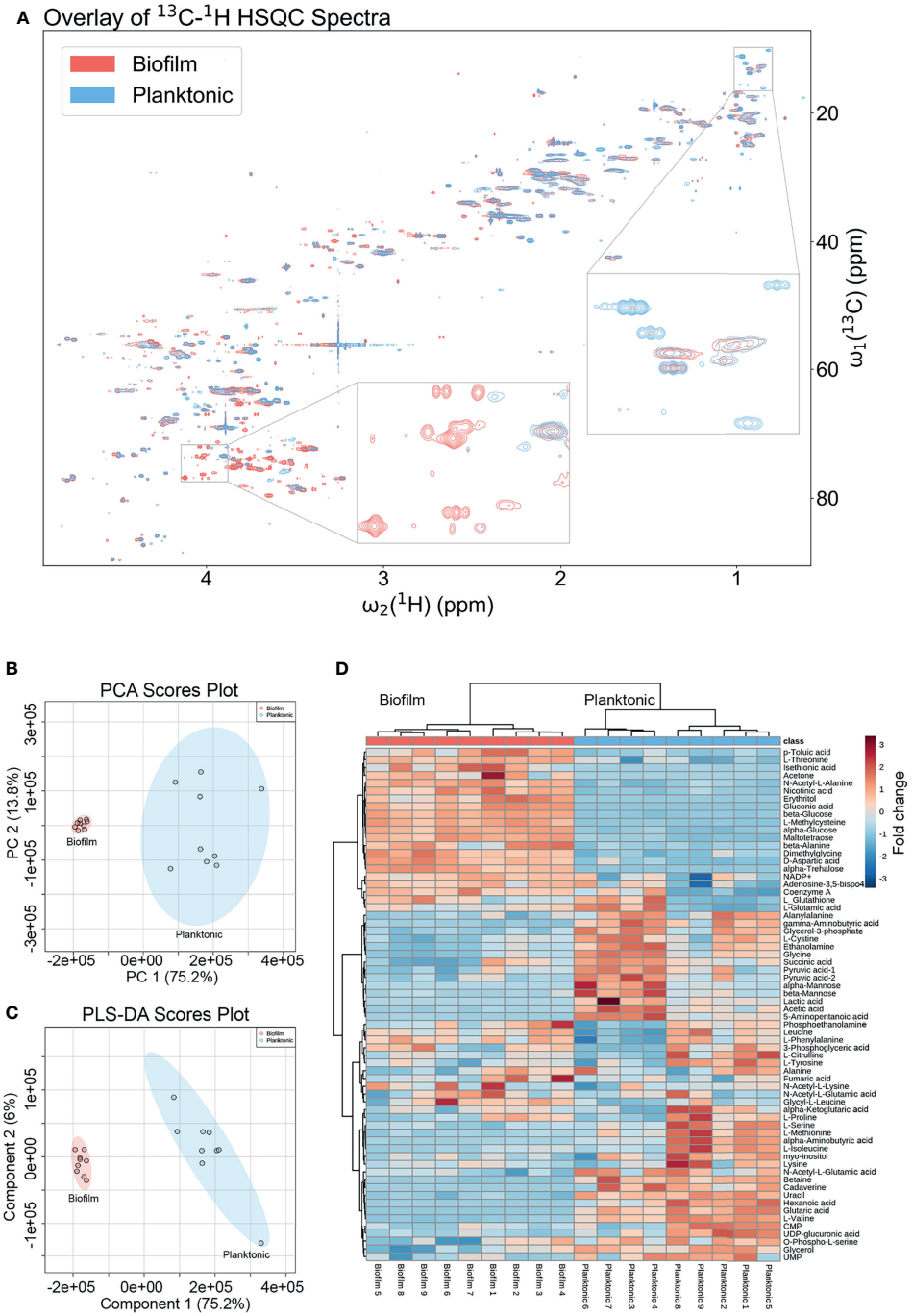

FIGURE 2 | Metabolomics data analysis shows many unique metabolic differences between the biofilm and planktonic phenotypes. **(A)** Overlay of a representative region of the 2D ^{13}C-^{1}H HSQC spectra of a representative biofilm (red; bottom) and planktonic (blue; top) culture with select regions enlarged exemplifying peaks unique to each growth mode. Statistical analysis of metabolomics data distinguishes between biofilm and planktonic cohorts. Two-dimensional score plots for **(B)** principal component analysis (PCA) and **(C)** partial least squares discriminant analysis (PLS-DA) of biofilm (red) and planktonic (blue) sample cohorts (n=9) based on quantitation of identified metabolites show clustering of sample cohorts with no overlap of the ellipses (ellipses represent 95% confidence intervals), displaying good separation between and repeatability within cohorts. The heatmap **(D)** uses hierarchical clustering by Ward's method and Euclidean distance to accurately cluster samples into their respective cohorts and the color scale shows metabolite fold changes between cohorts.

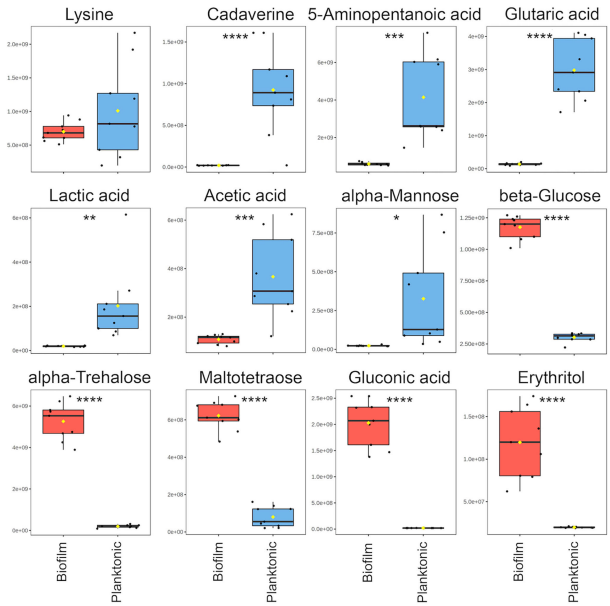

FIGURE 3 | Notable metabolite differences between planktonic and biofilm include intermediates of the cadaverine branch of the lysine degradation pathway (LDP), weak organic acids, and carbohydrate-related metabolites. Box plots represent a metabolite fold change analysis between biofilm (red) and planktonic (blue) cohorts (n=9). The black circles represent independent sample values, boxes represent upper and lower quartiles, black bars represent median, yellow diamonds (♦) represent mean value, whiskers represent minimum and maximum values, and asterisks denote significance (*$p < 0.05$, **$p < 0.01$, ***$p < 0.001$, ****$p < 0.0001$ by unpaired, two-tailed *t*-test).

whose abundance increased in biofilm were carbohydrate-related, such as mono- and disaccharides, sugar acids and alcohols, which increased from four to 102-fold. The only identified carbohydrate with the opposite trend was mannose, with about a six-fold decrease in biofilm. This is consistent with previous studies, which suggested that mannose acts as a competitive inhibitor of bacterial adherence by binding adhesion proteins or lectins in both *E. coli* and *P. aeruginosa* (Hauck et al., 2013; Scaglione et al., 2021). Weak organic acids (WOA) such as lactic and acetic acid were significantly decreased in biofilm about 10-fold and three-fold, respectively (**Figure 3**). A recent study showed that addition of lactic and acetic acid to culture in *E. coli* reduced production of extracellular polymeric substances, inhibited quorum sensing, and reduced biofilm formation (Amrutha et al., 2017). Therefore, lactic and acetic acid may also play a role in establishing growth mode in *P. aeruginosa*, favoring the planktonic phenotype.

In addition to the metabolites identified by querying the HSQC spectrum against known metabolites, 66.5% of the HSQC peaks belong to compounds that could not be matched to metabolites in the COLMAR database. Of these "unknown" peaks, 493 show statistically significant differences between planktonic and biofilm cohorts (**Supplementary Table 1**). Based on the average number of identified peaks per known metabolite, these "unknown" signals could belong to an estimated 75 additional metabolites differing significantly in quantity between phenotypes. Identification of the unknown metabolites and linking them to new proteins and biochemical pathways is an opportunity to advance our understanding of other biochemical changes that accompany the phenotypic changes and may offer new targets for biofilm control.

Identification of the Lysine Degradation Pathway for Its Possible Role in *P. aeruginosa* Growth Mode

Three metabolites including cadaverine (biofilm/planktonic = 0.02; $p = 8.74 \times 10^{-5}$), 5-aminopentanoic acid (biofilm/planktonic = 0.14; $p = 2.17 \times 10^{-4}$), and glutaric acid (biofilm/planktonic = 0.05; $p = 7.03 \times 10^{-8}$) (**Figures 3**, **4**) were found to be significantly decreased in biofilm and could be mapped on the cadaverine branch of the LDP (**Figure 4**) using the KEGG PATHWAY database (Fothergill and Guest, 1977; Indurthi et al., 2016; Kanehisa et al., 2017). The LDP is an important link in central metabolism as lysine is typically taken up from the growth media *via* transport channels and degraded to glutaric acid, which enters the tricarboxylic acid (TCA) cycle (Knorr et al., 2018). The majority of metabolites of the cadaverine branch of the LDP were detected and quantified by our NMR-based metabolomics analysis, namely lysine, cadaverine, 5-aminopentanoic acid, and glutaric acid (**Figure 4**). Since other intermediates of the LDP, namely 5-aminopentanal and glutarate semialdehyde, were not present in the COLMAR database, their presence based on NMR spectra alone is unknown. However, based on mass spectrometry they are likely to be present as at least one common adduct of each of these metabolites was detected within less than 0.77 ppm of their expected mass.

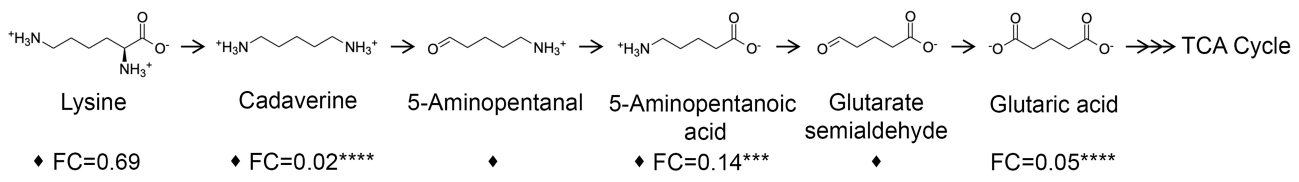

FIGURE 4 | Metabolites of the cadaverine branch of the lysine degradation pathway are significantly down-regulated in biofilm compared to planktonic cultures. Lysine is degraded to supplement the TCA cycle to increase cellular respiration. Metabolites identified and quantified by NMR show a fold change (FC) (biofilm/planktonic) (n=9) and asterisks denote significance (***$p < 0.001$, ****$p < 0.0001$ by unpaired, two-tailed *t*-test). Metabolites with at least one common adduct detected by mass spectrometry by direct injection in positive ion mode with a mass error of <0.77 ppm are denoted by a black diamond (♦).

All metabolites in the cadaverine pathway were detected by mass spectrometry for additional confirmation except for glutaric acid, which contains two carboxylic acid groups that are negatively charged and therefore may not be detectable in positive ion mode used here (**Supplementary Table 3**). While many metabolites of the cadaverine branch of the LDP were significantly different, lysine did not show a significant fold change (biofilm/planktonic = 0.69; p = 0.21) (**Figures 3**, **4**).

Exogenous Supplementation of Cadaverine Increases Planktonic Growth and Inhibits Biofilm Accumulation

Cadaverine belongs to a class of compounds known as polyamines, which have been reported to perform multiple roles in bacteria with links to cell growth, proliferation, bacterial carcinogenesis, escape from phagolysosomes, bacteriocin production, natural product synthesis, toxin activity, protection from oxidative and acidic stress, and electrostatic interactions (Shah and Swlatlo, 2008; Michael, 2016). Polyamines, such as spermidine and putrescine, have been shown to play a direct role in biofilm formation in *Vibrio cholera*, *Yersinia pestis*, *E. coli*, *Bacillus subtilis*, and *Neisseria gonorrheoae* (Karatan and Michael, 2013), yet it remains unknown whether there is a common function of polyamines in all biofilm-forming bacteria. Of the LDP intermediates, we find that cadaverine shows the largest difference between phenotypes and therefore may play a role in establishing growth mode. It is known that metabolites of a targeted pathway can be supplemented to trigger rapid changes in enzyme activity leading to reprogrammed metabolic activity (Wegner et al., 2015). To test this possibility for the cadaverine branch of the LDP, we supplemented cadaverine to the growth media in a concentration range of 0 - 3.30 mM and concurrently measured planktonic growth by OD_{600} and biofilm accumulation by crystal violet (CV) staining elution at OD_{590} after 24 hrs. With the addition of cadaverine, planktonic growth increased significantly whereas biofilm accumulation decreased significantly (**Figures 5A, B**). Moreover, addition of cadaverine was not bactericidal as the OD_{600} increased at most concentrations. Planktonic growth increases in a somewhat cadaverine-concentration dependent manner, however not all concentrations altered growth significantly, which is likely due to the variability in the planktonic samples. Planktonic growth increased maximally by 20.5 ± 4.2% with 3.30 mM cadaverine (**Figure 5A**). This contrasts the biofilm response to exogenous cadaverine: at low cadaverine concentration (25 μM) biofilm accumulation increased marginally before systematically decreasing with 200 μM to 3.30 mM cadaverine, leveling off at a 49.0 ± 3.5% decrease at the highest cadaverine concentration (**Figure 5B**). These results suggest that exogenous supplementation of cadaverine stimulates planktonic growth and inhibits biofilm accumulation post inoculation.

Because of its basic nature, cadaverine supplementation increased the pH of the media by up to 0.8 pH units (**Supplementary Figure 3A**) with the pH remaining in the normal growth range for *P. aeruginosa* (Klein et al., 2009). This small pH change by itself did not cause increased planktonic growth or reduced biofilm accumulation, as increasing the pH by addition of sodium hydroxide in lieu of cadaverine caused no systematic significant change in planktonic growth or biofilm accumulation (**Supplementary Figure 3B**).

Confirmation of Cadaverine Inhibition of Biofilm Accumulation by Confocal Laser Scanning Microscopy

To independently confirm the CV elution results by an alternative method, biofilm accumulation was measured by CLSM. 3.30 mM cadaverine was supplemented to the growth media in a confocal dish. At 24 hrs, samples were stained with SYTO 9 and stitched confocal images were collected and quantified by Fiji (Schindelin et al., 2012) (**Figure 6A**). Mean grayscale value (**Figure 6B**) showed a significant reduction in biofilm accumulation of 54.5 ± 26.0% and surface area coverage (**Figure 6C**) showed a significant reduction in biofilm accumulation by 79.8 ± 55.1%. Both visual inspection and quantification of the biofilm images show variation among replicates, likely partially due to the inherently heterogeneous nature of biofilms (Stewart and Franklin, 2008). Despite the heterogeneity, the average effect shows significant reduction in biofilm accumulation with cadaverine supplementation.

Exogenous Supplementation of Cadaverine Inhibits Biofilm Accumulation in the Presence of Pre-Formed Biofilm

To investigate whether cadaverine could also inhibit biofilm accumulation in the presence of pre-formed biofilm, cultures were grown for 24 hrs then supplemented with cadaverine and grown an additional 24 hrs for OD_{600} and CV staining elution. Planktonic growth was significantly increased by 5.8 ± 1.8%

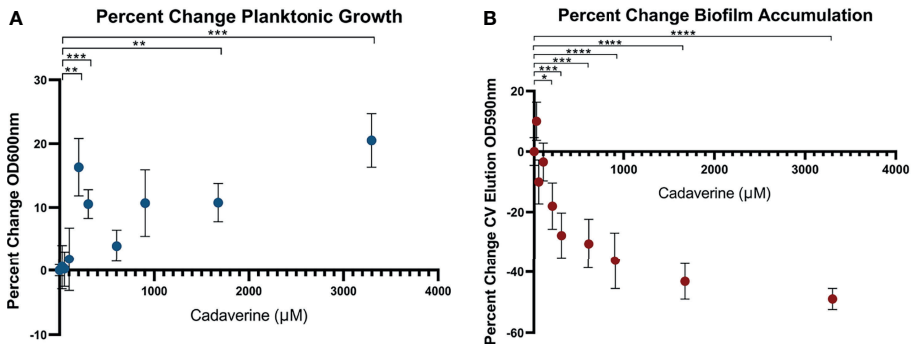

FIGURE 5 | Microtitre plate assays show cadaverine supplementation significantly increases planktonic growth and decreases biofilm accumulation post inoculation. Planktonic growth **(A)** and biofilm accumulation **(B)** are measured by OD_{600} and crystal violet staining elution at OD_{590}, respectively, after supplementation of 0-3.30mM cadaverine to the growth media for 24 hrs (n=18). Values are normalized to the control wells (no cadaverine) in each plate and reported as a percent change from control and asterisks denote significance (*$p < 0.05$, **$p < 0.01$, ***$p < 0.001$, ****$p < 0.0001$ by unpaired, two-tailed *t*-test). **(A)** Planktonic growth significantly increases at several cadaverine concentrations, maximally by 21%. **(B)** Biofilm accumulation significantly decreases in a cadaverine concentration dependent manner, maximally by 49%.

(**Supplementary Figure 4A**) and biofilm accumulation was significantly decreased by 39.8 ± 2.5% (**Supplementary Figure 4B**). These results are consistent with the previous assay, demonstrating that addition of cadaverine stimulates planktonic growth and inhibits biofilm accumulation, even in the presence of pre-formed biofilm.

Exogenous Supplementation of Cadaverine Causes a Macroscopic Alteration in Biofilm Morphology

The aforementioned assays measured biofilm accumulation of surface-attached biofilm after aspiration, washing, and staining. We also report a macroscopic alteration of biofilm morphology in standing liquid culture dishes grown for 24 hrs with cadaverine. The *P. aeruginosa* Td-tomato strain, utilized for visualization, supplemented with cadaverine showed a significant increase in planktonic growth by OD_{600} (**Supplementary Figure 5A**) and significant reduction in biofilm accumulation by CV staining elution (**Supplementary Figure 5B**), similarly to WT PAO1.

Representative macroscopic images of cultures in **Figure 7A** revealed altered biofilm morphology in the presence of supplemented cadaverine. In control cultures the biofilm appears in a web-like structure that is well attached and localized at the bottom of the dish. With 3.30 mM cadaverine, the biofilm appears more aggregate-like, in a pellicle, which consists of many small areas of biofilm accumulation toward the air-liquid interface (**Figure 7A**). The air-liquid interface of the cultures was imaged using an AmScope MU500 camera with an AmScope dissecting microscope, showing a microscopic image of the areas of pellicle biofilm appearing at the air-liquid interface with the addition of cadaverine (**Figure 7B**). In the control, no biofilm growth appears at the air-liquid interface.

Macroscopic photos, dissecting microscope images, and IVIS images in **Figures 7C–E** were also collected with the constitutive bioluminescent PAO1 derivative Xen41. Representative photos (**Figure 7C**) and dissecting microscope images (**Figure 7D**) of the air-liquid interface similarly showed pellicle biofilm with cadaverine supplementation. To determine the metabolic state of the bacteria within the pellicle and surrounding supernatant, we utilized an IVIS imaging system, which captures light from bioluminescence that is proportional to the cell numbers and metabolic activity. IVIS images of cultures with cadaverine supplemented show that the pellicle biofilm emits more light, which is proportional to the accumulation of more cells in biofilm at the air-liquid interface (**Figure 7E**). The light production is localized to the areas of pellicle, indicating that they are metabolically active (**Figure 7E** and **Supplementary Figure 6**). In contrast, biofilm attached at the bottom of the dish in the control cultures emits low levels of luminescence, likely resulting from reduced oxygen and a limited dynamic range with the strong signal collected at the air-liquid interface of the test cultures. Therefore, along with significantly less total biofilm accumulation, cadaverine supplementation stimulates the altered macroscopic morphology to a pellicle biofilm. We also found the cadaverine-induced pellicle biofilm was more easily aspirated than the more strongly attached, web-like control biofilm (**Figure 7**). This likely contributes to the reduced surface-attached biofilm accumulation measured *via* the CV assay and microscopy (**Figures 5**, **6**).

DISCUSSION

Our untargeted NMR-based metabolomics approach enabled us to uncover specific metabolites and pathways involved in regulation of growth mode and biofilm formation. Of the significant metabolite changes identified by our new COLMARq web server, the cadaverine branch of the LDP was the pathway that showed the most significant differences between planktonic and biofilm phenotypes, with significant reduction in the biofilm phenotype. Exogenous supplementation of cadaverine to cultures significantly stimulated planktonic growth and inhibited

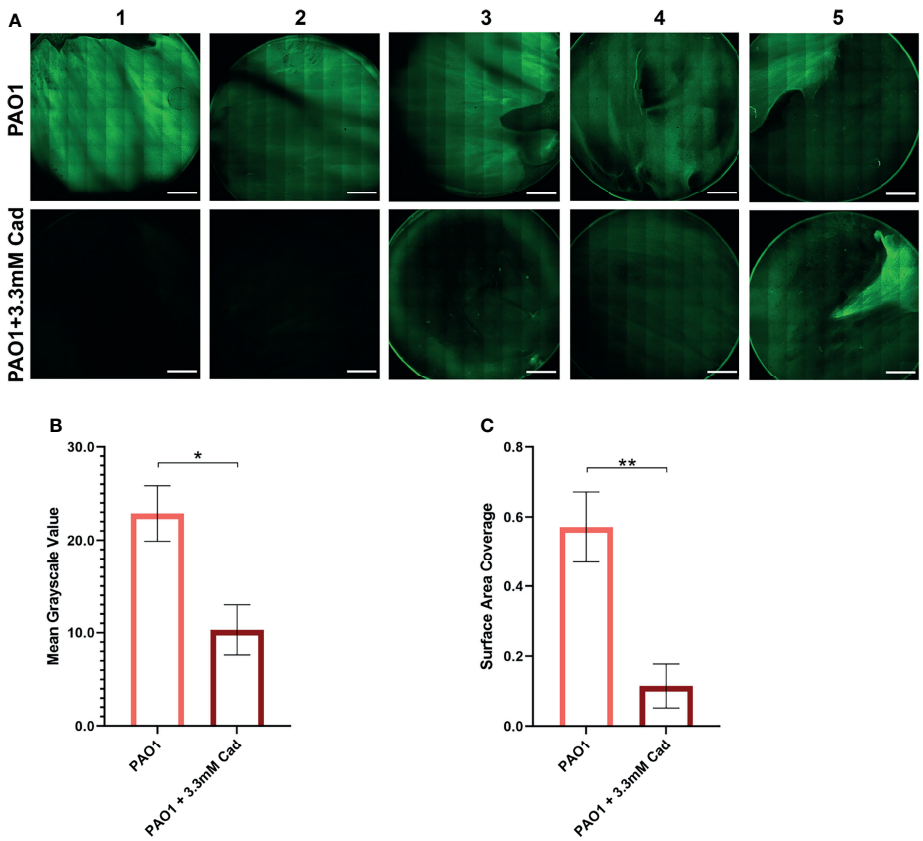

FIGURE 6 | Stitched confocal microscopy images show a significant reduction in biofilm accumulation with cadaverine by image quantification. **(A)** 3.30mM cadaverine (cad) is supplemented to the PAO1 culture in a 35 by 10mm dish, grown 24 hrs, stained with SYTO 9, and stitched confocal images (n=5; paired to control cultures) are taken at laser power 4.5%. Scale bars in the lower right corner of images represent 0.2 cm. Images are quantified in Fiji by **(B)** mean grayscale value and **(C)** surface area coverage with the auto threshold set to 13 and asterisks denote significance (*$p < 0.05$, **$p < 0.01$ by unpaired, two-tailed *t*-test). Mean grayscale value and surface area coverage show 55% and 80% reduction in biofilm accumulation, respectively, with supplementation of cadaverine.

biofilm accumulation (**Figure 5**). This suggests exogenous supplementation of cadaverine may reprogram cellular metabolism to maintain a more planktonic-like metabolic state leading to reduced biofilm formation. To our knowledge, this is the first association of the cadaverine pathway to biofilm accumulation in *P. aeruginosa*. Other polyamines have been shown to play varied roles in biofilm formation in other pathogens (Rojo, 2010), indicating that the role of each polyamine is specific, requiring a separate mechanistic investigation for each system.

The observed stimulation of planktonic growth by cadaverine reported here may be related to previous findings of possible roles of cadaverine, including combatting cellular stress (Miller-Fleming et al., 2015; Soksawatmaekhin et al., 2004), increase of cell viability in the stationary phase (Sakamoto et al., 2012), stimulation of protein synthesis (Igarashi and Kashiwagi, 2018), and increase of cellular respiration and growth (Nie et al., 2017; Knorr et al., 2018), thereby contributing to the favoring of the planktonic phenotype. Polyamines in *E. coli* have been shown to form complexes with RNA, stimulate assembly of the ribosome, and increase general protein synthesis about two-fold (Igarashi and Kashiwagi, 2018), which may contribute to increased growth. The cadaverine pathway also increases cellular respiration by supplementing the TCA cycle (Nie et al., 2017; Knorr et al., 2018). Metabolic intermediates such as cadaverine and glutaric acid serve as better carbon and nitrogen sources than lysine itself (Fothergill and Guest, 1977; Indurthi et al., 2016). Since nutrient restriction has been associated with stimulating biofilm formation (Zhang et al., 2012), increased metabolic activity in *P. aeruginosa* may generally favor the planktonic phenotype.

Alternatively, inhibition of biofilm accumulation by cadaverine may be related to its ability to alter adhesion protein expression (Torres et al., 2005). Restoration of lysine decarboxylase after inhibition to produce cadaverine in *E. coli* led to reduced production of intimin, an adhesion protein (Torres et al., 2005). Therefore, cadaverine may act on biofilm matrix components contributing to more weakly attached biofilms and reduced biofilm accumulation.

Another proposed mechanism of the regulation of biofilm formation in *P. aeruginosa* is modulation of the second messenger bis-(3'-5')-cyclic dimeric guanosine monophosphate

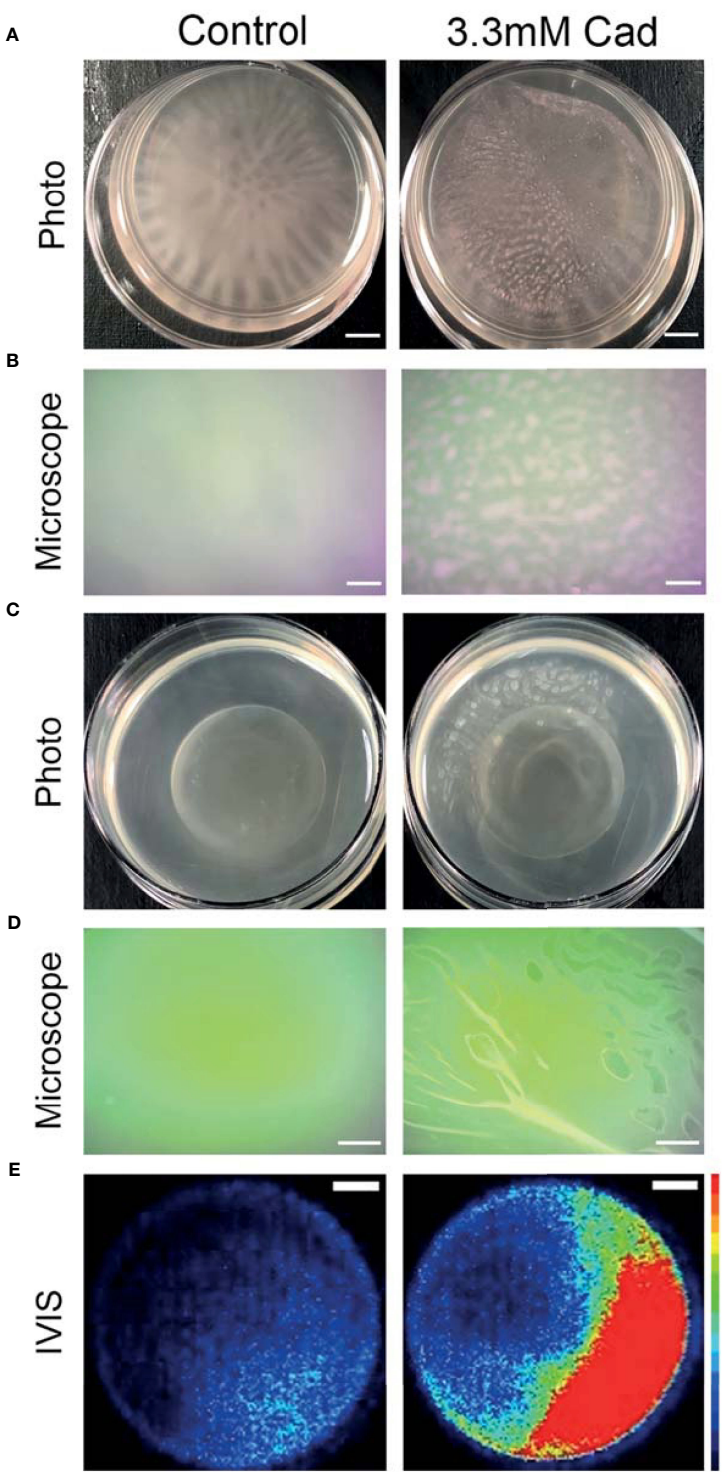

FIGURE 7 | Cadaverine supplementation causes altered biofilm morphology to pellicle biofilm at the air-liquid interface that is metabolically active. Representative iPhone8 photos (scale bar = 2.9mm) **(A)** and dissecting microscope images of culture air-liquid interfaces (scale bar = 0.14mm) **(B)** are taken of PAO1 Td-tomato supplemented with 3.30mM cadaverine (cad) showing pellicle biofilm. Representative iPhone8 photos (scale bar = 3.6mm) **(C)**, dissecting microscope images of culture air-liquid interfaces (scale bar = 0.18mm) **(D)**, and IVIS images of air-liquid interfaces (scale bar = 3.8mm) with red being the most metabolically active (scale on right of images) **(E)** are shown of PAO1 Xen41 supplemented with 3.30mM cadaverine. Cadaverine supplementation leads to biofilm formation at the air-liquid interface compared to the control, where biofilm is localized to the bottom of the dish.

(c-di-GMP) (Romling et al., 2013; Randall et al., 2021). In most cases, the mechanism that leads to alterations in c-di-GMP levels is unknown (Barrientos-Moreno et al., 2020). However, a most recent study shows that the polyamine putrescine and its metabolic precursor L-arginine increase biofilm formation in *P. aeruginosa*, at least in part through increasing c-di-GMP levels (Liu et al., 2021). Cadaverine production through lysine catabolism is coupled with arginine metabolism *via* the arginine-responsive regulator (Chou et al., 2010). This association could suggest that cadaverine regulates biofilm formation in part through affecting c-di-GMP levels. Measuring metabolic pathway changes and c-di-GMP after exogenous cadaverine supplementation is an interesting future direction to inform further on metabolic mechanisms underlying biofilm regulation.

Our findings highlight the potential of NMR-based metabolomics as a viable tool for diagnosis and identification of new targets for prevention and control of *P. aeruginosa* infection and biofilm. Detection of certain types of infections, such as periprosthetic joint infection, is difficult and requires time-consuming culturing methods, making early and pathogen-specific intervention unfeasible in many cases and there are no clinical biomarkers for the presence of biofilms (Glaudemans et al., 2019; Wasterlain et al., 2020). As a highly reproducible and quantitative method, NMR spectroscopy has the potential to identify metabolite biomarkers or fingerprints of infection in bodily fluids such as serum and synovial fluid (Hugle et al., 2012; Ammons et al., 2014; Palama et al., 2016). With 782 HSQC peaks identified that manifest significant concentration fold changes (up to 100-fold) between *P. aeruginosa* planktonic and biofilm, unique metabolites or metabolomic signatures, if detectable *in vivo*, could be used as culture-free diagnostic markers. These markers have the potential to enable rapid identification of bacterial growth mode and to aid in deciding the optimal treatment. In addition, combining biofilm-controlling compounds with antibiotics has been identified as an effective strategy to control biofilm infections (Estrela and Abraham, 2010). We found supplementation of cadaverine did not have a bactericidal or bacteriostatic effect while reducing biofilm accumulation post inoculation and in the presence of pre-formed biofilm, indicating that it could act to reduce biofilm formation and potentially increase susceptibility to antibiotics. Previous studies have shown cadaverine enhances the effectiveness of many β-lactams against *P. aeruginosa* (Kwon and Lu, 2006; Manuel et al., 2010). Cadaverine is a natural metabolite found in all living organisms (Miller-Fleming et al., 2015) and can stem from microbiota or have endogenous origin (Amin et al., 2021). Cadaverine supplementation shows low acute oral toxicity at 2,000 mg/kg body weight in rats (Til et al., 1997), and negligible cytotoxicity up to 70 mM in HT29 intestinal cells (del Rio et al., 2019). Therefore, adding cadaverine to the *P. aeruginosa* infection prevention or treatment course is a potentially viable new strategy that warrants further investigation.

Our quantitative untargeted metabolomics approach can be directly applied to the characterization of biofilm versus planktonic phenotypes of *P. aeruginosa* and other biofilm-forming bacteria in growth media and environments other than those studied here. Our cultures were grown in LB media that contains a mixture of carbon sources including amino acids and glucose among other nutrients. *P. aeruginosa* utilizes a carbon catabolite repression system to select preferred carbon sources and optimize growth in various environments (Karatan and Michael, 2013). *P. aeruginosa* prefers organic acids or amino acids over standard nutrients like glucose. With preferred nutrients available, we detected alteration of the LDP, an amino acid pathway, to modulate growth between planktonic and biofilm phenotypes. Utilizing other growth conditions will provide more insight about the generality of the role of the lysine degradation pathway in *P. aeruginosa* biofilm formation or even may lead to the identification of other endogenous metabolites that can be used to modulate biofilm growth. In addition, utilizing clinical isolates and mimicking specific environments, for example artificial sputum in the case of cystic fibrosis lung infections or synovial fluid in the case of periprosthetic knee or hip joint infections, is expected to provide important new information about metabolic pathways associated with biofilm growth in specific conditions.

In conclusion, we have identified and quantified many specific metabolic differences between *P. aeruginosa* planktonic and biofilm phenotypes and discovered that the cadaverine pathway is linked to the establishment of the growth mode. Exogenous cadaverine supplementation to cultures led to stimulated planktonic growth, inhibited biofilm accumulation by up to 49%, and induced macroscopic pellicle biofilm structure. Our findings identify cadaverine and the LDP as a potential target for prevention and mitigation of *P. aeruginosa* biofilm infections. Additional studies of the effect of cadaverine metabolism in *P. aeruginosa* clinical isolates and the virulence and persistence of the induced pellicle biofilm *in vivo* are needed. Beyond cadaverine alone, treatment with a mixture of LDP pathway intermediates or other endogenous metabolites that are decreased in the biofilm phenotype could further increase effectiveness in modulating growth mode. Further advances in our understanding of the precise role of metabolic regulation in biofilm formation open new possibilities to the modulation of growth mode in *P. aeruginosa*. The metabolomics approach used here should be applicable to other biofilm-forming bacteria to deepen our understanding of the existence and role of metabolic pathways in these pathogens.

DATA AVAILABILITY STATEMENT

The original contributions presented in the study are included in the article/**Supplementary Material**. Further inquiries can be directed to the corresponding authors.

AUTHOR CONTRIBUTIONS

Conceptualization and design: AL, LB-L, RB, and PS. Investigation: AL, DS, AS, and NR. Data analysis: AL and DL. Figures: AL and NR.

Writing of the original draft: AL, RB, and PS. All authors read and approved the final version of the manuscript.

FUNDING

This work was supported by the National Institutes of Health [grants R01GM124436 (to PS), R01GM066041, and R35GM139482 (to RB)] and by a pilot grant from the Department of Microbial Infection and Immunity in the College of Medicine at OSU.

ACKNOWLEDGMENTS

All NMR experiments were performed at the CCIC NMR facility at The Ohio State University.

SUPPLEMENTARY MATERIAL

The Supplementary Material for this article can be found online at: https://www.frontiersin.org/articles/10.3389/fcimb.2022.833269/full#supplementary-material

REFERENCES

Amin, M., Tang, S. Y., Shalamanova, L., Taylor, R. L., Wylie, S., Abdullah, B. M., et al. (2021). Polyamine Biomarkers as Indicators of Human Disease. *Biomarkers* 26, 77–94. doi: 10.1080/1354750X.2021.1875506

Ammons, M. C., Tripet, B. P., Carlson, R. P., Kirker, K. R., Gross, M. A., Stanisich, J. J., et al. (2014). Quantitative NMR Metabolite Profiling of Methicillin-Resistant and Methicillin-Susceptible Staphylococcus Aureus Discriminates Between Biofilm and Planktonic Phenotypes. *J. Proteome Res.* 13 (6), 2973–2985. doi: 10.1021/pr500120c

Amrutha, B., Sundar, K., and Shetty, P. H. (2017). Effect of Organic Acids on Biofilm Formation and Quorum Signaling of Pathogens From Fresh Fruits and Vegetables. *Microb. Pathogenesis* 111, 156–162. doi: 10.1016/j.micpath.2017.08.042

Barrientos-Moreno, L., Molina-Henares, M. A., Ramos-Gonzalez, M. I., and Espinosa-Urgel, M. (2020). Arginine as an Environmental and Metabolic Cue for Cyclic Diguanylate Signalling and Biofilm Formation in Pseudomonas Putida. *Sci. Rep-Uk* 10, 13623. doi: 10.1038/s41598-020-70675-x

Benjamini, Y., and Hochberg, Y. (1995). Controlling the False Discovery Rate - a Practical and Powerful Approach to Multiple Testing. *J. R Stat. Soc. B* 57, 289–300. doi: 10.1111/j.2517-6161.1995.tb02031.x

Bingol, K., Li, D. W., Zhang, B., and Brüschweiler, R. (2016). Comprehensive Metabolite Identification Strategy Using Multiple Two-Dimensional NMR Spectra of a Complex Mixture Implemented in the COLMARm Web Server. *Anal. Chem.* 88, 12411–12418. doi: 10.1021/acs.analchem.6b03724

Bligh, E. G., and Dyer, W. J. (1959). A Rapid Method of Total Lipid Extraction and Purification. *Can. J. Biochem. Phys.* 37, 911–917. doi: 10.1139/y59-099

Borgos, S. E. F., Skjastad, R., Tondervik, A., Aas, M., Aasen, I. M., Brunsvik, A., et al. (2015). Rapid Metabolic Profiling of Developing Pseudomonas Aeruginosa Biofilms by High-Resolution Mass Spectrometry Fingerprinting. *Ann. Microbiol.* 65, 891–898. doi: 10.1007/s13213-014-0930-z

Chou, H. T., Hegazy, M., and Lu, C. D. (2010). L-Lysine Catabolism Is Controlled by L-Arginine and ArgR in Pseudomonas Aeruginosa PAO1. *J. Bacteriol* 192, 5874–5880. doi: 10.1128/JB.00673-10

Cornforth, D. M., Dees, J. L., Ibberson, C. B., Huse, H. K., Mathiesen, I. H., Kirketerp-Moller, K., et al. (2018). Pseudomonas Aeruginosa Transcriptome During Human Infection. *P Natl. Acad. Sci. U.S.A.* 115, E5125–E5134. doi: 10.1073/pnas.1717525115

del Rio, B., Redruello, B., Linares, D. M., Ladero, V., Ruas-Madiedo, P., Fernandez, M., et al. (2019). The Biogenic Amines Putrescine and Cadaverine Show *In Vitro* Cytotoxicity at Concentrations That can be Found in Foods. *Sci. Rep.* 9, 120. doi: 10.1038/s41598-018-36239-w

Delaglio, F., Grzesiek, S., Vuister, G. W., Zhu, G., Pfeifer, J., and Bax, A. (1995). Nmrpipe - A Multidimensional Spectral Processing System Based on Unix Pipes. *J. Biomol Nmr* 6, 277–293. doi: 10.1007/BF00197809

Dusane, D. H., Lochab, V., Jones, T., Peters, C. W., Sindeldecker, D., Das, A., et al. (2019). Electroceutical Treatment of Pseudomonas Aeruginosa Biofilms. *Sci. Rep-Uk* 9 (1). doi: 10.1038/s41598-018-37891-y

Estrela, A. B., and Abraham, W. R. (2010). Combining Biofilm-Controlling Compounds and Antibiotics as a Promising New Way to Control Biofilm Infections. *Pharmaceuticals.* 3, 1374–1393. doi: 10.3390/ph3051374

Favre, L., Ortalo-Magne, A., Pichereaux, C., Gargaros, A., Burlet-Schiltz, O., Cotelle, V., et al. (2018). Metabolome and Proteome Changes Between Biofilm and Planktonic Phenotypes of the Marine Bacterium Pseudoalteromonas Lipolytica TC8. *Biofouling* 34, 132–148. doi: 10.1080/08927014.2017.1413551

Fothergill, J. C., and Guest, J. R. (1977). Catabolism of L-Lysine by Pseudomonas-Aeruginosa. *J. Gen. Microbiol.* 99, 139–155. doi: 10.1099/00221287-99-1-139

Fuchs, A., Tripet, B. P., Ammons, M. C. B., and Copie, V. (2016). Optimization of Metabolite Extraction Protocols for the Identification and Profiling of Small Molecule Metabolites From Planktonic and Biofilm Pseudomonas Aeruginosa Cultures. *Curr. Metabol* 4, 141–147. doi: 10.2174/2213235X04666151126203043

Gjersing, E. L., Herberg, J. L., Horn, J., Schaldach, C. M., and Maxwell, R. S. (2007). NMR Metabolornics of Planktonic and Biofilm Modes of Growth in Pseudomonas Aeruginesa. *Anal. Chem.* 79, 8037–8045. doi: 10.1021/ac070800t

Glaudemans, A., Jutte, P. C., Cataldo, M. A., Cassar-Pullicino, V., Gheysens, O., Borens, O., et al. (2019). Consensus Document for the Diagnosis of Peripheral Bone Infection in Adults: A Joint Paper by the EANM, EBJIS, and ESR (With ESCMID Endorsement). *Eur. J. Nucl. Med. Mol. Imaging.* 46 (4), 957–970. doi: 10.1007/s00259-019-4262-x

Gowda, G. A. N., and Raftery, D. (2015). Can NMR Solve Some Significant Challenges in Metabolomics? *J. Magn. Reson.* 260, 144–160. doi: 10.1016/j.jmr.2015.07.014

Hall-Stoodley, L., Costerton, J. W., and Stoodley, P. (2004). Bacterial Biofilms: From the Natural Environment to Infectious Diseases. *Nat. Rev. Microbiol.* 2, 95–108. doi: 10.1038/nrmicro821

Hauck, D., Joachim, I., Frommeyer, B., Varrot, A., Philipp, B., Moller, H. M., et al. (2013). Discovery of Two Classes of Potent Glycomimetic Inhibitors of Pseudomonas Aeruginosa LecB With Distinct Binding Modes. *ACS Chem. Biol.* 8, 1775–1784. doi: 10.1021/cb400371r

Hoiby, N., Henneberg, K. A., Wang, H. S., Stavnsbjerg, C., Bjarnsholt, T., Ciofu, O., et al. (2019). Formation of Pseudomonas Aeruginosa Inhibition Zone During Tobramycin Disk Diffusion is Due to Transition From Planktonic to Biofilm Mode of Growth. *Int. J. Antimicrob. Ag* 53, 564–573. doi: 10.1016/j.ijantimicag.2018.12.015

Hügle, T., Kovacs, H., Heijnen, I. A., Daikeler, T., Baisch, U., Hicks, J. M., et al. (2012). Synovial Fluid Metabolomics in Different Forms of Arthritis Assessed by Nuclear Magnetic Resonance Spectroscopy. *Clin. Exp. Rheumatol.* 30 (2), 240–245.

Igarashi, K., and Kashiwagi, K. (2018). Effects of Polyamines on Protein Synthesis and Growth of Escherichia Coli. *J. Biol. Chem.* 293 (48), 18702–18709. doi: 10.1074/jbc.TM118.003465

Indurthi, S. M., Chou, H. T., and Lu, C. D. (2016). Molecular Characterization of lysR-lysXE, gcdR-gcdHG and amaR-amaAB Operons for Lysine Export and Catabolism: A Comprehensive Lysine Catabolic Network in Pseudomonas Aeruginosa PAO1. *Microbiol-Sgm* 162, 876–888. doi: 10.1099/mic.0.000277

Kanehisa, M., Furumichi, M., Tanabe, M., Sato, Y., and Morishima, K. (2017). KEGG: New Perspectives on Genomes, Pathways, Diseases and Drugs. *Nucleic Acids Res.* 45, D353–D361. doi: 10.1093/nar/gkw1092

Karatan, E., and Michael, A. J. (2013). A Wider Role for Polyamines in Biofilm Formation. *Biotechnol. Lett.* 35, 1715–1717. doi: 10.1007/s10529-013-1286-3

Klein, S., Lorenzo, C., Hoffmann, S., Walther, J. M., Storbeck, S., Piekarski, T., et al. (2009). Adaptation of Pseudomonas Aeruginosa to Various Conditions Includes tRNA-Dependent Formation of Alanyl-Phosphatidylglycerol. *Mol. Microbiol.* 71, 551–565. doi: 10.1111/j.1365-2958.2008.06562.x

Knorr, S., Sinn, M., Galetskiy, D., Williams, R. M., Wang, C. H., Muller, N., et al. (2018). Widespread Bacterial Lysine Degradation Proceeding *via* Glutarate and L-2-Hydroxyglutarate. *Nat. Commun.* 9 (1), 5071. doi: 10.1038/s41467-018-07563-6

Kwon, D. H., and Lu, C. D. (2006). Polyamines Increase Antibiotic Susceptibility in Pseudomonas Aeruginosa. *Antimicrob. Agents Ch.* 50, 1623–1627. doi: 10.1128/Aac.50.5.1623-1627.2006

Leggett, A., Wang, C., Li, D. W., Somogyi, A., Bruschweiler-Li, L., and Brüschweiler, R. (2019). Identification of Unknown Metabolomics Mixture Compounds by Combining NMR, MS, and Cheminformatics. *Method Enzymol.* 615, 407–422. doi: 10.1016/bs.mie.2018.09.003

Lewis, K. (2001). Riddle of Biofilm Resistance. *Antimicrob. Agents Ch* 45, 999–1007. doi: 10.1128/AAC.45.4.999-1007.2001

Liu, Z., Hossain, S. S., Morales Moreira, Z., and Haney, C. H. (2021). Putrescine and its Metabolic Precursor Arginine Promote Biofilm and C-Di-GMP Synthesis in Pseudomonas Aeruginosa. *J. Bacteriol.* 204 (1), e0029721. doi: 10.1128/JB.00297-21

Locke, L. W., Shankaran, K., Gong, L., Stoodley, P., Vozar, S. L., Cole, S. L., et al. (2020). Evaluation of Peptide-Based Probes Toward *In Vivo* Diagnostic Imaging of Bacterial Biofilm-Associated Infections. *ACS Infect. Dis.* 6, 2086–2098. doi: 10.1021/acsinfecdis.0c00125

Lu, H. T., Que, Y. M., Wu, X., Guan, T. B., and Guo, H. (2019). Metabolomics Deciphered Metabolic Reprogramming Required for Biofilm Formation. *Sci. Rep-Uk* 9 (1), 13160. doi: 10.1038/s41598-019-49603-1

Manuel, J., Zhanel, G. G., and de Kievit, T. (2010). Cadaverine Suppresses Persistence to Carboxypenicillins in Pseudomonas Aeruginosa PAO1. *Antimicrob. Agents Ch.* 54, 5173–5179. doi: 10.1128/Aac.01751-09

Markley, J. L., Brüschweiler, R., Edison, A. S., Eghbalnia, H. R., Powers, R., Raftery, D., et al. (2017). The Future of NMR-Based Metabolomics. *Curr. Opin. Biotech.* 43, 34–40. doi: 10.1016/j.copbio.2016.08.001

Michael, A. J. (2016). Polyamines in Eukaryotes, Bacteria, and Archaea. *J. Biol. Chem.* 291, 14896–14903. doi: 10.1074/jbc.R116.734780

Miller-Fleming, L., Olin-Sandoval, V., Campbell, K., and Ralser, M. (2015). Remaining Mysteries of Molecular Biology: The Role of Polyamines in the Cell. *J. Mol. Biol.* 427 (21), 3389–3406. doi: 10.1016/j.jmb.2015.06.020

Nie, H. Y., Nie, M. Q., Xiao, T., Wang, Y., and Tian, X. T. (2017). Hexadecane Degradation of *Pseudomonas aeruginosa* NY3 Promoted by Glutaric Acid. *Sci. Total Environ.* 575, 1423–1428. doi: 10.1016/j.scitotenv.2016.09.223

O'Toole, G. A., and Kolter, R. (1998). Flagellar and Twitching Motility are Necessary for Pseudomonas Aeruginosa Biofilm Development. *Mol. Microbiol.* 30, 295–304. doi: 10.1046/j.1365-2958.1998.01062.x

Palama, T. L., Canard, I., Rautureau, G. J. P., Mirande, C., Chatellier, S., and Elena-Herrman, B. (2016). Identification of Bacterial Species by Untargeted NMR Spectroscopy of the Exo-Metabolome. *Analyst* 141, 4558–4561. doi: 10.1039/c6an00393a

Pfeltz, R. F., Schmidt, J. L., and Wilkinson, B. J. (2001). A Microdilution Plating Method for Population Analysis of Antibiotic-Resistant Staphylococci. *Microb. Drug Resist.* 7, 289–295. doi: 10.1089/10766290152652846

Randall, T. E., Eckartt, K., Kakumanu, S., Prince-Whelan, A., Dietrich, L. E. P., and Harrison, J. J. (2021). Sensory Perception in Bacterial Cyclic Diguanylate Signal Transduction. *J. Bacteriol.* doi: 10.1128/JB.00433-21

Rieusset, L., Rey, M., Muller, D., Vacheron, J., Gerin, F., Dubost, A., et al. (2020). Secondary Metabolites From Plant-Associated Pseudomonas are Overproduced in Biofilm. *Microb. Biotechnol.* 13, 1562–1580. doi: 10.1111/1751-7915.13598

Rojo, F. (2010). Carbon Catabolite Repression in Pseudomonas: Optimizing Metabolic Versatility and Interactions With the Environment. *FEMS Microbiol. Rev.* 34, 658–684. doi: 10.1111/j.1574-6976.2010.00218.x

Romling, U., Galperin, M. Y., and Gomelsky, M. (2013). Cyclic Di-GMP: The First 25 Years of a Universal Bacterial Second Messenger. *Microbiol. Mol. Biol. R* 77, 1–52. doi: 10.1128/MMBR.00043-12

Sakamoto, A., Terui, Y., Yamamoto, T., Kasahara, T., Nakamura, M., Tomotori, H., et al. (2012). Enhanced Biofilm Formation and/or Cell Viability by Polyamines Through Stimulation of Response Regulators UvrY and CpxR in the Two-Component Signal Transducing Systems, and Ribosome Recycling Factor. *Int. J. Biochem. Cell Bio.* 44 (11), 1877–1886. doi: 10.1016/j.biocel.2012.07.010

Sauer, K., Camper, A. K., Ehrlich, G. D., Costerton, J. W., and Davies, D. G. (2002). Pseudomonas Aeruginosa Displays Multiple Phenotypes During Development as a Biofilm. *J. Bacteriol* 184, 1140–1154. doi: 10.1128/jb.184.4.1140-1154.2002

Scaglione, F., Musazzi, U. M., and Minghetti, P. (2021). Considerations on D-Mannose Mechanism of Action and Consequent Classification of Marketed Healthcare Products. *Front. Pharmacol.* 12. doi: 10.3389/fphar.2021.636377

Schindelin, J., Arganda-Carreras, I., Frise, E., Kaynig, V., Longair, M., Pietzsch, T., et al. (2012). Fiji: An Open-Source Platform for Biological-Image Analysis. *Nat. Methods* 9, 676–682. doi: 10.1038/nmeth.2019

Shah, P., and Swlatlo, E. (2008). A Multifaceted Role for Polyamines in Bacterial Pathogens. *Mol. Microbiol.* 68, 4–16. doi: 10.1111/j.1365-2958.2008.06126.x

Soksawatmaekhin, W., Kuraishi, A., Sakata, K., Kashiwagi, K., and Igarashi, K. (2004). Excretion and Uptake of Cadaverine by CadB and its Physiological Functions in Escherichia Coli. *Mol. Microbiol.* 51, 1401–1412. doi: 10.1046/j.1365-2958.2003.03913.x

Stewart, P. S., and Franklin, M. J. (2008). Physiological Heterogeneity in Biofilms. *Nat. Rev. Microbiol.* 6, 199–210. doi: 10.1038/nrmicro1838

Stipetic, L. H., Dalby, M. J., Davies, R. L., Morton, F. R., Ramage, G., and Burgess, K. E. V. (2016). A Novel Metabolomic Approach Used for the Comparison of Staphylococcus Aureus Planktonic Cells and Biofilm Samples. *Metabolomics* 12 (4), 75. doi: 10.1007/s11306-016-1002-0

Sudhir K. Shukla, T. S. R. (2017). An Improved Crystal Violet Assay for Biofilm Quantification in 96-Well Microtitre Plate. *bioRxiv* 100214. doi: 10.1101/100214

Sussulini, A. (2017). Erratum to: Chapters 1 and 11 of Metabolomics: From Fundamentals to Clinical Applications. *Adv. Exp. Med. Biol.* 965, E1–E2. doi: 10.1007/978-3-319-47656-8_14

Tang, T. S., Xu, Y., Wang, J. F., Tan, X., Zhao, X. N., Zhou, P., et al. (2021). Evaluation of the Differences Between Biofilm and Planktonic Brucella Abortus *via* Metabolomics and Proteomics. *Funct. Integr. Genomic* 21, 421–433. doi: 10.1007/s10142-021-00788-7

Til, H. P., Falke, H. E., Prinsen, M. K., and Willems, M. I. (1997). Acute and Subacute Toxicity of Tyramine, Spermidine, Spermine, Putrescine and Cadaverine in Rats. *Food Chem Toxicol.* 35, 337–348. doi: 10.1016/S0278-6915(97)00121-X

Torres, A. G., Vazquez-Juarez, R. C., Tutt, C. B., and Garcia-Gallegos, J. G. (2005). Pathoadaptive Mutation That Mediates Adherence of Shiga Toxin-Producing Escherichia Coli O111. *Infect. Immun.* 73, 4766–4776. doi: 10.1128/Iai.73.8.4766-4776.2005

Toyofuku, M., Inaba, T., Kiyokawa, T., Obana, N., Yawata, Y., and Nomura, N. (2016). Environmental Factors That Shape Biofilm Formation. *Biosci. Biotech. Bioch* 80, 7–12. doi: 10.1080/09168451.2015.1058701

Wagner, V. E., Li, L. L., Isabella, V. M., and Iglewski, B. H. (2007). Analysis of the Hierarchy of Quorum-Sensing Regulation in Pseudomonas Aeruginosa. *Anal. Bioanal Chem.* 387, 469–479. doi: 10.1007/s00216-006-0964-6

Waite, R. D., Papakonstantinopoulou, A., Littler, E., and Curtis, M. A. (2005). Transcriptome Analysis of Pseudomonas Aeruginosa Growth: Comparison of Gene Expression in Planktonic Cultures and Developing and Mature Biofilms. *J. Bacteriol* 187, 6571–6576. doi: 10.1128/JB.187.18.6571-6576.2005

Wasterlain, A. S., Goswami, K., Ghasemi, S. A., and Parvizi, J. (2020). Diagnosis of Periprosthetic Infection: Recent Developments. *J. Bone Joint Surg. Am.* 102, 1366–1375. doi: 10.2106/Jbjs.19.00598

Wegner, A., Meiser, J., Weindl, D., and Hiller, K. (2015). How Metabolites Modulate Metabolic Flux. *Curr. Opin. Biotech.* 34, 16–22. doi: 10.1016/j.copbio.2014.11.008

Whiteley, M., Bangera, M. G., Bumgarner, R. E., Parsek, M. R., Teitzel, G. M., Lory, S., et al. (2001). Gene Expression in Pseudomonas Aeruginosa Biofilms. *Nature* 413, 860–864. doi: 10.1038/35101627

Wilson, S., Hamilton, M. A., Hamilton, G. C., Schumann, M. R., and Stoodley, P. (2004). Statistical Quantification of Detachment Rates and Size Distributions of Cell Clumps From Wild-Type (PAO1) and Cell Signaling Mutant (JP1) Pseudomonas Aeruginosa Biofilms. *Appl. Environ. Microb.* 70, 5847–5852. doi: 10.1128/AEM.70.10.5847-5852.2004

Tacconelli, E., Magrini, N., Carmeli, Y., Harbarth, S., Kahlmeter, G., Kluytmans, J., et al. (2017). *Global Priority List of Antibiotic-Resistant Bacteria to Guide Research, Discovery, and Development of New Antibiotics*. World Health Organization, pp. 1–7. Available at: http://www.who.int/medicines/publications/WHO-PPL-Short_Summary_25Feb-ET_NM_WHO.pdf. Last date of access: January 30, 2022.

Xia, J. G., Psychogios, N., Young, N., and Wishart, D. S. (2009). MetaboAnalyst: A Web Server for Metabolomic Data Analysis and Interpretation. *Nucleic Acids Res.* 37, W652–W660. doi: 10.1093/nar/gkp356

Yeom, J., Shin, J. H., Yang, J. Y., Kim, J., and Hwang, G. S. (2013). H-1 NMR-Based Metabolite Profiling of Planktonic and Biofilm Cells in

Acinetobacter Baumannii 1656-2. *PloS One* 8 (3), e57730. doi: 10.1371/journal.pone.0057730

Zhang, L., Chiang, W. C., Gao, Q., Givskov, M., Tolker-Nielsen, T., Yang, L., et al. (2012). The Catabolite Repression Control Protein Crc Plays a Role in the Development of Antimicrobial-Tolerant Subpopulations in Pseudomonas Aeruginosa Biofilms. *Microbiol. (Reading)* 158 (Pt 12), 3014–3019. doi: 10.1099/mic.0.061192-0

Zhang, B., and Powers, R. (2012). Analysis of Bacterial Biofilms Using NMR-Based Metabolomics (Vol 4, Pg 1273, 2012). *Future Med. Chem.* 4, 1764–1764. doi: 10.4155/fmc.12.59

Conflict of Interest: The authors declare that the research was conducted in the absence of any commercial or financial relationships that could be construed as a potential conflict of interest.

Publisher's Note: All claims expressed in this article are solely those of the authors and do not necessarily represent those of their affiliated organizations, or those of the publisher, the editors and the reviewers. Any product that may be evaluated in this article, or claim that may be made by its manufacturer, is not guaranteed or endorsed by the publisher.

frontiers in Cellular and Infection Microbiology

REVIEW
published: 25 February 2022
doi: 10.3389/fcimb.2022.850030

Combination Therapies for Biofilm Inhibition and Eradication: A Comparative Review of Laboratory and Preclinical Studies

Sophia Hawas[1,2], *Anthony D. Verderosa*[1,2] *and Makrina Totsika*[1,2]*

[1] Centre for Immunology and Infection Control, Queensland University of Technology, Brisbane, QLD, Australia, [2] School of Biomedical Sciences, Queensland University of Technology, Brisbane, QLD, Australia

Microbial biofilms are becoming increasingly difficult to treat in the medical setting due to their intrinsic resistance to antibiotics. To combat this, several biofilm dispersal agents are currently being developed as treatments for biofilm infections. Combining biofilm dispersal agents with antibiotics is emerging as a promising strategy to simultaneously disperse and eradicate biofilms or, in some cases, even inhibit biofilm formation. Here we review studies that have investigated the anti-biofilm activity of some well-studied biofilm dispersal agents (e.g., quorum sensing inhibitors, nitric oxide/nitroxides, antimicrobial peptides/amino acids) in combination with antibiotics from various classes. This review aims to directly compare the efficacy of different combination strategies against microbial biofilms and highlight synergistic treatments that warrant further investigation. By comparing across studies that use different measures of efficacy, we can conclude that treating biofilms *in vitro* and, in some limited cases *in vivo*, with a combination of an anti-biofilm agent and an antibiotic, appears overall more effective than treating with either compound alone. The review identifies the most promising combination therapies currently under development as biofilm inhibition and eradication therapies.

Keywords: antimicrobial resistance (AMR), anti-biofilm, infection, nitroxides, antibiotics, nitric oxide (NO), quorum sensing inhibitors (QSI), antimicrobial peptides (AMPs)

OPEN ACCESS

Edited by:
Carina Almeida,
Instituto Nacional Investigaciao Agraria e Veterinaria (INIAV), Portugal

Reviewed by:
Sarah Maddocks,
Cardiff Metropolitan University, United Kingdom
Laura Cerqueira,
University of Porto, Portugal
Pilar Teixeira,
University of Minho, Portugal

***Correspondence:**
Makrina Totsika
makrina.totsika@qut.edu.au

Specialty section:
This article was submitted to Biofilms, a section of the journal Frontiers in Cellular and Infection Microbiology

Received: *07 January 2022*
Accepted: *04 February 2022*
Published: *25 February 2022*

Citation:
Hawas S, Verderosa AD and Totsika M (2022) Combination Therapies for Biofilm Inhibition and Eradication: A Comparative Review of Laboratory and Preclinical Studies. Front. Cell. Infect. Microbiol. 12:850030. doi: 10.3389/fcimb.2022.850030

INTRODUCTION

When planktonic bacterial cells contact a surface, whether biotic or abiotic, they can irreversibly attach to it, proliferate, and form complex three-dimensional communities known as biofilms (Vestby et al., 2020). Biofilms are inherently tolerant to environmental stress, antimicrobials, and host immune responses (McDougald et al., 2011; Vestby et al., 2020). Consequently, biofilms pose a major clinical challenge as biofilm-related infections are extremely difficult to treat or permanently eradicate, with very few viable treatments or management options available (Azevedo et al., 2020; Vishwakarma, 2020). Current strategies for managing biofilm-related infections are aimed at: (i) preventing biofilm formation, (ii) limiting biofilm expansion, or (iii) biofilm eradication by chemical or mechanical means (e.g. removal) (Vuotto and Donelli, 2019; Zhao et al., 2019 Azevedo et al., 2020).

Achieving complete biofilm eradication with antibiotics alone is extremely challenging, with even clinically significant bacterial reduction being often hard to achieve. The precise mechanism by which conventional antibiotics fail to eradicate biofilms is not fully understood and has been the topic of extensive investigation (Gilbert et al., 2002; Lewis, 2008; Høiby et al., 2010). Restricted drug penetration resulting from the presence of a protective extracellular matrix, reduced cell growth, and the presence of persister cells within biofilms (quiescent cells exhibiting extreme antimicrobial tolerance) are all thought to contribute to the high antibiotic tolerance of biofilms (McDougald et al., 2011). To address this challenge, several new and innovative strategies have come under intense investigation (Barraud et al., 2015; Brackman and Coenye, 2015; Pletzer and Hancock, 2016; Fleming and Rumbaugh, 2017). Many of these, such as the development of biofilm inhibition, dispersal, and eradication agents, have been extensively reviewed elsewhere (Fleming and Rumbaugh, 2017; Roy et al., 2018; Verderosa et al., 2019c; Ghosh et al., 2020). Here we focus on studies whereby biofilm dispersal agents are co-administered with antimicrobials and evaluated as combination treatment strategies against bacterial biofilms.

Biofilm dispersal agents rarely possess inherent antimicrobial activity. As such, their potential use as biofilm treatment strategies requires supplementation with an effective antimicrobial agent to successfully disperse and eradicate biofilms (Fleming and Rumbaugh, 2018). Several promising classes of biofilm dispersal agents have been reported to date (Kaplan, 2010); however, the true therapeutic potential of dispersal agents lies in their ability to restore or synergistically enhance the activity of commonly prescribed antimicrobials. In clinical settings, co-treatment is imperative as biofilm dispersal alone would result in translocation of live bacteria to new sites in the body and the subsequent seeding of new infection foci (Fleming and Rumbaugh, 2018). Upon combining a dispersal agent with an effective antibiotic/antimicrobial, the combined treatment both disperses and eradicates biofilm-residing cells, thus preventing further dissemination (**Figure 1**).

This review aims to collate and compare studies that have evaluated biofilm dispersal and eradication combination treatments against established biofilms from clinically relevant pathogens. Important details of the studies cited in this review have been summarised in a comprehensive table (**Table S1**), where the efficacy of the standalone treatments (biofilm dispersal agent or antibiotic) was compared to the efficacy of the combination treatment as reported within each study. For studies where the combination efficacy was greater than the sum of the standalone strategies, these have been included in a summary table (**Table 1**) showcasing the most promising anti-biofilm combination treatments currently under intense study.

CELL-SIGNALLING DISRUPTERS

Quorum Sensing Inhibitors (QSIs)

Quorum sensing (QS) is a bacterial communication system which allows neighbouring cells to send and receive signal molecules, called autoinducers, in a density-dependent manner. QS has been shown to play a pivotal role in biofilm regulation for many species (Brackman and Coenye, 2015). Targeting QS with inhibitors (QSIs) has been a significant innovation in the antibiofilm field, even though the role of QSIs in biofilm formation and dispersal is not always fully understood for different Gram-positive and Gram-negative bacteria (Brackman

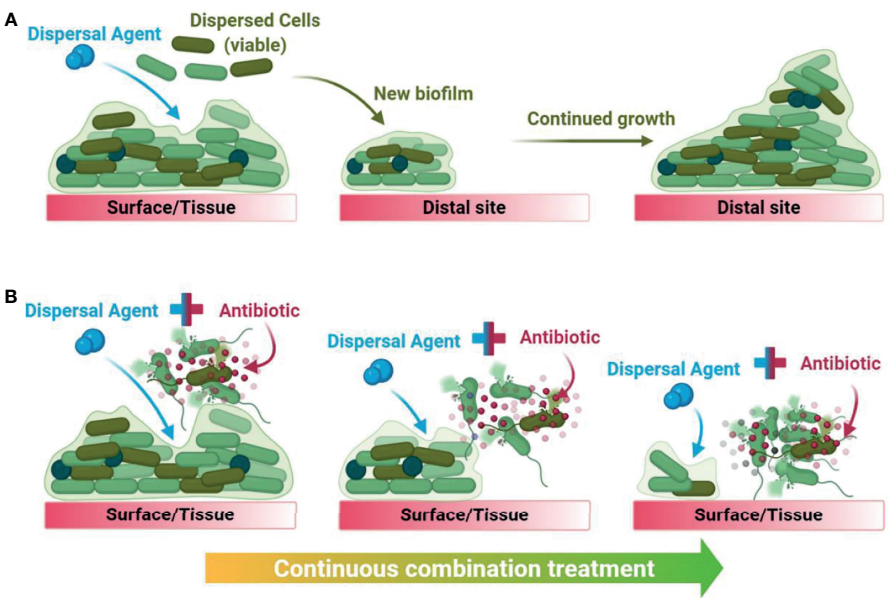

FIGURE 1 | Graphical summary of the downstream consequences of treating a biofilm with dispersal agents alone **(A)** versus with a biofilm dispersal-eradication combination strategy **(B)**, demonstrating how it is clinically and industrially relevant.

TABLE 1 | List of promising combination treatments against bacterial biofilms currently in development.

Dispersal Agent	Antibiotic	Tested Species	Treatment Efficacy (Reduction over untreated biofilm)			*In vivo*	Ref
			Combination	Dispersal Agent	Antibiotic		
Quorum Sensing Inhibitors (QSIs)							
Baicalin hydrate, cinnamaldehyde, hamamelitannin	Tobramycin, clindamycin, vancomycin	*P. aeruginosa*	**68-90%**[1]	<1%	45%		(Brackman et al., 2011)*
Hamamelitannin analogue 38	Vancomycin, cephalexin	*S. aureus*	**5.75-log**[2]	≤1-log	3.75-log	✓	(Vermote et al., 2016)*
Cyclodextrin– Hamamelitannin	Vancomycin	*S. aureus*	**5.5-log**[2]	1-log	3.5-log		(Brackman et al., 2016)*
C11	Ciprofloxacin, tobramycin, colistin	*P. aeruginosa*	**4-6-log**[3]	<1-2-log	1-2-log		(Furiga et al., 2015)*
3-amino-7-chloro-2-nonylquinazolin-4(3H)-one (ACNQ)	Ciprofloxacin	*P. aeruginosa*	**80%**[4]	10%	50%		(Singh et al., 2019)*
FS10	Tigecycline	*S. aureus*	**5.75-6-log**[2]	1.5-1.75-log	3.5-4-log	✓	(Simonetti et al., 2016)*
FS8	Tigecycline	*S. aureus*	**5-log**[2]	2-log	2-log	✓	(Simonetti et al., 2013)*
4-dimethylaminocinnamic acid (DCA) and 4-methoxycinnamic acid (MCA)	Tobramycin	*C. violaceum*	**>5-log**[2]	<1-log	≤1-log		(Cheng et al., 2020)
Nitric Oxide and Nitroxides							
NO (diazeniumdiolate nanoparticles)	Gentamicin	*P. aeruginosa*	**90%**[4]	≤30%	≤30%		(Nguyen et al., 2016)
NO (diethylamin-cephalosporin-30diazeniumdiolate)	Tobramycin	*P. aeruginosa*	**65%**[5]	50%	<1%		(Soren et al., 2020)
nitroxide 4-carboxy-2,2,6,6tetramethylpiperidine 1-oxyl (CTEMPO)	Ciprofloxacin	*P. aeruginosa*, EHEC	**87-99.3%**[6]	60-71%	<1%		(Reffuveille et al., 2015)
CTMIO	Ciprofloxacin	*S. aureus*	**1024 μM**[7]	>2048 μM	4096 μM		(Verderosa et al., 2019a)*
ciprofloxacin-CTMIO hybrid	N/A[11]		**64 μM**[7]	N/A	N/A		
CTEMPO	Ciprofloxacin	UPEC	**≤800 μM**[7]	>1000 μM	≤800 μM		(Verderosa et al., 2019b)*
Dinitroxide-ciprofloxacin hybrid (CDN11)	N/A		**≤400 μM**[7]	N/A	N/A		
Antimicrobial Peptides (AMPs)							
G10KHc	Tobramycin	*P. aeruginosa*	**4-log**[2]	<1-log	<1-log		(Eckert et al., 2006)
LFchimera	Doxycycline	*A. actinomycetemcomitans*	**87%**[8]	6%	3%		(Lachica et al., 2019)
Temporin A (TEMP-A), citropin 1.1 (CIT-1.1) and tachyplesin I linear analogue (TP-1-L)	Colistin	*P. aeruginosa*	**6-log**[2]	≤1-log	1-2-log		(Jorge et al., 2017)*
Melimine, Mel4	Ciprofloxacin	*P. aeruginosa*[9]	**84-90%**[5]	<1%	65%		(Yasir et al., 2020)*
Melittin (hydrogel)	Tobramycin	*P. aeruginosa*	**4.2-fold**[10]	no change	1.8-fold	✓	(Maiden et al., 2019)
AMP38	Imipenem	*P. aeruginosa*	**62.5 μg/mL**[7]	>500 μg/mL	>500 μg/mL		(Rudilla et al., 2016)*
Repurposed Drugs							
Ambroxol	Vancomycin	*S. epidermidis*	**7-log**[2]	<1 log	~3-log	✓	(Zhang et al., 2015)

[1]*% reduction in total biofilm colony forming units (CFU).*
[2]*log reduction in CFU/mL.*
[3]*log reduction in biofilm CFU/cm^2.*
[4]*% reduction in viable biofilm bacteria (CFU).*
[5]*% reduction in total biofilm biomass.*
[6]*% Biofilm eradication (CFU).*
[7]*Minimum Biofilm Eradication Concentration (MBEC).*
[8]*% reduction biofilm CFU/cm^2.*
[9]*against ciprofloxacin-sensitive isolates.*
[10]*fold reduction in biofilm bioluminescence.*
[11]*N/A denotes hybrid compound testing, hybrids already contained the antibiotic and were not tested in combination with additional antibiotics.*
**Low cytotoxicity to human cell lines or in tested in vivo model.*
*All studies investigating biofilm co-treatments cited in this review were compiled into a table comparing the efficacy of the dispersal agent, antibiotic alone, and combination treatment (**Table S1**). Where co-treatment was more effective than the sum of the standalone treatments, the combination treatment was deemed promising, and these studies are summarized here under different dispersal agent groups (QSIs, NO/Nitroxides, AMPs, Repurposed Drugs). Other study details provided include the name of the dispersal agent(s) and antibiotic(s), bacterial species tested, and if the combination treatment was tested against biofilm infection in vivo. Efficacy measures for each study are different (as marked in the combination column and relevant footnote); efficacy measures reported are in relation to untreated biofilm controls in all studies.*

and Coenye, 2015). QS inhibition can occur by inhibiting autoinducer synthesis, degradation of signalling molecules, interfering with signal binding, and inhibition of the signal transduction cascade, which results in dysregulated biofilm signalling and subsequently, dispersal or inhibition of the biofilm (Brackman and Coenye, 2015; Jiang et al., 2019). Most QSIs are derived from proteins (autoinducers, transcription factors and regulators) that mediate QS in the bacterial target, acting as competitive inhibitors of these systems.

Several studies have been conducted using QSIs in combination with antibiotics to either inhibit and/or eradicate biofilms. One of the earliest studies, conducted by Brackman et al., focused on the efficacies of baicalin hydrate, cinnamaldehyde, and hamamelitannin (structures shown in **Figure 2**) in combination with the antibiotics tobramycin, clindamycin, and vancomycin (Brackman et al., 2011). These compounds were tested against established (24-hour) *Pseudomonas aeruginosa* and *Staphylococcus aureus* biofilms in Mueller-Hinton agar (Brackman et al., 2011). Initial *in vitro* testing showed that individual treatment with inhibitor or antibiotic alone was largely ineffective (<10% reduction in biofilm bacterial numbers) against *P. aeruginosa* ATCC 9027 and *S. aureus* CS1 and Mu50. Tobramycin alone reduced only *P. aeruginosa* PAO1 biofilm bacterial numbers by 45% (Brackman et al., 2011). When biofilms were treated with a combination of QSI and antibiotic, viable bacteria for all strains showed a 68-90% reduction (**Table 1**), except *S. aureus* Mu50, which were only reduced by 6% when treated with clindamycin and a QSI (Brackman et al., 2011). This strain has been shown to be resistant to clindamycin planktonically, which may explain reduced efficacy also against its biofilms (Cui et al., 2009).

These QSI-antibiotic combinations were also evaluated *in vivo* against *Burkholderia cenocepacia* and *Burkholderia multivorans*, in a *Caenorhabditis elegans* and *Galleria mellonella* survival model and in a mouse lung infection model (Brackman et al., 2011). QSIs alone exacted a strain-dependent effect on the survival of *G. mellonella*, with a minimal protective effect observed against the *Burkholderia* spp. (0-30% survival) but very high protection in larvae infected with *S. aureus* (70-100% survival) (Brackman et al., 2011). In *C. elegans*, none of the QSIs alone exhibited any protective effect (<10% survival) (Brackman et al., 2011). Standalone antibiotic treatment in *C. elegans* showed increased survival compared to the inhibitor only, and this was also observed for *G. mellonella* (Brackman et al., 2011). Combination treatment exhibited the most protective effect, with most combinations resulting in 80-100% survival when infected with either *P. aeruginosa* and *S. aureus*. These outcomes were further confirmed in the mouse model, which showed that the combination of tobramycin (30 mg/kg) and baicalin hydrate (2 mg/kg) reduced pulmonary bacterial numbers by 99.9% (Brackman et al., 2011).

The same authors extended their investigation of hamamelitannin, by testing it in combination with several antibiotics (vancomycin, cefazolin, cefalonium, cephalexin, cefoxitin, daptomycin, linezolid, tobramycin, fusidic acid) against established *S. aureus* biofilms (Brackman et al., 2016). Here they measured the efficacy of single treatment (antibiotic only) and compared it to combination treatment (antibiotic and hamamelitannin). For all antibiotics, combination treatment was at least equally as effective but, in most cases, resulted in greatly increased efficacy (40-70% additional biofilm eradication compared to antibiotic treatment alone) (Brackman et al., 2016). The most effective combinations were hamamelitannin with cefazolin, cefoxitin, tobramycin or fusidic acid, which resulted in ≥90% eradication of the biofilm (Brackman et al., 2016). Similarly, Vermote et al. derived a hamamelitannin analogue (compound-38) that was reported to have a 20-fold lower median minimum bactericidal (MBC_{50}) value against *S. aureus* Mu50 planktonic cells (Vermote et al., 2016). Mirroring the initial hamamelitannin study (Brackman et al., 2011), all combinations were at least as, or more effective than their standalone counterpart (Vermote et al., 2016). The most effective combinations were compound-38 with vancomycin, cefazolin, daptomycin or tobramycin (≥90% eradication, **Table 1**) (Vermote et al., 2016). Combined, these studies

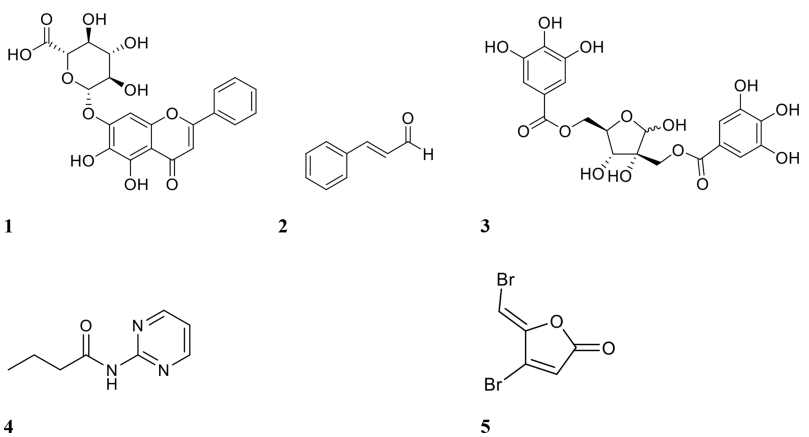

FIGURE 2 | Chemical structures of QSIs 1 baicalin, 2 cinnamaldehyde, 3 hamamelitannin, 4 *N*- (2-pyrimidyl)butanamide (C11), and 5 furanone C-30.

suggest that hamamelitannin is most effective against biofilm bacteria when administered with the antibiotics cefazolin and tobramycin (Brackman et al., 2016; Vermote et al., 2016).

In a different study, Brackman et al. incorporated hamamelitannin into a delivery system to improve its efficacy against *S. aureus* biofilms (Brackman et al., 2016). They achieved this by incorporating the inhibitor into a cyclodextrin complex which could release the QSI and an antibiotic at a controlled rate (Brackman et al., 2016). Utilising these complexes as a delivery system increased efficacy *in vitro*, and the use of the delivery system with hamamelitannin alone reduced biofilm CFU by 1 log (Brackman et al., 2016). However, when the system was used in combination with both vancomycin and hamamelitannin, biofilm CFUs were reduced by 5.5 logs (**Table 1**) (Brackman et al., 2016). Hamamelitannin thus appears to demonstrate a broad-spectrum of biofilm-eradication potentiating activity when administered as a co-treatment with antibiotics. Furthermore, it synergised well with antibiotics from different classes. These properties make hamamelitannin one of the more promising QSIs reviewed here, warranting further exploration into its synergistic capabilities. Given that hamamelitannin has already been tested *in vivo* in mice, this warrants further investigation into its potential toxicity and side effects, before moving into clinical development. As successful analogues with similar efficacies have also been developed (Vermote et al., 2016), this dispersal agent has potential to be modified chemically as well.

Other promising QSIs have also been tested in combination with antibiotics against biofilms. Some of these include furanone C-30 and C11 (structures shown in **Figure 2**), ajoene (garlic extract), 3-amino-7-chloro-2-nonylquinazolin-4(3H)-one (ACNQ) (PqsR receptor inhibitor), derivatives of cinnamic acid, horseradish extract and alkylquinolone-based inhibitors. Christensen et al. investigated combinations of tobramycin and the inhibitors furanone C-30, ajoene, and horseradish extract against *P. aeruginosa* biofilm infection *in vivo* using a mouse intraperitoneal implant model (Christensen et al., 2012). Tobramycin alone failed to reduce bacterial numbers by more than 1 log, but combination treatment reduced bacteria by up to 3 logs (Christensen et al., 2012). Treatment with inhibitor alone however, also showed similar efficacy, suggesting that the interaction between the two compounds was additive rather than synergistic. A derivative of a signalling molecule in *P. aeruginosa* QS, C11, was also tested in combination with the antibiotics ciprofloxacin, tobramycin, ceftazidime, and colistin against forming *P. aeruginosa* biofilms (Furiga et al., 2015). Treatment with individual agents reduced biofilm surface area (CFU/cm^2) by 1-2 logs, while combination treatment with antibiotics and C11 resulted in a 4-6-log reduction (**Table 1**) (Furiga et al., 2015). The only combination which was not synergistic was ceftazidime and C11, reducing biofilm surface area only by 1-2 logs (Furiga et al., 2015).

Building upon this work, Singh et al. used an inhibitor similar to C11 which also targets QS in *Pseudomonas* spp (Singh et al., 2019). Using engineered polymeric nanoparticles as a delivery system, they co-delivered the inhibitor ACNQ (4 μg/mL) and ciprofloxacin (60 μg/mL) to treat established *P. aeruginosa* biofilms (Singh et al., 2019). Individual treatments with the inhibitor and antibiotic were somewhat effective (10% and 50% eradication, respectively), however, combination treatment significantly enhanced eradication of established biofilms (80% eradication; **Table 1**) (Singh et al., 2019). Using an alternative delivery system, Ho et al. tested the alkylquinolone QSI [1] (20 μM) in combination with tobramycin (25 μg/mL) to treat *P. aeruginosa* biofilms (24-hours) (Ho et al., 2020). Here they employed a squalenyl hydrogen sulfate nanoparticle delivery system to deliver both compounds at the same time (Ho et al., 2020). Treatment with the antibiotic alone resulted in a 4-5-log reduction in biofilm CFU compared to the untreated control, regardless of the mode of delivery (Ho et al., 2020). Combination treatment with the delivery system achieved complete eradication (>6-log reduction), whereas combination treatment without the delivery system resulted in 3-4-log less eradication (Ho et al., 2020). Thus, the design of the delivery system is important for combination treatment with QSIs. The dual nature of a combination treatment suggests that for it to be successful, both compounds must be in the same environment at the same time to work effectively, as depicted in **Figure 1B**. As standalone treatments do not need to interact with any other compounds, this may be why the delivery system had no impact on their efficacy, as reported in this study. This should be taken into consideration when designing future co-treatment strategies.

Another studied QSI is baicalin (**Figure 2**), a flavonoid isolated from the roots of *Scutellaria baicalensis* (Chinese skullcap) (Slachmuylders et al., 2018). Using this compound, Slachmuylders et al. examined biofilm eradication in combination with tobramycin, gentamicin, kanamycin or neomycin (Slachmuylders et al., 2018). Tobramycin was the most effective against several strains of *Burkholderia* spp. when combined with baicalin hydrate (75-95% increase in biofilm eradication against 5 out of 9 strains tested, compared to antibiotic treatment alone) (Slachmuylders et al., 2018). Similarly, Luo et al. tested baicalin in combination with levofloxacin, amikacin, and ceftazidime against *P. aeruginosa* biofilms (Luo et al., 2017). Amikacin and baicalin were the most effective combination for biofilm inhibition *in vitro*, while *in vivo* (mouse peritoneal implant model), ceftazidime and baicalin were the most effective combination for reducing bacterial numbers (Luo et al., 2017).

Another series of QS inhibitors shown to be active against *S. aureus* are analogues of the RNA-III inhibiting peptide (RIP) (Cirioni et al., 2013; Simonetti et al., 2013; Simonetti et al., 2016). Mouse studies using the QSIs FS3 and FS8 with daptomycin and tigecycline, respectively, demonstrated additive and synergistic efficacy against *S. aureus* biofilms (Cirioni et al., 2013; Simonetti et al., 2013). In these studies, Cirioni et al. and Simonetti et al. implanted grafts (with or without inhibitor) and injected *S. aureus* into the graft site while the antibiotic was administered intraperitoneally (Cirioni et al., 2013; Simonetti et al., 2013; Simonetti et al., 2016). Treatment with the QSI or antibiotic alone resulted in a 2-3-log reduction in bacterial numbers after 7 days of infection, compared to the untreated control group (Cirioni et al., 2013; Simonetti et al., 2013).

Treatment with both compounds resulted in an additive effect for FS3 and daptomycin (4-log reduction) and a synergistic effect for FS8 and tigecycline (5-log reduction, **Table 1**) (Cirioni et al., 2013; Simonetti et al., 2013). Following on from this, FS10 was also tested in combination with tigecycline and showed similar results in the same mouse infection model against both methicillin-susceptible *S. aureus* (MSSA) and MRSA (Simonetti et al., 2016). Groups treated with FS10 alone showed minimal CFU reduction after 7 days post implantation (1-2-log reduction), while groups treated with tigecycline only showed higher log reduction in bacterial numbers (3.5-4 logs, **Table 1**) (Simonetti et al., 2016). Combination treatment was the most efficacious against both MSSA and MRSA, reducing bacterial numbers by 5.5-6 logs (Simonetti et al., 2016). Considering that the inhibitor and antibiotic are administered separately, administration of both at the same site could potentially improve efficacy.

Lastly, cinnamic acid, a metabolite of *Cinnamomum cassia* (Chinese cinnamon), has recently been shown to inhibit quorum sensing in bacteria (Vasconcelos et al., 2018). In a study by Cheng et al., two synthesised cinnamic acid derivatives, 4-dimethylaminocinnamic acid (DCA) and 4-methoxycinnamic acid (MCA) were tested in combination with tobramycin against *Chromobacterium violaceum* biofilms (Cheng et al., 2020). Individual treatments were largely ineffective at eradicating established biofilms (≤1-log reduction in biofilm CFU counts), though combination treatment was highly successful and resulted in a 5-log CFU reduction compared to the untreated control, see **Table 1** (Cheng et al., 2020). It is also noteworthy that the core structures of these compounds are amenable to synthetic modification, which makes them ideal candidates for the development of more potent derivatives. In conjunction with this, additional *in vivo/ex vivo* studies should be conducted to test the toxicity of newly modified inhibitors while also assessing discrepancies between *in vitro vs. in vivo* effects.

Overall, quorum sensing inhibitors are a promising class of biofilm disruptors. Most QSI studies to date demonstrate that while they are not effective at eradicating biofilms on their own, when used together with antibiotics they can effectively eradicate established biofilms both *in vitro* and *in vivo*. Continued research into QSIs is sorely needed, as many of the mechanisms inhibited by them are poorly understood (Brackman and Coenye, 2015). Additionally, further manipulation of the structures of these inhibitors would open many avenues of therapeutic development, considering their amenability to synthetic modification.

Nitric Oxide

Nitric oxide (NO) is a free radical colourless gas (at room temperature), and a well-established signalling molecule in eukaryotic organisms (Barraud et al., 2015). One of the earliest uses of NO as a biofilm dispersal agent was documented by Barraud et al. (2006) and since then its potential as a biofilm dispersal agent has been widely documented. While NO concentrations at the mM range are antibacterial (Barraud et al., 2015), inhalation of NO gas at such high concentrations is also acutely toxic to the respiratory tract of humans (Weinberger et al., 2001). However, NO-mediated biofilm dispersal occurs at concentrations sublethal for bacteria (nM range) (Barraud et al., 2006). Thus, the use of NO as an effective biofilm eradication strategy requires supplementation with an antimicrobial agent. NO signals dispersal of bacterial biofilms by interacting with enzymes that affect intracellular concentrations of bis-(3′-5′)-cyclic dimeric guanosine monophosphate (c-di-GMP) (Williams and Boon, 2019). The molecular mechanism was recently characterised in some species of bacteria, including *P. aeruginosa*, *Nitrosomonas europaea*, and *Shewanella oneidensis* (Hossain and Boon, 2017; Hossain et al., 2017; Nisbett et al., 2019). Interaction of NO with NO-sensitive enzymes stimulates the activity of phosphodiesterases (PDEs), which degrade c-di-GMP and signal biofilm dispersal (McDougald et al., 2011).

Several studies have tested NO for its ability to potentiate antibiotics *in vitro* (Barraud et al., 2009; Nguyen et al., 2016; Liu et al., 2020; Soren et al., 2020). NO is a difficult molecule to work with due to its gaseous form at room temperature and high reactivity (Barraud et al., 2015). Hence, most studies have used NO donors, such as sodium nitroprusside (SNP) and (Z)-1-[N-Methyl-N-[6-(N-methylammoniohexyl)amino]]diazen-1-ium-1,2-diolate (MAHMA NONOate) (Barraud et al., 2009; Barnes et al., 2013; Marvasi et al., 2015) (structure shown in **Figure 3**), which albeit are also known to be inherently unstable molecules (Wang et al., 2002). In order to address this, several NO delivery

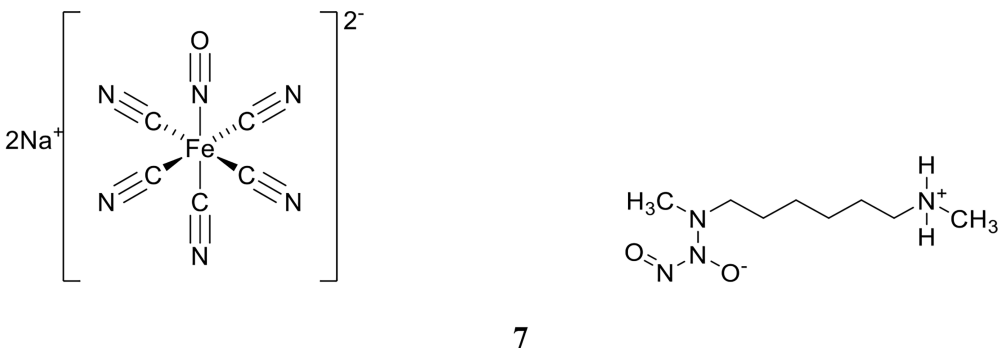

6 7

FIGURE 3 | Chemical structures of 6 sodium nitroprusside (SNP) and 7 (Z)-1-[N-Methyl-N-[6-(N-methylammoniohexyl)amino]diazen-1-ium-1,2-diolate (MAHMA NONOate).

systems have been reported to release NO in a controlled manner at the target site (Lu et al., 2013; Nguyen et al., 2016; Ren et al., 2016; Liu et al., 2020). Examples of these include diazeniumdiolate (NONOate), micro/nanoparticles, and amphiphilic poly(amidoamine) (PAMAM) dendrimers (Lu et al., 2013; Nguyen et al., 2016; Soren et al., 2020). These systems improve handling and dose mediation, prevent or limit off-target effects, and increase the efficacy of biofilm dispersal by NO while minimising cytotoxicity to the host (Davies et al., 2001; Findlay et al., 2004; Poh et al., 2017; Yang et al., 2018; Verderosa et al., 2019c). In this section, we review studies that have combined NO with antibiotics for either dispersing or eradicating clinically relevant biofilms, while excluding studies which have only tested NO alone *in vitro*.

In one of the earlier *in vitro* studies, Barraud et al. investigated the potentiation of tetracycline by NO against biofilms from a variety of different bacterial species, using the NO-donor sodium nitroprusside (SNP) (Barraud et al., 2009). Pre-treating *Vibrio cholerae* biofilms with NO and then adding tetracycline reduced the biofilm surface area by 90% compared to untreated biofilms (Barraud et al., 2009). NO alone reduced the biofilm surface area by 67%, while tetracycline alone only afforded a 21% biofilm reduction (Barraud et al., 2009). The study also investigated the ability of NO to potentiate chlorine used for water treatment. Similar to tetracycline, NO treatment of *V. cholerae* biofilms followed by chlorine resulted in significant biofilm reduction (85-90%) compared to untreated controls (Barraud et al., 2009). The authors concluded that NO could enhance the activity of tetracycline and chlorine against biofilms when administered sequentially (NO treatment followed by tetracycline/chlorine treatment), however co-treatment with NO and tetracycline was not investigated, nor was the viability of the dispersed cells.

While sequential treatment of biofilms with a dispersal agent followed by an antibiotic is informative and may find use in industrial settings, such as water treatment, this approach would not be suited to the clinical setting. Dispersing a clinical biofilm prior to antimicrobial intervention can lead to systemic bacterial dissemination, which can result in spread of infection, septicaemia, and bacteraemia (Fleming and Rumbaugh, 2018; Müsken et al., 2018). For this reason, subsequent biofilm studies have focused on NO co-treatment with antibiotics.

NO co-administration with antibiotics has been facilitated by delivery systems such as those developed by Soren et al. which use the prodrug diethylamin-cephalosporin-30diazeniumdiolate (DEA-C3D) to investigate the delivery of NO in combination with tobramycin to eradicate *P. aeruginosa* biofilms (Barraud et al., 2012; Soren et al., 2020). DEA-C3D belongs to a class of NO-donor prodrugs known as cephalosporin-30-diazeniumdiolates (C3Ds), which contain the phenacetyl side chain of the first-generation cephalosporin cefaloram and the NO donor diazeniumdiolate (Soren et al., 2020). These compounds deliver NO by local release upon contact with bacterial β-lactamase enzymes (Soren et al., 2020). When used to deliver NO for the treatment of *P. aeruginosa* biofilms, NO alone reduced biofilm biomass by 50%, while treatment with the antibiotic tobramycin alone had no effect on biofilm biomass. However, NO and tobramycin co-delivery reduced biofilm biomass by 65%. While the potentiation of tobramycin was relatively modest, it should be noted that the concentration of antibiotic used in the study was sublethal (Soren et al., 2020), suggesting that efficacy could be likely increased by using tobramycin at higher concentrations. A similar potentiation trend was also observed for colistin. Despite colistin treatment alone being extremely effective against *P. aeruginosa* biofilms (90% biomass reduction), co-treatment with DEA-C3D resulted in almost complete biofilm eradication (98% reduction, **Table 1**) (Soren et al., 2020). The design of this NO delivery strategy is certainly innovative; however, its application is limited to β-lactamase-producing bacteria, and furthermore, it is unfortunate that the antibacterial properties of the delivery system (β-lactam) are lost upon NO release, which was an intentional design feature (Soren et al., 2020). The authors comment that the ultimate goal of this delivery system is to deliver NO to a targeted site, containing β-lactamase-producing bacteria, to reduce tissue damage from NO's reactivity (Soren et al., 2020). In addition, as the study determined biofilm eradication by visualising remaining cells, dispersed cells were not studied. This makes it difficult to evaluate the efficacy of this treatment in the context of a "disperse and eradicate" strategy, as it is important to determine whether dispersed cells remained viable or were killed.

Another study targeting *P. aeruginosa* biofilms used a diazeniumdiolate nanoparticle delivery system in combination with the antibiotic gentamicin (Nguyen et al., 2016). Here, Nguyen and co-workers designed and produced a polymeric nanoparticle delivery system that simultaneously released NO and gentamicin at a target site by placing a gentamicin-NONOate complex (generated by reacting gentamicin and NO gas) at the core of the nanoparticle (Nguyen et al., 2016). Co-treatment with NO and gentamicin reduced biofilm viability by 90%, whereas treatment with the individual compounds only reduced viability by ≤30%, (**Table 1**) (Nguyen et al., 2016). These results are promising and should the compound prove to be non-toxic to mammalian cells, a property that was not examined, the strategy would certainly merit *in vivo* analysis. Similarly, Liu et al. engineered a NO delivery system using a derivative of a naturally occurring compound, chitosan (Liu et al., 2020). The donor, chitosan-graft-poly(amidoamine) dendrimer (CS-PAMAM), was used to deliver methicillin and NO to methicillin-resistant *Staphylococcus aureus* (MRSA) biofilms (Liu et al., 2020). They observed that despite the strains being methicillin resistant, co-treatment with methicillin increased biofilm eradication a further 10% than with NO treatment alone (Liu et al., 2020). This study is unique as the target pathogen has acquired resistance to the antibiotic yet co-treatment with NO had an effect, which we speculate suggests that NO was likely dispersing cells from the biofilm outer layer and allowing higher levels of methicillin to access and kill underlying biofilm-residing cells.

The above studies have showcased the promising potential of NO as a biofilm dispersal agent with and without antibiotics *in vitro*. However, studies on NO co-treatments of clinical biofilms using *in vivo* models (cystic fibrosis, urinary tract infections, chronic wounds, etc. (Vestby et al., 2020)] are currently lacking. Nevertheless several *in vivo* studies on NO have provide valuable

insight into its potential use as an infection treatment and or control strategy (Webert et al., 2000; Miller et al., 2012; Miller et al., 2013).

Inhaled NO has been studied as a standalone treatment for pneumonia in rats and has more recently progressed to phase I human trials (Webert et al., 2000; Miller et al., 2012; Miller et al., 2013; Deppisch et al., 2016). A rat model of *P. aeruginosa* pneumonia was initially used to test the efficacy of inhaled NO (Webert et al., 2000; Miller et al., 2012; Miller et al., 2013). Rats were injected intratracheally with 10^8 colony forming units (CFU) of *P. aeruginosa* and then monitored over time for any physiological changes and for bacterial carriage in the lungs (Webert et al., 2000). The study successfully demonstrated that NO could reduce the pulmonary bacterial load after 24 hours of NO inhalation at a concentration of 40 ppm (Webert et al., 2000). A follow up study by the same group demonstrated that an even higher concentration of NO (160 ppm) given intermittently was also effective at lowering viable *P. aeruginosa* counts in the lungs of infected rats (Miller et al., 2013). This confirmed previous *in vitro* studies, which had shown that at a concentration of 160ppm, NO is bactericidal (Schairer et al., 2012). The success of these preclinical animal studies paved the way for a small Phase I study on 10 healthy adult volunteers, which confirmed the same dosing regimen of 160 ppm for 30 minutes was safe (Miller et al., 2012). A follow-up pilot clinical study treated eight cystic fibrosis patients suffering from long term (>6 months) bacterial and/or fungal lung infection(s) with gaseous NO for 30 minutes, three times daily, at a concentration of 160 ppm for two periods of five days over two weeks (Deppisch et al., 2016). Patients were followed over the course of seven months and post-NO treatment were all found to have an average log-reduction of 3.6 and 3.0, respectively, of bacteria and fungi (regardless of species) in their sputum samples (Deppisch et al., 2016). In addition to this, ESBL-producing *Escherichia coli* or *Aspergillus* spp. biofilms were undetectable after treatment. This study is one of the first of its kind and is unique from other NO dispersal studies in that it did not require the use of a NO delivery system. Additionally, these studies demonstrate the safety of NO administration even at bactericidal concentrations, which are higher than the concentrations shown to be required to disperse bacterial biofilms *in vitro*. Future clinical studies will greatly enhance the development of new respiratory therapeutics with potential benefits for other respiratory diseases.

Nitroxides

The development of antibacterial and antibiofilm therapies based on NO is often limited by its high reactivity, instability, and inherent human toxicity at high concentrations (Barraud et al., 2015; Verderosa et al., 2019c). Thus, alternatives that mimic the behaviour of NO, but lack its limitations, have recently been explored (de la Fuente-Núñez et al., 2013; O'Loughlin et al., 2013; Rajasekaran et al., 2019).

Nitroxides are structurally similar to NO as both contain an unpaired electron delocalised over the nitrogen-oxygen bond. However, unlike NO, nitroxides are generally air-stable crystalline solids at room temperature, which makes their handling and delivery far more convenient than NO. Furthermore, nitroxides have been recently shown to exhibit similar antibiofilm properties to NO *in vitro* (de la Fuente-Núñez et al., 2013; Verderosa et al., 2016). The antibiofilm properties of nitroxides were first explored by de la Fuente Núñez et al., who showed that nitroxides not only mimicked the biofilm dispersal activity of NO but also prevented biofilm formation *in vitro* (de la Fuente-Núñez et al., 2013). In a follow up study by the same group, nitroxides were shown to potentiate the action of ciprofloxacin against both *P. aeruginosa* and *E. coli* biofilms (Reffuveille et al., 2015). Here, they investigated the ability of the nitroxide 4-carboxy-2,2,6,6tetramethylpiperidine 1-oxyl (CTEMPO) (structure shown in **Figure 4**) to potentiate the activity of ciprofloxacin when administered as a co-treatment (Reffuveille et al., 2015). CTEMPO (20 μM) alone dispersed *P. aeruginosa* and enterohemorrhagic *E. coli* (EHEC) biofilms resulting in significantly reduced biomass (60% and 71%, respectively, **Table 1**) (Reffuveille et al., 2015). At the same concentration, CTEMPO also potentiated ciprofloxacin activity against *P. aeruginosa* and EHEC biofilms, eradicating 99.3% and 93%, respectively (Reffuveille et al., 2015). This occurred at a ciprofloxacin concentration of just 320 ng/mL for *P. aeruginosa* and 20 ng/mL for EHEC when ciprofloxacin treatment alone had

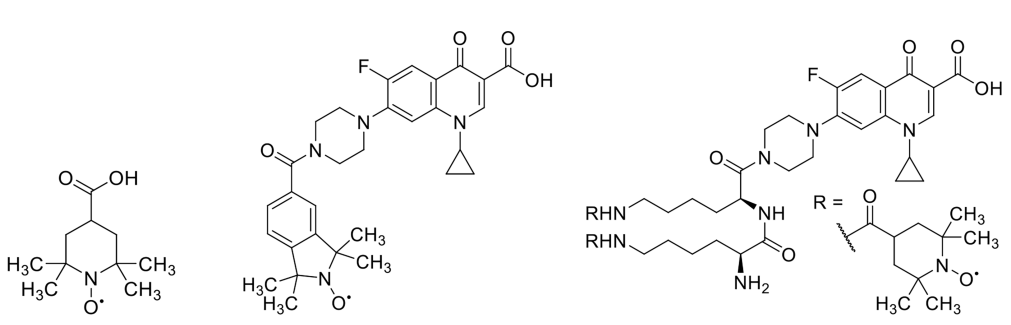

FIGURE 4 | Chemical structures of 8 4-carboxy-2,2,6,6tetramethylpiperidine 1-oxyl (CTEMPO), 9 ciprofloxacin-nitroxide hybrid-27 and 10 dinitroxide-ciprofloxacin hybrid 11 (CDN-11).

no or minimal effect on biofilm biovolume (Reffuveille et al., 2015). Dispersed cells from CTEMPO treated *P. aeruginosa* biofilms were also collected and quantified at 3-, 6- and 24-hours post treatment. Between the 3 and 6 hour treatment timepoints, there was minimal change in bacterial numbers, however after 24 hours, there was a minimum 5-fold change in dispersed bacterial counts (Reffuveille et al., 2015). This suggests that after 24 hours of CTEMPO treatment, the biofilm has been sufficiently dispersed that many cells are becoming dislodged and flowing out of the system.

Verderosa et al. built upon this work by synthetically linking the nitroxide to the ciprofloxacin moiety to create a variety of ciprofloxacin-nitroxide hybrids (Verderosa et al., 2016; Verderosa et al., 2017; Verderosa et al., 2019a; Verderosa et al., 2019b). These hybrid compounds were effective in dispersing and eradicating both Gram-negative (*P. aeruginosa*, uropathogenic *E. coli* (UPEC)) as well as Gram-positive (*S. aureus*) biofilms *in vitro* (Verderosa et al., 2017; Verderosa et al., 2019a; Verderosa et al., 2019b). *P. aeruginosa* biofilms were 94% eradicated with ciprofloxacin-nitroxide hybrid-27 (structure shown in **Figure 4**) treatment at 20 μM (Verderosa et al., 2017). Treatment with the hybrid was on par with the synergy reported previously against *P. aeruginosa* biofilms using CTEMPO and ciprofloxacin co-treatment (Reffuveille et al., 2015). However, hybrid compounds provide some intrinsic advantages over co-treatments, such as *i*) more favourable pharmacokinetic and pharmacodynamic properties and *ii*) insurance that the dual action of dispersal and eradication are contained in the one compound, which is especially important for *in vivo* studies (Verderosa et al., 2017; Fleming and Rumbaugh, 2018). In a follow-up study by Verderosa et al., co-treatment and treatment with hybrid compounds was tested against *S. aureus* biofilms (Verderosa et al., 2019a). Co-treatment with nitroxide (8 μM for CTEMPO) and ciprofloxacin (256 μM) was effective at eradicating biofilms, affording a 16-fold improvement (**Table 1**) in the minimum biofilm eradication concentration (MBEC) (99.9% eradication) compared to ciprofloxacin treatment alone (Verderosa et al., 2019a). Interestingly, treatment with the ciprofloxacin-nitroxide hybrid-27 at 64 μM was 4-fold more potent than co-treatment and 64-fold more potent than ciprofloxacin alone, suggesting that hybrid compounds (dispersal agent linked to antibiotic) may provide distinct advantages over co-treatments against some species (Verderosa et al., 2019a). In a subsequent study, the authors developed a synthetic strategy for altering the ratio of nitroxide to antibiotic producing a dinitroxide-ciprofloxacin hybrid (CDN-11, structure shown in **Figure 4**) with potent activity against UPEC biofilms *in vitro* (Verderosa et al., 2019b). CDN-11 was effective in eradicating biofilm residing UPEC, with a 99% reduction in bacterial numbers (*vs.* untreated group) at 12.5 μM (**Table 1**) (Verderosa et al., 2019b). The use of nitroxides in the eradication of biofilms is certainly encouraging, especially considering how well they can potentiate the activity of ciprofloxacin (either as a co-treatment or in hybrid compounds). However, their ability to potentiate the activity of other classes of antibiotics remains to be explored as does their antibiofilm activity *in vivo*. The lack of human cell toxicity reported for nitroxides and nitroxide functionalised antibiotics (Sadowska-Bartosz et al., 2015; Verderosa et al., 2017) however supports their further development as antibiofilm antimicrobials.

Clearly, NO and nitroxides are effective biofilm dispersal agents and based on *in vitro* and *in vivo* studies, they both hold genuine promise as treatment strategies for biofilm related infections. As co-treatment agents they have also showed synergy with several antibiotics and proved to be effective at eradicating established biofilms. While the combined use of NO, nitroxides and antibiotics is still in early preclinical testing, its development towards clinical applications is likely to progress. Continued assessment against other biofilm-forming organisms (*in vitro* and *in vivo*) is needed to ascertain how broad-spectrum these combinations can be. NO has already been tested against several well established biofilm-forming species, including the fungal pathogen *Candida albicans*, and proven efficacious for biofilm dispersal (Barraud et al., 2009). Further work expanding the testing of such combination treatments towards several other species would aid both their development as therapeutics and understanding of the mechanism behind NO's biofilm dispersing ability, which is likely to differ between microbes.

PEPTIDES/MEMBRANE DISRUPTERS

Antimicrobial Peptides

Antimicrobial peptides (AMPs) are small cationic and amphipathic molecules of 12-50 amino acids that have the ability to disrupt bacterial membranes (Grassi et al., 2017). AMPs exhibit a broad-spectrum of activity and have a high potential to target metabolically dormant cells in biofilms (Grassi et al., 2017). AMPs are often studied in combination with antibiotics and other antibiofilm compounds, and many of these studies have been briefly described by Grassi et al. in 2017 (Grassi et al., 2017). Here, we report the efficacy afforded through combination treatment compared to standalone and also include studies that have been published since then.

An early study on AMP-antibiotic combinations assessed the synergistic activity of the synthetic AMP G10KHc (amino acid sequence shown in **Table 2**) in combination with tobramycin for the eradication of *P. aeruginosa* biofilms (Eckert et al., 2006). Treatment with G10KHc or tobramycin alone (each at 100 μg/mL) for 4 and 24 hours had little effect on established biofilms (Eckert et al., 2006). However, when used together at the same concentrations, a 4-log reduction in bacterial numbers (**Table 1**) was observed after 4 hours of co-treatment, with no viable CFU recovered from the biofilms after 24 hours (Eckert et al., 2006). The same group further investigated how G10KHc potentiated tobramycin activity by staining cells with propidium iodide (PI) and observing whether the dye was present in treated cells, as it cannot enter cells with intact membranes (Krishan, 1975; Eckert et al., 2006). Bacterial cells treated with G10KHc were found to fluoresce, indicating that the peptide disrupted the cell membrane, subsequently allowing tobramycin to enter and kill cells (Eckert et al., 2006).

TABLE 2 | Amino acid sequences of antimicrobial peptides (AMPs) with notable antibiofilm activity.

Peptide Name	Type	Sequence
G10KHc	Synthetic	KKHRKHRKHRKHGGSGGSKNLRRIIRKGIHIIKKYG
Nisin-A	Natural	MSTKDFNLDLVSVSKKDSGASPRITSIS LCTPGCKTGALMGCNMKTATCHCSIHVSK
Melittin	Natural	NH_2-GIGAVLKVLTTGLPALISWIKRKRQQ-$CONH_2$
1018	Synthetic	VRLIVAVRIWRR-NH_2
DJK-6	Synthetic	VQWRRIRVWVIR-$CONH_2$

Naturally Derived Antimicrobial Peptides

A wide variety of inherently antimicrobial peptides exist in nature serving as innate defence proteins against bacteria and produced by many species. Tachyplesin III, for example, is a short peptide from Southeast Asian horseshoe crabs that is similar in structure to the protegrin peptide family, which is also known for its antimicrobial properties (Minardi et al., 2007). Minardi et al. investigated the synergy between Tachyplesin III and piperacillin-tazobactam to treat *P. aeruginosa* biofilms in a rat ureteral stent model (Minardi et al., 2007). Treatment with either Tachyplesin III (10 mg/L stent coating) or piperacillin-tazobactam (120 mg/kg intraperitoneally) resulted in a 3-log reduction of bacterial numbers compared to untreated controls (Minardi et al., 2007). Administered together however, the combination treatment resulted in a 5-log reduction of bacterial numbers, demonstrating synergistic activity (Minardi et al., 2007). In a subsequent study, the AMP BMAP-28 was used in combination with vancomycin to treat *Enterococcus faecalis* and *S. aureus* biofilms (Orlando et al., 2008). The co-treatment was tested both *in vitro* and *in vivo*, again in the rat stent model (Orlando et al., 2008). *In vitro*, a 4-fold decrease in MBEC value was observed, compared to individual treatments (Orlando et al., 2008). *In vivo*, stent cultures taken 5 days post implantation and urine cultures taken 24 hours post implantation showed a 2-3 log reduction in bacterial numbers for both bacterial species when compared to individual treatment groups, and a 5-log reduction compared to untreated controls (Orlando et al., 2008). Despite the agreement between *in vitro* and *in vivo* results, it is important to note that they are not directly comparable, as the methods for quantifying biofilm eradication were different (MBEC *vs* CFU quantification).

Similar to Tachyplesin III, lactoferrin is another peptide with antibacterial and bacterial anti-adhesion properties, and is commonly found in human blood and secreted fluids (Ammons and Copié, 2013). Wakabayashi et al. showed that treatment of *Porphyromonas gingivalis* biofilms with a combination of lactoferrin and ciprofloxacin was very effective, reducing biofilm biomass by 80% (0.5 mg/mL lactoferrin, 10 μg/mL ciprofloxacin) whereas the compounds alone only reduced biofilm biomass by 50% and 40%, respectively (Wakabayashi et al., 2009). Following on from this work, Lachica et al. tested lactoferrin chimera (LFchimera) against *Aggregatibacter actinomycetemcomitans* biofilms, a major causative agent of periodontitis (Lachica et al., 2019). Treatment with LFchimera alone or in combination with doxycycline was assessed for biofilm surface area. Combination treatment was most effective, reducing surface area by 87% compared to the untreated control, while individual treatments only reduced area by <10%, (**Table 1**) (Lachica et al., 2019).

Another naturally derived AMP, nisin, has also been assessed for antibiotic potentiation against biofilms *in vitro*. Nisin is a 34 amino acid peptide that originates from *Lactococcus lactis* and is commonly used as a food preservative (amino acid sequence shown in **Table 2**) (Tong et al., 2014) as it has been shown to have strong antimicrobial activity against many Gram-positive bacteria (Tong et al., 2014). Tong et al. investigated the synergy between nisin and several antibiotics for the eradication of *E. faecalis* biofilms *in vitro* (Tong et al., 2014). All nisin-antibiotic combinations were more effective than individual treatments, except for sulphapyridine, metronidazol, and polymyxin, which demonstrated no improved activity over standalone treatment (Tong et al., 2014). Conversely, for Gram-negative bacteria, Field et al. found that combining nisin with polymyxin and colistin was effective in preventing *P. aeruginosa* biofilm formation (Field et al., 2016). Biofilm formation was only slightly inhibited by the compounds alone at sub-MIC levels, but the combination of nisin (at ¼ MIC) and polymyxin or colistin (at either ½ or ⅕ MIC) completely prevented biofilm growth up to 24 hours (Field et al., 2016). The difference between these two studies suggests that nisin is more synergistic with colistin over polymyxin, despite the antibiotics belonging to the same class. Colistin is a membrane-disrupting antibiotic that serves as a last resort treatment for multidrug resistant infections (Bialvaei and Samadi Kafil, 2015). Synergy between AMPs and colistin was also investigated by Jorge et al, using the AMPs temporin A (TEMP-A), citropin 1.1 (CIT-1.1) and tachyplesin I linear analogue (TP-1-L). AMPs were tested individually and in combination with colistin against *P. aeruginosa* and *S. aureus* biofilms (Jorge et al., 2017). All AMP-antibiotic combinations were effective in inhibiting biofilm formation by at least 2 log (CFU/cm^2) (**Table 1**) (Jorge et al., 2017). The most effective combination was colistin with CIT-1.1, which inhibited formation of *P. aeruginosa* (PAO1) biofilms by 7.7 logs (Jorge et al., 2017). All combinations were also tested for eradication activity against 24-hour established biofilms with only colistin and TP-1-L reported to completely eradicate (6-log reduction in bacterial numbers) *P. aeruginosa* biofilms (Jorge et al., 2017). All other combinations and individual treatments only reduced bacterial numbers by 2 logs or less (Jorge et al., 2017), which suggests that these colistin-AMP combinations are more useful for inhibiting rather than eradicating biofilms. These findings were supported by Mataraci et al., who tested several AMPs (indolicidin, CAMA (cecropin (1-7)–melittin A (2-9) amide), and nisin with multiple antibiotics (daptomycin, linezolid,

teicoplanin, ciprofloxacin, and azithromycin) to prevent the formation of methicillin-resistant *S. aureus* biofilms *in vitro* (Mataraci and Dosler, 2012). All combination treatments (AMP/AMP, AMP/antibiotic and antibiotic/antibiotic) were equally effective at preventing biofilm formation (Mataraci and Dosler, 2012). These findings suggest that biofilms are more susceptible to combination treatment during early development stages. This may be due to lack or reduced biofilm features known to contribute to intrinsic resistance [i.e. a matrix of extracellular polymeric substances (EPS) and persister cells (Verderosa et al., 2019c)], allowing access of AMPs and antibiotics to actively growing biofilm cells.

Kalsy et al. investigated antibiotic combinations with the insect derived peptide cecropin A, which is involved in innate immune defence (Kalsy et al., 2020). Cecropin A was tested for synergy with nalidixic acid against uropathogenic *E. coli* (UPEC) biofilms (Kalsy et al., 2020). Interestingly, cecropin A was highly effective at inhibiting both forming and established biofilms, but combination with nalidixic acid did not improve its eradication activity (Kalsy et al., 2020), supporting the tenet that AMPs in general appear to be more effective at inhibiting biofilm formation over eradication. The fractional inhibitory concentration (FIC) index for cecropin A and nalidixic acid was calculated using the FIC formula (**Figure 5**) (Hall et al., 1983), which was reported <0.5 (indicating synergy), which conflicts with their previous findings (Kalsy et al., 2020). The authors state that UPEC was unlikely to harbour intrinsic resistance to the combination treatment, as its mode of action disrupts the bacterial outer membrane and overcoming this would be genetically and metabolically taxing (Kalsy et al., 2020). They then tested cecropin A and nalidixic acid *in vivo* using a *G. mellonella* (greater wax moth) larvae infection model (Kalsy et al., 2020). Combination treatment of moth larvae was also not protective against UPEC challenge (Kalsy et al., 2020). However, when a protease inhibitor was co-administered, all larvae treated with both cecropin A (50 μg/mL) and nalidixic acid (0.5 ng/mL) survived up to six days post injection with *E. coli* (Kalsy et al., 2020). They proposed that the addition of the protease inhibitor prevented proteolytic degradation of cecropin A *in vivo*, allowing it to have maximal activity in combination with nalidixic acid (Kalsy et al., 2020).

Thappeta et al., investigated the efficacy of the naturally derived chitosan-based peptide CSM5-K5 (structure shown in **Figure 6**) against *S. aureus* biofilms in combination with the antibiotics oxacillin, meropenem or streptomycin (Thappeta et al., 2020). MBC values were 2-3 fold lower with co-treatment compared to standalone treatment, a finding that was confirmed *in vivo* against *S. aureus*, *E. faecalis* and uropathogenic *E. coli* in a mouse wound excision model (Thappeta et al., 2020). The authors also reported little resistance development after 15 days of serially passaging the bacteria *in vitro* in the presence of CSM5-K5 (Thappeta et al., 2020). Similarly, Yasir et al. reported no resistance development to the AMPs melimine and Mel4 against *P. aeruginosa* biofilms after 30 days of exposure at sub-MIC levels (Yasir et al., 2020). Melimine is a cationic chimera of two naturally occurring peptides: melittin and protamine, and Mel4 is a derivative of melimine with demonstrated antibiofilm activity against *P. aeruginosa* (Yasir et al., 2020). Synergy between these AMPs and the antibiotic ciprofloxacin was assessed by measuring reduction in biomass in established (24-hour) ciprofloxacin resistant or sensitive *P. aeruginosa* biofilms (Yasir et al., 2020). Treatment with each peptide or ciprofloxacin alone at 1x MIC had no effect on ciprofloxacin resistant biofilms, but combination treatment at 1x MIC resulted in 61-66% reduction in biofilm mass (**Table 1**) (Yasir et al., 2020). Synergy was also reported against ciprofloxacin sensitive biofilms, where peptide only treatment at 1x MIC had no effect, and while ciprofloxacin reduced biofilm mass by 65%, combination treatment reduced biofilm mass by 84-90% (Yasir et al., 2020).

Recent advances in clinical treatment include the use of hydrogels as scaffolds for long-term drug release in wounds, to maintain wound sterility and aid healing (Azevedo et al., 2020). Maiden et al. investigated the integration of the AMP melittin (amino acid sequence shown in **Table 2**) in an agarose-based hydrogel in addition to co-treatment with the antibiotic tobramycin. Using an *in vivo* mouse wound model, they reported that tobramycin alone reduced biofilm bioluminescence (used here as a measure of biomass) by 1.8-fold after 4 hours, with melittin having no effect (Maiden et al., 2019). However, incorporating both compounds into the hydrogels reduced biofilm bioluminescence 4.2-fold (**Table 1**) (Maiden et al., 2019). Other studies incorporating hydrogels as delivery systems have also reported increased combination treatment efficacy, potentially due to simultaneous release of compounds, and engineered slow release of the compounds over time (Marvasi et al., 2015; Anjum et al., 2018; Maiden et al., 2019).

$$\frac{A}{MIC_A} + \frac{B}{MIC_B} = FIC_A + FIC_B = \textbf{FIC Index Value}$$

FIGURE 5 | Fractional inhibitory concentration (FIC) index formula. The equation used to calculate synergy, indifference, or antagonism between two compounds (Hall et al., 1983). "A" refers to the MIC value of compound A in combination with compound B, where "MIC_A" refers to the MIC of compound A alone. "B" refers to the MIC value of compound B in combination with compound A, where "MIC_B" refers to the MIC of compound B alone. These values added together output the FIC index value, where < 0.5 indicates synergy, 0.5-4 indifference, and > 4 antagonism.

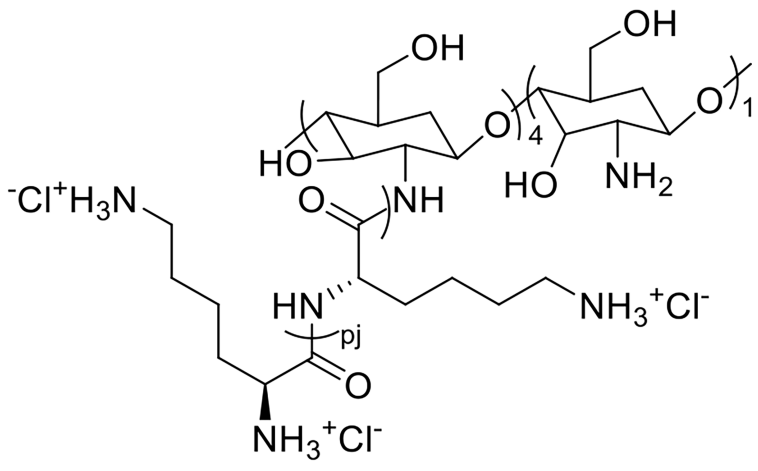

FIGURE 6 | Chemical structure of 11 CSM5-K5.

These studies on naturally derived AMPs have collectively demonstrated their activity in inhibiting biofilm formation and expansion. However, natural AMPs appear less effective at eradicating established biofilms when administered alone or as part of co-treatment strategies. To overcome this, synthetic AMPs based on natural peptides have recently been engineered and trialled as biofilm eradication agents.

Synthetic Antimicrobial Peptides

Synthetic AMPs are peptides that have been synthesised *de novo* and engineered to have antimicrobial properties. As such, they have become a focus for many antibiotic co-treatment studies involving biofilms. Amongst the first synthetic peptides with confirmed antibacterial activities were those engineered by Kovacs et al., who reported their efficacy against Gram-positive and Gram-negative bacteria (Kovacs et al., 1960). Following that, several other synthetic AMPs have been designed and tested against a variety of bacterial pathogens. Synthetic peptide 1018 (amino acid sequence shown in **Table 2**) has been one studied extensively for its activity to potentiate antibiotics against biofilms. Reffuveille et al. initially tested the ability of 1018 to potentiate ciprofloxacin against *P. aeruginosa* biofilms (Reffuveille et al., 2014). Treating biofilms with ciprofloxacin alone at MIC, 10x MIC, and even 100x MIC had little eradication effect. However, combining peptide 1018 with ciprofloxacin, mostly eradicated *P. aeruginosa* biofilms and any remaining cells were small microcolonies of dead cells (Reffuveille et al., 2014). The efficacy of peptide 1018 in combination with other antibiotics was also tested against biofilms from multiple species (*E. coli, S. aureus, Klebsiella pneumoniae, Acinetobacter baumannii*, and *Salmonella enterica*) with combination treatment found always to be most effective when visually comparing biomass reduction and bacterial cell viability (Reffuveille et al., 2014). De la Fuente Núñez et al. also treated *P. aeruginosa* biofilms with the D-enantiomeric peptides DJK-5 and DJK-6 (DJK-6 amino acid sequence shown in **Table 2**) in combination with multiple antibiotics (ceftazidime, ciprofloxacin, imipenem, and tobramycin) (de la Fuente-Núñez et al., 2015). Using confocal microscopy and an *in vivo C. elegans* model, they showed that regardless of the combination, the concentration of antibiotic needed to inhibit biofilm growth was decreased at least 2-fold and in certain cases up to 16-fold with addition of the peptides (de la Fuente-Núñez et al., 2015). Similarly, DJK-6 potentiated meropenem against *K. pneumoniae* biofilms, reducing its MBEC value 16-fold, despite the fact that the tested isolates were carbapenemase producers (Ribeiro et al., 2015). Rudilla et al. also investigated combinations of synthetic peptides with imipenem, reporting that peptide AMP38 decreased by 8-fold the imipenem MBC value for *P. aeruginosa* biofilms (**Table 1**) (Rudilla et al., 2016). Swedan et al. tested AMP WLBU2 in combination with imipenem, tobramycin, amoxicillin-clavulanate or ciprofloxacin against *K. pneumoniae* and *A. baumannii* biofilms, reporting that all combination treatments decreased MBEC values from 6- to 200-fold compared to treatment with WLBU2 alone, the dramatic 200-fold improvement being in combination with ciprofloxacin against *K. pneumoniae* (Swedan et al., 2019). However, when testing cytotoxicity at MBEC values, a significant reduction in eukaryotic cell viability was observed for all tested concentrations of WLBU2 (Swedan et al., 2019). Due to their high cytotoxicity, WLBU2 combination treatment strategies might be more suitable for eradication of biofilms found in the environment e.g. on hospital surfaces or instruments. Alternatively, future efforts could be directed to modifying the chemical structure of WLBU2 to reduce cytotoxicity and facilitate the development of clinically viable antibiofilm agents.

In a more recent study, Pletzer et al. examined optimal combinations of synthetic AMPs with antibiotics to treat ESKAPE pathogen biofilms in an *in vivo* subcutaneous mouse abscess model (Pletzer et al., 2018). Mice infected with fluorescently tagged strains from the ESKAPE group and *E. coli*, inoculated at a dose of $\geq 10^7$ bacteria to simulate a chronic human wound, were monitored non-invasively for disease progression and treatment efficacy (Pletzer et al., 2018).

Treatments were directly injected into the wound and were administered at approximate *in vitro* MIC concentrations (Pletzer et al., 2018). Antibiotic monotherapy even when administered at higher than MIC concentrations was often ineffective against high-density (biofilm) infections, highlighting that *in vitro* MICs are not reliably predictive of *in vivo* efficacy, which the authors also noted (Pletzer et al., 2018). Treatment with AMPs alone reduced wound size and moderately reduced bacterial numbers in the wound (2.2-22-fold decrease) (Pletzer et al., 2018). Notably, the AMP DJK-5 was very effective in combination with antibiotics (ciprofloxacin, gentamicin, meropenem, and vancomycin) in terms of reducing bacterial numbers in all species tested (ESKAPE and *E. coli*) (Pletzer et al., 2018).

While synthetic AMPs have not been studied as extensively as natural AMPs for antibiotic potentiation against biofilms, their promising potential has been clearly demonstrated. Their distinct advantages over naturally occurring AMPs - they can be readily improved *via* chemical manipulation, can be potentially linked to antibiotics, and engineered to be less toxic to mammalian cells- makes this class of antibiofilm agents very promising.

Amino Acids

Amino acids can exist in nature as a D-isomer or L-isomer, where the orientation of the alpha carbon in the molecule determines its chirality. The L-isomer is most common in ribosomal peptide synthesis, but recently D-amino acids have also been found in mammals as regulators of neurogenesis and brain receptor function, and also components of some bacterial membranes (Cava et al., 2011). These have recently emerged as a class of potential biofilm dispersal agents given their role as regulators of biofilm dispersal (Cava et al., 2011). So far, the mode of action for D-amino acids has only been delineated in *Bacillus subtilis* biofilm dispersal, where the bacteria were reported to release D-leucine, -methionine, -tyrosine, and -tryptophan, which disrupted the amyloid fibers linking biofilm cells together at nanomolar concentrations (Kolodkin-Gal et al., 2010).

While their exact mode of action has yet to be elucidated in other species, a few studies have been conducted using amino acids and antibiotics together as a biofilm treatment strategy. In one of these studies, Sanchez et al. investigated the ability of D-amino acids and antibiotics to inhibit *P. aeruginosa* and *S. aureus* biofilm formation (Sanchez et al., 2014). Here, an equimolar mixture of D-amino acids (methionine, phenylalanine, and tryptophan) in combination with rifampicin were shown to reduce the minimum biofilm inhibition concentration (MBIC) by 4-fold and a >2-log reduction in viable bacteria was reported with treated *S. aureus* biofilms (Sanchez et al., 2014). Similar results were observed for *P. aeruginosa*, with a >2-log reduction in viable bacteria when treated with 64 μg/mL rifampicin, and 5 mM of the D-amino acid mixture (Sanchez et al., 2014). Another study investigating amino acids in combination with antibiotics, conducted by Warraich et al., reported that compared to standalone treatment, lower concentrations of ciprofloxacin and D-amino acids were synergistic (<40 mM amino acids, <90.54 μM ciprofloxacin), and resulted in almost 97% inhibition of biofilm formation and 97.6% dispersal (D-isomer structures shown in **Figure 7**). However, biofilm eradication activity was not tested. The study also investigated the ability of L-amino acids to inhibit biofilm formation, and found that L-isomers of aspartic acid and glutamic acid were equally as effective as the D-isomers at 40mM (Warraich et al., 2020). Only two other studies have reported similar findings with L-amino acids (aspartate and glutamate) (Tong et al., 2014; Yang et al., 2015), challenging the dogma that L-isomers do not have antibiofilm activity. Conflicting evidence reports that L-amino acids can even encourage biofilm formation in some species (Hochbaum et al., 2011; Velmourougane and Prasanna, 2017).

For D-amino acids the evidence is more clear-cut, with several studies reporting some antibiofilm activity (inhibition and dispersal) and in a range of settings, from the industrial to development of drug delivery systems (Si et al., 2014; Wei et al., 2015; Li et al., 2016; Zilm et al., 2017). In these studies, D-amino acids (d-leucine, -methionine, -tyrosine, and -tryptophan) alone and in combination with other compounds effectively inhibited *Desulfovibrio vulgaris* biofilms and polymicrobial biofilms (Si et al., 2014; Wei et al., 2015; Li et al., 2016; Zilm et al., 2017). Li et al. and Si et al. investigated disruption of established *D. vulgaris* biofilms that had been grown on carbon steel coupons (Li et al., 2016) or multi-species aggregates collected from an activated sludge reactor (Si et al., 2014) that had grown for longer than 10 days and up to 6 months (Si et al., 2014; Li et al., 2016). Both studies reported that combinations of D-amino acids with other compounds (hydroxymethyl phosphonium sulfate (THPS) and norspermidine) disrupted biofilm surface attachment (Si et al., 2014; Li et al., 2016). Titanium oxide

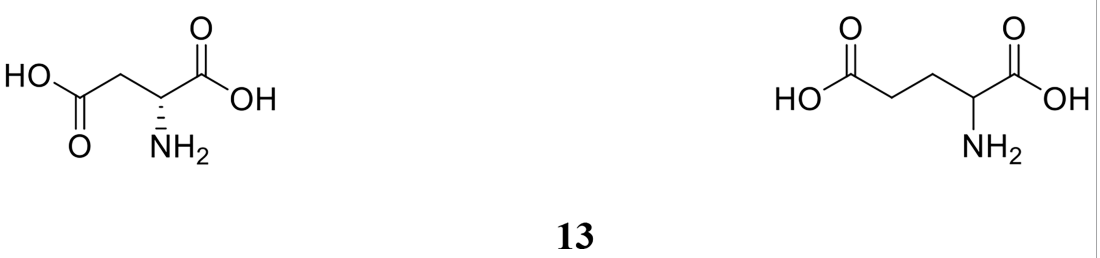

12 **13**

FIGURE 7 | Chemical structures of 12 D-aspartic acid and 13 D-glutamic acid.

nanoparticles engineered to release D-amino acids upon stimulation with UV light were also shown effective in dispersing *B. subtilis* biofilms (Wei et al., 2015), and D-amino acids were also found to inhibit *E. faecalis* biofilm formation *in vitro* (Zilm et al., 2017). Some conflicting evidence exists around the capacity of D-amino acids to disperse *P. aeruginosa* and *S. aureus* biofilms (Sarkar and Pires, 2015; Kao et al., 2017). Kao et al. investigated the ability of D-amino acids alanine, leucine, methionine, tryptophan, and tyrosine (10 μM, 1 mM, and 10mM) to inhibit biofilm formation of *P. aeruginosa* strains PAO1 and PA14. Here they concluded that D-amino acids slow biofilm growth but do not prevent its formation (Kao et al., 2017), which Sarkar et al. also report for *S. aureus* biofilms treated with D-tryptophan and D-tyrosine at 1 and 5 mM (Sarkar and Pires, 2015).

Several questions remain unanswered about the antibiofilm properties of amino acids and thus their potential to be employed in future antibiofilm strategies needs more fundamental research. This should aim to resolve the role of both D- and L- isomers in biofilm inhibition and dispersal and explore the specificity of their activity in key biofilm-producing species, such as *P. aeruginosa* and *S. aureus*. Their mode of action is likely to vary between species, and so, future research on this group of potential antibiofilm agents should be prioritized.

REPURPOSED DRUGS

Drug repurposing is a common strategy used in the field of medicine to maximise the potential of any individual drug for broader clinical applications outside of its original use (Farha and Brown, 2019). A small number of U.S. Food and Drug Administration (FDA)-approved drugs have been investigated against biofilms to date, particularly drugs involved in mucous degradation. *N*-acetyl cysteine (structure shown in **Figure 8**) is a drug commonly prescribed to cystic fibrosis patients to break down mucus in the lung (Samuni et al., 2013). Moon et al. investigated *N*-acetyl cysteine in combination with several antibiotics for dispersal of *Prevotella intermedia* biofilms, a major oral pathogen (Moon et al., 2015). They demonstrated that *N*-acetyl cysteine was highly effective in preventing biofilm growth but was ineffective against pre-formed biofilms *in vitro* (Moon et al., 2015). Zhang et al. also investigated the efficacy of ambroxol (another FDA-approved drug for mucus degradation) in combination with vancomycin to treat *Staphylococcus epidermidis* biofilms *in vitro* and *in vivo* (Zhang et al., 2015). Interestingly, they reported that the combination of ambroxol and vancomycin was highly effective at eradicating mature biofilms in a rabbit intravenous catheter model, reducing catheter bacterial load by an impressive 7 logs compared to the control group (**Table 1**), which were only treated with heparin (Zhang et al., 2015). This result is very promising, and this combination should be further investigated with other bacterial species and other FDA-approved drugs used for mucus degradation.

Another FDA-approved drug with promising antibiofilm activity is auranofin. This gold-containing compound is usually prescribed for the treatment of rheumatoid arthritis, but has since been tested in combination with antibiotics against *S. aureus* and *E. faecalis* biofilms both *in vitro* and *in vivo* (She et al., 2019). Auranofin and the antibiotics fosfomycin, linezolid and chloramphenicol were synergistic at eradicating these biofilms *in vitro*, with compound combinations reducing individual $MBEC_{50}$ values by 2- to over 8-fold (She et al., 2019). *In vivo*, combination treatment was reported to be similarly effective. In a *S. aureus* cutaneous infection mouse model, individual treatment with either auranofin, fosfomycin or linezolid resulted in a <2-log reduction in viable bacterial numbers, while combination treatment with an antibiotic and auranofin resulted in >3-log reduction in *S. aureus* CFU (She et al., 2019). In the same mouse model, however, treatment of *E. faecalis* infection was not reduced by more than 1-log in viable CFU irrespective of the treatment strategy, indicating that *E. faecalis* may have intrinsic resistance to auranofin both planktonically and in sessile form *in vivo*, despite the drug having activity *in vitro* (She et al., 2019).

While the potential use of FDA-approved drugs against biofilms is supported by some impressive results to date, evidence remains sporadic and additional studies are warranted. It would be interesting to investigate other existing mucolytic drugs, as well as approved anticoagulant/antithrombotic and expectorant agents already approved for clinical use.

CONCLUSIONS

The combination of biofilm dispersal agents and antibiotics are an effective treatment strategy for both the prevention and eradication of bacterial biofilms. Many of these combinations have been successfully tested *in vitro*, and some also *in vivo*. All studies reviewed here have focused on single-species biofilms, however multi-species biofilms are also a major clinical and industrial issue (Del Pozo, 2018; Vishwakarma, 2020; Rather et al., 2021). Very few studies have been conducted investigating the dispersal of multi-species biofilms (Mei et al., 2013; Oliveira et al., 2014; Si et al., 2015; Wu et al., 2016; Ioannidis et al., 2019), and none featuring co-treatments with antibiotics. Multi-species biofilms are classically harder to eradicate than single-species biofilms given their heterogeneous composition, and research into the molecular interplay between participating species should illuminate potential therapeutic avenues (single or combination approaches) and advance the biofilm field going forward.

In most of these studies co-treatment or hybrid compounds have been much more effective in terms of biofilm inhibition and/or eradication than standalone treatments, with either the antibiofilm agent or antibiotic alone. This trend is evident across all classes of dispersal agents, suggesting that a two-pronged approach of biofilm dispersal and eradication could translate to a successful treatment strategy. Furthermore, there appears to be a distinct advantage to the simultaneous delivery and or release of the two agents at the target site, an effect which was demonstrated by the production of hybrid molecules, and delivery and release systems. However, very

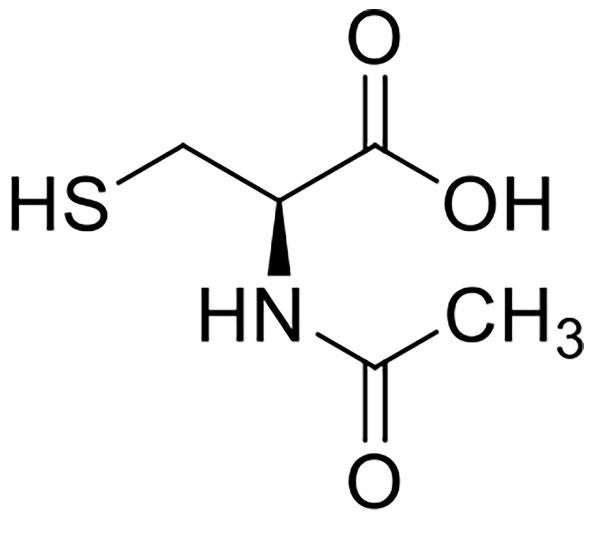

FIGURE 8 | Chemical structure of 14 N-acetyl cysteine.

few cotreatments have been explored for their potential as hybrids drugs. This review has highlighted a multitude of effective cotreatments that would be ideal for future development into hybrid drugs.

Despite the advantages of some combination strategies having been demonstrated both *in vitro* and *in vivo*, follow-up *in vivo* studies are often lacking for co-treatments with confirmed anti-biofilm activity *in vitro*. Indeed, out of the 45 studies reviewed, only 17 (~38%) progressed from *in vitro* testing to preclinical evaluation in an *in vivo* model. Furthermore, out of the hundreds of newly discovered antibiofilm agents currently reported in the literature, only a handful have been tested for activity *in vitro* in assays comparing single agents over co-treatment. This highlights that there is still a lot of untapped potential for the development of new effective anti-biofilm combination therapies. Future studies on novel antibiofilm agents should follow a co-treatment design from early testing, first examining the agent's antibiotic potentiation activity *in vitro* and if successful progress into *in vivo* testing in relevant animal models. While this process can appear tedious, it is necessary in order to shortlist promising combination leads for clinical development. We posit that this review has provided examples that are already following this process successfully and identified others that represent promising candidates to follow this path.

Of the agents reviewed here, QSIs, NO, and nitroxides appear to hold the most promise for the development of biofilm-eradication treatments based on the co-treatment strategy. While the efficacy of co-treatments using QSIs has been demonstrated *in vivo* in some species, both NO and nitroxides remain to be examined *in vivo* despite their promising *in vitro* results. Any of these candidates would be ideal to examine in *in vivo* models.

Biofilm-related infection remains a critical healthcare issue worldwide, and new and innovative strategies need to be devised. Co-treatment using antibiofilm agents with antibiotics appears to hold great promise as one such strategy, and our review provides useful information required to progress and assist in the development of candidates along this strategy.

AUTHOR CONTRIBUTIONS

AV and MT contributed to conception and design of the review. SH and AV compiled and reviewed relevant studies. SH wrote the first draft of the manuscript, figures, and tables. AV and MT wrote sections of the manuscript and edited tables. All authors contributed to the article and approved the submitted version.

FUNDING

SH is the recipient of an Australian Government Research Training Program (RTP) Scholarship.

ACKNOWLEDGMENTS

MT gratefully acknowledges funding support from the Australian Research Council (Discovery Projects DP190101613 and DP210101317, and a Georgina Sweet Award for Women in Quantitative Biomedical Science), the National Health and Medical Research Council of Australia (Project Grant GNT1144046), and the Clive and Vera Ramaciotti Foundations (Health Investment Grant 2017HIG0119).

SUPPLEMENTARY MATERIAL

The Supplementary Material for this article can be found online at: https://www.frontiersin.org/articles/10.3389/fcimb.2022.850030/full#supplementary-material

REFERENCES

Ammons, M. C., and Copié, V. (2013). Mini-Review: Lactoferrin: A Bioinspired, Anti-Biofilm Therapeutic. *Biofouling* 29 (4), 443–455. doi: 10.1080/08927014.2013.773317

Anjum, A., Sim, C. H., and Ng, S. F. (2018). Hydrogels Containing Antibiofilm and Antimicrobial Agents Beneficial for Biofilm-Associated Wound Infection: Formulation Characterizations and *In Vitro* Study. *AAPS PharmSciTech* 19 (3), 1219–1230. doi: 10.1208/s12249-017-0937-4

Azevedo, M. M., Lisboa, C., Cobrado, L., Pina-Vaz, C., and Rodrigues, A. (2020). Hard-To-Heal Wounds, Biofilm and Wound Healing: An Intricate Interrelationship. *Br. J. Nurs.* 29 (5), S6–s13. doi: 10.12968/bjon.2020.29.5.S6

Barnes, R. J., Bandi, R. R., Wong, W. S., Barraud, N., McDougald, D., Fane, A., et al. (2013). Optimal Dosing Regimen of Nitric Oxide Donor Compounds for the Reduction of Pseudomonas Aeruginosa Biofilm and Isolates From Wastewater Membranes. *Biofouling* 29 (2), 203–212. doi: 10.1080/08927014.2012.760069

Barraud, N., Hassett, D. J., Hwang, S. H., Rice, S. A., Kjelleberg, S., and Webb, J. S. (2006). Involvement of Nitric Oxide in Biofilm Dispersal of Pseudomonas Aeruginosa. *J. Bacteriol.* 188 (21), 7344–7353. doi: 10.1128/JB.00779-06

Barraud, N., Kardak, B. G., Yepuri, N. R., Howlin, R. P., Webb, J. S., Faust, S. N., et al. (2012). Cephalosporin-3'-Diazeniumdiolates: Targeted NO-Donor Prodrugs for Dispersing Bacterial Biofilms. *Angew Chem. Int. Ed. Engl.* 51 (36), 9057–9060. doi: 10.1002/anie.201202414

Barraud, N., Kelso, M. J., Rice, S. A., and Kjelleberg, S. (2015). Nitric Oxide: A Key Mediator of Biofilm Dispersal With Applications in Infectious Diseases. *Curr. Pharm. Des.* 21 (1), 31–42. doi: 10.2174/1381612820666140905112822

Barraud, N., Storey, M. V., Moore, Z. P., Webb, J. S., Rice, S. A., and Kjelleberg, S. (2009). Nitric Oxide-Mediated Dispersal in Single- and Multi-Species Biofilms of Clinically and Industrially Relevant Microorganisms. *Microb. Biotechnol.* 2 (3), 370–378. doi: 10.1111/j.1751-7915.2009.00098.x

Bialvaei, A. Z., and Samadi Kafil, H. (2015). Colistin, Mechanisms and Prevalence of Resistance. *Curr. Med. Res. Opin.* 31 (4), 707–721. doi: 10.1185/03007995.2015.1018989

Brackman, G., Breyne, K., De Rycke, R., Vermote, A., Van Nieuwerburgh, F., Meyer, E., et al. (2016). The Quorum Sensing Inhibitor Hamamelitannin Increases Antibiotic Susceptibility of Staphylococcus Aureus Biofilms by Affecting Peptidoglycan Biosynthesis and eDNA Release. *Sci. Rep.* 6, 20321. doi: 10.1038/srep20321

Brackman, G., and Coenye, T. (2015). Quorum Sensing Inhibitors as Anti-Biofilm Agents. *Curr. Pharm. Des.* 21 (1), 5–11. doi: 10.2174/1381612820666140905114627

Brackman, G., Cos, P., Maes, L., Nelis, H. J., and Coenye, T. (2011). Quorum Sensing Inhibitors Increase the Susceptibility of Bacterial Biofilms to Antibiotics *In Vitro* and In Vivo. *Antimicrob. Agents Chemother.* 55 (6), 2655–2661. doi: 10.1128/AAC.00045-11

Brackman, G., Garcia-Fernandez, M. J., Lenoir, J., De Meyer, L., Remon, J. P., De Beer, T., et al. (2016). Dressings Loaded With Cyclodextrin-Hamamelitannin Complexes Increase Staphylococcus Aureus Susceptibility Toward Antibiotics Both in Single as Well as in Mixed Biofilm Communities. *Macromol. Biosci.* 16 (6), 859–869. doi: 10.1002/mabi.201500437

Cava, F., Lam, H., de Pedro, M. A., and Waldor, M. K. (2011). Emerging Knowledge of Regulatory Roles of D-Amino Acids in Bacteria. *Cell Mol. Life Sci.* 68 (5), 817–831. doi: 10.1007/s00018-010-0571-8

Cheng, W. J., Zhou, J. W., Zhang, P. P., Luo, H. Z., Tang, S., Li, J. J., et al. (2020). Quorum Sensing Inhibition and Tobramycin Acceleration in Chromobacterium Violaceum by Two Natural Cinnamic Acid Derivatives. *Appl. Microbiol. Biotechnol.* 104 (11), 5025–5037. doi: 10.1007/s00253-020-10593-0

Christensen, L. D., van Gennip, M., Jakobsen, T. H., Alhede, M., Hougen, H. P., Høiby, N., et al. (2012). Synergistic Antibacterial Efficacy of Early Combination Treatment With Tobramycin and Quorum-Sensing Inhibitors Against Pseudomonas Aeruginosa in an Intraperitoneal Foreign-Body Infection Mouse Model. *J. Antimicrob. Chemother.* 67 (5), 1198–1206. doi: 10.1093/jac/dks002

Cirioni, O., Mocchegiani, F., Cacciatore, I., Vecchiet, J., Silvestri, C., Baldassarre, L., et al. (2013). Quorum Sensing Inhibitor FS3-Coated Vascular Graft Enhances Daptomycin Efficacy in a Rat Model of Staphylococcal Infection. *Peptides* 40, 77–81. doi: 10.1016/j.peptides.2012.12.002

Cui, L., H-m, N., Shoji, M., and Hiramatsu, K. (2009). Contribution of vraSR and graSR Point Mutations to Vancomycin Resistance in Vancomycin-Intermediate Staphylococcus Aureus. *Antimicrob Agents Chemother.* 53 (3), 1231–1234. doi: 10.1128/AAC.01173-08

Davies, K. M., Wink, D. A., Saavedra, J. E., and Keefer, L. K. (2001). Chemistry of the Diazeniumdiolates. 2. Kinetics and Mechanism of Dissociation to Nitric Oxide in Aqueous Solution. *J. Am. Chem. Soc.* 123 (23), 5473–5481. doi: 10.1021/ja002899q

de la Fuente-Núñez, C., Reffuveille, F., Fairfull-Smith, K. E., and Hancock, R. E. (2013). Effect of Nitroxides on Swarming Motility and Biofilm Formation, Multicellular Behaviors in Pseudomonas Aeruginosa. *Antimicrob. Agents Chemother.* 57 (10), 4877–4881. doi: 10.1128/AAC.01381-13

de la Fuente-Núñez, C., Reffuveille, F., Mansour, S. C., Reckseidler-Zenteno, S. L., Hernández, D., Brackman, G., et al. (2015). D-Enantiomeric Peptides That Eradicate Wild-Type and Multidrug-Resistant Biofilms and Protect Against Lethal Pseudomonas Aeruginosa Infections. *Chem. Biol.* 22 (2), 196–205. doi: 10.1016/j.chembiol.2015.01.002

Del Pozo, J. L. (2018). Biofilm-Related Disease. *Expert Rev. Anti Infect. Ther.* 16 (1), 51–65. doi: 10.1080/14787210.2018.1417036

Deppisch, C., Herrmann, G., Graepler-Mainka, U., Wirtz, H., Heyder, S., Engel, C., et al. (2016). Gaseous Nitric Oxide to Treat Antibiotic Resistant Bacterial and Fungal Lung Infections in Patients With Cystic Fibrosis: A Phase I Clinical Study. *Infection* 44 (4), 513–520. doi: 10.1007/s15010-016-0879-x

Eckert, R., Brady, K. M., Greenberg, E. P., Qi, F., Yarbrough, D. K., He, J., et al. (2006). Enhancement of Antimicrobial Activity Against Pseudomonas Aeruginosa by Coadministration of G10KHc and Tobramycin. *Antimicrob. Agents Chemother.* 50 (11), 3833–3838. doi: 10.1128/AAC.00509-06

Farha, M. A., and Brown, E. D. (2019). Drug Repurposing for Antimicrobial Discovery. *Nat. Microbiol.* 4 (4), 565–577. doi: 10.1038/s41564-019-0357-1

Field, D., Seisling, N., Cotter, P. D., Ross, R. P., and Hill, C. (2016). Synergistic Nisin-Polymyxin Combinations for the Control of Pseudomonas Biofilm Formation. *Front. Microbiol.* 7, 1713. doi: 10.3389/fmicb.2016.01713

Findlay, V. J., Townsend, D. M., Saavedra, J. E., Buzard, G. S., Citro, M. L., Keefer, L. K., et al. (2004). Tumor Cell Responses to a Novel Glutathione S-Transferase–Activated Nitric Oxide-Releasing Prodrug. *Mol. Pharmacol.* 65 (5), 1070. doi: 10.1124/mol.65.5.1070

Fleming, D., and Rumbaugh, K. P. (2017). Approaches to Dispersing Medical Biofilms. *Microorganisms* 5 (2), 15. doi: 10.3390/microorganisms5020015

Fleming, D., and Rumbaugh, K. (2018). The Consequences of Biofilm Dispersal on the Host. *Sci. Rep.* 8 (1), 10738. doi: 10.1038/s41598-018-29121-2

Furiga, A., Lajoie, B., El Hage, S., Baziard, G., and Roques, C. (2015). Impairment of Pseudomonas Aeruginosa Biofilm Resistance to Antibiotics by Combining the Drugs With a New Quorum-Sensing Inhibitor. *Antimicrob. Agents Chemother.* 60 (3), 1676–1686. doi: 10.1128/AAC.02533-15

Ghosh, A., Jayaraman, N., and Chatterji, D. (2020). Small-Molecule Inhibition of Bacterial Biofilm. *ACS Omega* 5 (7), 3108–3115. doi: 10.1021/acsomega.9b03695

Gilbert, P., Maira-Litran, T., McBain, A. J., Rickard, A. H., and Whyte, F. W. (2002). The Physiology and Collective Recalcitrance of Microbial Biofilm Communities. *Adv. Microb. Physiol.* 46, 202–256. doi: 10.1016/S0065-2911(02)46005-5

Grassi, L., Maisetta, G., Esin, S., and Batoni, G. (2017). Combination Strategies to Enhance the Efficacy of Antimicrobial Peptides Against Bacterial Biofilms. *Front. Microbiol.* 8, 2409. doi: 10.3389/fmicb.2017.02409

Høiby, N., Bjarnsholt, T., Givskov, M., Molin, S., and Ciofu, O. (2010). Antibiotic Resistance of Bacterial Biofilms. *Int. J. Antimicrob. Agents* 35 (4), 322–332. doi: 10.1016/j.ijantimicag.2009.12.011

Hall, M. J., Middleton, R. F., and Westmacott, D. (1983). The Fractional Inhibitory Concentration (FIC) Index as a Measure of Synergy. *J. Antimicrob. Chemother.* 11 (5), 427–433. doi: 10.1093/jac/11.5.427

Hochbaum, A. I., Kolodkin-Gal, I., Foulston, L., Kolter, R., Aizenberg, J., and Losick, R. (2011). Inhibitory Effects of D-Amino Acids on Staphylococcus Aureus Biofilm Development. *J. Bacteriol* 193 (20), 5616–5622. doi: 10.1128/JB.05534-11

Ho, D. K., Murgia, X., De Rossi, C., Christmann, R., Hüfner de Mello Martins, A. G., Koch, M., et al. (2020). Squalenyl Hydrogen Sulfate Nanoparticles for Simultaneous Delivery of Tobramycin and an Alkylquinolone Quorum

Sensing Inhibitor Enable the Eradication of *P aeruginosa Biofilm Infect. Angew Chem. Int. Ed Engl.* 59 (26), 10292–10296. doi: 10.1002/anie.202001407

Hossain, S., and Boon, E. M. (2017). Discovery of a Novel Nitric Oxide Binding Protein and Nitric-Oxide-Responsive Signaling Pathway in Pseudomonas Aeruginosa. *ACS Infect. Dis.* 3 (6), 454–461. doi: 10.1021/acsinfecdis.7b00027

Hossain, S., Nisbett, L. M., and Boon, E. M. (2017). Discovery of Two Bacterial Nitric Oxide-Responsive Proteins and Their Roles in Bacterial Biofilm Regulation. *Acc Chem. Res.* 50 (7), 1633–1639. doi: 10.1021/acs.accounts.7b00095

Ioannidis, K., Niazi, S., Mylonas, P., Mannocci, F., and Deb, S. (2019). The Synthesis of Nano Silver-Graphene Oxide System and its Efficacy Against Endodontic Biofilms Using a Novel Tooth Model. *Dent. Mater.* 35 (11), 1614–1629. doi: 10.1016/j.dental.2019.08.105

Jiang, Q., Chen, J., Yang, C., Yin, Y., and Yao, K. (2019). Quorum Sensing: A Prospective Therapeutic Target for Bacterial Diseases. *BioMed. Res. Int.* 2019, 2015978. doi: 10.1155/2019/2015978

Jorge, P., Grzywacz, D., Kamysz, W., Lourenço, A., and Pereira, M. O. (2017). Searching for New Strategies Against Biofilm Infections: Colistin-AMP Combinations Against Pseudomonas Aeruginosa and Staphylococcus Aureus Single- and Double-Species Biofilms. *PloS One* 12 (3), e0174654. doi: 10.1371/journal.pone.0174654

Kalsy, M., Tonk, M., Hardt, M., Dobrindt, U., Zdybicka-Barabas, A., Cytrynska, M., et al. (2020). The Insect Antimicrobial Peptide Cecropin A Disrupts Uropathogenic Escherichia Coli Biofilms. *NPJ Biofilms Microbiomes* 6 (1), 6. doi: 10.1038/s41522-020-0116-3

Kao, W. T., Frye, M., Gagnon, P., Vogel, J. P., and Chole, R. (2017). D-Amino Acids do Not Inhibit Pseudomonas Aeruginosa Biofilm Formation. *Laryngoscope Investig. Otolaryngol.* 2 (1), 4–9. doi: 10.1002/lio2.34

Kaplan, J. B. (2010). Biofilm Dispersal: Mechanisms, Clinical Implications, and Potential Therapeutic Uses. *J. Dent. Res.* 89 (3), 205–218. doi: 10.1177/0022034509359403

Kolodkin-Gal, I., Romero, D., Cao, S., Clardy, J., Kolter, R., and Losick, R. (2010). D-Amino Acids Trigger Biofilm Disassembly. *Science* 328 (5978), 627–629. doi: 10.1126/science.1188628

Kovacs, K., Kotai, A., and Szabo, I. (1960). Synthetic Polypeptide Derivatives With Anti-Bacterial Activities. *Nature* 185, 266–267. doi: 10.1038/185266a0

Krishan, A. (1975). Rapid Flow Cytofluorometric Analysis of Mammalian Cell Cycle by Propidium Iodide Staining. *J. Cell Biol.* 66 (1), 188–193. doi: 10.1083/jcb.66.1.188

Lachica, M., Anutrakunchai, C., Prajaneh, S., Nazmi, K., Bolscher, J. G. M., and Taweechaisupapong, S. (2019). Synergistic Effects of LFchimera and Antibiotic Against Planktonic and Biofilm Form of Aggregatibacter Actinomycetemcomitans. *PloS One* 14 (7), e0217205. doi: 10.1371/journal.pone.0217205

Lewis, K. (2008). Multidrug Tolerance of Biofilms and Persister Cells. *Curr. Top. Microbiol. Immunol.* 322, 107–131. doi: 10.1007/978-3-540-75418-3_6

Li, Y., Jia, R., Al-Mahamedh, H. H., Xu, D., and Gu, T. (2016). Enhanced Biocide Mitigation of Field Biofilm Consortia by a Mixture of D-Amino Acids. *Front. Microbiol.* 7, 896. doi: 10.3389/fmicb.2016.00896

Liu, S., Cai, X., Xue, W., Ma, D., and Zhang, W. (2020). Chitosan Derivatives Co-Delivering Nitric Oxide and Methicillin for the Effective Therapy to the Methicillin-Resistant *S. aureus Infection. Carbohydr Polym* 234, 115928. doi: 10.1016/j.carbpol.2020.115928

Luo, J., Dong, B., Wang, K., Cai, S., Liu, T., Cheng, X., et al. (2017). Baicalin Inhibits Biofilm Formation, Attenuates the Quorum Sensing-Controlled Virulence and Enhances Pseudomonas Aeruginosa Clearance in a Mouse Peritoneal Implant Infection Model. *PloS One* 12 (4), e0176883. doi: 10.1371/journal.pone.0176883

Lu, Y., Slomberg, D. L., Shah, A., and Schoenfisch, M. H. (2013). Nitric Oxide-Releasing Amphiphilic Poly(Amidoamine) (PAMAM) Dendrimers as Antibacterial Agents. *Biomacromolecules* 14 (10), 3589–3598. doi: 10.1021/bm400961r

Maiden, M. M., Zachos, M. P., and Waters, C. M. (2019). Hydrogels Embedded With Melittin and Tobramycin Are Effective Against Pseudomonas Aeruginosa Biofilms in an Animal Wound Model. *Front. Microbiol.* 10, 1348. doi: 10.3389/fmicb.2019.01348

Marvasi, M., Durie, I. A., McLamore, E. S., Vanegas, D. C., and Chaturvedi, P. (2015). Salmonella Enterica Biofilm-Mediated Dispersal by Nitric Oxide Donors in Association With Cellulose Nanocrystal Hydrogels. *AMB Express* 5, 28. doi: 10.1186/s13568-015-0114-7

Mataraci, E., and Dosler, S. (2012). *In Vitro* Activities of Antibiotics and Antimicrobial Cationic Peptides Alone and in Combination Against Methicillin-Resistant Staphylococcus Aureus Biofilms. *Antimicrob. Agents Chemother.* 56 (12), 6366–6371. doi: 10.1128/AAC.01180-12

McDougald, D., Rice, S. A., Barraud, N., Steinberg, P. D., and Kjelleberg, S. (2011). Should We Stay or Should We Go: Mechanisms and Ecological Consequences for Biofilm Dispersal. *Nat. Rev. Microbiol.* 10 (1), 39–50. doi: 10.1038/nrmicro2695

Mei, M. L., Li, Q. L., Chu, C. H., Lo, E. C., and Samaranayake, L. P. (2013). Antibacterial Effects of Silver Diamine Fluoride on Multi-Species Cariogenic Biofilm on Caries. *Ann. Clin. Microbiol. Antimicrob.* 12, 4. doi: 10.1186/1476-0711-12-4

Miller, C. C., Hergott, C. A., Rohan, M., Arsenault-Mehta, K., Döring, G., and Mehta, S. (2013). Inhaled Nitric Oxide Decreases the Bacterial Load in a Rat Model of Pseudomonas Aeruginosa Pneumonia. *J. Cyst Fibros* 12 (6), 817–820. doi: 10.1016/j.jcf.2013.01.008

Miller, C., Miller, M., McMullin, B., Regev, G., Serghides, L., Kain, K., et al. (2012). A Phase I Clinical Study of Inhaled Nitric Oxide in Healthy Adults. *J. Cyst Fibros* 11 (4), 324–331. doi: 10.1016/j.jcf.2012.01.003

Minardi, D., Ghiselli, R., Cirioni, O., Giacometti, A., Kamysz, W., Orlando, F., et al. (2007). The Antimicrobial Peptide Tachyplesin III Coated Alone and in Combination With Intraperitoneal Piperacillin-Tazobactam Prevents Ureteral Stent Pseudomonas Infection in a Rat Subcutaneous Pouch Model. *Peptides* 28 (12), 2293–2298. doi: 10.1016/j.peptides.2007.10.001

Moon, J. H., Jang, E. Y., Shim, K. S., and Lee, J. Y. (2015). *In Vitro* Effects of N-Acetyl Cysteine Alone and in Combination With Antibiotics on Prevotella Intermedia. *J. Microbiol.* 53 (5), 321–329. doi: 10.1007/s12275-015-4500-2

Müsken, M., Pawar, V., Schwebs, T., Bähre, H., Felgner, S., Weiss, S., et al. (2018). Breaking the Vicious Cycle of Antibiotic Killing and Regrowth of Biofilm-Residing Pseudomonas Aeruginosa. *Antimicrob. Agents Chemother.* 62 (12), e01635–18. doi: 10.1128/AAC.01635-18

Nguyen, T. K., Selvanayagam, R., Ho, K. K. K., Chen, R., Kutty, S. K., Rice, S. A., et al. (2016). Co-Delivery of Nitric Oxide and Antibiotic Using Polymeric Nanoparticles. *Chem. Sci.* 7 (2), 1016–1027. doi: 10.1039/C5SC02769A

Nisbett, L. M., Binnenkade, L., Bacon, B., Hossain, S., Kotloski, N. J., Brutinel, E. D., et al. (2019). NosP Signaling Modulates the NO/H-NOX-Mediated Multicomponent C-Di-GMP Network and Biofilm Formation in Shewanella Oneidensis. *Biochemistry* 58 (48), 4827–4841. doi: 10.1021/acs.biochem.9b00706

O'Loughlin, C. T., Miller, L. C., Siryaporn, A., Drescher, K., Semmelhack, M. F., and Bassler, B. L. (2013). A Quorum-Sensing Inhibitor Blocks Pseudomonas Aeruginosa Virulence and Biofilm Formation. *Proc. Natl. Acad. Sci. U. S. A.* 110 (44), 17981–17986. doi: 10.1073/pnas.1316981110

Oliveira, S. A., Zambrana, J. R., Iorio, F. B., Pereira, C. A., and Jorge, A. O. (2014). The Antimicrobial Effects of Citrus Limonum and Citrus Aurantium Essential Oils on Multi-Species Biofilms. *Braz. Oral. Res.* 28, 22–27. doi: 10.1590/S1806-83242013005000024

Orlando, F., Ghiselli, R., Cirioni, O., Minardi, D., Tomasinsig, L., Mocchegiani, F., et al. (2008). BMAP-28 Improves the Efficacy of Vancomycin in Rat Models of Gram-Positive Cocci Ureteral Stent Infection. *Peptides* 29 (7), 1118–1123. doi: 10.1016/j.peptides.2008.03.005

Pletzer, D., and Hancock, R. E. (2016). Antibiofilm Peptides: Potential as Broad-Spectrum Agents. *J. Bacteriol.* 198 (19), 2572–2578. doi: 10.1128/JB.00017-16

Pletzer, D., Mansour, S. C., and Hancock, R. E. W. (2018). Synergy Between Conventional Antibiotics and Anti-Biofilm Peptides in a Murine, Sub-Cutaneous Abscess Model Caused by Recalcitrant ESKAPE Pathogens. *PloS Pathog.* 14 (6), e1007084. doi: 10.1371/journal.ppat.1007084

Poh, W. H., Barraud, N., Guglielmo, S., Lazzarato, L., Rolando, B., Fruttero, R., et al. (2017). Furoxan Nitric Oxide Donors Disperse Pseudomonas Aeruginosa Biofilms, Accelerate Growth, and Repress Pyoverdine Production. *ACS Chem. Biol.* 12 (8), 2097–2106. doi: 10.1021/acschembio.7b00256

Rajasekaran, G., Dinesh Kumar, S., Nam, J., Jeon, D., Kim, Y., Lee, C. W., et al. (2019). Antimicrobial and Anti-Inflammatory Activities of Chemokine CXCL14-Derived Antimicrobial Peptide and its Analogs. *Biochim. Biophys. Acta Biomembr.* 1861 (1), 256–267. doi: 10.1016/j.bbamem.2018.06.016

Rather, M. A., Gupta, K., Bardhan, P., Borah, M., Sarkar, A., Eldiehy, K. S. H., et al. (2021). Microbial Biofilm: A Matter of Grave Concern for Human Health and Food Industry. *J. Basic Microbiol.* 61 (5), 380–395. doi: 10.1002/jobm.202000678

Reffuveille, F., de la Fuente-Núñez, C., Mansour, S., and Hancock, R. E. (2014). A Broad-Spectrum Antibiofilm Peptide Enhances Antibiotic Action Against Bacterial Biofilms. *Antimicrob. Agents Chemother.* 58 (9), 5363–5371. doi: 10.1128/AAC.03163-14

Reffuveille, F., Fuente-Núñez Cde, L., Fairfull-Smith, K. E., and Hancock, R. E. (2015). Potentiation of Ciprofloxacin Action Against Gram-Negative Bacterial Biofilms by a Nitroxide. *Pathog. Dis.* 73 (5), ftv016. doi: 10.1093/femspd/ftv016

Ren, H., Wu, J., Colletta, A., Meyerhoff, M. E., and Xi, C. (2016). Efficient Eradication of Mature Pseudomonas Aeruginosa Biofilm *via* Controlled Delivery of Nitric Oxide Combined With Antimicrobial Peptide and Antibiotics. *Front. Microbiol.* 7, 1260. doi: 10.3389/fmicb.2016.01260

Ribeiro, S. M., de la Fuente-Núñez, C., Baquir, B., Faria-Junior, C., Franco, O. L., and Hancock, R. E. (2015). Antibiofilm Peptides Increase the Susceptibility of Carbapenemase-Producing Klebsiella Pneumoniae Clinical Isolates to β-Lactam Antibiotics. *Antimicrob. Agents Chemother.* 59 (7), 3906–3912. doi: 10.1128/AAC.00092-15

Roy, R., Tiwari, M., Donelli, G., and Tiwari, V. (2018). Strategies for Combating Bacterial Biofilms: A Focus on Anti-Biofilm Agents and Their Mechanisms of Action. *Virulence* 9 (1), 522–554. doi: 10.1080/21505594.2017.1313372

Rudilla, H., Fusté, E., Cajal, Y., Rabanal, F., Vinuesa, T., and Viñas, M. (2016). Synergistic Antipseudomonal Effects of Synthetic Peptide AMP38 and Carbapenems. *Molecules* 21 (9), 1223. doi: 10.3390/molecules21091223

Sadowska-Bartosz, I., Gajewska, A., Skolimowski, J., Szewczyk, R., and Bartosz, G. (2015). Nitroxides Protect Against Peroxynitrite-Induced Nitration and Oxidation. *Free Radic. Biol. Med.* 89, 1165–1175. doi: 10.1016/j.freeradbiomed.2015.11.002

Samuni, Y., Goldstein, S., Dean, O. M., and Berk, M. (2013). The Chemistry and Biological Activities of N-Acetylcysteine. *Biochim. Biophys. Acta* 1830 (8), 4117–4129. doi: 10.1016/j.bbagen.2013.04.016

Sanchez, C. J. Jr., Akers, K. S., Romano, D. R., Woodbury, R. L., Hardy, S. K., Murray, C. K., et al. (2014). D-Amino Acids Enhance the Activity of Antimicrobials Against Biofilms of Clinical Wound Isolates of Staphylococcus Aureus and Pseudomonas Aeruginosa. *Antimicrob. Agents Chemother.* 58 (8), 4353–4361. doi: 10.1128/AAC.02468-14

Sarkar, S., and Pires, M. M. (2015). D-Amino Acids do Not Inhibit Biofilm Formation in Staphylococcus Aureus. *PloS One* 10 (2), e0117613. doi: 10.1371/journal.pone.0117613

Schairer, D. O., Chouake, J. S., Nosanchuk, J. D., and Friedman, A. J. (2012). The Potential of Nitric Oxide Releasing Therapies as Antimicrobial Agents. *Virulence* 3 (3), 271–279. doi: 10.4161/viru.20328

She, P., Zhou, L., Li, S., Liu, Y., Xu, L., Chen, L., et al. (2019). Synergistic Microbicidal Effect of Auranofin and Antibiotics Against Planktonic and Biofilm-Encased S. Aureus and E. Faecalis. *Front. Microbiol.* 10, 2453. doi: 10.3389/fmicb.2019.02453

Simonetti, O., Cirioni, O., Cacciatore, I., Baldassarre, L., Orlando, F., Pierpaoli, E., et al. (2016). Efficacy of the Quorum Sensing Inhibitor FS10 Alone and in Combination With Tigecycline in an Animal Model of Staphylococcal Infected Wound. *PloS One* 11 (6), e0151956. doi: 10.1371/journal.pone.0151956

Simonetti, O., Cirioni, O., Mocchegiani, F., Cacciatore, I., Silvestri, C., Baldassarre, L., et al. (2013). The Efficacy of the Quorum Sensing Inhibitor FS8 and Tigecycline in Preventing Prosthesis Biofilm in an Animal Model of Staphylococcal Infection. *Int. J. Mol. Sci.* 14 (8), 16321–16332. doi: 10.3390/ijms140816321

Singh, N., Romero, M., Travanut, A., Monteiro, P. F., Jordana-Lluch, E., Hardie, K. R., et al. (2019). Dual Bioresponsive Antibiotic and Quorum Sensing Inhibitor Combination Nanoparticles for Treatment of Pseudomonas Aeruginosa Biofilms *In Vitro* and Ex Vivo. *Biomater. Sci.* 7 (10), 4099–4111. doi: 10.1039/C9BM00773C

Si, X., Quan, X., Li, Q., and Wu, Y. (2014). Effects of D-Amino Acids and Norspermidine on the Disassembly of Large, Old-Aged Microbial Aggregates. *Water Res.* 54, 247–253. doi: 10.1016/j.watres.2014.02.007

Si, X., Quan, X., and Wu, Y. (2015). A Small-Molecule Norspermidine and Norspermidine-Hosting Polyelectrolyte Coatings Inhibit Biofilm Formation by Multi-Species Wastewater Culture. *Appl. Microbiol. Biotechnol.* 99 (24), 10861–10870. doi: 10.1007/s00253-015-6943-0

Slachmuylders, L., Van Acker, H., Brackman, G., Sass, A., Van Nieuwerburgh, F., and Coenye, T. (2018). Elucidation of the Mechanism Behind the Potentiating Activity of Baicalin Against Burkholderia Cenocepacia Biofilms. *PloS One* 13 (1), e0190533. doi: 10.1371/journal.pone.0190533

Soren, O., Rineh, A., Silva, D. G., Cai, Y., Howlin, R. P., Allan, R. N., et al. (2020). Cephalosporin Nitric Oxide-Donor Prodrug DEA-C3D Disperses Biofilms Formed by Clinical Cystic Fibrosis Isolates of Pseudomonas Aeruginosa. *J. Antimicrob. Chemother.* 75 (1), 117–125. doi: 10.1093/jac/dkz378

Swedan, S., Shubair, Z., and Almaaytah, A. (2019). Synergism of Cationic Antimicrobial Peptide WLBU2 With Antibacterial Agents Against Biofilms of Multi-Drug Resistant Acinetobacter Baumannii and Klebsiella Pneumoniae. *Infect. Drug Resist.* 12, 2019–2030. doi: 10.2147/IDR.S215084

Thappeta, K. R. V., Vikhe, Y. S., Yong, A. M. H., Chan-Park, M. B., and Kline, K. A. (2020). Combined Efficacy of an Antimicrobial Cationic Peptide Polymer With Conventional Antibiotics to Combat Multidrug-Resistant Pathogens. *ACS Infect. Dis.* 6 (5), 1228–1237. doi: 10.1021/acsinfecdis.0c00016

Tong, Z., Zhang, L., Ling, J., Jian, Y., Huang, L., and Deng, D. (2014). An *In Vitro* Study on the Effect of Free Amino Acids Alone or in Combination With Nisin on Biofilms as Well as on Planktonic Bacteria of Streptococcus Mutans. *PloS One* 9 (6), e99513. doi: 10.1371/journal.pone.0099513

Tong, Z., Zhang, Y., Ling, J., Ma, J., Huang, L., and Zhang, L. (2014). An *In Vitro* Study on the Effects of Nisin on the Antibacterial Activities of 18 Antibiotics Against Enterococcus Faecalis. *PloS One* 9 (2), e89209. doi: 10.1371/journal.pone.0089209

Vasconcelos, N. G., Croda, J., and Simionatto, S. (2018). Antibacterial Mechanisms of Cinnamon and its Constituents: A Review. *Microb. Pathog.* 120, 198–203. doi: 10.1016/j.micpath.2018.04.036

Velmourougane, K., and Prasanna, R. (2017). Influence of L-Amino Acids on Aggregation and Biofilm Formation in Azotobacter Chroococcum and Trichoderma Viride. *J. Appl. Microbiol.* 123 (4), 977–991. doi: 10.1111/jam.13534

Verderosa, A. D., de la Fuente-Núñez, C., Mansour, S. C., Cao, J., Lu, T. K., Hancock, R. E. W., et al. (2017). Ciprofloxacin-Nitroxide Hybrids With Potential for Biofilm Control. *Eur. J. Med. Chem.* 138, 590–601. doi: 10.1016/j.ejmech.2017.06.058

Verderosa, A. D., Dhouib, R., Fairfull-Smith, K. E., and Totsika, M. (2019a). Nitroxide Functionalized Antibiotics Are Promising Eradication Agents Against Staphylococcus Aureus Biofilms. *Antimicrob. Agents Chemother.* 64 (1), e01685–19. doi: 10.1128/AAC.01685-19

Verderosa, A. D., Harris, J., Dhouib, R., Totsika, M., and Fairfull-Smith, K. E. (2019b). Eradicating Uropathogenic Escherichia Coli Biofilms With a Ciprofloxacin-Dinitroxide Conjugate. *Medchemcomm* 10 (5), 699–711. doi: 10.1039/C9MD00062C

Verderosa, A. D., Mansour, S. C., de la Fuente-Núñez, C., Hancock, R. E., and Fairfull-Smith, K. E. (2016). Synthesis and Evaluation of Ciprofloxacin-Nitroxide Conjugates as Anti-Biofilm Agents. *Molecules* 21 (7), 841. doi: 10.3390/molecules21070841

Verderosa, A. D., Totsika, M., and Fairfull-Smith, K. E. (2019c). Bacterial Biofilm Eradication Agents: A Current Review. *Front. Chem.* 7, 824. doi: 10.3389/fchem.2019.00824

Vermote, A., Brackman, G., Risseeuw, M. D., Vanhoutte, B., Cos, P., Van Hecke, K., et al. (2016). Hamamelitannin Analogues That Modulate Quorum Sensing as Potentiators of Antibiotics Against Staphylococcus Aureus. *Angew Chem. Int. Ed Engl.* 55 (22), 6551–6555. doi: 10.1002/anie.201601973

Vestby, L. K., Grønseth, T., Simm, R., and Nesse, L. L. (2020). Bacterial Biofilm and its Role in the Pathogenesis of Disease. *Antibiotics (Basel)* 9 (2), 59. doi: 10.3390/antibiotics9020059

Vishwakarma, V. (2020). Impact of Environmental Biofilms: Industrial Components and its Remediation. *J. Basic Microbiol.* 60 (3), 198–206. doi: 10.1002/jobm.201900569

Vuotto, C., and Donelli, G. (2019). Novel Treatment Strategies for Biofilm-Based Infections. *Drugs* 79 (15), 1635–1655. doi: 10.1007/s40265-019-01184-z

Wakabayashi, H., Yamauchi, K., Kobayashi, T., Yaeshima, T., Iwatsuki, K., and Yoshie, H. (2009). Inhibitory Effects of Lactoferrin on Growth and Biofilm Formation of Porphyromonas Gingivalis and Prevotella Intermedia. *Antimicrob. Agents Chemother.* 53 (8), 3308–3316. doi: 10.1128/AAC.01688-08

Wang, P. G., Xian, M., Tang, X., Wu, X., Wen, Z., Cai, T., et al. (2002). Nitric Oxide Donors: Chemical Activities and Biological Applications. *Chem. Rev.* 102 (4), 1091–1134. doi: 10.1021/cr000040l

Warraich, A. A., Mohammed, A. R., Perrie, Y., Hussain, M., Gibson, H., and Rahman, A. (2020). Evaluation of Anti-Biofilm Activity of Acidic Amino Acids and Synergy With Ciprofloxacin on Staphylococcus Aureus Biofilms. *Sci. Rep.* 10 (1), 9021. doi: 10.1038/s41598-020-66082-x

Webert, K. E., Vanderzwan, J., Duggan, M., Scott, J. A., McCormack, D. G., Lewis, J. F., et al. (2000). Effects of Inhaled Nitric Oxide in a Rat Model of Pseudomonas Aeruginosa Pneumonia. *Crit. Care Med.* 28 (7), 2397–2405. doi: 10.1097/00003246-200007000-00035

Wei, W., Bing, W., Ren, J., and Qu, X. (2015). Near Infrared-Caged D-Amino Acids Multifunctional Assembly for Simultaneously Eradicating Biofilms and Bacteria. *Chem. Commun. (Camb)* 51 (63), 12677–12679. doi: 10.1039/C5CC04729C

Weinberger, B., Laskin, D. L., Heck, D. E., and Laskin, J. D. (2001). The Toxicology of Inhaled Nitric Oxide. *Toxicol. Sci.* 59 (1), 5–16. doi: 10.1093/toxsci/59.1.5

Williams, D. E., and Boon, E. M. (2019). Towards Understanding the Molecular Basis of Nitric Oxide-Regulated Group Behaviors in Pathogenic Bacteria. *J. Innate Immun.* 11 (3), 205–215. doi: 10.1159/000494740

Wu, Y., Quan, X., Si, X., and Wang, X. (2016). A Small Molecule Norspermidine in Combination With Silver Ion Enhances Dispersal and Disinfection of Multi-Species Wastewater Biofilms. *Appl. Microbiol. Biotechnol.* 100 (12), 5619–5629. doi: 10.1007/s00253-016-7394-y

Yang, H., Wang, M., Yu, J., and Wei, H. (2015). Aspartate Inhibits Staphylococcus Aureus Biofilm Formation. *FEMS Microbiol. Letters* 362 (7), fnv025. doi: 10.1093/femsle/fnv025

Yang, T., Zelikin, A. N., and Chandrawati, R. (2018). Progress and Promise of Nitric Oxide-Releasing Platforms. *Adv. Sci. (Weinh)* 5 (6), 1701043. doi: 10.1002/advs.201701043

Yasir, M., Dutta, D., and Willcox, M. D. P. (2020). Activity of Antimicrobial Peptides and Ciprofloxacin Against Pseudomonas Aeruginosa Biofilms. *Molecules* 25 (17), 3843. doi: 10.3390/molecules25173843

Zhang, Y., Fu, Y., Yu, J., Ai, Q., Li, J., Peng, N., et al. (2015). Synergy of Ambroxol With Vancomycin in Elimination of Catheter-Related Staphylococcus Epidermidis Biofilm *In Vitro* and In Vivo. *J. Infect. Chemother.* 21 (11), 808–815. doi: 10.1016/j.jiac.2015.08.017

Zhao, Y., Liu, D., Huang, W., Yang, Y., Ji, M., Nghiem, L. D., et al. (2019). Insights Into Biofilm Carriers for Biological Wastewater Treatment Processes: Current State-of-the-Art, Challenges, and Opportunities. *Bioresour Technol.* 288, 121619. doi: 10.1016/j.biortech.2019.121619

Zilm, P. S., Butnejski, V., Rossi-Fedele, G., Kidd, S. P., Edwards, S., and Vasilev, K. (2017). D-Amino Acids Reduce Enterococcus Faecalis Biofilms *In Vitro* and in the Presence of Antimicrobials Used for Root Canal Treatment. *PloS One* 12 (2), e0170670. doi: 10.1371/journal.pone.0170670

Conflict of Interest: The authors declare that the research was conducted in the absence of any commercial or financial relationships that could be construed as a potential conflict of interest.

Publisher's Note: All claims expressed in this article are solely those of the authors and do not necessarily represent those of their affiliated organizations, or those of the publisher, the editors and the reviewers. Any product that may be evaluated in this article, or claim that may be made by its manufacturer, is not guaranteed or endorsed by the publisher.

frontiers in Cellular and Infection Microbiology

ORIGINAL RESEARCH
published: 28 February 2022
doi: 10.3389/fcimb.2022.831887

Sleep Disordered Breathing and Recurrent Tonsillitis Are Associated With Polymicrobial Bacterial Biofilm Infections Suggesting a Role for Anti-Biofilm Therapies

Tulia Mateus[1,2‡], *Elke J. Seppanen*[2‡], *Camilla de Gier*[1,2], *Sharon Clark*[1,2], *Harvey Coates*[1,2], *Shyan Vijayasekaran*[1,3], *Karen Prosser*[3], *Selma P. Wiertsema*[1†], *Angela Fuery*[2], *Lea-Ann S. Kirkham*[2,4], *Peter C. Richmond*[1,2,3,4] *and Ruth B. Thornton*[2,4*]

[1] School of Medicine, University of Western Australia, Perth, WA, Australia, [2] Wesfarmers Centre of Vaccines and Infectious Diseases, Telethon Kids Institute, Perth, WA, Australia, [3] Perth Children's Hospital, Perth, WA, Australia, [4] Centre for Child Health Research, University of Western Australia, Perth, WA, Australia

Background: The underlying pathogenesis of pediatric obstructive sleep disordered breathing (SDB) and recurrent tonsillitis (RT) are poorly understood but need to be elucidated to develop less invasive treatment and prevention strategies.

Methods: Children aged between 1- and 16-years undergoing adenoidectomy, tonsillectomy or adenotonsillectomy for SDB (n=40), RT alone (n=18), or both SDB and RT (SDB+RT) (n=17) were recruited with age-matched healthy controls (n=33). Total bacterial load and species-specific densities of nontypeable *Haemophilus influenzae* (NTHi), *Staphylococcus aureus, Streptococcus pyogenes, Streptococcus pneumoniae* and *Moraxella catarrhalis* were measured by qPCR in nasopharyngeal swabs, oropharyngeal swabs, adenoid and tonsillar tissue from children with SDB, SDB+RT and RT, and in naso- and oro- pharyngeal swabs from healthy children. A subset of tonsil biopsies were examined for biofilms using 16S rRNA FISH (n=3/group).

Results: The 5 bacterial species were detected in naso- and oro- pharyngeal samples from all children. These species were frequently detected in adenotonsillar tissue (except *S. aureus*, which was absent in adenoids) from children with SDB, SDB+RT and RT. NTHi and *S. aureus* were observed in tonsils from 66.7-88.2% and 33.3-58.8% of children respectively. Similar total and species-specific bacterial densities were observed in adenotonsillar tissue from children with SDB, SDB+RT or RT. Nasopharyngeal and oropharyngeal swabs were more likely to have multiple bacterial species co-detected than adenotonsillar tissue where one or two targeted species predominated.

Edited by:
Carina Almeida, Instituto Nacional Investigaciao Agraria e Veterinaria (INIAV), Portugal

Reviewed by:
Mainul Haque, National Defence University of Malaysia, Malaysia
Juliana Cardoso, Universidade Federal de Goiás, Brazil

***Correspondence:**
Ruth B. Thornton
ruth.thornton@uwa.edu.au

†Present address:
Selma P. Wiertsema, Immunology group, Danone Nutricia, Utrecht, Netherlands

‡*These authors have contributed equally to this work and share first authorship*

Specialty section:
This article was submitted to Biofilms, a section of the journal Frontiers in Cellular and Infection Microbiology

Received: *09 December 2021*
Accepted: *03 February 2022*
Published: *28 February 2022*

Citation:
Mateus T, Seppanen EJ, de Gier C, Clark S, Coates H, Vijayasekaran S, Prosser K, Wiertsema SP, Fuery A, Kirkham LS, Richmond PC and Thornton RB (2022) Sleep Disordered Breathing and Recurrent Tonsillitis Are Associated With Polymicrobial Bacterial Biofilm Infections Suggesting a Role for Anti-Biofilm Therapies. Front. Cell. Infect. Microbiol. 12:831887. doi: 10.3389/fcimb.2022.831887

Polymicrobial biofilms and intracellular bacteria were observed in tonsils from children with adenotonsillar disease.

Conclusions: Antimicrobials, particularly anti-biofilm therapies, may be a strategy for managing children with SDB.

Keywords: pediatric sleep disordered breathing, recurrent tonsillitis, nontypeable *Haemophilus influenzae*, *Streptococcus pneumoniae*, *Streptococcus pyogenes*, bacteria, biofilms

INTRODUCTION

Adenotonsillectomy Is the Most Common Pediatric Surgery in Australia

Adenotonsillectomy is a common surgical procedure performed on children in high-income countries (Harris et al., 2008). In Australia, it is estimated that ~750 per 100,000 children undergo tonsillectomy (with or without adenoidectomy) each year. This rate has increased by 3% between 2012 and 2018 (Australian Commision on Safety and Quality in Health Care, 2021). Children undergo adenotonsillectomy to treat a range of adenotonsillar diseases associated with infection and/or hypertrophy of the adenotonsillar tissue including sleep disordered breathing (SDB), recurrent tonsillitis (RT), or a combination of both. A definitive diagnosis of obstructive sleep apnoea (OSA) in children with SDB is hampered by the difficulty in obtaining a polysomnogram (PSG). Based on the recommendations most children with a clinical diagnosis of SDB undergo surgery without formal polysomnography (Mitchell et al., 2019). While most children benefit from adenotonsillectomy, with a reduction in primary symptoms and improved quality of life (Marcus et al., 2013), surgery is not without risks nor is it always successful. Post-operative bleeding is the most common complication and accounts for readmissions in ~5% of patients (Ostvoll et al., 2018). Due to long surgical waitlists, many children are left untreated or are managed inefficiently for years before undergoing surgery. Thus, alternative treatment strategies are needed. One potential strategy is to specifically target the pathogen/s or their survival mechanisms that may be associated with adenotonsillar enlargement, and chronic/recurrent infection. Surprisingly, few studies exist comparing the underlying pathogenesis in each of these diseases (Roberts et al., 2012; Viciani et al., 2016; Johnston et al., 2019). Thus, we sought to investigate the presence and densities of common upper respiratory tract bacteria in specimens from children undergoing adenotonsillectomy for SDB, RT or a combination of both. A better understanding of microbial involvement in each of these diseases will facilitate development of alternative or adjunct therapies to surgery.

Evidence for Microbial Involvement in Sleep Disordered Breathing

While there is considerable evidence for microbial infection driving adenotonsillar enlargement in children with RT (Brodsky et al., 1988; Diaz et al., 2011), a role for microbes in the pathogenesis of SDB is controversial. Recent studies suggest that persistent bacterial infection may drive chronic inflammation, hypertrophy, and airway obstruction in SDB including OSA (Viciani et al., 2016; Johnston et al., 2019; Radcliff et al., 2019), the most severe form of SDB. *Streptococcus pyogenes*-positive throat swabs have been identified in 30% children with OSA compared to 48% of children with RT (Johnston et al., 2019). However, a lack of surface-associated bacterial biofilms on adenoidal and tonsillar surfaces have been shown in children with OSA, while extensive biofilms have been demonstrated in children with RT, and other ear, nose and throat diseases including otitis media and chronic rhinosinusitis (Coticchia et al., 2007; Galli et al., 2007; Zuliani et al., 2009). A recent analysis of bacterial communities from the adenoids and tonsils of children with both RT and SDB revealed that *Proteobacteria* (represented by *Haemophilus*, *Moraxella* and *Neisseria species*) dominated (Johnston et al., 2019). This suggests that these bacteria play a role in adenotonsillar diseases in addition to *S. pyogenes*, which is a well-recognized pathogen associated with RT. Together, these data indicate that the types and densities of bacteria present, and the mechanisms by which they persist in the respiratory tracts and tissues, may contribute to disease pathogenesis and thus, offer targets for new treatment strategies.

Rationale for Study Design

There is a continuum of diagnoses associated with adenotonsillar disease, with some children diagnosed with RT alone, some having overlapping diagnoses of both SDB and RT, while others are diagnosed with SDB alone. In this study, to represent the continuum of disease and assess associated risk factors, we included children with the aforementioned diagnoses, as well as healthy children with no history of adenotonsillar disease. We evaluated the presence, density, and relative abundance of 5 species of respiratory bacteria that are associated with upper airway and respiratory tissue infections: *S. pyogenes*, *Staphylococcus aureus, Streptococcus pneumoniae*, nontypeable *Haemophilus influenzae* (NTHi) and *Moraxella catarrhalis*, in nasopharyngeal swabs, oropharyngeal swabs, and in adenoid and tonsil tissue from children with adenotonsillar diseases, and in nasopharyngeal and oropharyngeal swabs from healthy controls. We hypothesized that 1) we would detect higher densities of the 5 pathogens in respiratory tissues and swabs from children with RT (or SDB and RT), but lower densities in children with SDB alone who would be more similar to healthy control children; 2) pathogens would be present in polymicrobial biofilms within the tonsils from children with RT but not SDB.

METHODS

Population

Cases and controls aged between 1 and 16 years were recruited in Perth, Australia between 2005 and 2009. Cases were recruited from the tertiary children's hospital, Princess Margaret Hospital for Children and controls from the Vaccine Trials Group Database at the Telethon Kids Institute. Data on host and environmental risks factors and antibiotic treatment were collected using a standardized parental questionnaire (Goodwin et al., 2003) and medical records. Written informed consent was obtained from parents or guardians, and assent obtained from children 10 years of age or older prior to any study procedure.

Exclusion criteria for all groups: any chromosomal or craniofacial disorders, known immunodeficiency or receiving immunosuppressive therapy.

Inclusion criteria for Adenotonsillar disease groups: Children were diagnosed as having SDB by the treating otorhinolaryngologist. Due to long waitlists and limited availability of PSG, and in keeping with clinical practice guidelines, the majority of patients with a clinical diagnosis of SDB had surgery without pre-operative PSG. Diagnosis of SDB was based on the history and examination of the child by pediatric otorhinolaryngologists. Specifically, a diagnosis of SDB was assigned if the child had a history of snoring, apneic episodes while sleeping, struggling to breathe, severe dysphagia for solids such as meat, tiredness in the morning, daytime sleepiness, neurocognitive and behavioral issues. Other quality of life symptoms were also considered such as enuresis, night terrors, sleeping in unusual positions, frequent arousals, hypersomnolence, failure to thrive, and obesity. A combination of these findings with the child's physical examination including consideration of tonsillar size, and any other diagnostic procedures eg radiological or endoscopic examinations. For the purpose of this study, these diagnoses were further supported by the outcomes of the Tucson Children's Assessment of Sleep Apnoea Study (TuCASA) questionnaire. Of the 13 children that had a PSG conducted in this study, all were confirmed to have OSA. For ease of interpretation, all patients with a clinical diagnosis of SDB or sleep-study proven OSA were analyzed as a single group. Children were diagnosed with RT if they had a history of either 7 tonsillar infections in the preceding 12 months, 5 episodes per year for the previous 24 months, or 3 episodes per year for the previous 36 months (Harris et al., 2008). Two children in the RT group were diagnosed as having chronic tonsillitis exclusively as they had at least one episode of tonsillitis that persisted for 3 or more months as evidenced by daily sore throats, halitosis, cryptic debris, or tonsil stones. Children with concurrent diagnoses of both SDB and RT were grouped into a SDB+RT group. All diagnoses were confirmed by the treating otorhinolaryngologist. Recruitment of children undergoing adenotonsillar surgery was approved by the Princess Margaret Hospital for Children Human Research Ethics Committee, Perth, Australia (1046/EP).

Inclusion criteria for Healthy Controls: Children were considered healthy if they had no significant history of chronic or recurrent respiratory disease including otitis media, lung disease, sinusitis, SDB and recurrent or chronic tonsillitis. Children were recruited through the Vaccine Trials Group at Princess Margaret Hospital for Children, Perth, Australia (1385/EP).

Specimen Acquisition and Sample Preparation

Nasopharyngeal and oropharyngeal swabs were collected from children with SDB and/or RT at the time of surgery, and from healthy controls when attending the study clinic using flocked swabs (Copan, Italy). Swabs were stored in 1 mL of sterile skim milk tryptone glucose glycerol broth (STGGB), placed on ice and transported to the Princess Margaret Hospital for Children, Children's Clinical Research Facility laboratory within 4h. Samples were vortexed for 30 sec and stored at −80°C.

Adenoids and tonsils were obtained from children undergoing adenotonsillectomy for SDB and/or RT. Tissues were placed in sterile containers on ice and transported to the Princess Margaret Hospital for Children, Children's Clinical Research Facility laboratory within 4h of collection. Biopsies, approximately 5mm^3, were excised from each tonsil and adenoid tissue sample. Biopsies were individually homogenized using hand-held homogenization pestles and placed in cryovials containing 1mL STGGB and stored at −80°C. The remaining tissue was fixed overnight at 4°C in 4% paraformaldehyde, before being washed 3x each for 30min in PBS. They were then stored in 50% PBS/Ethanol at -20°C until sectioning for fluorescence *in situ* hybridization.

Microbiological Assays

Quantitative PCR

Genomic DNA (gDNA) was extracted from nasopharyngeal and oropharyngeal swabs, and from bacterial reference strains NTHi 86-028NP (Bakaletz et al., 1988), *M. catarrhalis* ATCC 25238, *S. pneumoniae* ATCC 7466, *S. pyogenes* ATCC 19615 and *S. aureus* ATCC 25923 using the QIAGEN-DNA Mini Kit (Qiagen, Chadstone, VIC, Australia) as described previously (de Gier et al., 2016). Adenoid and tonsil tissue homogenates were thawed and vortexed for 30 seconds. 200µL of tissue homogenate was used for gDNA extraction. Homogenates were centrifuged at 13000rpm for 7 min to ensure maximum recovery of tissue. The supernatant was discarded, and the pellet resuspended in 180µL of ATL buffer and incubated with 20µL of proteinase K at 56 °C for 3 h. Tissue lysates were loaded into the S-Block from the QIAcube HT Kit (QIAGEN) and gDNA extraction was performed with the QIAcube HT following the manufacturer's protocol for tissue samples.

Real-time qPCR was conducted using the CFX96 real-time PCR detection system (Bio-Rad, CA, USA) using validated qPCR primers, probes and reaction conditions as described previously (Bhuiyan et al., 2018). Nasopharyngeal and oropharyngeal swab gDNA was diluted 1:20 and adenotonsillar samples, 1:30 in nuclease-free water to reduce assay interference with human DNA. GAPDH qPCR was used on all tissue samples to determine the number of human cells present. The number of bacterial copies were then normalized to the number of human cells to account for variation in biopsy size (Tasker et al., 2010).

16S rRNA FISH

Fluorescence *in situ* hybridization (FISH) was conducted using previously described methods and validated 16S rRNA probes labelled with AlexaFluor 488, 546 or 633 dyes (Invitrogen Technologies, Thornton, NSW) (Hall-Stoodley et al., 2006; Thornton et al., 2011) (**Supplementary Table 1**) to determine persistence mechanisms. A subset of tonsillar biopsies (n=3 children/group) were selected based on a positive qPCR result for at least 1 of the 5 bacterial species tested. 3 FISH probes and 1 nucleic acid stain were used per sample. Slides were mounted using an in-house, low-fade mounting media and imaged using a Nikon A1 confocal laser scanning microscope with 60x oil Plan Apo objectives. Images were analyzed for presence of any bacteria, specific bacterial species, biofilm structure and composition.

Samples were considered positive for biofilm presence when images showed characteristic biofilm morphology and bacterial aggregates resembling microcolonies. Bacterial presence was confirmed by assessment of bacterial morphology based on size (0.5–2 μm), shape (cocci or coccobacilli) and fluorescence in the appropriate channel. Host cells were identified by Hoechst 33342 nucleic acid stain. Bacteria were deemed intracellular when discrete clusters of bacteria were in close proximity to intact host cell nuclei as described previously (Thornton et al., 2011).

Statistical Analyses

Chi-squared tests were used to compare categorical variables between groups. Kruskal Wallis with *post-hoc* pairwise analyses were used to assess differences in age, episodes of tonsillitis, bacterial species density and total bacterial load between groups. Samples with qPCR measurements below the limit of detection (LOD) were assigned half of this LOD value for statistical analyses. A p value ≤ 0.05 was considered significant. Statistical analyses were performed with SPSS version 23.0 for Windows (SPSS Inc., Chicago, IL, USA) and data were plotted using GraphPad version 8 for Windows (GraphPad Software, La Jolla California USA).

RESULTS

Population Characteristics

Forty children were recruited into the SDB group, 17 into the SDB +RT group, 18 into the RT group and 33 into the healthy group. The median age was similar across all 4 groups including healthy controls (p=0.083, **Table 1**). Gender was evenly distributed. Use of antibiotics in the month preceding surgery was higher in children with adenotonsillar diseases compared to healthy controls (p=0.009). Children with RT (with or without concurrent SDB) were more likely to have used antibiotics in the month prior to surgery than children with SDB (RT vs SDB, p=0.015; SDB+RT vs SDB, p=0.024). Only 1 child in the SDB+RT group was on antibiotics at the time of surgery. Although obesity is commonly associated with SDB (Daar et al., 2016), this was not observed in our study with a similar mean body mass index (BMI) observed for each group (means 17.6 to 19.1, p=0.404; **Table 1**). The proportion of children with adenotonsillar diseases presenting

TABLE 1 | Study population.

	SDB n = 40	SDB+RT n = 17	RT n = 18	Healthy n = 33	p value
Median age in years (range)	6.0 (1.1-13.6)	6.0 (2.3-13.6)	7.8 (2.8-15.8)	9.1 (2.0-16.6)	0.083
Male Gender n(%)	22 (55.0)	11 (64.7)	10 (55.6)	13 (39.4)	0.329
Median no. of acute tonsillitis episodes (range)	1.0# (0-10)	13.0# (5-45)	20.0^ (8-65)	0 (0-3)	0.000
Procedure					
- **Adenotosillectomy**	36	16	14	N/A	0.282
- **Tonsillectomy**	2	1	4	N/A	0.097
- **Adenoidectomy**	2	0	0	N/A	0.407
Mean BMI (+/- SD)^	17.6 (5.2)	17.9 (3.4)	19.1 (3.8)	17.9 (3.3)	0.157
Antibiotics in last month n(%)	2# (5.4)	4# (17.6)	5 (27.3)	0#	0.009
Adenoid hypertrophy (Grade 3 or 4) n(%)	18* (52.9)	9* (64.3)	6* (37.5)	N/A	0.333
Tonsillar hypertrophy (Grade 3 or 4) n(%)	22# (56.4)	12 (70.6)	8 (44.4)	N/A	0.295
Confirmatory PSG for OSA	12 (30.0)	1^^ (6.7)	0	N/A	–
TuCASA					
- **Excessive daytime sleepiness**	16# (41.0)	7# (43.8)	8** (47.1)	1 (3.0)	0.001
- **Witnessed apnoea**	23 (57.5)	9# (56.3)	1** (5.9)	0	0.000
- **Snoring**	36 (90.0)	13# (81.3)	7 (38.9)	0	0.000
- **Learning problems**	10 (25.0)	3# (18.8)	2** (11.8)	0	0.022
Allergic presentations					
- **Hay fever**	2 (5.0)	0#	1 (5.6)	3 (9.1)	0.629
- **Asthma**	12# (30.8)	3# (18.8)	4 (22.2)	5 (15.6)	0.446
- **Rhinitis**	25 (62.5)	9^ (64.3)	7 (38.9)	6 (18.2)	0.001
- **Rhinitis with itchy eyes**	8 (20.0)	5# (31.3)	5 (27.8)	1 (3.0)	0.041
- **Eczema or dermatitis**	11 (27.5)	6# (37.5)	6 (33.3)	7 (21.2)	0.631

SDB, sleep disordered breathing; RT, recurrent tonsillitis; BMI, body mass index; PSG, polysomnogram; OSA, obstructive sleep apnoea; SD, standard deviation.
*^Information is missing for 4 subjects in SDB group (n = 36), 3 subjects in SDB+RT group (n = 14) and 2 subjects in RT group (n = 16); #information is missing for missing for 1 subject in SDB group (n = 39),1 subject in SDB+RT group (n = 16) and 12 in HC group (n = 21); *Adenoids were not graded from 6 children with SDB (n = 34), 3 children with SDB+RT (n = 14), and 2 children with RT (n = 16); ^^Information is missing for 2 subjects in the SDB+RT group (n = 15); **Information is missing for 1 subject in the RT group (n = 17).*
N/A, not applicable.

with adenotonsillar hypertrophy as determined by grade 3 or 4 adenoids or tonsils on the Brodsky scale (Brodsky et al., 1988) was similar across groups. OSA was confirmed by PSG for 12 of 40 children with SDB and 1 of 17 children with SDB+RT. As PSG could not be obtained for all children diagnosed with SDB, parents were asked to complete the validated Tucson Children's Assessment of Sleep Apnoea Study (TuCASA) questionnaire (Goodwin et al., 2003) to assess respiratory sleep disturbances. TuCASA responses revealed that healthy children did not exhibit clinical symptoms of respiratory sleep disturbances whereas children diagnosed with an adenotonsillar disease did; witnessed apnoea and snoring were more prevalent in children diagnosed with SDB and SDB+RT compared to RT (p=0.001; p<0.0001 respectively). Learning problems and excessive daytime sleepiness were comparable between children with SDB, SDB+RT and RT. As allergy is also considered as a risk factor for SDB (Gadi et al., 2017; Zheng et al., 2017), we compared allergic presentations across groups. Rhinitis and itchy eyes were more prevalent in children with adenotonsillar diseases compared to healthy controls (p=0.001 and p=0.041) but prevalence amongst children with either SDB, SDB+RT or RT (p=0.625) was similar. The frequency of physician diagnosed hay fever, asthma and eczema/dermatitis were similar across all 4 groups (**Table 1**).

All Bacterial Species Were Frequently Detected in Nasopharyngeal and Oropharyngeal Swabs From Children With Adenotonsillar Diseases as Well as Healthy Controls

S. pyogenes, *S. aureus, S. pneumoniae*, NTHi and *M. catarrhalis* were detected in nasopharyngeal and oropharyngeal swabs from children with adenotonsillar diseases as well as healthy controls. *S. pyogenes* was detected at relatively low frequencies in nasopharyngeal swabs compared to the other species, with only 2 out of 18 children diagnosed with RT (11.1%) positive for *S. pyogenes* in their nasopharynx compared to 27.5% of children with SDB, 43.8% of children with SDB+RT, and 18.8% of healthy children. *S. pyogenes* was detected more often in oropharyngeal swabs than nasopharyngeal swabs, with similar frequency of detection across all groups. *S. aureus* was detected more frequently in nasopharyngeal swabs from children with SDB, SDB+RT and healthy children compared to those with RT alone although this was not statistically different (60%, 62.5%, 65.6% and 33.3% respectively; p=0.143). In oropharyngeal swabs, *S. aureus* was detected more often from children with SDB (62.9%), SDB+RT (75%) and RT (75%) compared to healthy children (33.3%), (p=0.007). *S. pneumoniae* was frequently detected in nasopharyngeal swabs (>61%) and frequency did not differ between groups including healthy children. In contrast, *S. pneumoniae* was detected more frequently in oropharyngeal swabs from children with SDB, SDB+RT and RT compared to healthy children (91.4%, 87.5%, 87.5% and 66.7% respectively; p=0.046). NTHi was also frequently detected in oropharyngeal swabs, with more than 81% of children in each group including healthy controls being positive. In the nasopharynx, NTHi was detected in 19% to 35% of children with similar frequencies between groups including healthy children. *M. catarrhalis* was frequently detected in nasopharyngeal swabs, with over 60% of children positive. Similarly, this pathogen was detected in over 48% of oropharyngeal swabs, with a similar detection frequency across groups (**Figure 1**).

Species-Specific Bacterial Densities in Oropharyngeal Swabs Were Lower in Healthy Children

Children with SDB alone had higher total bacterial loads in their nasopharyngeal swabs when compared to healthy children (p=0.001). While total bacterial loads in the nasopharynx were similar in children with SDB+RT, RT and healthy children. Total bacterial loads in the oropharynx were higher than in the nasopharynx and were similar between groups (**Figure 1A**).

The median density of *S. pyogenes* in nasopharyngeal swabs was higher in children with adenotonsillar diseases compared to healthy controls (SDB vs healthy p<0.0001; SDB+RT vs healthy p<0.0001; RT vs healthy p=0.003) (**Figure 1B**). While the median densities of *S. aureus, S. pneumoniae*, NTHi and *M. catarrhalis* in nasopharyngeal swabs were similar across groups (**Figures 1C–F**). In oropharyngeal swabs, the median densities of *S. pyogenes* and *S. aureus* were similar across all groups (**Figures 1B, C**). The density of *S. pneumoniae* in oropharyngeal swabs was higher in children with SDB and SDB+RT compared to healthy children (p<0.0001 and p=0.034 respectively) (**Figure 1D**). NTHi densities were also higher in children with SDB compared to healthy controls (p=0.002) but similar between other groups (**Figure 1E**). The densities of *M. catarrhalis* were higher in children with SDB and SDB+RT compared to healthy controls (p=0.01 and p=0.02 respectively) (**Figure 1F**).

NTHi Was the Most Frequently Detected Pathogen in Tonsils From Children With Adenotonsillar Diseases

S. pyogenes, *S. pneumoniae*, NTHi and *M. catarrhalis* were detected in both adenoid and tonsil tissue from children with adenotonsillar diseases. NTHi was the predominant species detected in adenoid and tonsil tissue, with detection rates above 47% in adenoids and above 84% in tonsils from children with SDB and SDB+RT. The frequency of NTHi detection was lower in adenoids and tonsils from children with RT (30% and 66% respectively) but this was not significantly different when compared to other disease groups (**Figure 2E**). The frequency of *S. pyogenes* detection in adenoids was higher in children with RT compared to those with SDB (p=0.03). However, this was not the case in tonsil tissue with similar detection frequency of *S. pyogenes* across all disease groups (**Figure 2B**). *S. aureus* was also commonly detected in tonsil tissue from all children with adenotonsillar disease (33 to 58%), but was only present in the adenoid tissue from one child (**Figure 2C**). *S. pneumoniae* detection frequency in adenoids and tonsils was also similar across groups (23-30%), although only 1 child with RT had detectable *S. pneumoniae* in their tonsil tissue. The frequency of

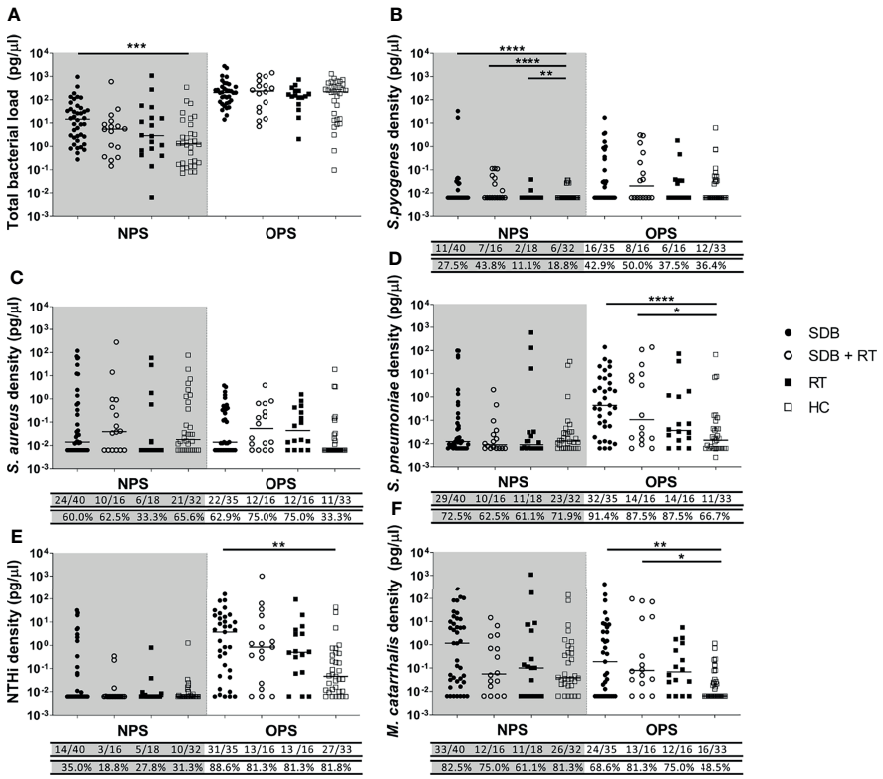

FIGURE 1 | Total bacterial load **(A)** and specific bacterial density **(B–F)** in the nasopharyngeal swabs (NPS) and oropharyngeal swabs (OPS) from children with SDB (•), SDB+RT (o), RT (▪) and healthy children (HC) (▫). p value * < 0.05; **< 0.01; *** < 0.001; **** < 0.0001. Numbers underneath each graph represent the proportion of children in each group considered positive for each bacterial species with numbers on the top row and the corresponding proportion in the bottom. Samples not available: 1 NPS from a child with SDB+RT and 1 NPS from a healthy child; 5 OPS from children with SDB, 1 OPS from a child with SDB+RT and 2 OPS from children with RT.

M. catarrhalis detection in adenoids was higher in children with SDB compared to RT (p=0.036) while the frequency of detection in tonsils was similar across groups (**Figure 2F**).

Children Had Similar Total Bacterial and Species-Specific Densities in Their Adenotonsillar Tissue Regardless of Clinical Diagnosis

Total bacterial loads in adenoids and tonsils were similar between all children with adenotonsillar disease regardless of clinical diagnosis (**Figure 2A**). The densities of specific bacterial species were similar in adenoids and tonsils from children in all groups (**Figures 2B–F**). The density of *S. pyogenes* in adenoids tended to be higher in children with RT although this was not significant (p=0.054) (**Figure 2B**). *S. aureus* was found at high densities and at similar levels across groups in tonsils but was rarely detected in adenoids (**Figure 2C**). Densities of *S. pneumoniae* were comparable between groups in both adenoid and tonsil tissue (**Figure 2D**). NTHi was also present at similar densities in adenoids and tonsils across groups (**Figure 2E**). Densities of *M. catarrhalis* were low and comparable between groups in both adenoid and tonsil tissue (**Figure 2F**).

Polymicrobial Detection Was More Common in Nasopharyngeal and Oropharyngeal Swabs Than Adenotonsillar Tissue

Concurrent detection of 3 or more of the 5 respiratory pathogens tested was common in nasopharyngeal and oropharyngeal swabs from children across all groups. Although, in oropharyngeal swabs, concurrent detection of 3 or more of the 5 respiratory pathogens occurred more frequently in children with adenotonsillar disease compared to healthy children (80% versus 57%, p=0.043). Adenoid and tonsillar tissues, only taken from children with adenotonsillar disease, were more likely to have only 1 or 2 species detected. The frequency of detection was similar across the 3 adenotonsillar groups (**Supplementary Table 2**).

When relative abundance of each species was compared, nasopharyngeal and oropharyngeal swabs exhibited high densities and diversity of detected species, although overall densities were lower in healthy children compared to those with adenotonsillar diseases (**Supplementary Figure 1**). Less polymicrobial interactions were observed in the adenoid and tonsillar tissues where usually only 1 or 2 species were present (**Supplementary Figure 2**).

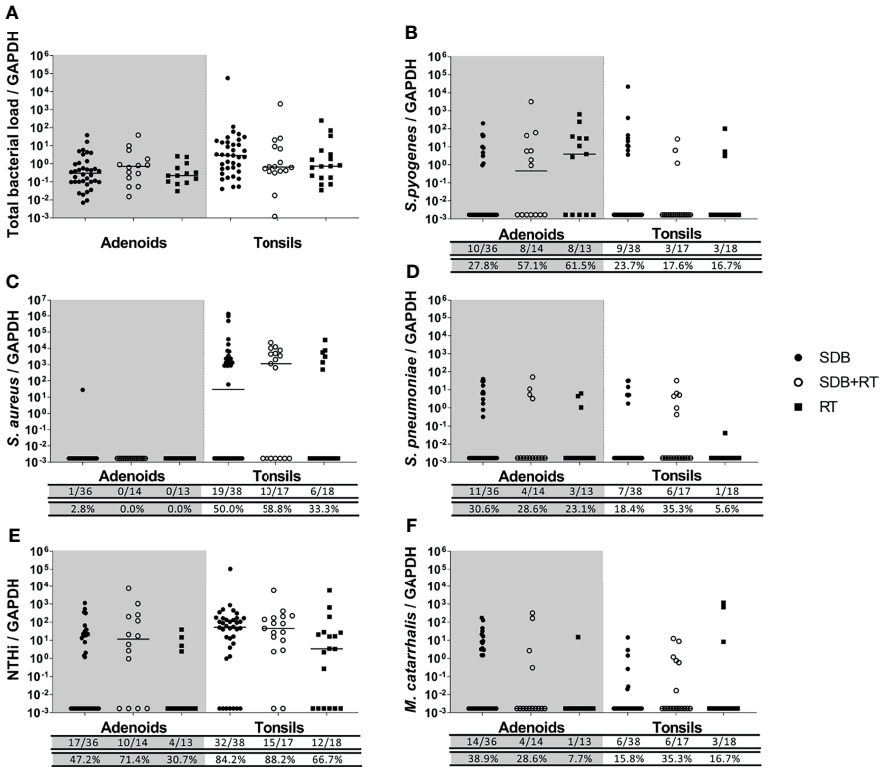

FIGURE 2 | Total bacterial load **(A)** and specific bacterial density **(B–F)** in adenoids and tonsils from children with SDB (•), SDB+RT (○), RT (■). Numbers underneath each graph represent the number of children in each group considered positive for each bacterial species (top row) and the corresponding proportion (bottom row). Samples not available: 4 adenoids from children with SDB, 3 adenoids from children with SDB+RT and 5 adenoids from children with RT; 2 tonsils from children with SDB.

Tonsillar Polymicrobial Biofilms Are Also Evident in Children With SDB

Polymicrobial biofilms were detected in the tonsil crypts and on the tonsillar surfaces of tissue irrespective of clinical diagnosis (**Figure 3**). Biofilm presence, location and detection of intracellular bacteria were similar between the 3 disease groups (**Supplementary Table 3**). Species-specific probes identified the same bacterial species as were detected by qPCR with the universal bacterial probe confirming that other unidentified bacterial species were also abundant in biofilms. Some bacterial species were observed using FISH that were not detected using qPCR.

DISCUSSION

This study demonstrates the presence of 5 common respiratory pathogens in the upper respiratory tract and adenotonsillar tissues from children with adenotonsillar diseases. We observed that these 5 bacterial species are present just as often and at similar densities in children with SDB (including OSA) when compared to children diagnosed with RT, and in those with concurrent diagnoses of SDB and RT. Moreover, we have demonstrated surface and crypt-associated polymicrobial biofilms and intracellular bacterial pods in tonsil tissue from a subset of children presenting with each of these adenotonsillar diseases. Together, these data demonstrate the presence of bacteria in high densities and in formations that may contribute to the chronicity of infection in patients, including those presenting with SDB. Traditionally, children with SDB are considered to have disease of non-infectious origins in comparison to children diagnosed with RT, and have even been used as healthy comparators to children with RT in previous reports (Subtil et al., 2017; Dan et al., 2019). Our study challenges this dogma, and instead proposes that that the broad range of clinical presentations in children with SDB and RT may actually have a shared microbial aetiology. Our data also suggest that it is unlikely that a single bacterial species drives either an obstructive sleep phenotype or recurrent tonsillitis. We also showed that nasopharyngeal and oropharyngeal swabs, which have greater diversity of detected species, are not representative of the microbial profile of adenoids and tonsil tissues demonstrating that these swabs cannot be used as surrogates to determine what is happening in adenoids and tonsils leading to clinical disease. While these findings are contrary to our original hypothesis that children with SDB would have reduced bacterial loads and a lack of biofilms compared to those with RT, our data demonstrate an

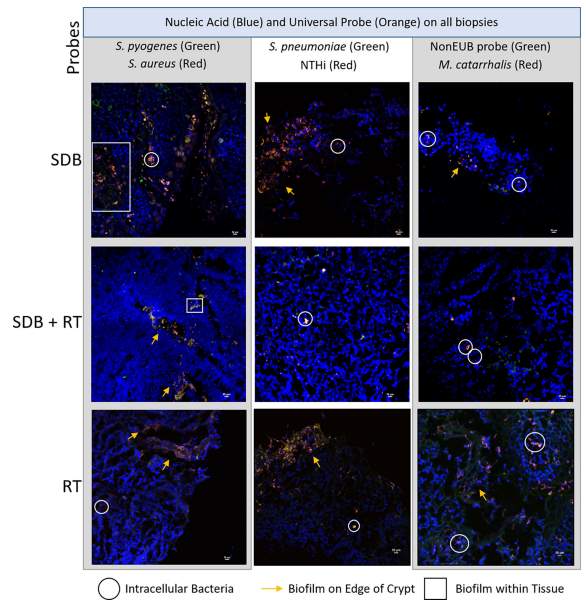

FIGURE 3 | Representative maximum projections of intracellular bacteria, biofilms on surfaces and within tonsillar tissue from children with SDB, SDB+RT and RT. Scale bars represent 10μM.

infectious phenotype associated with SDB and a high prevalence of NTHi and *S. aureus* infection. Importantly, these pathogens were demonstrated to be present within biofilms regardless of diagnoses which likely contributes to the chronicity of infection. The frequent and dense detection of NTHi and *S. aureus* in tonsillar tissue from our pediatric samples are consistent with previous studies. In tonsils removed from children and adults with OSA or RT, *H. influenzae* and *S. aureus* were the most frequently isolated species (particularly in children), implicating these species as major pathogens in adenotonsillar diseases. The authors also showed that biofilms were associated with clinical symptoms of tonsillar diseases such as apnoea and sore throat, suggesting that the recalcitrant nature of these diseases is due to microbial persistence (Alasil et al., 2013). In another study, which compared groups of children with RT to those with OSA, *S. aureus* was more frequently identified than *S. pyogenes* in tonsil tissue and at similar frequencies between the groups (Radcliff et al., 2019). This further supports the evidence that *S. pyogenes* is neither the sole nor major pathogenic determinant driving adenotonsillar disease and has implications for the clinical management of children with adenotonsillar disease. We recommend the investigation into the use of anti-biofilm agents or perhaps even NTHi and/or *S. aureus* targeted therapies while children with adenotonsillar disease are awaiting surgery or even before they reach this severe end of the disease spectrum.

Microbial involvement in SDB is further supported by recent studies. Bacterial 16S RNA sequencing revealed that the microbial profiles of adenoid and tonsil tissues in children with clinical symptoms of SDB were similar to children with RT, with frequent detection of *Streptococcus*, *Haemophilus*, *Moraxella*, *Neiserria* and *Staphylococcus* species and an overall dominance of *Haemophilus* (Johnston et al., 2019) Given that we and others have shown that the same bacterial species are involved in the pathogenesis of SDB as well as RT, host responses to these pathogens also need to be considered to explain the clinical presentations specific to each diagnosis. There are limited data on this in the context of adenotonsillar diseases, but it has been demonstrated that *S. aureus* isolates from tonsils from children with OSA or RT had mitogenic capacity, and that *S. aureus* presence was associated with elevated peripheral blood and tonsillar mucosal-associated invariant T (MAIT) cells, likely responding to the bacterially-derived superantigens. Interestingly, the proportion of tonsillar MAIT cells were reduced in children with RT compared to OSA but there were no differences between other CD4+ and CD8+ T cell compartments (Radcliff et al., 2019). These data suggest that there may be differences in immune development that influences disease pathogenesis, which should be investigated in future studies.

While the development of vaccines targeting NTHi and *S. aureus* may be important for the treatment/prevention of pediatric respiratory diseases, including adenotonsillar diseases, anti-biofilm agents may also be required. The identification of polymicrobial biofilms on tonsillar surfaces, in crypts and intracellularly in the small sub-group assessed in our study suggests that these persistence mechanisms contribute to the chronicity of infection in these clinical conditions. It may be pertinent in the future to investigate the potential use of topical anti-biofilm treatments (Brockson et al., 2014; Novotny et al., 2020), bacteriophage therapy (Kornienko et al., 2020), or vaccines targeting important proteins involved in biofilm formation and maintenance (Mokrzan et al., 2018; Novotny et al., 2019), to both prevent and treat these conditions, thus reducing the need for long term antibiotics or surgical intervention.

LIMITATIONS

In Australia, due to considerable wait times for polysomnography versus adenotonsillectomy surgery, not all children with physician diagnosed SDB underwent polysomnography to confirm OSA. As a result only 23% of children with SDB had confirmatory polysomnography in our study and thus we used the validated TuCASA questionnaire (Goodwin et al., 2003) as a secondary tool to verify the SDB diagnosis. We acknowledge that the small group sizes in our study may not be representative of the complete spectrum of pediatric adenotonsillar diseases. However, our groups sizes are comparable (if not, slightly larger) to other studies investigating the aetiology and pathogenesis of adenotonsillar diseases. Furthermore, unlike other studies, we included groups of children to represent the breadth of adenotonsillar disease diagnoses, enabling assessment of microbial profiles that may have been unique to each. By using a targeted PCR approach focusing on the 5 major respiratory pathogens, we may have missed important microbes present in the

tonsillar microbiota, but this was safe-guarded by using a universal bacterial qPCR and universal bacterial FISH probe to detect all bacteria present (Johnston et al., 2019). Future studies should include non-targeted profiling in conjunction with quantitative species-specific assays.

CONCLUSIONS AND RECOMMENDATIONS FOR DEVELOPMENT OF FUTURE THERAPEUTICS

We have shown that a similar polymicrobial infectious phenotype exists in children with SDB, RT alone, or with concurrent diagnoses of SDB and RT. Differences in clinical presentations are likely driven by host responses. The microbial profiles of the nasopharynx and oropharynx are not representative of the adenoids and tonsils. We identified NTHi and *S. aureus* as species to target and suggest that antimicrobial (including anti-biofilm) approaches may be relevant for treating children with SDB and/or RT. Vaccines targeting these pathogens may also be useful in reducing the overall prevalence of these diseases in pediatric populations.

DATA AVAILABILITY STATEMENT

The raw data supporting the conclusions of this article will be made available by the authors, without undue reservation.

ETHICS STATEMENT

The studies involving human participants were reviewed and approved by Princess Margaret Hospital for Children Human Research Ethics Committee, Perth, Australia (1046/EP)(1385/EP). Written informed consent to participate in this study was provided by the participants' legal guardian/next of kin.

AUTHOR CONTRIBUTIONS

RT had full access to all of the data in the study and takes responsibility for the integrity of the data and the accuracy of the data analysis. Concept and design: TM, RT, PR, LK, SV, KP, and HC. Acquisition, analysis or interpretation of data: all authors. Drafting of the manuscript: ES, RT, PR, and LK. Critical revision of the manuscript for important intellectual content: all authors. Statistical analysis: ES. Administrative, technical or material support: TM, SV, KP, and HC. Supervision: RT, PR, and LK. All authors contributed to the article and approved the submitted version.

FUNDING

This study was funded by the Western Australia Department of Health Telethon Perth Children's Hospital Research Fund. TM was a recipient of a University of Western Australia International Postgraduate Fellowship and Stan and Jean Perron top-up scholarship. LK was a recipient of an Australian National Health and Medical Research Council (NHMRC) Career Development Fellowship (#1061428). RT was a recipient of a BrightSpark postdoctoral fellowship.

ACKNOWLEDGMENTS

We thank the families and hospital staff for taking part in this study. The authors acknowledge the facilities, and the scientific and technical assistance of Microscopy Australia at the Centre for Microscopy, Characterisation & Analysis, The University of Western Australia, a facility funded by the University, State and Commonwealth Governments.

SUPPLEMENTARY MATERIAL

The Supplementary Material for this article can be found online at: https://www.frontiersin.org/articles/10.3389/fcimb.2022.831887/full#supplementary-material

REFERENCES

Alasil, S. M., Omar, R., Ismail, S., Yusof, M. Y., Dhabaan, G. N., and Abdulla, M. A. (2013). Evidence of Bacterial Biofilms Among Infected and Hypertrophied Tonsils in Correlation With the Microbiology, Histopathology, and Clinical Symptoms of Tonsillar Diseases. *Int. J. Otolaryngol* 2013, 408238. doi: 10.1155/2013/408238

Australian Commision on Safety and Quality in Health Care. (2021). "3.1 Tonsillectomy Hospitalisations, 17 Years and Under," in *Variation TFAAoH*.

Bakaletz, L. O., Tallan, B. M., Hoepf, T., DeMaria, T. F., Birck, H. G., and Lim, D. J. (1988). Frequency of Fimbriation of Nontypable Haemophilus Influenzae and its Ability to Adhere to Chinchilla and Human Respiratory Epithelium. *Infect. Immun.* 56 (2), 331–335.

Bhuiyan, M. U., Snelling, T. L., West, R., Lang, J., Rahman, T., Borland, M. L., et al. (2018). Role of Viral and Bacterial Pathogens in Causing Pneumonia Among Western Australian Children: A Case-Control Study Protocol. *BMJ Open* 8 (3), e020646. doi: 10.1136/bmjopen-2017-020646

Brockson, M. E., Novotny, L. A., Mokrzan, E. M., Malhotra, S., Jurcisek, J. A., Akbar, R., et al. (2014). Evaluation of the Kinetics and Mechanism of Action of Anti-Integration Host Factor-Mediated Disruption of Bacterial Biofilms. *Mol. Microbiol.* 93 (6), 1246–1258. doi: 10.1111/mmi.12735

Brodsky, L., Moore, L., Stanievich, J. F., and Ogra, P. L. (1988). The Immunology of Tonsils in Children: The Effect of Bacterial Load on the Presence of B- and T-Cell Subsets. *Laryngoscope* 98 (1), 93–98. doi: 10.1288/00005537-198801000-00019

Coticchia, J., Zuliani, G., Coleman, C., Carron, M., Gurrola, J.2nd, Haupert, M., et al. (2007). Biofilm Surface Area in the Pediatric Nasopharynx: Chronic Rhinosinusitis vs Obstructive Sleep Apnea. *Arch. Otolaryngol Head Neck Surg.* 133 (2), 110–114. doi: 10.1001/archotol.133.2.110

Daar, G., Sari, K., Gencer, Z. K., Ede, H., Aydin, R., and Saydam, L. (2016). The Relation Between Childhood Obesity and Adenotonsillar Hypertrophy. *Eur. Arch. Otorhinolaryngol* 273 (2), 505–509. doi: 10.1007/s00405-015-3554-4

Dan, J. M., Havenar-Daughton, C., Kendric, K., Al-Kolla, R., Kaushik, K., Rosales, S. L., et al. (2019). Recurrent Group A Streptococcus Tonsillitis is an

Immunosusceptibility Disease Involving Antibody Deficiency and Aberrant TFH Cells. *Sci. Transl. Med.* 11 (478). doi: 10.1126/scitranslmed.aau3776

de Gier, C., Pickering, J. L., Richmond, P. C., Thornton, R. B., and Kirkham, L. A. (2016). Duplex Quantitative PCR Assay for Detection of Haemophilus Influenzae That Distinguishes Fucose- and Protein D-Negative Strains. *J. Clin. Microbiol.* 54 (9), 2380–2383. doi: 10.1128/JCM.00982-16

Diaz, R. R., Picciafuoco, S., Paraje, M. G., Villegas, N. A., Miranda, J. A., Albesa, I., et al. (2011). Relevance of Biofilms in Pediatric Tonsillar Disease. *Eur. J. Clin. Microbiol. Infect. Dis.* 30 (12), 1503–1509. doi: 10.1007/s10096-011-1249-3

Gadi, G., Wali, S., Koshak, E., Albar, M., Fida, A., Abdelaziz, M., et al. (2017). The Prevalence of Allergic Rhinitis and Atopic Markers in Obstructive Sleep Apnea. *J. Epidemiol. Glob Health* 7 (1), 37–44. doi: 10.1016/j.jegh.2016.06.001

Galli, J., Calo, L., Ardito, F., Imperiali, M., Bassotti, E., Fadda, G., et al. (2007). Biofilm Formation by Haemophilus Influenzae Isolated From Adeno-Tonsil Tissue Samples, and its Role in Recurrent Adenotonsillitis. *Acta Otorhinolaryngol Ital* 27 (3), 134–138.

Goodwin, J. L., Kaemingk, K. L., Fregosi, R. F., Rosen, G. M., Morgan, W. J., Sherrill, D. L., et al. (2003). Clinical Outcomes Associated With Sleep-Disordered Breathing in Caucasian and Hispanic Children–the Tucson Children's Assessment of Sleep Apnea Study (TuCASA). *Sleep* 26 (5), 587–591. doi: 10.1093/sleep/26.5.587

Hall-Stoodley, L., Hu, F. Z., Gieseke, A., Nistico, L., Nguyen, D., Hayes, J., et al. (2006). Direct Detection of Bacterial Biofilms on the Middle-Ear Mucosa of Children With Chronic Otitis Media. *JAMA* 296 (2), 202–211. doi: 10.1001/jama.296.2.202

Harris, M. A., Coates, H., Harari, M., Kennedy, D., Lannigan, F., Richmond, P., et al. (2008). Indications for Tonsillectomy and Adenotonsillectomy in Children. *Paediatrics & Child Health Division of The Royal Australasian College of Physicians and The Australian Society of Otolaryngology Head and Neck Surgery*.

Johnston, J., Hoggard, M., Biswas, K., Astudillo-Garcia, C., Radcliff, F. J., Mahadevan, M., et al. (2019). Pathogen Reservoir Hypothesis Investigated by Analyses of the Adenotonsillar and Middle Ear Microbiota. *Int. J. Pediatr. Otorhinolaryngol* 118, 103–109. doi: 10.1016/j.ijporl.2018.12.030

Johnston, J., McLaren, H., Mahadevan, M., and Douglas, R. G. (2019). Clinical Characteristics of Obstructive Sleep Apnea Versus Infectious Adenotonsillar Hyperplasia in Children. *Int. J. Pediatr. Otorhinolaryngol* 116, 177–180. doi: 10.1016/j.ijporl.2018.11.004

Kornienko, M., Kuptsov, N., Gorodnichev, R., Bespiatykh, D., Guliaev, A., Letarova, M., et al. (2020). Contribution of Podoviridae and Myoviridae Bacteriophages to the Effectiveness of Anti-Staphylococcal Therapeutic Cocktails. *Sci. Rep.* 10 (1), 18612. doi: 10.1038/s41598-020-75637-x

Marcus, C. L., Moore, R. H., Rosen, C. L., Giordani, B., Garetz, S. L., Taylor, H. G., et al. (2013). A Randomized Trial of Adenotonsillectomy for Childhood Sleep Apnea. *N Engl. J. Med.* 368 (25), 2366–2376. doi: 10.1056/NEJMoa1215881

Mitchell, R. B., Archer, S. M., Ishman, S. L., Rosenfeld, R. M., Coles, S., Finestone, S. A., et al. (2019). Clinical Practice Guideline: Tonsillectomy in Children (Update). *Otolaryngol Head Neck Surg.* 160 (1_suppl), S1–S42. doi: 10.1177/0194599818801757

Mokrzan, E. M., Novotny, L. A., Brockman, K. L., and Bakaletz, L. O. (2018). Antibodies Against the Majority Subunit (PilA) of the Type IV Pilus of Nontypeable Haemophilus Influenzae Disperse Moraxella Catarrhalis From a Dual-Species Biofilm. *mBio* 9 (6). doi: 10.1128/mBio.02423-18

Novotny, L. A., Goodman, S. D., and Bakaletz, L. O. (2019). Redirecting the Immune Response Towards Immunoprotective Domains of a DNABII Protein Resolves Experimental Otitis Media. *NPJ Vaccines* 4, 43. doi: 10.1038/s41541-019-0137-1

Novotny, L. A., Goodman, S. D., and Bakaletz, L. O. (2020). Targeting a Bacterial DNABII Protein With a Chimeric Peptide Immunogen or Humanised Monoclonal Antibody to Prevent or Treat Recalcitrant Biofilm-Mediated Infections. *EBioMedicine* 59, 102867. doi: 10.1016/j.ebiom.2020.102867

Ostvoll, E., Sunnergren, O., and Stalfors, J. (2018). Increasing Readmission Rates for Hemorrhage After Tonsil Surgery: A Longitudinal (26 Years) National Study. *Otolaryngol Head Neck Surg.* 158 (1), 167–176. doi: 10.1177/0194599817725680

Radcliff, F. J., Waldvogel-Thurlow, S., Clow, F., Mahadevan, M., Johnston, J., Li, G., et al. (2019). Impact of Superantigen-Producing Bacteria on T Cells From Tonsillar Hyperplasia. *Pathogens* 8 (3). doi: 10.3390/pathogens8030090

Roberts, A. L., Connolly, K. L., Kirse, D. J., Evans, A. K., Poehling, K. A., Peters, T. R., et al. (2012). Detection of Group A Streptococcus in Tonsils From Pediatric Patients Reveals High Rate of Asymptomatic Streptococcal Carriage. *BMC Pediatr.* 12, 3. doi: 10.1186/1471-2431-12-3

Subtil, J., Rodrigues, J. C., Reis, L., Freitas, L., Filipe, J., Santos, A., et al. (2017). Adenoid Bacterial Colonization in a Paediatric Population. *Eur. Arch. Otorhinolaryngol* 274 (4), 1933–1938. doi: 10.1007/s00405-017-4493-z

Tasker, S., Peters, I. R., Mumford, A. D., Day, M. J., Gruffydd-Jones, T. J., Day, S., et al. (2010). Investigation of Human Haemotropic Mycoplasma Infections Using a Novel Generic Haemoplasma qPCR Assay on Blood Samples and Blood Smears. *J. Med. Microbiol.* 59 (Pt 11), 1285–1292. doi: 10.1099/jmm.0.021691-0

Thornton, R. B., Rigby, P. J., Wiertsema, S. P., Filion, P., Langlands, J., Coates, H. L., et al. (2011). Multi-Species Bacterial Biofilm and Intracellular Infection in Otitis Media. *BMC Pediatr.* 11, 94. doi: 10.1186/1471-2431-11-94

Viciani, E., Montagnani, F., Tavarini, S., Tordini, G., Maccari, S., Morandi, M., et al. (2016). Paediatric Obstructive Sleep Apnoea Syndrome (OSAS) is Associated With Tonsil Colonisation by Streptococcus Pyogenes. *Sci. Rep.* 6, 20609. doi: 10.1038/srep20609

Zheng, M., Wang, X., Ge, S., Gu, Y., Ding, X., Zhang, Y., et al. (2017). Allergic and Non-Allergic Rhinitis Are Common in Obstructive Sleep Apnea But Not Associated With Disease Severity. *J. Clin. Sleep Med.* 13 (8), 959–966. doi: 10.5664/jcsm.6694

Zuliani, G., Carlisle, M., Duberstein, A., Haupert, M., Syamal, M., Berk, R., et al. (2009). Biofilm Density in the Pediatric Nasopharynx: Recurrent Acute Otitis Media Versus Obstructive Sleep Apnea. *Ann. Otol. Rhinol. Laryngol* 118 (7), 519–524. doi: 10.1177/000348940911800711

Conflict of Interest: The authors declare that the research was conducted in the absence of any commercial or financial relationships that could be construed as a potential conflict of interest.

frontiers in Cellular and Infection Microbiology

ORIGINAL RESEARCH
published: 28 February 2022
doi: 10.3389/fcimb.2022.851784

Pseudomonas aeruginosa Is More Tolerant Under Biofilm Than Under Planktonic Growth Conditions: A Multi-Isolate Survey

Janne G. Thöming[1,2] *and Susanne Häussler*[1,2,3,4]*

[1] Department of Clinical Microbiology, University Hospital Copenhagen, Rigshospitalet, Copenhagen, Denmark, [2] Molecular Bacteriology, Twincore Center for Experimental and Clinical Infection Research GmbH, Hannover, Germany, [3] Molecular Bacteriology, Helmholtz Centre for Infection Research, Braunschweig, Germany, [4] Cluster of Excellence RESIST (EXC 2155), Hannover Medical School, Hannover, Germany

OPEN ACCESS

Edited by:
Lauren O. Bakaletz,
Nationwide Children's Hospital,
United States

Reviewed by:
Oana Ciofu,
University of Copenhagen, Denmark
Laura Sherrard,
Queen's University Belfast,
United Kingdom

***Correspondence:**
Susanne Häussler
Susanne.haeussler@helmholtz-hzi.de

Specialty section:
This article was submitted to Biofilms, a section of the journal Frontiers in Cellular and Infection Microbiology

Received: 10 January 2022
Accepted: 24 January 2022
Published: 28 February 2022

Citation:
Thöming JG and Häussler S (2022) Pseudomonas aeruginosa Is More Tolerant Under Biofilm Than Under Planktonic Growth Conditions: A Multi-Isolate Survey. Front. Cell. Infect. Microbiol. 12:851784. doi: 10.3389/fcimb.2022.851784

Biofilm-associated bacteria exhibit profound changes in bacterial physiology. They thrive in the environment but also in the human host in protected sessile communities. Antimicrobial therapy usually fails, despite the absence of genotypic resistance, and it is commonly accepted that biofilm-grown bacteria are up to 1,000-fold more resistant than planktonic cells. We are only at the beginning to understand the reasons for biofilm recalcitrance, and systematic approaches to describe biofilm-induced tolerance phenotypes are lacking. In this study, we investigated a large and highly diverse collection of 352 clinical *Pseudomonas aeruginosa* isolates for their antimicrobial susceptibility profiles under biofilm growth conditions towards the antibiotics ciprofloxacin, tobramycin, and colistin. We discovered characteristic patterns of drug-specific killing activity and detected conditional tolerance levels far lower (in the range of the minimal inhibitory concentration (MIC)), but also far higher (up to 16,000-fold increase compared to planktonic cells) than generally believed. This extremely broad distribution of biofilm-induced tolerance phenotypes across the clinical isolates was greatly influenced by the choice of the antibiotic. We furthermore describe cross-tolerance against ciprofloxacin and tobramycin, but not colistin, and observed an additive activity between biofilm-induced tolerance and genetically determined resistance. This became less evident when the biofilm-grown cells were exposed to very high antibiotic concentrations. Although much more remains to be learned on the molecular mechanisms underlying biofilm-induced tolerance, our data on intra-species variations in tolerance profiles provide valuable new insights. Furthermore, our observation that colistin appears to act independently of the tolerance mechanisms of individual clinical

strains could make colistin a valuable therapeutic option in chronic biofilm-associated infections characterized by the presence of particularly tolerant strains.

Keywords: conditional tolerance, biofilms, *Pseudomonas aeruginosa*, biofilm-associated chronic infections, clinical isolates, antimicrobial susceptibility testing (AST), biofilm-induced tolerance, antibiotic treatment

INTRODUCTION

Frequent use of antibiotics favors bacterial strains that have acquired mechanisms to overcome drug inhibition and lethality. Various genetically inherited mechanisms have been identified in bacteria that reduce the efficacy of a drug. These include, for example, mutations of the target structures, enzymatic inactivation of the antibiotic, or the reduction of its intracellular concentrations through reduced influx and/or increased efflux. The phenotypic consequences of genetically conferred resistance are usually monitored by the use of standard antimicrobial susceptibility testing (AST), which largely relies on the determination of the minimal inhibitory concentration (MIC) values of the antibiotic. While the assessment of MICs has a significant impact on the choice of a therapeutic strategy, it has been argued that the predictive power of MIC measurements is less suitable for the implementation of successful treatment regimens in patients with chronic, biofilm-associated infections (Smith et al., 2003). The ability of bacteria to survive a transient exposure of high antibiotic concentrations in a non-specific way, for example when the bacteria temporarily stop growing, is commonly described as tolerance and might be more relevant than inherited drug resistance, when it comes to describing the inability of our currently used drugs to combat biofilm-associated infections.

The biofilm mode of growth enables bacteria to evade the attacks from the immune system and to survive exposure to high concentrations of antimicrobial agents. It is commonly accepted that bacteria exhibit an up to 1,000-fold increased tolerance towards a broad range of different classes of antibiotics under biofilm- as opposed to planktonic growth conditions (conditional tolerance) (e.g. Costerton et al., 1987; Lewis, 2001; Lebeaux et al., 2014; Hall and Mah, 2017; Ciofu and Tolker-Nielsen, 2019). Of note, this does not seem to be true for all antibiotics when the tolerance profile of biofilm-grown cells is compared with that of planktonic cells from the stationary phase (Spoering and Lewis, 2001). However, despite the great attention and clinical importance, the reason for the recalcitrance of biofilm-grown bacteria is only incompletely understood and there is only a limited number of studies on the biofilm-induced tolerance profile of a larger panel of bacterial isolates (Ceri et al., 1999; Moskowitz et al., 2004; Müsken et al., 2017).

In this study, we investigated overall 352 clinical *Pseudomonas aeruginosa* isolates and determined their susceptibility profiles against the three commonly used antibiotics tobramycin, ciprofloxacin, and colistin under biofilm growth conditions. We describe an extremely broad distribution of conditional tolerance phenotypes across the various clinical isolates, which are dependent on the individual strain background and influenced by the choice of the antibiotic. We furthermore describe an additive activity between biofilm-induced tolerance and genetically determined resistance, which however becomes less apparent if the biofilm-grown cells are exposed to very high antibiotic concentrations.

METHODS

Strains, Media and Growth Conditions

For this study, we selected 352 well characterized clinical *P. aeruginosa* isolates, which have been previously collected across Europe (Hornischer et al., 2019). The strains have been isolated from diverse infection sites, including acute as well as chronic infections (**Electronic Supplementary Table ES1**). Minimal inhibitory concentrations (MIC) of all isolates are publicly available (Khaledi et al., 2020). Biofilm formation was assessed by confocal microscopy in the course of a previous study (Thöming et al., 2020). Bacteria were grown in standard rich medium culture conditions (lysogeny broth, LB) at 37°C. Overnight cultures were incubated with constant shaking (180 rpm); biofilms were grown statically without shaking.

Antimicrobial Susceptibility Testing Under Biofilm-Growth Conditions

We performed large-scale antimicrobial susceptibility testing of the clinical isolate collection for tobramycin, ciprofloxacin, and colistin under biofilm growth conditions as previously described (Müsken et al., 2010; Donnert et al., 2020). In brief, overnight cultures of clinical isolates were adjusted to an OD_{600} of 0.02 and 100 µl of the bacterial suspension were added to the wells of a sterile half-area, 96-well µClear microtiter plate (Greiner Bio-One). The plate was sealed with an air-permeable BREATHseal cover foil (Greiner Bio-One) and incubated without shaking at 37°C in humid atmosphere. After 24 h, 60 µl of antibiotic solution in diluted LB media were carefully added, resulting in a total volume of 160 µl per well. Antibiotic solutions were adjusted to final concentrations of 1; 4; 16; 64; 256; and 1,024 µg/ml. For the growth control, 60 µl diluted LB media (1:3 in deionized water) without antibiotics were added. The antibiotic exposed biofilms were incubated for 24 h and subsequently resuspended by the use of a multichannel pipette. Tenfold serial dilutions were spotted onto rectangular LB agar plates and incubated at 37°C. Growth was evaluated after 16 h of incubation and further monitored over a period of 48 h to ensure that all surviving bacteria were detected. Colony-forming units (CFU) per ml were calculated for surviving bacteria.

Determination of the Minimum Antibiotic Concentration of Killing (MCK) and the Biofilm Tolerance Factors

Antibiotic concentration-dependent killing of biofilm-grown cells was determined based on the reduction of CFUs following

the addition of different antibiotic concentrations as compared to an untreated control well. The number of surviving bacteria for each clinical isolate for overall six different concentrations of the three different antibiotics was recorded. From those data the minimum antibiotic concentrations of killing (MCK) that resulted in a CFU reduction of biofilm-grown cells of at least 1-log, 2-log, 3-log, 4-log, 5-log, 6-log or eradication (below the detection limit) could be deduced.

To quantify biofilm-induced tolerance of the individual isolates, the biofilm tolerance factor (BTF) was introduced. The BTF results from the ratio of the concentration that is required to achieve a certain log-CFU reduction in biofilm-grown cells, and the respective MIC of the strain:

$$\mathrm{BTF} = \frac{\mathrm{MCK\ (CFU\ log-reduction)}}{\mathrm{MIC}}$$

BTF: Biofilm tolerance factor; MCK(CFU log-reduction): minimum antibiotic concentration of killing at which a certain log-reduction [1 log (BTF-1), 2 log (BTF-2), 3 log (BTF-3), 4 log (BTF-4), 5 log (BTF-5), or 6 log (BTF-6) units as well as eradication (BTF-E)] in the CFUs of biofilm-grown cells was observed; MIC: minimal inhibitory concentration

Correlation Analyses and Hierarchical Clustering Using Biofilm Tolerance Factors

An integrated analysis of biofilm tolerance factors (BTFs) for the three antibiotics tested was used to uncover cross-tolerance and characteristic patterns in the tolerance behavior of biofilm-grown cells. Only discrete BTFs were used, where the highest antibiotic concentration tested (1,024 μg/ml) resulted in a measurable reduction of CFUs. BTFs were log2-transformed prior to further analyses.

Correlation analyses were performed in order to access cross-tolerance. Correlation coefficients for log2-transformed BTFs for the different antibiotics were calculated pairwise using the Correlation analysis tool in Microsoft Excel. Simple linear regression was calculated and plotted in GraphPad Prism (v 8.3.0). A hierarchical clustering approach was performed using the web tool ClustVis (Metsalu and Vilo, 2015) to group clinical isolates (n = 352) into six clusters of strains with characteristic biofilm tolerance patterns. Log2-transformed BTFs for all three antibiotics and all possible log-reductions were used as input data resulting in a heatmap of 352 rows (clinical isolates) and 21 columns (BTFs). No scaling was applied to rows. Rows were clustered using Euclidian distance and Ward linkage.

RESULTS

Antimicrobial Susceptibility Testing of Planktonic and Biofilm-Grown Clinical *P. aeruginosa* Isolates

Antimicrobial susceptibility testing of planktonic as well as biofilm-grown bacterial cells was performed on a collection of overall 352 clinical *P. aeruginosa* strains isolated from various infection sites (**Electronic Supplementary Table ES1**). While the minimal inhibitory concentration (MIC) values of the planktonically grown cells have been determined in a previous study (Khaledi et al., 2020) and are publicly available (Hornischer et al., 2019), we recorded antimicrobial activities on biofilm-grown bacteria in this study. We restricted our analysis to the anti-biofilm activity of tobramycin (an aminoglycoside), ciprofloxacin (a fluoroquinolone), and colistin (a polymyxin), all of which are frequently used to treat chronic *P. aeruginosa* infections e.g. of the respiratory tract of cystic fibrosis patients (Banerjee and Stableforth, 2000). Based on their MIC values and according to the CLSI guidelines (Weinstein et al., 2021), the great majority of isolates included in this study was classified as susceptible to tobramycin (86 % of the 352 clinical isolates) and colistin (82 %), while 44 % of the strains were ciprofloxacin-susceptible (**Supplementary Figure 1**; **Supplementary Table 1**).

We found that the different clinical isolates exhibit a very wide distribution of susceptibility to the three antibiotics when grown under biofilm conditions, even when they exhibited similar antimicrobial susceptibility profiles (MIC values) under planktonic conditions. Some clinical *P. aeruginosa* isolates proved to be remarkably responsive towards antimicrobial killing and already low antibiotic concentrations resulted in a significant reduction of biofilm-grown cells (**Figure 1A**). However, other isolates were largely non-responsive and the numbers of surviving biofilm-grown cells decreased only at very high antibiotic concentrations (**Figure 1B**).

Figures 1C–E depict the killing efficiency of the three antibiotics (tobramycin, ciprofloxacin, and colistin) on all 352 biofilm-grown clinical isolates. The minimum antibiotic concentration of killing (MCK) at which the colony-forming units (CFUs) of biofilm-grown bacteria was reduced by 1-log, 2-log, 3-log, 4-log, 5-log and 6-log units compared to growth of the untreated control in the individual isolates, as well as eradicated below the detection limit, is depicted (**Figures 1C–E**; **Electronic Supplementary Table ES1**). In general, higher reductions in the CFUs of biofilm-grown cells required higher concentrations of the antibiotic. For tobramycin, a gradual increase in the median MCKs was observed, indicating that the killing efficiency increases proportionally with the antibiotic concentration (**Figure 1C**). In contrast, we observed a disproportional increase in the median MCKs for ciprofloxacin (**Figure 1D**). While ciprofloxacin seems to be quite potent to achieve low (2-log) reductions in biofilm-grown clinical isolates at low antibiotic concentrations, much higher concentrations had to be applied to achieve reductions of ≥ 3 logs across the isolates. The profile was different again with colistin. We observed that a concentration of 256 μg/ml was required to achieve a 2-log reduction in CFUs in the vast majority of biofilm-grown strains (**Figure 1E**). However, once this colistin concentration threshold (256 μg/ml) was reached, the eradication of biofilm-grown cells across the clinical isolates became largely concentration-independent (all-or-none phenomenon).

Of note, several clinical isolates showed a remarkable biofilm recalcitrance, particularly towards tobramycin and ciprofloxacin. Even the highest concentration applied in this screening (1,024

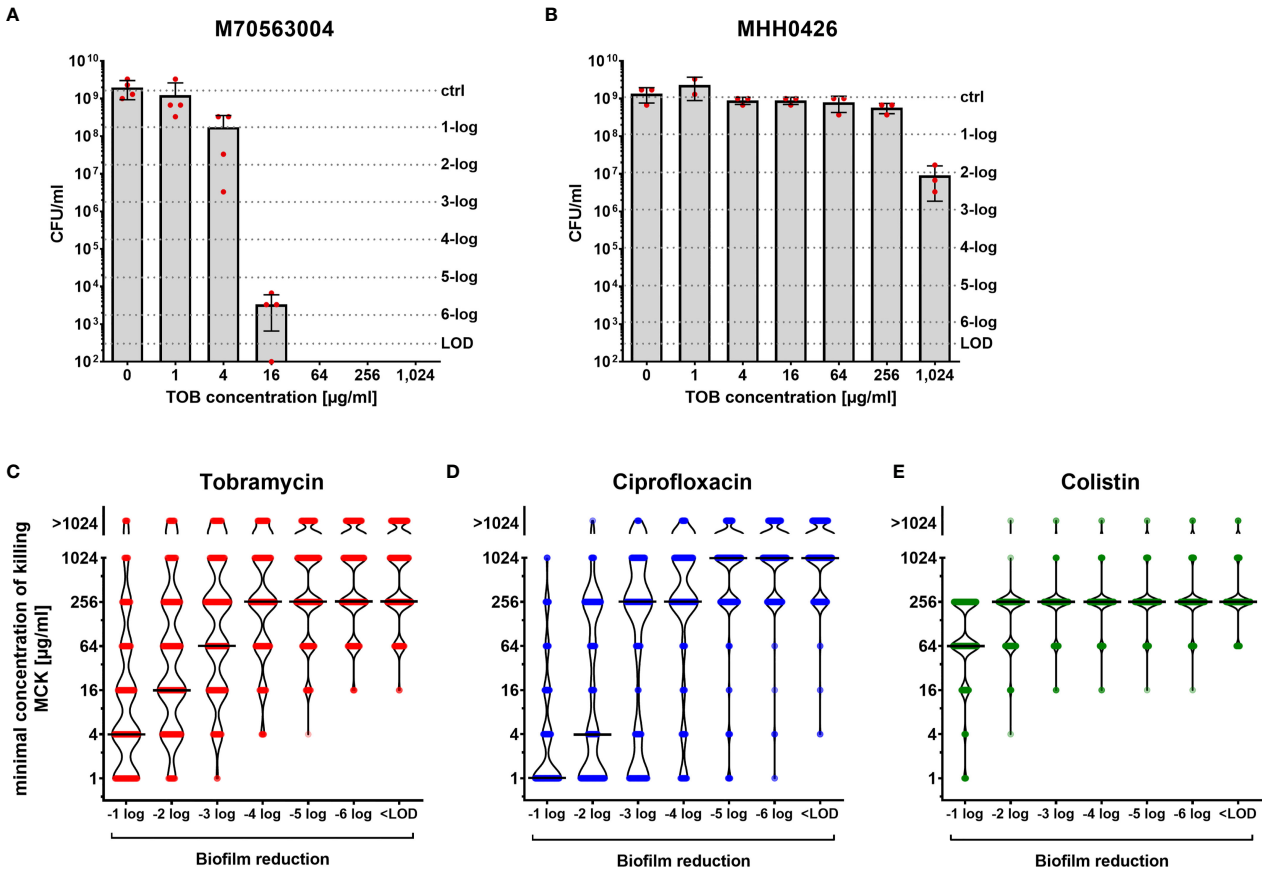

FIGURE 1 | Concentration-dependent killing of biofilm-grown clinical *P. aeruginosa* isolate cells. Isolate-specific killing profiles are exemplarily shown for two tobramycin susceptible clinical isolates, which exhibit the same minimal inhibitory concentration (MIC) value (MIC = 1 µg/ml). M70563004 biofilm-grown cells are responsive to tobramycin treatment **(A)**, whereas MHH0426 biofilm-grown cells are far less responsive **(B)**. Mean and standard deviations of the CFU/ml following the antibiotic treatment of biofilm-grown cells at the indicated tobramycin concentrations for 24 h are depicted. Results of the individual independent experiments are indicated by red dots (n = 4 for M70563004; n = 3 for MHH0426). The antibiotic concentration (minimal concentration of killing, MCK) that was required to lead to a 1-log, 2-log, 3-log, 4-log, 5-log, and 6-log unit reduction (dashed lines) in colony forming units (CFU) as compared to the untreated growth control can be deduced. The violin plots **(C–E)** depict the minimal concentrations of killing (MCK) to achieve a 1-log, 2-log, 3-log, 4-log, 5-log, 6-log unit reduction in colony forming units (CFU), and eradication below the limit of detection (< LOD), respectively for all 352 clinical isolates. Black lines indicate the median MCKs of tobramycin **(C)**, ciprofloxacin **(D)** and colistin **(E)**. Each dot represents one clinical isolate. TOB, tobramycin; CIP, ciprofloxacin; COL, colistin; LOD, limit of detection.

µg/ml of the antibiotic) was not sufficient to reduce the CFUs of biofilm-grown cells (**Figures 1C–E**).

Strains With Higher Ciprofloxacin and Tobramycin MICs Require Higher Antimicrobial Concentrations to Reduce the CFUs of Biofilm-Grown Cells

Our biofilm susceptibility screening has shown that the higher the antibiotic concentrations, the more pronounced are the CFU reductions across the biofilm-grown clinical isolates. However, we also observed that the minimum concentrations of killing (MCK) required for a certain reduction in CFUs were very different across the individual clinical strains. To evaluate whether killing efficiency is dependent on the underlying MIC, we sorted the 352 clinical strains according to their MIC values and depicted the MCKs for those clinical strains that exhibited a MIC around the CLSI breakpoints (**Figure 2**). For the vast majority of clinical isolates, we recorded MCKs far above their MICs, confirming the generally higher recalcitrance of biofilm-grown cells as compared to their planktonic counterparts (**Figure 2**; **Supplementary Figure 2**). Interestingly, in general – despite the very broad distribution of MCKs even in clinical isolates exhibiting the same MIC – the median MCK99.99 (antibiotic concentrations required for a 4-log CFU reduction, **Figures 2A, B**) and the median MCK99 (required for a 2-log reduction, **Supplementary Figures 2A, B**) gradually increased in clinical isolates that exhibited increased MICs for tobramycin and ciprofloxacin. Thus, the proportion of strains that did not respond to the highest concentration used in this screening (1,024 µg/ml tobramycin or ciprofloxacin) was highest among resistant strains (**Supplementary Figures 2D, E**), while strains responsive to low concentrations of antibiotics under biofilm growth conditions, were almost exclusively found among strains exhibiting low MIC values. As opposed to ciprofloxacin and

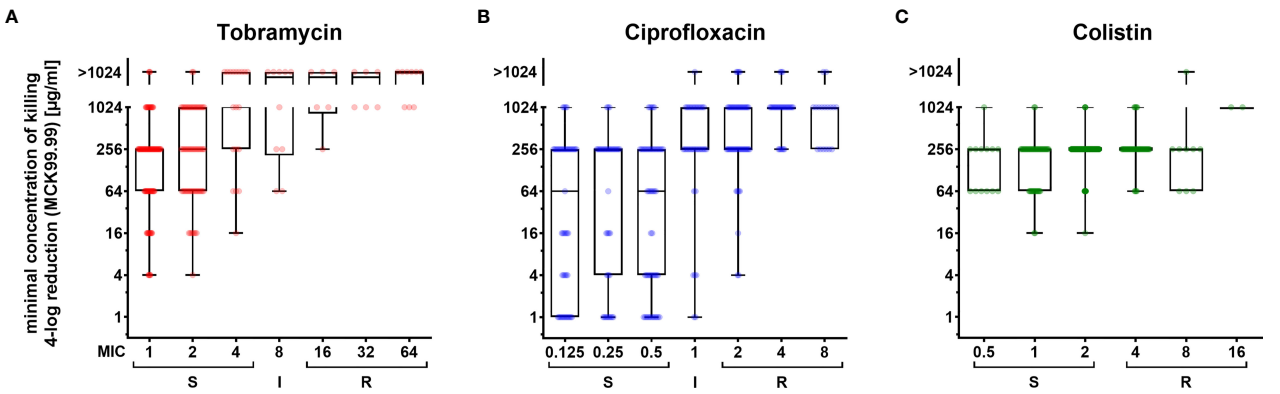

FIGURE 2 | Concentration-dependent killing of biofilm-grown clinical *P. aeruginosa* isolate cells exhibiting different resistance levels. Minimum concentrations of killing (MCK) for tobramycin **(A)**, ciprofloxacin **(B)** and colistin **(C)** that are required to reduce biofilm-grown cells by 99.99 % (4-log reduction of CFU; MCK99.99) are depicted in box-plots for clinical isolates, which were categorized into sub-groups exhibiting the same MIC values (x-axis). Boxplot elements are: center line – median; box limits – upper and lower quartiles; whiskers – minimum and maximum. Each dot represents one clinical isolate. S, susceptible; I, intermediate; R, resistant. Strains were categorized according to breakpoints defined by CLSI guidelines.

tobramycin, colistin-mediated killing of biofilm-grown cells was found to act independently of the MIC of the respective individual strains. The MCK99, MCK99.99 and the 6-log kill rate were stable (256 µg/ml) for most of the strains despite differing MICs (**Figure 2C**; **Supplementary Figures 2C, F**).

Biofilm-Induced Tolerance Versus Antimicrobial Resistance in the Individual Clinical Isolates

It is commonly claimed that biofilm-grown bacteria exhibit an up to 1,000-fold increased tolerance towards antibiotics as compared to their planktonically grown counterparts. In order to provide a better data basis, we determined the biofilm tolerance factor (BTF) of the clinical isolates against the three tested antibiotics. The BTF indicates which multiple of antibiotic concentration under biofilm-growth conditions as compared to the MIC (determined under planktonic growth conditions) must be used to achieve a CFU reduction of at least 1 log (BTF-1), 2 log (BTF-2), 3 log (BTF-3), 4 log (BTF-4), 5 log (BTF-5), 6 log (BTF-6) units or to observe eradication (BTF-E) below the detection limit (**Electronic Supplementary Table ES1**). Histograms of the BTFs of the individual clinical isolates are shown in **Figure 3**. Of note, BTFs could only be determined for strains for which a concentration of 1,024 µg/ml was sufficient to reach the respective log-reduction in the CFUs of biofilm-grown cells (**Supplementary Table 1**).

We found that for 1-log CFU reductions the median biofilm tolerance factor (BTF-1) across the clinical isolates was 4 for tobramycin, 2 for ciprofloxacin and 32 for colistin. This factor shifted to a median BTF-E (biofilm tolerance factor for eradication) of 256 for tobramycin, and 1,024 for ciprofloxacin, while it reached the maximum of 128 for colistin already at BTF-2 (**Figure 3**). Thus, depending on the antibiotic, this factor varies substantially, and is additionally greatly influenced by the *P. aeruginosa* strain background. We identified a small number of *P. aeruginosa* isolates, in which an antibiotic concentration around the MIC (of ciprofloxacin and less frequently tobramycin) was sufficient to achieve a 2-log (99 %) CFU reduction of biofilm-grown bacteria (**Figures 3A, H**). However, there were also isolates for which antibiotic concentrations of > 4,000 times the MIC for tobramycin or > 16,000 times the MIC for ciprofloxacin, were required to achieve a 2-log reduction in CFUs of biofilm-grown bacteria.

Our data also illustrate that the distribution of the BTFs among the clinical isolates was different in the three antibiotics tested. The fraction of clinical isolates that were effectively reduced by 2-log already at a low BTF was highest for ciprofloxacin. However, the proportion of isolates that required a high BTF to achieve a substantial reduction in the CFU of biofilm-grown bacteria was also highest for ciprofloxacin (**Figures 3H–N**). The opposite was found for colistin. Most clinical isolates required already a high BTF to achieve even a 2-log CFU reduction (**Figure 3P**). However, on the other end of the scale more clinical isolates were eradicated with overall only slightly higher colistin BTFs (**Figure 3U**). It seems that once a certain colistin killing concentration is reached, this concentration seems to efficiently eradicate biofilm-grown cells in a concentration-independent manner and independent on the resistance background within the clinical isolate.

Cross-Tolerance of the Clinical Isolates Against Ciprofloxacin and Tobramycin

In order to determine whether there is cross-tolerance in individual clinical biofilm-grown isolates towards the activity of the three antibiotics, we performed correlation analyses. While we found there was no correlation between colistin BTFs and those of ciprofloxacin or tobramycin, there was a positive correlation (correlation coefficient of 0.4148) between the killing efficiency of ciprofloxacin and tobramycin (reduction of 99.99 % of the biofilm-grown cells (BTF-4), **Figure 4**). We observed a similar trend for smaller (BTF-2) and larger log-CFU reductions (BTF-6) (**Supplementary Figure 3**).

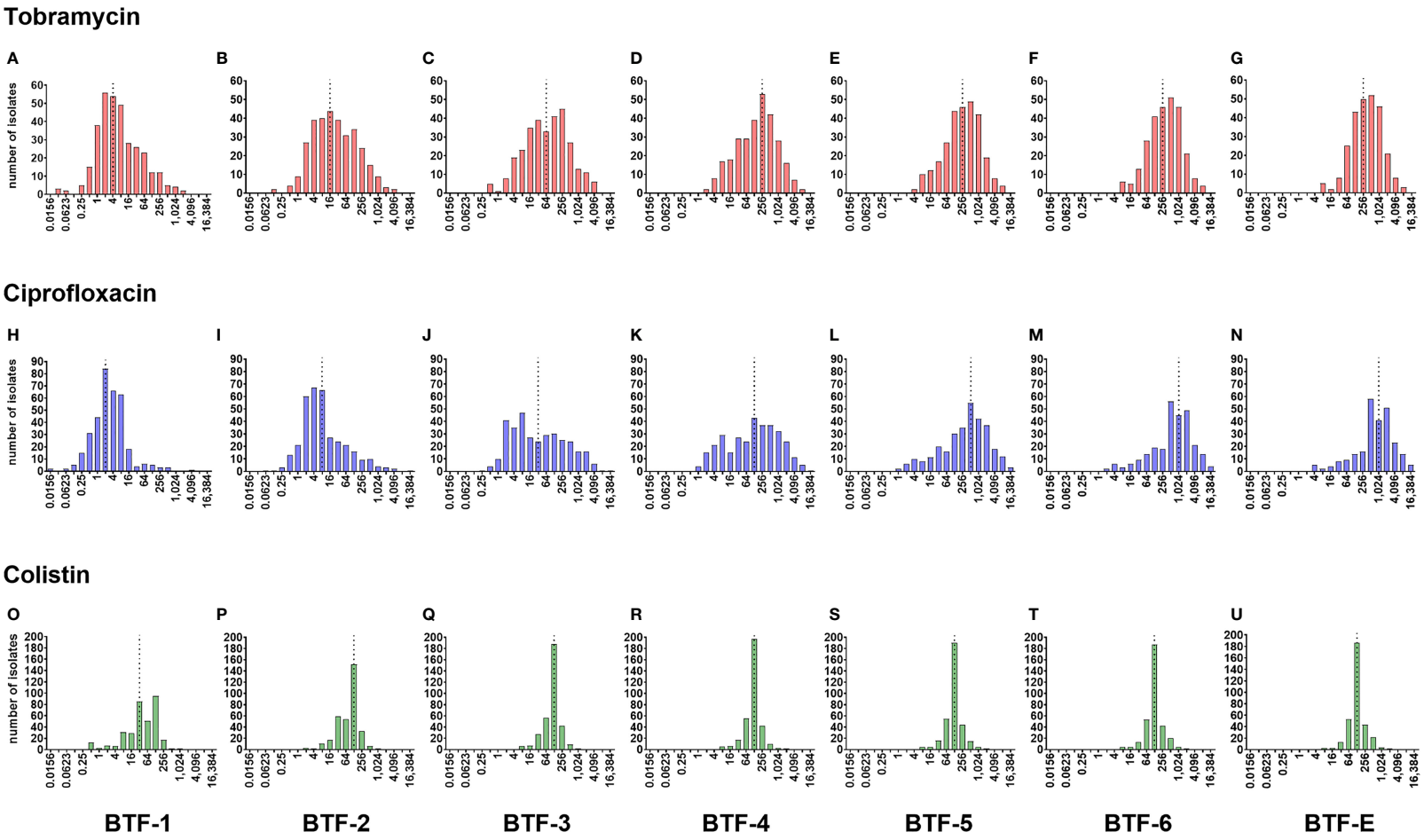

FIGURE 3 | Histograms of the biofilm tolerance factors (BTFs) of the individual clinical isolates. Distributions of biofilm tolerance factors (BTF) by which the minimal inhibitory concentration (MIC) has to be multiplied to achieve a reduction in the CFUs of the individual biofilm-grown clinical isolates by 1-log (BTF-1), 2-log (BTF-2), 3-log (BTF-3), 4-log (BTF-4), 5-log (BTF-5), 6-log (BTF-6) reduction and eradication below the detection limit (BTF-E), respectively, are shown for tobramycin **(A–G)**, ciprofloxacin **(H–N)**, and colistin **(O–U)**. Tested clinical isolates: n = 352. BTF = MCK/MIC. Graphs only include strains with discrete BTF, where the highest antibiotic concentration tested (1,024 μg/ml) resulted in the indicated reduction of biofilm CFU. Median biofilm tolerance factors are indicated by a dashed line.

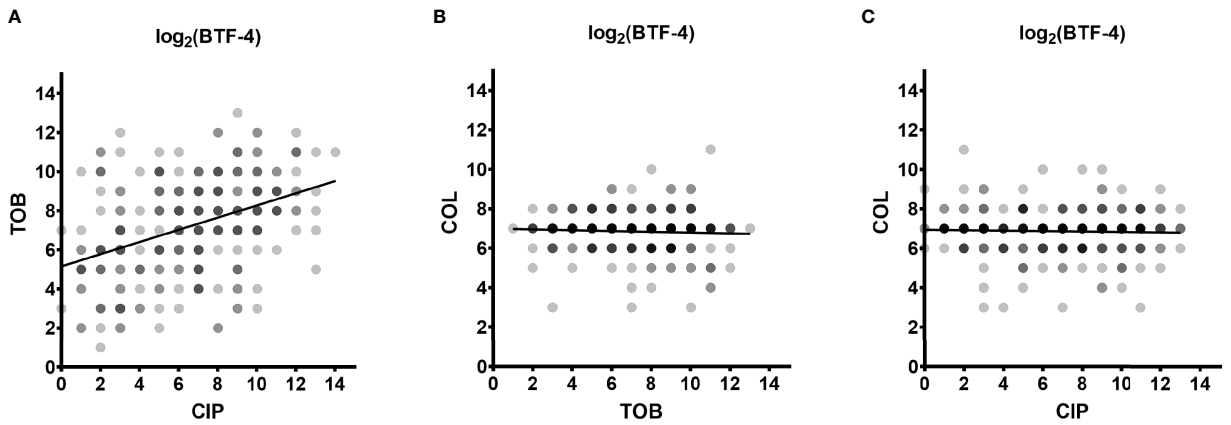

FIGURE 4 | Cross-tolerance of biofilm-grown cells. The dependence between the log2-transformed BTF-4 of the three antibiotics on all clinical isolates is depicted. The correlation coefficient between the BTF-4 of tobramycin (TOB) and ciprofloxacin (CIP) was 0.4148 **(A)**. No correlation was observed between the BTF-4 of colistin (COL) and TOB **(B)** or CIP **(C)**. BTF-4 - minimum antibiotic concentration killing 99.99 % of the biofilm-grown cells (MCK99.99; 4-log reduction) divided by the minimal inhibitory concentration (MIC) of the individual isolate. Dots represent the log2-transformed BTF-4 of the individual clinical isolates. Darker shades indicate overlapping datapoints.

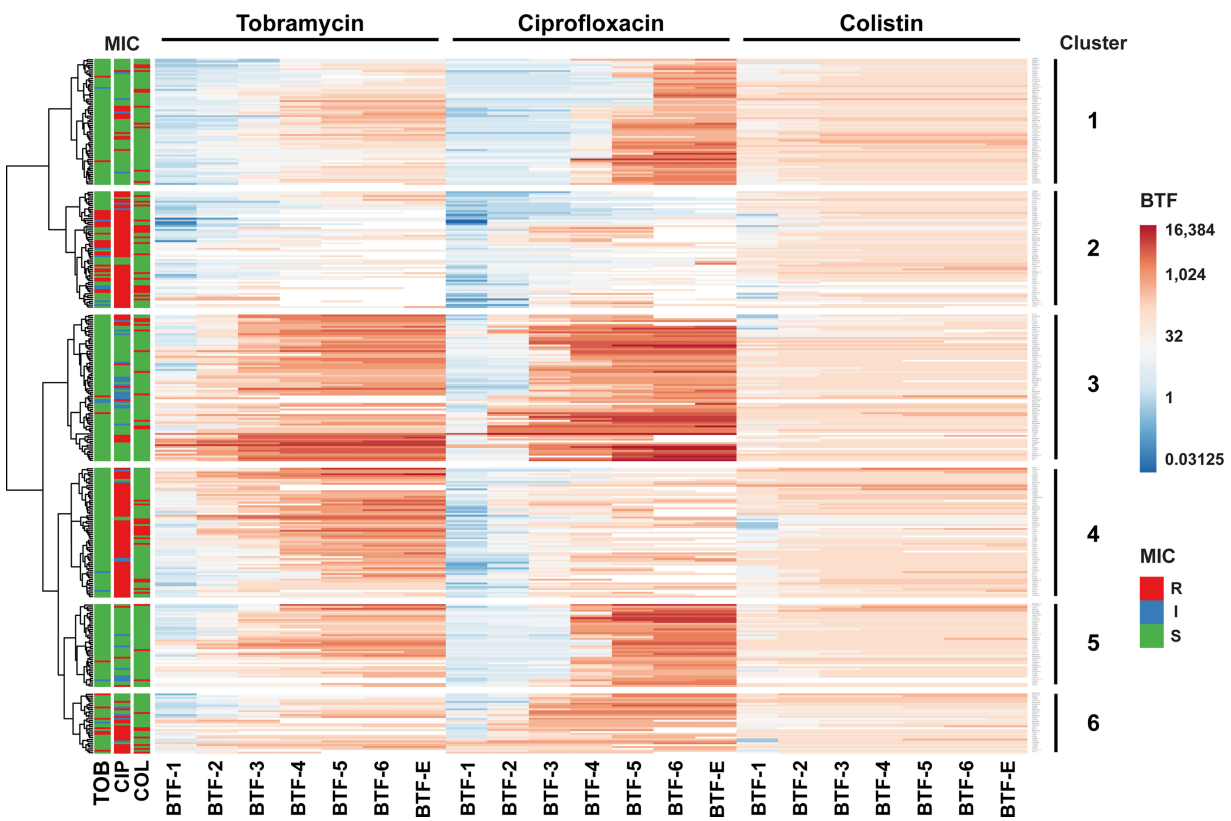

FIGURE 5 | Hierarchical clustering of biofilm tolerance factors. The 352 clinical isolates were clustered based on their biofilm tolerance factors for all three antibiotics. The result of the hierarchical clustering calculation is displayed in a heat map and uncovers six groups of strains (indicated on the right) that exhibit similar tolerance patterns. Hierarchical clustering was based on log2-transformed BTFs, using Euclidian distance and Ward linkage in ClustVis (Metsalu and Vilo, 2015). Only discrete BTFs are shown, where the highest antibiotic concentration tested (1,024 µg/ml) resulted in a measurable reduction of CFUs. The MIC-based susceptibility profiles of clinical isolates (according to CLSI breakpoints) are displayed on the left. R, resistant (marked in red); I, intermediate (blue); S, susceptible (green).

The Higher the Ciprofloxacin and Tobramycin MIC Values, the Lower the BTFs

In order to characterize the conditional tolerance phenotype of the individual clinical isolates in more detail, we integrated all data on the BTFs of the three antibiotics and performed a hierarchical cluster analysis across all clinical isolates. We identified six clusters of clinical strains with characteristic patterns in their biofilm tolerance factors (**Figure 5**; **Electronic Supplementary Table ES1**). Clinical isolates in cluster 2 and in cluster 4 generally exhibited lower ciprofloxacin BTFs, whereas isolates in cluster 2 exhibited additionally lower tobramycin BTFs. Interestingly, a majority of strains assigned to cluster 4 exhibited elevated ciprofloxacin MICs, whereas the isolates in cluster 2 exhibited elevated ciprofloxacin as well as tobramycin MICs. This result shows that strains that have inherited genetically encoded resistance mechanisms to tobramycin and/or ciprofloxacin show an increase in overall tolerance under biofilm-growth conditions that is less pronounced compared to the increase in tolerance observed in clinical strains with low MIC values.

DISCUSSION

In order to get a full picture of biofilm-growth mediated tolerance phenotypes in the opportunistic pathogen *P. aeruginosa*, we investigated the efficiency of three different classes of antibiotics to kill biofilm-grown cells in a large collection of diverse clinical isolates (n = 352). Those have been isolated from various infection sites and from acute and chronic infections. As opposed to previous studies, which had introduced the minimum duration of killing (MDK) as a quantitative indicator for tolerance of planktonic cultures in time-resolved killing experiments (Brauner et al., 2016), we determined the minimum antibiotic concentration of killing (MCK) as a quantitative measure of biofilm-induced tolerance in concentration-dependent killing experiments. Typically, MDK99 values (time to kill 99 % of the bacterial cells) are used to describe tolerance on a population level. Here, we recorded the MCK99 value (antibiotic concentration required to kill 99 % of the bacterial cells) and additionally the MCK90, MCK99.9, MCK99.99, MCK99.999, MCK99.9999 as well as the MCK that is required to eradicate biofilm-grown cells (below the detection limit).

Our data showed first of all, that the MCKs were impacted to a very large extent by the individual strain background. We found very susceptible clinical isolates that were killed by a comparatively low antibiotic concentration under biofilm-growth conditions, while other strains were only effectively killed after exposure to very high antibiotic concentrations. For some strains, up to 8,000 times the MIC for tobramycin and up to 16,000 times the MIC for ciprofloxacin were required in order to kill 99.99 % of the biofilm-grown cells. Interestingly, this inter-strain variation of the MCKs was very much dependent on the antibiotic. The highest variation of the MCKs among the individual clinical isolates was observed for ciprofloxacin. While a ciprofloxacin concentration of 4 μg/ml or less killed 99 % of the biofilm cells in more than half of the tested isolates (54 %), a concentration of 256 μg/ml or more was required to achieve the same biofilm killing in 31 % of the isolates.

Variation in tobramycin MCKs was lower, while the clinical isolates responded most consistently to colistin. The great majority of the clinical isolates (90 %) were eradicated at a colistin concentration of 256 μg/ml. While this concentration was required to kill at least 90 % of the biofilm-grown bacterial population, the same colistin concentration was also sufficient to eradicate the biofilm-grown cells to levels below the detection limit.

Our observation of a broad distribution of the MCK values across the clinical isolates is remarkable and suggests that while the biofilm growth mode in itself is sufficient to explain tolerance in clinical isolates, the respective tolerance levels seem to be largely modulated by the individual strain background. Interestingly, biofilm-induced tolerance against ciprofloxacin and tobramycin, but not colistin, were correlated in the individual clinical isolates. This result underlines that the conditional tolerance phenotype seems to be non-specific and is determined both, by the biofilm growth pattern and by additional isolate-specific, tolerance-promoting mechanisms that help bacteria survive transient exposure to high antibiotic concentrations. Despite extensive research on the identification of bacterial factors that determine tolerance-promoting phenotypes, we are only at the beginning to understand the molecular mechanisms that drive bacterial tolerance. It seems that changes in the activity of the tricarboxylic acid (TCA) cycle, cellular respiration, the proton motive force as well as shifts in the intracellular pH drive bacterial tolerance phenotypes (Allison et al., 2011; Meylan et al., 2017; Crabbé et al., 2019; Donnert et al., 2020; Zheng et al., 2020; Arce-Rodríguez et al., 2022). Furthermore, it is conceivable that additional factors contribute to biofilm tolerance phenotypes, such as restricted penetration of the antibiotic through the biofilm matrix, a biofilm-specific expression of resistance genes, or the presence of a sub-population of dormant persister cells (Stewart, 1996; Hentzer et al., 2001; Lewis, 2001; Pamp et al., 2008; Zhang and Mah, 2008; Chiang et al., 2013; Hall and Mah, 2017).

Despite the large variability in the MCKs, our extensive data on many clinical isolates allowed the detection of a positive correlation between the MIC values of the individual isolates and the concentration of antibiotics (MCK) that was required to kill biofilm-grown cells. These results suggest that genetically inherited resistance mechanisms affect the biofilm-induced tolerance phenotype. In general, strains found to be resistant as categorized by elevated MIC levels also required high concentrations of antibiotics to achieve biofilm reduction of 4-logs or more. A synergistic interaction between tolerance and resistance has been described previously (Levin-Reisman et al., 2019) and it has been speculated that genetically inherited resistance factors might be more effective in slow growing cells, and thus might act synergistically with tolerance to protect biofilm-grown cells.

Strikingly, at the same time we observed that the strains exhibiting high MIC values seemed to express lower biofilm-specific tolerance factors (BTFs) as defined by the multiple of the MIC concentration required to kill the biofilm-grown population. Thus, it seems that once a certain threshold concentration of an

antibiotic is reached, biofilm-grown bacteria are efficiently killed, independent on their individual genetically determined resistance profile. A recent study demonstrated that antibiotic exposed strains developed either high-level multidrug tolerance or antibiotic resistance, but not both (Santi et al., 2021). It could be argued that once high-level tolerance is reached, additional genetically determined resistance mechanisms do not add further to survival.

It has already been shown several times that antibiotic susceptibility profiles of biofilm-grown cells cannot be predicted on the basis of MIC profiles. Thus MIC determinations cannot serve as an approximation on which is the best therapy to apply to treat patients suffering from chronic biofilm-associated diseases (Moskowitz et al., 2004; Keays et al., 2009; Waters and Ratjen, 2015; Brady et al., 2017; Müsken et al., 2017; Coenye et al., 2018). However, our study also revealed that leveraging drug-specific properties might have great potential to optimize future treatments of biofilm-associated infections. If a certain threshold concentration of colistin can be reached in e.g. the respiratory tract of CF patients, then not only the great majority of the clinical isolates, independent on their individual strain background, might be efficiently killed, but this killing also becomes concentration independent. It appears that colistin overcomes the conditional tolerance mechanisms of the individual clinical strains, and thus, as suggested before (Pamp et al., 2008; Elborn et al., 2009; Kolpen et al., 2016), it might be a valuable therapeutic option for chronic biofilm-associated infections characterized by the presence of particularly tolerant strains.

DATA AVAILABILITY STATEMENT

The original contributions presented in the study are included in the article/**Supplementary Material**. Further inquiries can be directed to the corresponding author.

AUTHOR CONTRIBUTIONS

JT, conception and design, acquisition and curation of the data, analysis and interpretation of the data, drafting and revising the manuscript. SH, conception and design, analysis and interpretation of the data, drafting and revising the manuscript, funding acquisition. All authors have read and agreed to the published version of the manuscript.

FUNDING

SH was funded by the European Union (EU, ERC Consolidator Grant COMBAT 724290) and received funding as part of the excellence cluster RESIST (Resolving Infection Susceptibility; EXC 2155). Furthermore, SH received funding from the German Research Foundation (DFG SPP 1879) and the Novo Nordisk Foundation (NNF 18OC0033946).

ACKNOWLEDGMENTS

We acknowledge Dr. Mathias Müsken for valuable contributions and fruitful discussions, and gratefully thank Maximilian Kink and Carolina Arévalo Schüring for support with the biofilm tolerance screening.

SUPPLEMENTARY MATERIAL

The Supplementary Material for this article can be found online at: https://www.frontiersin.org/articles/10.3389/fcimb.2022.851784/full#supplementary-material

REFERENCES

Allison, K. R., Brynildsen, M. P., and Collins, J. J. (2011). Metabolite-Enabled Eradication of Bacterial Persisters by Aminoglycosides. *Nature* 473, 216–220. doi: 10.1038/nature10069

Arce-Rodríguez, A., Pankratz, D., Preusse, M., Nikel, P. I., and Häussler, S. (2022). Dual Effect: High NADH Levels Contribute to Efflux-Mediated Antibiotic Resistance But Drive Lethality Mediated by Reactive Oxygen Species. *MBio* 13, e02434-21. doi: 10.1128/mbio.02434-21

Banerjee, D., and Stableforth, D. (2000). The Treatment of Respiratory *Pseudomonas* Infection in Cystic Fibrosis. *Drugs* 60, 1053–1064. doi: 10.2165/00003495-200060050-00006

Brady, A. J., Laverty, G., Gilpin, D. F., Kearney, P., and Tunney, M. (2017). Antibiotic Susceptibility of Planktonic- and Biofilm-Grown Staphylococci Isolated From Implant-Associated Infections: Should MBEC and Nature of Biofilm Formation Replace MIC? *J. Med. Microbiol.* 66, 461–469. doi: 10.1099/jmm.0.000466

Brauner, A., Fridman, O., Gefen, O., and Balaban, N. Q. (2016). Distinguishing Between Resistance, Tolerance and Persistence to Antibiotic Treatment. *Nat. Rev. Microbiol.* 14, 320–330. doi: 10.1038/nrmicro.2016.34

Ceri, H., Olson, M. E., Stremick, C., Read, R. R., Morck, D., and Buret, A. (1999). The Calgary Biofilm Device: New Technology for Rapid Determination of Antibiotic Susceptibilities of Bacterial Biofilms. *J. Clin. Microbiol.* 37, 1771–1776. doi: 10.1128/JCM.37.6.1771-1776.1999

Chiang, W.-C., Nilsson, M., Jensen, P.Ø., Høiby, N., Nielsen, T. E., Givskov, M., et al. (2013). Extracellular DNA Shields Against Aminoglycosides in *Pseudomonas Aeruginosa* Biofilms. *Antimicrob. Agents Chemother.* 57, 2352–2361. doi: 10.1128/AAC.00001-13

Ciofu, O., and Tolker-Nielsen, T. (2019). Tolerance and Resistance of Pseudomonas Aeruginosa Biofilms to Antimicrobial Agents—How *P. Aeruginosa* Can Escape Antibiotics. *Front. Microbiol.* 10, 913. doi: 10.3389/fmicb.2019.00913

Coenye, T., Goeres, D., Van Bambeke, F., and Bjarnsholt, T. (2018). Should Standardized Susceptibility Testing for Microbial Biofilms be Introduced in Clinical Practice? *Clin. Microbiol. Infect.* 24, 570–572. doi: 10.1016/J.CMI.2018.01.003

Costerton, J. W., Cheng, K. J., Geesey, G. G., Ladd, T. I., Nickel, J. C., Dasgupta, M., et al. (1987). Bacterial Biofilms in Nature and Disease. *Annu. Rev. Microbiol.* 41, 435–464. doi: 10.1146/annurev.mi.41.100187.002251

Crabbé, A., Ostyn, L., Staelens, S., Rigauts, C., Risseeuw, M., Dhaenens, M., et al. (2019). Host Metabolites Stimulate the Bacterial Proton Motive Force to Enhance the Activity of Aminoglycoside Antibiotics. *PloS Pathog.* 15, e1007697. doi: 10.1371/journal.ppat.1007697

Donnert, M., Elsheikh, S., Arce-Rodriguez, A., Pawar, V., Braubach, P., Jonigk, D., et al. (2020). Targeting Bioenergetics is Key to Counteracting the Drug-Tolerant State of Biofilm-Grown Bacteria. *PloS Pathog.* 16, e1009126. doi: 10.1371/journal.ppat.1009126

Elborn, J. S., Hodson, M., and Bertram, C. (2009). Implementation of European Standards of Care for Cystic Fibrosis - Control and Treatment of Infection. *J. Cyst. Fibros.* 8, 211–217. doi: 10.1016/j.jcf.2009.03.001

Hall, C. W., and Mah, T.-F. (2017). Molecular Mechanisms of Biofilm-Based Antibiotic Resistance and Tolerance in Pathogenic Bacteria. *FEMS Microbiol. Rev.* 41, 276–301. doi: 10.1093/femsre/fux010

Hentzer, M., Teitzel, G. M., Balzer, G. J., Heydorn, A., Molin, S., Givskov, M., et al. (2001). Alginate Overproduction Affects *Pseudomonas Aeruginosa* Biofilm Structure and Function. *J. Bacteriol.* 183, 5395–5401. doi: 10.1128/JB.183.18.5395-5401.2001

Hornischer, K., Khaledi, A., Pohl, S., Schniederjans, M., Pezoldt, L., Casilag, F., et al. (2019). BACTOME—A Reference Database to Explore the Sequence- and Gene Expression-Variation Landscape of Pseudomonas Aeruginosa Clinical Isolates. *Nucleic Acids Res.* 47, D716–D720. doi: 10.1093/nar/gky895

Keays, T., Ferris, W., Vandemheen, K. L., Chan, F., Yeung, S.-W., Mah, T.-F., et al. (2009). A Retrospective Analysis of Biofilm Antibiotic Susceptibility Testing: A Better Predictor of Clinical Response in Cystic Fibrosis Exacerbations. *J. Cyst. Fibros.* 8, 122–127. doi: 10.1016/J.JCF.2008.10.005

Khaledi, A., Weimann, A., Schniederjans, M., Asgari, E., Kuo, T., Oliver, A., et al. (2020). Predicting Antimicrobial Resistance in Pseudomonas Aeruginosa With Machine Learning-Enabled Molecular Diagnostics. *EMBO Mol. Med.* 12, e10264. doi: 10.15252/emmm.201910264

Kolpen, M., Appeldorff, C. F., Brandt, S., Mousavi, N., Kragh, K. N., Aydogan, S., et al. (2016). Increased Bactericidal Activity of Colistin on *Pseudomonas Aeruginosa* Biofilms in Anaerobic Conditions. *Pathog. Dis.* 74, ftv086. doi: 10.1093/femspd/ftv086

Lebeaux, D., Ghigo, J.-M., and Beloin, C. (2014). Biofilm-Related Infections: Bridging the Gap Between Clinical Management and Fundamental Aspects of Recalcitrance Toward Antibiotics. *Microbiol. Mol. Biol. Rev.* 78, 510–543. doi: 10.1128/MMBR.00013-14

Levin-Reisman, I., Brauner, A., Ronin, I., and Balaban, N. Q. (2019). Epistasis Between Antibiotic Tolerance, Persistence, and Resistance Mutations. *Proc. Natl. Acad. Sci. U. S. A.* 116, 14734–14739. doi: 10.1073/pnas.1906169116

Lewis, K. (2001). Riddle of Biofilm Resistance. *Antimicrob. Agents Chemother.* 45, 999–1007. doi: 10.1128/AAC.45.4.999-1007.2001

Metsalu, T., and Vilo, J. (2015). ClustVis: A Web Tool for Visualizing Clustering of Multivariate Data Using Principal Component Analysis and Heatmap. *Nucleic Acids Res.* 43, W566–W570. doi: 10.1093/nar/gkv468

Meylan, S., Porter, C. B. M., Yang, J. H., Belenky, P., Gutierrez, A., Lobritz, M. A., et al. (2017). Carbon Sources Tune Antibiotic Susceptibility in *Pseudomonas Aeruginosa via* Tricarboxylic Acid Cycle Control. *Cell Chem. Biol.* 24, 195–206. doi: 10.1016/J.CHEMBIOL.2016.12.015

Moskowitz, S. M., Foster, J. M., Emerson, J., and Burns, J. L. (2004). Clinically Feasible Biofilm Susceptibility Assay for Isolates of *Pseudomonas Aeruginosa* From Patients With Cystic Fibrosis. *J. Clin. Microbiol.* 42, 1915–1922. doi: 10.1128/JCM.42.5.1915-1922.2004

Müsken, M., Di Fiore, S., Römling, U., and Häussler, S. (2010). A 96-Well-Plate-Based Optical Method for the Quantitative and Qualitative Evaluation of *Pseudomonas Aeruginosa* Biofilm Formation and its Application to Susceptibility Testing. *Nat. Protoc.* 5, 1460–1469. doi: 10.1038/nprot.2010.110

Müsken, M., Klimmek, K., Sauer-Heilborn, A., Donnert, M., Sedlacek, L., Suerbaum, S., et al. (2017). Towards Individualized Diagnostics of Biofilm-Associated Infections: A Case Study. *NPJ Biofilms Microbiomes* 3, 22. doi: 10.1038/s41522-017-0030-5

Pamp, S. J., Gjermansen, M., Johansen, H. K., and Tolker-Nielsen, T. (2008). Tolerance to the Antimicrobial Peptide Colistin in *Pseudomonas Aeruginosa* Biofilms Is Linked to Metabolically Active Cells, and Depends on the Pmr and mexAB-oprM Genes. *Mol. Microbiol.* 68, 223–240. doi: 10.1111/j.1365-2958.2008.06152.x

Santi, I., Manfredi, P., Maffei, E., Egli, A., and Jenal, U. (2021). Evolution of Antibiotic Tolerance Shapes Resistance Development in Chronic *Pseudomonas Aeruginosa* Infections. *MBio* 12, 1–17. doi: 10.1128/mBio.03482-20

Smith, A. L., Fiel, S. B., Mayer-Hamblett, N., Ramsey, B., and Burns, J. L. (2003). Susceptibility Testing of *Pseudomonas Aeruginosa* Isolates and Clinical Response to Parenteral Antibiotic Administration. *Chest* 123, 1495–1502. doi: 10.1378/chest.123.5.1495

Spoering, A. L., and Lewis, K. (2001). Biofilms and Planktonic Cells of *Pseudomonas Aeruginosa* Have Similar Resistance to Killing by Antimicrobials. *J. Bacteriol.* 183, 6746–6751. doi: 10.1128/JB.183.23.6746-6751.2001

Stewart, P. S. (1996). Theoretical Aspects of Antibiotic Diffusion Into Microbial Biofilms. *Antimicrob. Agents Chemother.* 40, 2517–2522. doi: 10.1128/AAC.40.11.2517

Thöming, J. G., Tomasch, J., Preusse, M., Koska, M., Grahl, N., Pohl, S., et al. (2020). Parallel Evolutionary Paths to Produce More Than One *Pseudomonas Aeruginosa* Biofilm Phenotype. *NPJ Biofilms Microbiomes* 6, 1–13. doi: 10.1038/s41522-019-0113-6

Waters, V., and Ratjen, F. (2015). "Standard Versus Biofilm Antimicrobial Susceptibility Testing to Guide Antibiotic Therapy in Cystic Fibrosis", in *Cochrane Database of Systematic Reviews*. Ed. V. Waters (Chichester, UK: John Wiley & Sons, Ltd). doi: 10.1002/14651858.CD009528.pub3

Weinstein M, M. P., Lewis, J. S.II, P, Bobenchik, P, A. M., Campeau, P, S., Cullen, B, S. K., Galas, M. F., et al. (2021). *CLSI M100-ED31:2021 Performance Standards for Antimicrobial Susceptibility Testing*. Available at: http://em100.edaptivedocs.net/GetDoc.aspx?doc=CLSIM100ED31:2021&scope=user.

Zhang, L., and Mah, T.-F. (2008). Involvement of a Novel Efflux System in Biofilm-Specific Resistance to Antibiotics. *J. Bacteriol.* 190, 4447–4452. doi: 10.1128/JB.01655-07

Zheng, E. J., Stokes, J. M., and Collins, J. J. (2020). Eradicating Bacterial Persisters With Combinations of Strongly and Weakly Metabolism-Dependent Antibiotics. *Cell Chem. Biol.* 27, 1544–1552.e3. doi: 10.1016/j.chembiol.2020.08.015

Conflict of Interest: The authors declare that the research was conducted in the absence of any commercial or financial relationships that could be construed as a potential conflict of interest.

Publisher's Note: All claims expressed in this article are solely those of the authors and do not necessarily represent those of their affiliated organizations, or those of the publisher, the editors and the reviewers. Any product that may be evaluated in this article, or claim that may be made by its manufacturer, is not guaranteed or endorsed by the publisher.

frontiers | Frontiers in Cellular and Infection Microbiology

ORIGINAL RESEARCH
published: 07 April 2022
doi: 10.3389/fcimb.2022.835754

Contribution of *Pseudomonas aeruginosa* Exopolysaccharides Pel and Psl to Wound Infections

Derek Fleming[1], *Brandon Niese*[2], *Whitni Redman*[1], *Emily Vanderpool*[1], *Vernita Gordon*[2,3] *and Kendra P. Rumbaugh*[1,4]*

[1] Department of Surgery, Texas Tech University Health Sciences, Lubbock, TX, United States, [2] Department of Physics, Center for Nonlinear Dynamics, The University of Texas at Austin, Austin TX, United States, [3] Interdisciplinary Life Sciences Graduate Programs, LaMontagne Center for Infectious Disease, The University of Texas at Austin, Austin, TX, United States, [4] Burn Center for Research Excellence, Texas Tech University Health Sciences, Lubbock, TX, United States

Biofilms are the cause of most chronic bacterial infections. Living within the biofilm matrix, which is made of extracellular substances, including polysaccharides, proteins, eDNA, lipids and other molecules, provides microorganisms protection from antimicrobials and the host immune response. Exopolysaccharides are major structural components of bacterial biofilms and are thought to be vital to numerous aspects of biofilm formation and persistence, including adherence to surfaces, coherence with other biofilm-associated cells, mechanical stability, protection against desiccation, binding of enzymes, and nutrient acquisition and storage, as well as protection against antimicrobials, host immune cells and molecules, and environmental stressors. However, the contribution of specific exopolysaccharide types to the pathogenesis of biofilm infection is not well understood. In this study we examined whether the absence of the two main exopolysaccharides produced by the biofilm former *Pseudomonas aeruginosa* would affect wound infection in a mouse model. Using *P. aeruginosa* mutants that do not produce the exopolysaccharides Pel and/or Psl we observed that the severity of wound infections was not grossly affected; both the bacterial load in the wounds and the wound closure rates were unchanged. However, the size and spatial distribution of biofilm aggregates in the wound tissue were significantly different when Pel and Psl were not produced, and the ability of the mutants to survive antibiotic treatment was also impaired. Taken together, our data suggest that while the production of Pel and Psl do not appear to affect *P. aeruginosa* pathogenesis in mouse wound infections, they may have an important implication for bacterial persistence *in vivo.*

Keywords: biofilm, *Pseudomonas aeruginosa*, wound infection, exopolysaccharides, aggregate, Pel, Psl

OPEN ACCESS

Edited by:
Lauren O. Bakaletz, Nationwide Children's Hospital, United States

Reviewed by:
Daniel Wozniak, The Ohio State University, United States
Laura K. Jennings, University of Montana, United States

***Correspondence:**
Kendra P. Rumbaugh
kendra.rumbaugh@ttuhsc.edu

Specialty section:
This article was submitted to Biofilms, a section of the journal Frontiers in Cellular and Infection Microbiology

Received: *14 December 2021*
Accepted: *01 March 2022*
Published: *07 April 2022*

Citation:
Fleming D, Niese B, Redman W, Vanderpool E, Gordon V and Rumbaugh KP (2022) Contribution of Pseudomonas aeruginosa Exopolysaccharides Pel and Psl to Wound Infections. Front. Cell. Infect. Microbiol. 12:835754. doi: 10.3389/fcimb.2022.835754

INTRODUCTION

Microbes in chronic infections most commonly exist as biofilms; communities of microorganisms dwelling within a matrix made of largely self-produced extracellular substances (EPS), including polysaccharides, proteins, eDNA, lipids and other molecules (Flemming and Wingender, 2010). In fact, biofilms have been estimated to be involved in 80% of all human bacterial infections, and 90%

of chronic wound infections (Attinger and Wolcott, 2012; Romling and Balsalobre, 2012). Living within the protection of the EPS matrix is thought to provide microorganisms greatly increased tolerances to antimicrobials and the host immune response (Rogers et al., 2010; Lewis, 2012). These tolerances arise from several mechanisms, including physical and chemical protection by the EPS matrix and reduced metabolic activity of many of the microorganisms in the biofilm. Lowering metabolic activity decreases susceptibility to the majority of antibiotics that target metabolically-active cells (Koo et al., 2017).

Given their prevalence in chronic infection, and the magnitude of their impact on human health, biofilms have been studied extensively over the past several decades. While many great strides have been made in understanding the pathophysiological mechanisms and genetics of biofilm formation and persistence, the vast majority of the work has been performed in artificial, *in vitro* environments with limited clinical relevance. Indeed, it has become clear that biofilm properties vary greatly between *in vitro* and *in vivo* settings, and even across differing infection sites and conditions *in vivo* (Bjarnsholt et al., 2013; Roberts et al., 2015; Ibberson et al., 2017; Redman et al., 2020). It is thus vital to investigate the properties of biofilms *in situ* to better understand their influence on infection. A proper understanding of how and when microbes form biofilms during infection and how these structures are composed is also needed to design new biofilm-targeting therapies.

For many microorganisms, biofilm formation varies considerably both temporally and from environment to environment (Stanley and Lazazzera; 2004, Karatan and Watnick, 2009; Yang et al., 2011; Redman et al., 2020). This is true for *Pseudomonas aeruginosa*, a biofilm-forming opportunistic pathogen that is involved in a wide range of infection types. One key way that *P. aeruginosa* can alter its EPS matrix composition is by differential expression of its three exopolysaccharides, Pel, Psl, and alginate (Ryder et al., 2007; Colvin et al., 2012; Rahman et al., 2021). Exopolysaccharides are major structural components of bacterial biofilms (Flemming and Wingender, 2010) and contribute to numerous aspects of biofilm formation and persistence, including adherence to surfaces, coherence with other biofilm cells, mechanical stability, protection against desiccation, binding of enzymes, nutrient acquisition and storage, and protection against antimicrobials, host immune cells and molecules, and environmental stressors (Flemming and Wingender, 2010). Pel is a cationic polysaccharide, containing acetylgalactosamine and acetylglucosamine sugars, that has been shown to aid in cell-cell adherence, surface attachment, DNA crosslinking, and protection against aminoglycosides (Colvin et al., 2011; Jennings et al., 2015a; Jennings et al., 2015b). Psl is a mannose, glucose, and rhamnose-rich polysaccharide that is also involved in cell-cell interactions and surface attachment (Irie et al; Ma et al., 2007; Byrd et al., 2009). Indeed, it has been suggested that Pel and Psl are structurally redundant, with successful *P. aeruginosa* strains often expressing one or the other, including the common laboratory strains PAO1 and PA14, which produce Psl-dominant and Pel-dominant biofilms respectively (Colvin et al., 2011). Alginate is a mucoid polysaccharide, composed of guluronic and mannuronic acid, that is strongly associated with *P. aeruginosa* lung infection isolates from cystic fibrosis (CF) patients (Franklin et al., 2011). Alginate is thought to aid in biofilm formation and immune evasion, but doesn't appear to play a significant role outside of the CF lung (Wozniak et al., 2003).

P. aeruginosa infection is highly prevalent in chronic wounds, estimated to be present in about 25% of all cases (Wolcott et al., 2016). However, since most *P. aeruginosa* biofilm studies have been performed *in vitro*, little is known about how different exopolysaccharides impact *P. aeruginosa* infection or the host response. In this study, we used a murine chronic wound model, and a selection of *P. aeruginosa* strains with different patterns of exopolysaccharide production, to examine the impact of differential polysaccharide composition on the size and spacing of bacterial aggregates, infection load, antibiotic susceptibility, and interaction with host cells.

Overall, we saw that the lack of Pel and Psl had little effect on the severity of wound infection, as bacterial loads in wounds and wound closure were unaffected. However, we saw significant differences in the spatial properties of *P. aeruginosa* aggregates in wound tissue when Pel and/or Psl were absent. Specifically, the absence of Pel and Psl resulted in much smaller aggregates spaced further apart. We also noted differences in the number of host cells surrounding these aggregates, which could have implications for an immune response. Importantly, the loss of both Pel and Psl affected the ability of *P. aeruginosa* to survive aminoglycoside treatment. These results are important to our understanding of how composition of the biofilm matrix can influence wound infection and bacterial persistence *in vivo*.

RESULTS

Neither the Deletion Nor Overproduction of Pel or Psl Affects Wound Infection in a Mouse Model

In theory, the ability to form robust biofilms should confer protection to bacteria from the host immune system during infection. While studies examining *in vivo* biofilm formation and biofilm/host interactions are few, there is some support that the ability to make a biofilm is a fitness attribute and potentially increases virulence *in vivo* (Pestrak et al., 2018). To examine the role of Pel and Psl in wound infections, we used the wild-type (WT) strain PAO1 and 4 mutants derived from PAO1 with deletions in different genes affecting exopolysaccharide production (Δ*pel*, Δ*psl*, Δ*pel*Δ*psl*, Δ*wspF*, **Table 1**).

The *wspF* gene encodes the regulatory protein of the diguanylate synthase, WspR (Hickman et al., 2005). It has previously been established that deletion of WspF results in the elevated production of the matrix protein CdrA and the pro-biofilm secondary messenger molecule, cyclic-di-GMP, resulting in a constitutive upregulation of Pel and Psl and biofilms with significantly more biomass (Hickman et al., 2005; Rybtke et al., 2012a). Thus we sought to determine if a Δ*wspF* mutant would cause a more virulent or persistent infection *in vivo*. We also sought to determine if the absence of Pel and/or Psl would affect *in vivo* fitness. To test this, mice were administered surgical excision wounds and infected with

TABLE 1 | Description of the *P. aeruginosa* strains used in this study.

Strain	Mutation	Impact of Mutation on EPS Exopolysaccharide Composition	Reference
PAO1	NA	Wild-type strain originally isolated from wound, capable of producing Psl, Pel and alginate	(Holloway, 1955)
PAO1Δ*pel*	*pelA*; polar mutant of the pel operon	Does not make the polysaccharide Pel	(Kirisits et al., 2005; Borlee et al., 2010)
PAO1Δ*psl*	*pslBCD*; polar mutant of psl operon	Does not make the polysaccharide Psl, overproduces Pel	(Kirisits et al., 2005)
PAO1Δ*pel*Δ*psl*	*pelA* and *pslBCD*; polar mutations	Does not make the polysaccharides Psl and Pel	(Rybtke et al., 2012b)
PAO1Δ*wspF*	In frame deletion of *wspF*	Constitutively over-expresses cyclic-di-GMP, which acts as a signal for biofilm development. Pel, Psl and CdrA overexproduced	(Starkey et al., 2009)

PAO1 or an exopolysaccharide mutant. Groups of mice were euthanized on post-infection days 2 and 7 and the bacterial loads in their wound beds and spleens were assessed. Significant differences were not observed (**Figure 1**), indicating that neither overexpression nor absence of Pel and Psl altered the ability of *P. aeruginosa* to establish an infection and survive in this *in vivo* model. While bacteria were detected in the spleens of some mice, they were low in number and not significantly different between groups. This likely represents a low level of transient systemic spread, which did not result in any morbidity or mortality.

Biofilms are thought to impact healing by acting as mechanical barriers that impede re-epithelialization and by causing a perpetual state of inflammation (Watters et al., 2013; Zhao et al., 2013). To determine whether wound closure was affected by the overexpression or absence of Pel and Psl, we measured the area of infected wounds daily for 14 days. We saw that wound closure rates were similar across all infection groups, indicating that Pel and Psl were not significant contributing factors to wound resolution in this model (**Figure 2**). These observations are somewhat consistent with those of Pestrak et al., who used a similar mouse model to examine the impact of Pel and Psl on *P. aeruginosa* wound infection (Pestrak et al., 2019). While the investigators did see significantly lower bacterial loads in wounds infected with PAO1Δ*pel*/Δ*psl* than with PAO1 WT at

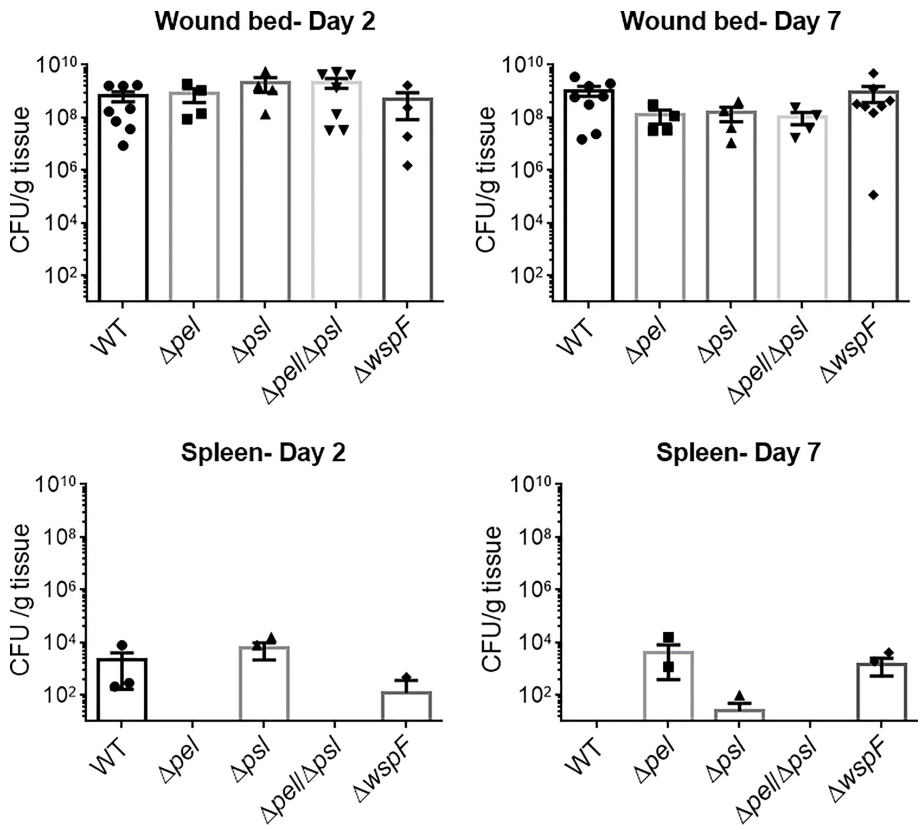

FIGURE 1 | No significant differences in wound or spleen bacterial load were observed between groups. Mice were wounded and infected with indicated *P. aeruginosa* strains. After 2 or 7 days, wound tissue and spleens were harvested and processed for CFU determination. One-way analysis of variance and a Dunn's or Dunnett's multiple comparison test was used to test for differences between groups. n=4-8 mice/strain.

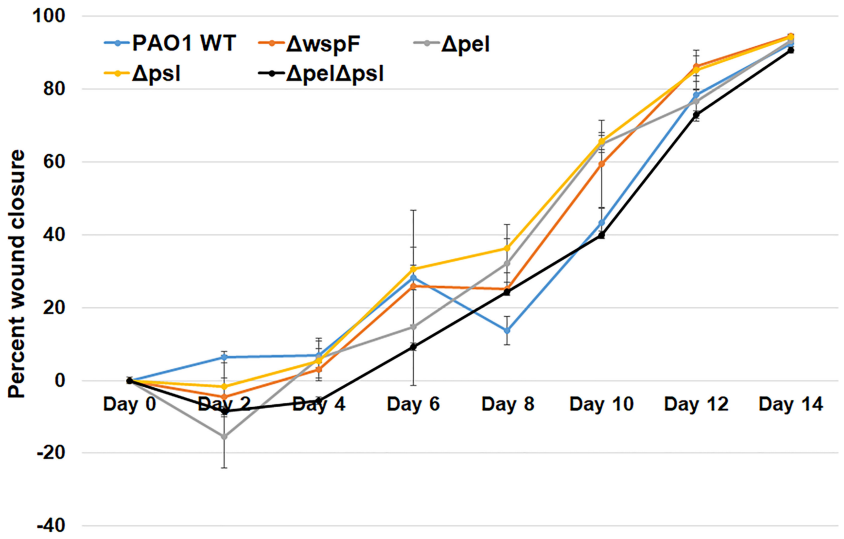

FIGURE 2 | No significant differences in wound closure rates were observed between groups. Mice were wounded and infected with indicated *P. aeruginosa* strains. Every 2 days they were anesthetized and their wounds were imaged and measured. One-way analysis of variance and a Tukey's multiple comparison test was used to test for differences between groups. n=4-8 mice/strain.

2 and 3 days post-infection, the differences were not significant by 4 days post-infection and wound closure was not assessed (Pestrak et al., 2019).

Overexpression of Pel and Psl by the PAO1Δ*wspF* mutant resulted in biofilms with significantly more biomass *in vitro* (Hickman et al., 2005) (Borlee et al., 2010). However, we observed that infection loads and wound closure rates were similar to those caused by the other strains *in vivo*. In a porcine, full thickness burn wound model, PAO1Δ*wspF* caused a greater bacterial burden in wounds that healed more slowly than those infected with PAO1 (Pestrak et al., 2018). However, these differences were only seen after 35 days post-infection. At early time points (7 days post-infection for bacterial load, and 7 and 14 days post-infection for wound size) there was no statistical difference between PAO1Δ*wspF* and the PAO1 parent strain (Pestrak et al., 2018). Taken together, these current and previous findings suggest that in a more acute murine wound model Pel and Psl have little impact on virulence, but in a more chronic pig model they appear to become important later in infection and their overproduction may impact the ability of wounds to heal.

Absence of Pel and Psl Alters Spatial Properties of Biofilm Aggregates in Wounds

The sizes and shapes of biofilms grown *in vitro* can vary due to a number of factors, and the production of Pel and Psl has been shown to contribute to this variation in some *in vitro* models. For example, in flow cell experiments, Colvin et al. observed distinct differences in the structures of Pel and Psl mutant biofilms in comparison to WT PAO1 biofilms after 5 days of growth (Colvin et al., 2012). While the *pelA* mutation had virtually no effect on microcolony development, a lack of Psl resulted in an absence of microcolony development and reduced biomass. However, while biofilm structure has been heavily scrutinized in flow cells, it is unclear how or if alteration in biofilm structure relates to infection. As opposed to biofilms formed unperturbed *in vitro*, biofilms in infection are typically present as aggregates that can vary greatly in size (Bjarnsholt et al., 2013; Jennings et al., 2021). To determine if changes to the exopolysaccharides produced would affect the number or size of aggregates in wounds, we performed imaging analysis on tissue from wounds infected with PAO1 and strains lacking Pel and/or Psl.

The spatial properties of biofilm aggregates in mouse wounds were examined by performing immunohistochemistry with a *P. aeruginosa* antibody on sections from wounds that had been infected with PAO1 or exopolysaccharide mutants for 10 days (**Figure 3**). We chose this time point based on our experience with this model, were aggregates are difficult to visualize until at least 10-12 days post infection (Dalton et al., 2011; Watters et al., 2013). To ascertain whether the antibody bound the strains similarly, we methanol fixed planktonic cells on slides, and then performed immunohistochemistry as described in the manuscript. We imaged the slides and performed analysis in ImageJ to determine if the antibody signals on cells were similar and if similar numbers of cells were labelled with antibody (**Supplemental Figure 1**). While the average antibody signal appeared to be less for all of the mutant strains in comparison to PAO1, the differences were not significant and did not visually appear different. We also did not see a significant difference in the number of cells (identified by DAPI) that were labelled by the antibody as determined by the mean of Pearson's coefficient.

Using image analysis, we analyzed 30 images from each infection group (i.e. 10 images per mouse and 3 mice infected with each strain) and determined the number, size and spatial distribution of 17,827 bacterial aggregates within the wound

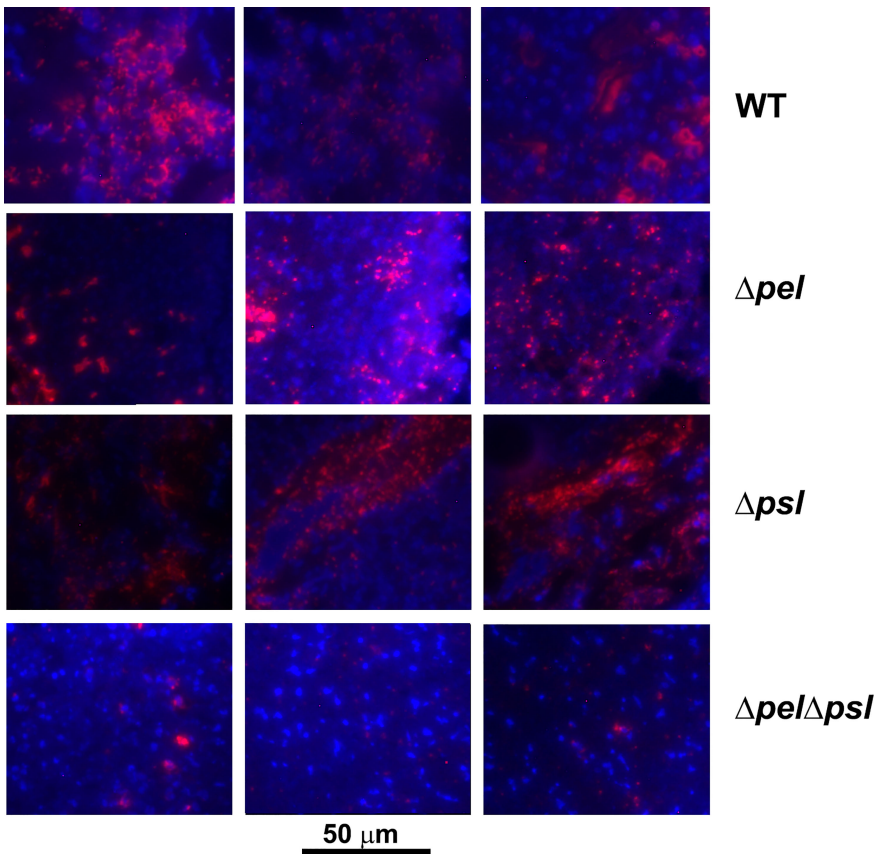

FIGURE 3 | Representative images of murine wound tissue infected with PAO1 exopolysaccharide mutants (red: Alexa Fluor® 594) embedded in host tissue (blue: DAPI). Mice were wounded and infected with indicated *P. aeruginosa* strains. After 10 days, wound tissue was harvested and processed for immunohistochemistry. Three representative images are shown from different mice and different sections to highlight the variability of aggregates observed.

tissue (**Figure 4**). We found that the lack of both Pel and Psl resulted in fewer and smaller aggregates. This was surprising considering that CFU analysis on infected tissue showed similar bacterial loads (**Figure 1**) and likely indicates that more of the PAO1 Δ*pel*Δ*psl* are present in the tissue as single cells, which are below the threshold of detection in our image analysis. We also found that aggregates of the double mutant were spaced further apart than were aggregates of either the single mutant strains or the wild-type (**Figure 4**, Nearest Neighbor), which makes sense as they are fewer and smaller. Similarly, as aggregates of the single knockouts were significantly larger than those of the double mutant, we also saw that they were spaced more closely together (**Figure 4**, Nearest Neighbor). Surprisingly, the spacing between aggregates of the double mutant and the wild-type were statistically indistinguishable. This is likely due to these two groups having the largest distances between aggregates, as well as the largest standard deviation between measurements.

We also investigated whether the absence of Pel or Psl would affect the abundance of host cells near bacterial aggregates. We measured the relative abundance of host material by taking the ratio of blue (DAPI; host cells) to red (*P. aeruginosa*) light intensity (**Figure 5**). Surprisingly, we found that deletion of Pel, but not Psl or even deletion of both exopolysaccharides, resulted in a lower host cell to bacterial cell ratio. If we assume that a large portion of these host cells are immune infiltrate, one explanation for this observation is that the lack of Pel results in a less active immune response. However, the mutant lacking both Pel and Psl did not show a similarly lower host cell to bacterial cell ratio. This could suggest the reduced host-cell signal is due to Psl being employed as the primary matrix scaffold during infection with PAO1Δ*pel*. Psl production by mucoid strains of *P. aeruginosa* has been shown to stimulate inflammation in murine lungs (Jones and Wozniak, 2017), thus it is unclear why Psl production in murine wounds would not also cause inflammation. Additionally, it is possible that these host cells are not immune infiltrate, but other cell types (e.g. epithelial, keratinocyte, fibroblasts) and their abundance may be a reflection of other factors within the infection microenvironment that are different between infection groups. For example, perhaps overproduction of Psl by the Δ*pel* strain is detrimental to host cells, causing cell death in the infected wound tissue. Psl production by *P. aeruginosa* in a keratitis infection model is was shown to be involved in a 'dead-zone' around aggregates, which was thought to involve neutrophil extracellular traps (Thanabalasuriar et al., 2019). As DAPI indiscriminately stains both the intracellular

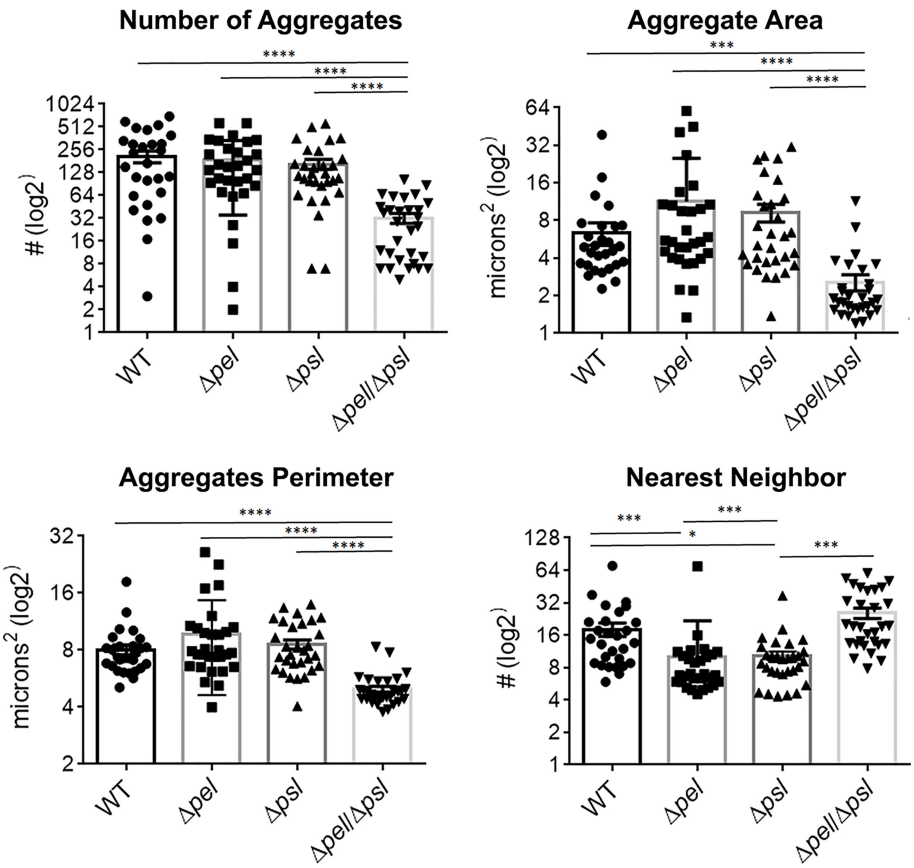

FIGURE 4 | *P. aeruginosa* aggregate characteristics of exopolysaccharide mutants in wound infections. Mice were wounded and infected with indicated *P. aeruginosa* strains. After 10 days, wound tissue was harvested and processed for immunohistochemistry. Images of aggregates in wound tissue were acquired and analyzed using image analysis. One-way analysis of variance and a Dunn's multiple comparison test was used to test for differences between groups. *, P<0.05; ***, P<0.001; ****, P<0.0001. n=30 images per strain (10 images/mouse and 3 mice/strain).

and extracellular DNA of both host cells and bacteria, future experiments will be needed to determine if a similar process is occurring in wound infections.

The Lack of Pel and Psl Reduces Antibiotic Tolerance in Wounds

The contribution of the biofilm matrix to survival of antibiotic treatment has been well studied *in vitro*. Although there have been confounding reports regarding mechanisms, it is generally accepted that exopolysaccharides produced by *P. aeruginosa* can help confer protection against antibiotics, especially to aminoglycosides, and that tolerance typically increases with greater biomass (Colvin et al., 2012; Tseng et al., 2013; Goltermann and Tolker-Nielsen, 2017; Ray et al., 2017; Jennings et al., 2021). Given the smaller and fewer aggregates created by the Pel and Psl mutant in our *in vivo* model, we sought to determine if antibiotic tolerance was affected (**Figure 6**). We found that wound beds infected with the double mutant, which had the smallest aggregates of all strains studied, were significantly less tolerant to gentamicin sulfate than WT PAO1 and the PAO1Δ*pel* strain, when treated *ex vivo*. We also saw that the Psl mutant was significantly less tolerant to gentamicin sulfate treatment than the PAO1Δ*pel* strain. As there was no difference in aggregate size between these two strains, it is clear that tolerance to gentamicin was not solely due to biomass. It is possible that the physical or chemical make-up of the PAO1Δ*psl* aggregates or the way they associate with host components decreases their tolerance.

MATERIALS AND METHODS

Bacterial *Strains* and Growth Conditions

Bacterial strains used are described in **Table 1**. Frozen bacterial stocks were stored at -80°C prior to culture. Using an inoculating loop, the bacterial stock was streaked onto LB (Luria-Bertani) agar and grown overnight at 37°C. One colony of the resulting streak was inoculated into 10 mL of LB broth and grown for 16 hours at 37°C in a 125 mL Erlenmeyer flask, with shaking at 220 RPM. Following incubation, overnight *P. aeruginosa* cultures were diluted to an optical density of 0.4 at 600 nm (OD_{600}). After that, 1 mL of the bacterial culture was prepared by centrifugation

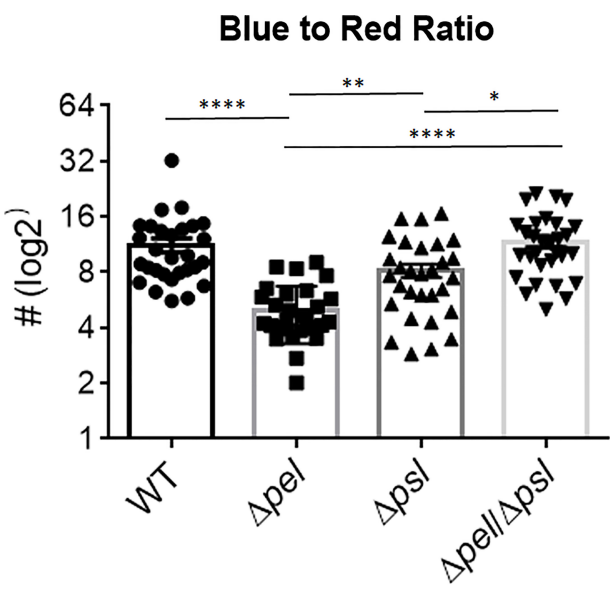

FIGURE 5 | Pel deletion results in a smaller host to bacteria ratio. Mice were wounded and infected with indicated *P. aeruginosa* strains. After 10 days, wound tissue was harvested and processed for immunohistochemistry. DAPI (blue) signal was used as a proxy for 'host' and Alexa Fluor® 594 (red) was used as a proxy for bacteria. Images of aggregates in wound tissue were acquired and analyzed using image analysis. One-way analysis of variance and a Dunn's multiple comparison test was used to test for differences between groups. *, P<0.05; **, P<0.01; ****, P<0.0001. n=30 images per strain (10 images/mouse and 3 mice/strain).

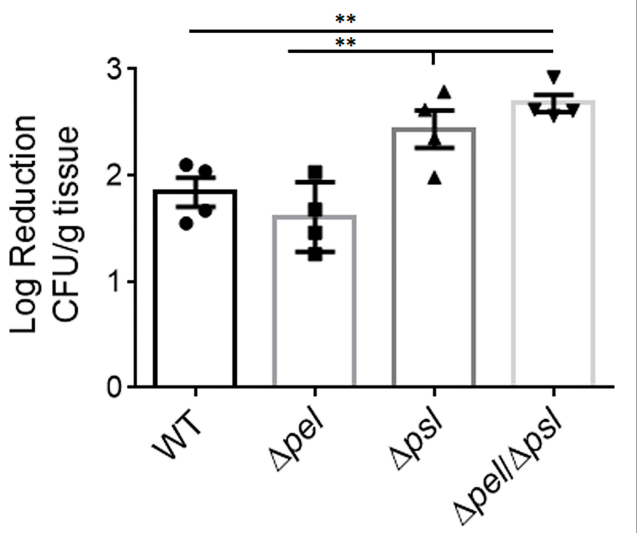

FIGURE 6 | Deletion of both Pel and Psl results in significantly reduced tolerance of *P. aeruginosa* to gentamicin sulfate. Mice were wounded and infected with indicated *P. aeruginosa* strains. After 4 days, wound tissue was harvested and treated *ex vivo* with gentamicin sulfate. One-way analysis of variance and a Dunn's multiple comparison test was used to test for differences between groups. **, P<0.01; n=4 mice/strain).

(10,000 X G for 5 minutes), washed and re-suspended in 1 X Phosphate Buffered Saline (PBS).

Murine Chronic Wound Infection Model

Our murine surgical excision wound model has been previously described (Brown and Greenhalgh, 1997; Rumbaugh et al., 2009; Wolcott et al., 2010; Dalton et al., 2011; Fleming et al., 2017; Fleming et al., 2020; Redman et al., 2021). Briefly, mice were anesthetized by intraperitoneal injection of ketamine and xylazine. After a surgical plane of anesthesia was reached, the backs were shaved and administered a full-thickness, dorsal excisional skin wound to the level of panniculus muscle with surgical scissors. Wounds were then covered with a semipermeable polyurethane dressing (OPSITE dressing; Smith & Nephew®), under which 10^4 bacterial cells were injected into the wound bed, and biofilm formation was allowed to proceed for the indicated time, after which the animals were sacrificed and their wound beds harvested for colony forming unit (CFU) analysis or imaging.

Imaging of Infected Mouse Wound Tissue

Mice were infected with the strains indicated as described above. After 10 days of infection, wound tissue was harvested, fixed in 10% formalin, embedded in paraffin, and cut into 10 μm sections. Sections were de-paraffinized, and labelled with an anti-*Pseudomonas* primary antibody (Chicken anti-*P. aeruginosa*; Abcam, PLC: ab74980) coupled to a red-fluorescent 2°antibody (Goat anti-chicken IgY H&L; Abcam, PLC: ab150176), and mounted with DAPI (ProLong® Diamond Antifade ThermoFisher: P36962) for immediate imaging with a Nikon eclipse TS 100-F Epifluorescence microscope.

Wound Bacterial Load Quantification

After 2 or 7 days of infection, entire wound beds were harvested, weighed, and placed into FischerScientific™ 2mL Pre-Filled Bead Mill Tubes with 1 mL of PBS and homogenized at 5 m/s for 60 seconds using a FastPrep-24™ MP Biomedical Benchtop Homogenizer. The resulting homogenates were then serially diluted 1:10 in PBS and plated on Pseudomonas Isolation Agar (Difco™). Plates were incubated at 37°C overnight, after which the bacterial loads were determined by CFU quantification.

Wound Closure Rate Quantification

Wounds were measured by daily imaging with a SilhouetteStar™ (ARANZ Medical) wound imaging camera. Percent wound closure was determined by subtracting the area of the wound measured on each day from the area on day 0, dividing by the area on day 0, and multiplying by 100.

Ex Vivo Antibiotic Tolerance

Equal-sized tissue sections from the wounds of infected mice were suspended in 200 μg/mL gentamicin sulfate (Sigma Aldrich) or PBS for 5 hours. Antibiotic treatment was removed with 3 washes of PBS. The samples were then homogenized as described in wound bacterial load quantification, serially diluted and plated on *Pseudomonas* isolation agar to quantitate CFU/g. The number of cells viable after antibiotic treatment was

compared to the number of cells viable after the PBS treatment to determine a log reduction.

Image Analysis of Infected Wound Tissue

The image analysis for this project was done in Fiji (Schindelin et al., 2012) and Python. In Fiji, images of infected mouse wound sections were split into red and blue channels to create 2 greyscale 8-bit images. The red and blue channels correspond to the Alexa Fluor® 594 secondary antibody used to detect bacteria, and the DAPI DNA binding dye, respectively. From each of the images, Intensity values and shape parameters were obtained using Fiji's "Measure" function and used as a measure of total bacteria and total host wound material. Then, a threshold was applied to the red ("bacteria") channel to create a black and white 8-bit image. From the thresholded image, area and center of mass position were obtained for all bacterial clusters using Fiji's built-in "Analyze Particle…" function.

Nearest neighbor distance is defined as the two-dimensional Euclidean distance from the bacterial cluster's center-of-mass position to the closest neighboring bacterial cluster's center-of-mass position. The following Python function returns a list of the nearest neighbors for all the aggregates given a 2D list of ["x","y"] coordinates.

```
def NN(dlist)
NN_list = [ ]
for i in range(len(dlist)):
NN = 100000000
for j in range(len(dlist)):
if i != j:
temp = (((dlist[i](0) - dlist[j](0)) ** 2) + (dlist[i](1) - dlist[j] (1)) ** 2) ** .5
if temp < NN:
NN = temp
NN_list . append (NN)
return NN_list
```

Statistical *Analysis*

GraphPad Prism (GraphPad Software, Inc.) was used for statistical analysis. Specific statistical tests used are provided in the figure legends.

Vertebrate Animal Use

All animal experiments were carried out in strict accordance with the recommendations in the Guide for the Care and Use of Laboratory Animals of the National Institutes of Health. The protocol was approved by the Institutional Animal Care and Use Committee of Texas Tech University Health Sciences Center (Protocol Number: 07044).

Immunohistochemistry of Planktonic Cells

Planktonic cultures were grown overnight in Luria Bertani Broth at 37C, with shaking at 200 rpm. Overnight cultures were diluted to 10^7 cfu/mL and placed dropwise on a slide. Samples were allowed to dry and subsequently methanol fixed. Prepared slides were incubated overnight at 4C in Primary Antibody (Abcam ab74980 Chicken Anti-Pseudomonas aeruginosa) diluted in PBS with 4% Dried Milk. Slides were washed with PBST before being incubated for 1 hour at room temperature in Secondary antibody (Abcam ab105176 Goat Anti-Chicken with Alexa594) diluted in PBST. Slides were washed following secondary incubation and prepared for imaging with ProLong Diamond Anti-Fade Mountant with DAPI (Invitrogen). Images were captured using a Nikon Eclipse 80i Fluorescent Scope with DS-Fi1 camera. Analysis was performed using ImageJ. For automated counting of antibody-positive cells, thresholds were applied to the images using the IJ_IsoData threshold function, followed by Analyzing Particles. For Corrected Total Fluorescence per area, integrated density was summed for each image, mean background subtracted, and the resulting difference was divided by the total fluorescence area. For colocalization, the Colocalization Threshold function was applied to determine P and Pearson's coefficient for each antibody-DAPI image pair.

DISCUSSION

P. aeruginosa is an opportunistic pathogen that uses at least three different exopolysaccharides, Pel, Psl and alginate, in its biofilm EPS. The production of these exopolysaccharides depends on the specific bacterial strain and on growth conditions (Colvin et al., 2012). However, it is thought that the primary exopolysaccharides produced in wounds are Pel and Psl (Wozniak et al., 2003). While the roles of Pel and Psl have been characterized to a large degree *in vitro*, how this characterization correlates with their roles *in vivo* is poorly understood. From *in vitro* studies it is apparent that Pel and Psl serve many functions including surface attachment, structural integrity of the biofilm, and antimicrobial and immune tolerance (Maunders and Welch, 2017), but few studies have sought to determine if these functions extend to infection.

Here we used a mouse wound model to characterize infections produced by a WT strain of *P. aeruginosa*, compared to PAO1 mutant strains that either did not produce Pel and/or Psl, or over-produced them (**Table 1**). We compared overall infection progression in mouse wounds, assessing bacterial load and wound closure as surrogate markers for virulence at 2 and 7 days post-infection. We discovered no significant differences between the bacterial loads in the wounds or spleens of mice infected with any of the bacterial strains studied. It should be noted however, that despite similar wound bioburden, infection with the mutant lacking both Pel and Psl resulted in no detectable bacteria in the spleens at either time point. This is the only strain in which this was the case, which could indicate that lacking both Pel and Psl leads to decreased hematogenous spread (i.e. decreased dispersal potential, decreased protection against the immune system, etc.). However it is more likely that the low number of bacteria detected in the spleens represents transient spread. We also saw no difference in wound closure rates over 14 days between infection groups.

Given the reported importance of Pel and Psl *in vitro*, it was unexpected that our data showed that their absence did not

grossly affect the progression and resolution of *P. aeruginosa* wound infection. Our *in vivo* results are somewhat consistent with those reported by Pestrak et al. (2019). Using a similar mouse excisional wound model, they compared bioburden in wounds infected with either PAO1 or PAO1Δ*pel* Δ*psl* at 1, 24, 48, 72, or 96 hours post-infection. They observed significant reductions in the bacterial load of wounds infected with PAO1Δ*pel* Δ*psl* at 48 and 72 hours post-infection, but by 96 hours, the difference was not significant. Wound size was not measured, so it is unclear if there were differences. They concluded that loss of Pel and Psl impacted initial colonization, but did not affect the long-term outcome of an infection (Pestrak et al., 2019). However, data from another study by Pestrak et al. showed that infection of porcine wounds with the Pel/Psl overproducing strain Δ*wspF* caused a different infection outcome than with WT PAO1 (Pestrak et al., 2018). In the porcine wound infection model, significant differences in the bacterial load of wounds infected with PAO1 versus Δ*wspF* were detected at 7, 14 and 35 days post-infection. However, these differences were not consistent. At 7 and 14 days post-infection, wounds infected with WT PAO1 had higher bioburden, while at 35 days the PAO1Δ*wspF* infected wounds had higher bioburden. Importantly, wounds infected with PAO1Δ*wspF* were significantly larger at 35 days post-infection than those infected with WT PAO1 (Pestrak et al., 2018). This led the authors to suggest that PAO1Δ*wspF* caused a more persistent and severe infection in pigs, impairing wound healing. We did not see this with PAO1Δ*wspF*, which could be primarily due to the animal model used. Porcine wound models are superior to mouse models because the dermal structure and mechanisms for healing much more closely resemble that of humans (Zindle et al., 2021). Therefore they are thought to more accurately model chronic infection. Taken together, these results demonstrate that the importance of Pel and Psl *in vivo* varies considerably between models and may only be apparent after a long period of chronic infection.

Since exopolysaccharides affect biofilm structure *in vitro*, we sought to investigate whether the spatial structure of the multicellular bacterial aggregates would be influenced by the loss of Pel and/or Psl *in vivo*. Using immunofluorescence microscopy and image analysis, we determined that infections with the mutant lacking both Pel and Psl exhibited fewer, smaller aggregates with greater spacing between aggregates. The fact that these differences in aggregate spatial structure exist despite similar bacterial loads suggests that much of the population of the Pel/Psl deficient cells exist as unaggregated single cells that are difficult to visualize with standard imaging techniques in wound tissue (Fleming et al., 2020). If true, one would expect these single cells to be more susceptible to clearance by the immune system. However, the similar bacterial loads indicate that this was not the case. We also saw that the intensity ratio of the blue (DAPI; host cells) and red (*P. aeruginosa*) signal in the immunofluorescent images was not affected by the loss of both Pel and Psl, which would be expected if there was a large difference in immune infiltrate. Instead, we saw that deletion of Pel alone resulted in a lower host cell to bacterial cell ratio. At this time we cannot explain this finding. However, it will be important in future studies to clearly identify the types of host cells that are less abundant around PAO1Δ*pel* aggregates.

Finally, we sought to investigate what role Pel and Psl play in antibiotic tolerance in wounds. Exopolysaccharides are clearly involved in the increased tolerance biofilm cells display to antibiotics. Specifically, the polycationic polymer Pel has especially been linked to tolerance to positively charged aminoglycoside antibiotics (Colvin et al., 2011; Jennings et al., 2015b; Jennings et al., 2021). Psl has also been shown to play a protective role against some antibiotics, but the mechanism is less understood (Billings et al., 2013). Thus we hypothesized that aggregates devoid of at least Pel would be more susceptible to killing by aminoglycosides. Our data supported this hypothesis as we saw that PAO1Δ*pel*Δ*psl* in wound tissue displayed a reduced ability to survive gentamicin treatment; however, we also saw that PAO1Δ*pel* did not exhibit this same tolerance. Instead, PAO1Δ*psl* in wound tissue was similarly tolerant to gentamicin treatment as PAO1Δ*pel*Δ*psl*. This result is perplexing since Pel is thought to play the major role in protection against aminoglycoside antibiotics. It also suggests that Psl may play a role in protecting *P. aeruginosa* from antibiotics *in vivo*, which has also been observed by other investigators *in vitro* (Billings et al., 2013). Other factors such as metabolism of the biofilm population may also be involved in our observations. Future studies will aim to better understand the interactions between the exopolysaccharides produced and efficacy of different classes of antibiotics.

There were several limitations to this study. Firstly, although there is evidence to support the production of Pel and Psl in aggregates during infection (Ray et al., 2017; Jennings et al., 2021), extensive characterization of *in vivo* exopolysaccharide production has not been reported, and we did not specifically verify that Pel and Psl are produced in mouse wounds. This is because the methods and reagents to specifically identify these exopolysaccharides amongst the myriad of host components present *in vivo* are still not readily available. We also acknowledge that since PelA is a deacetylase, it is possible that PAO1Δ*pel* could produce an acetylated version of Pel, which isn't recognized by Pel antisera. To explore this, future experiments should include other *pel* mutants. Future studies will also benefit from thorough assessment of which exopolysaccharides are produced during different stages of wound infection. Additionally, while Pel and Psl are thought to be the major exopolysaccharides produced by *P. aeruginosa* in chronic wound infections (Wozniak et al., 2003), alginate is also produced by PAO1 and its involvement cannot be discounted. It is possible that alginate production by one or more of these mutants can help explain some of our findings. Another limitation is that the imaging studies were performed at one time point, yet the EPS composition of *P. aeruginosa* may change over time *in vivo*, as it does *in vitro* (Yang et al., 2011). For example, one exopolysaccharide may dominate the EPS at early stages of the infection, and other exopolysaccharides may dominate at later stages of infection. If this is the case, the results presented herein should be taken as indicative of the contributions of

polysaccharides to established wound infections. Going forward, a time course examination of aggregate spatial properties during the course of infection may help resolve some of these uncertainties.

To conclude, in this study we attempted to define the roles of the Pel and Psl polysaccharides in chronic wound infection with *P. aeruginosa*, particularly in respect to bacterial load, wound closure rates, aggregate size and spacing, and antibiotic tolerance. We found that, despite similar bacterial loads and wound closure rates, the bacterial aggregates resulting from infection with a *P. aeruginosa* strain that is incapable of producing both Pel and Psl were smaller and fewer, and the cells were more susceptible to gentamicin sulfate. We also showed that deletion of Pel alone likely resulted in lesser immune cell recruitment, despite the double mutant showing similar host cell recruitment as the wild type strain. While this study takes a step forward in investigating *in vivo* polysaccharide production in chronic *P. aeruginosa* wound infection, further work is needed to determine how these affects change temporally over the course of an infection, the potential impact of alginate production, and the identity of the host cells involved.

DATA AVAILABILITY STATEMENT

The raw data supporting the conclusions of this article will be made available by the authors, without undue reservation.

ETHICS STATEMENT

The animal study was reviewed and approved by TTUHSC IACUC.

AUTHOR CONTRIBUTIONS

DF, KR, and VG contributed to conception and design of the study. BN performed the image analysis. KR performed the statistical analysis. DF wrote the first draft of the manuscript. DF, EV, WR, and BN collected and analyzed data. All authors wrote sections of the manuscript and contributed to manuscript revision, read, and approved the submitted version.

FUNDING

This work was supported by grants from the National Institutes of Health (1R01AI121500-01A1, National Institute of Allergy and Infectious Diseases), the National Science Foundation (727544; Biomechanics and Mechanobiology; Civil, Mechanical, and Manufacturing Innovation), to VG; National Institutes of Health (R21 AI137462-01A1), the Ted Nash Long Life Foundation, and The Jasper L. and Jack Denton Wilson Foundation, to KR.

ACKNOWLEDGMENTS

The authors would like to thanks Garrett Welch, Hua Hui and EV for help with animal experiments and immunohistochemistry. We also thank Matt Parsek for sharing the *P. aeruginosa* strains used in this study.

SUPPLEMENTARY MATERIAL

The Supplementary Material for this article can be found online at: https://www.frontiersin.org/articles/10.3389/fcimb.2022.835754/full#supplementary-material.

Supplementary Figure 1 | Comparison of antibody binding to methanol-fixed planktonic cells. **(A)** Examples of immunohistochemistry images from WT PAO1 and PAO1Δ*pel*Δ*psl* methanol-fixed planktonic cells with Alexa594 conjugated *P. aeruginosa* antibody in the first colomn, DAPI staining in the second, and an overlay in the third. **(B)** To alayze the average antibody signal per cell, ImageJ analysis of the mean corrected total fluorescence was divided by the total fluorescent area in fluorescence units/0.24 um^2, N=3 images per strain. Bars are standard error of the mean and groups were not significant by One-way ANOVA, $p < 0.05$. **(C)** Mean of Pearson's coefficient showing that the number of DAPI-stained cells, which were also antibody positive, was not significantly different between strains by One-way ANOVA, $p < 0.05$. n=3 per strain. P for colocalization is 1.00 for all images.

REFERENCES

Attinger C., Wolcott R. (2012). Clinically Addressing Biofilm in Chronic Wounds. *Adv. Wound Care (New Rochelle)* 1, 127–132. doi: 10.1089/wound.2011.0333

Billings N., Millan M., Caldara M., Rusconi R., Tarasova Y., Stocker R., et al. (2013). The Extracellular Matrix Component Psl Provides Fast-Acting Antibiotic Defense in Pseudomonas Aeruginosa Biofilms. *PloS Pathog.* 9, e1003526. doi: 10.1371/journal.ppat.1003526

Bjarnsholt T., Alhede M., Alhede M., Eickhardt-Sørensen S. R., Moser C., Kühl M., et al. (2013). The *In Vivo* Biofilm. *Trends Microbiol.* 21, 466–474. doi: 10.1016/j.tim.2013.06.002

Borlee B. R., Goldman A. D., Murakami K., Samudrala R., Wozniak D. J., Parsek M. R. (2010). Pseudomonas Aeruginosa Uses a Cyclic-Di-GMP-Regulated Adhesin to Reinforce the Biofilm Extracellular Matrix. *Mol. Microbiol.* 75, 827–842. doi: 10.1111/j.1365-2958.2009.06991.x

Brown R. L., Greenhalgh D. G. (1997). Mouse Models to Study Wound Closure and Topical Treatment of Infected Wounds in Healing-Impaired and Normal Healing Hosts. *Wound Repair Regener.* 5, 198–204. doi: 10.1046/j.1524-475X.1997.50213.x

Byrd M. S., Sadovskaya I., Vinogradov E., Lu H., Sprinkle A. B., Richardson S. H., et al. (2009). Genetic and Biochemical Analyses of the Pseudomonas Aeruginosa Psl Exopolysaccharide Reveal Overlapping Roles for Polysaccharide Synthesis Enzymes in Psl and LPS Production. *Mol. Microbiol.* 73, 622–638. doi: 10.1111/j.1365-2958.2009.06795.x

Colvin K. M., Gordon V. D., Murakami K., Borlee B. R., Wozniak D. J., Wong G. C. L., et al. (2011). The Pel Polysaccharide can Serve a Structural and Protective Role in the Biofilm Matrix of Pseudomonas Aeruginosa. *PloS Pathog.* 7, e1001264-e1001264. doi: 10.1371/journal.ppat.1001264

Colvin K. M., Irie Y., Tart C. S., Urbano R., Whitney J. C., Ryder C., et al. (2012). The Pel and Psl Polysaccharides Provide Pseudomonas Aeruginosa Structural Redundancy Within the Biofilm Matrix. *Environ. Microbiol.* 14, 1913–1928. doi: 10.1111/j.1462-2920.2011.02657.x

Dalton T., Dowd S. E., Wolcott R. D., Sun Y., Watters C., Griswold J. A., et al. (2011). An *In Vivo* Polymicrobial Biofilm Wound Infection Model to Study

Interspecies Interactions. *PloS One* 6, e27317. doi: 10.1371/journal.pone.0027317

Fleming D., Chahin L., Rumbaugh K. (2017). Glycoside Hydrolases Degrade Polymicrobial Bacterial Biofilms in Wounds. *Antimicrob. Agents Chemother.* 61, e01998–16. doi: 10.1128/AAC.01998-16

Fleming D., Redman W., Welch G. S., Mdluli N. V., Rouchon C. N., Frank K. L., et al. (2020). Utilizing Glycoside Hydrolases to Improve the Quantitation and Visualization of Biofilm Bacteria. *Biofilm* 2, 100037. doi: 10.1016/j.bioflm.2020.100037

Flemming H.-C., Wingender J. (2010). The Biofilm Matrix. *Nat. Rev. Microbiol.* 8, 623–633. doi: 10.1038/nrmicro2415

Franklin M. J., Nivens D. E., Weadge J. T., Howell P. L. (2011). Biosynthesis of the Pseudomonas Aeruginosa Extracellular Polysaccharides, Alginate, Pel, and Psl. *Front. Microbiol.* 2, 167. doi: 10.3389/fmicb.2011.00167

Goltermann L., Tolker-Nielsen T. (2017). Importance of the Exopolysaccharide Matrix in Antimicrobial Tolerance of Pseudomonas Aeruginosa Aggregates. *Antimicrob. Agents Chemother.* 61, e02696–16. doi: 10.1128/AAC.02696-16

Hickman J. W., Tifrea D. F., Harwood C. S. (2005). A Chemosensory System That Regulates Biofilm Formation Through Modulation of Cyclic Diguanylate Levels. *Proc. Natl. Acad. Sci. U.S.A.* 102, 14422–14427. doi: 10.1073/pnas.0507170102

Holloway B. (1955). Genetic Recombination in Pseudomonas Aeruginosa. *Microbiology* 13, 572–581. doi: 10.1099/00221287-13-3-572

Ibberson C. B., Stacy A., Fleming D., Dees J. L., Rumbaugh K., Gilmore M. S., et al. (2017). Co-Infecting Microorganisms Dramatically Alter Pathogen Gene Essentiality During Polymicrobial Infection. *Nat. Microbiol.* 2, 17079. doi: 10.1038/nmicrobiol.2017.79

Irie Y., Roberts Aled E. L., Kragh Kasper N., Gordon Vernita D., Hutchison J., Allen Rosalind J., et al. (2017). The Pseudomonas Aeruginosa PSL Polysaccharide Is a Social But Noncheatable Trait in Biofilms. *mBio* 8, e00374–e00317. doi: 10.1128/mBio.00374-17

Jennings L. K., Dreifus J. E., Reichhardt C., Storek K. M., Secor P. R., Wozniak D. J., et al. (2021). Pseudomonas Aeruginosa Aggregates in Cystic Fibrosis Sputum Produce Exopolysaccharides That Likely Impede Current Therapies. *Cell Rep.* 34, 108782. doi: 10.1016/j.celrep.2021.108782

Jennings L. K., Storek K. M., Ledvina H. E., Coulon C., Marmont L. S., Sadovskaya I., et al. (2015a). Pel Is a Cationic Exopolysaccharide That Cross-Links Extracellular DNA in the Pseudomonas Aeruginosa Biofilm Matrix. *Proc. Natl. Acad. Sci. U.S.A.* 112, 11353–11358. doi: 10.1073/pnas.1503058112

Jennings L. K., Storek K. M., Ledvina H. E., Coulon C., Marmont L. S., Sadovskaya I., et al. (2015b). Pel is a Cationic Exopolysaccharide That Cross-Links Extracellular DNA in the Pseudomonas Aeruginosa Biofilm Matrix. *Proc. Natl. Acad. Sci.* 112, 11353. doi: 10.1073/pnas.1503058112

Jones C. J., Wozniak D. J. (2017). Psl Produced by Mucoid Pseudomonas Aeruginosa Contributes to the Establishment of Biofilms and Immune Evasion. *mBio* 8, e00864–17. doi: 10.1128/mBio.00864-17

Karatan E., Watnick P. (2009). Signals, Regulatory Networks, and Materials That Build and Break Bacterial Biofilms. *Microbiol. Mol. Biol. Rev.* 73, 310–347. doi: 10.1128/MMBR.00041-08

Kirisits M. J., Prost L., Starkey M., Parsek M. R. (2005). Characterization of Colony Morphology Variants Isolated From Pseudomonas Aeruginosa Biofilms. *Appl. Environ. Microbiol.* 71, 4809–4821. doi: 10.1128/AEM.71.8.4809-4821.2005

Koo H., Allan R. N., Howlin R. P., Stoodley P., Hall-Stoodley L. (2017). Targeting Microbial Biofilms: Current and Prospective Therapeutic Strategies. *Nat. Rev. Microbiol.* 15, 740–755. doi: 10.1038/nrmicro.2017.99

Lewis K. (2012). Persister Cells: Molecular Mechanisms Related to Antibiotic Tolerance. *Handb. Exp. Pharmacol.* 211, 121–133. doi: 10.1007/978-3-642-28951-4_8

Ma L., Lu H., Sprinkle A., Parsek M. R., Wozniak D. J. (2007). Pseudomonas Aeruginosa Psl Is a Galactose- and Mannose-Rich Exopolysaccharide. *J. bacteriol* 189, 8353–8356. doi: 10.1128/JB.00620-07

Maunders E., Welch M. (2017). Matrix Exopolysaccharides; the Sticky Side of Biofilm Formation. *FEMS Microbiol. Lett.* 364, 1–10. doi: 10.1093/femsle/fnx120

Pestrak M. J., Baker P., Dellos-Nolan S., Hill P. J., Passos da Silva D., Silver H., et al. (2019). Treatment With the Pseudomonas Aeruginosa Glycoside Hydrolase PslG Combats Wound Infection by Improving Antibiotic Efficacy and Host Innate Immune Activity. *Antimicrob. Agents Chemother.* 63, e00234–19. doi: 10.1128/AAC.00234-19

Pestrak M. J., Chaney S. B., Eggleston H. C., Dellos-Nolan S., Dixit S., Mathew-Steiner S. S., et al. (2018). Pseudomonas Aeruginosa Rugose Small-Colony Variants Evade Host Clearance, are Hyper-Inflammatory, and Persist in Multiple Host Environments. *PloS Pathog.* 14, e1006842. doi: 10.1371/journal.ppat.1006842

Rahman M. U., Fleming D. F., Sinha I., Rumbaugh K. P., Gordon V. D., Christopher G. F. (2021). Effect of Collagen and EPS Components on the Viscoelasticity of Pseudomonas Aeruginosa Biofilms. *Soft Matter* 17, 6225–6237. doi: 10.1039/D1SM00463H

Ray V. A., Hill P. J., Stover C. K., Roy S., Sen C. K., Yu L., et al. (2017). Anti-Psl Targeting of Pseudomonas Aeruginosa Biofilms for Neutrophil-Mediated Disruption. *Sci. Rep.* 7, 16065. doi: 10.1038/s41598-017-16215-6

Redman W. K., Welch G. S., Rumbaugh K. P. (2020). Differential Efficacy of Glycoside Hydrolases to Disperse Biofilms. *Front. Cell Infect. Microbiol.* 10, 379. doi: 10.3389/fcimb.2020.00379

Redman W. K., Welch G. S., Rumbaugh K. P. (2021). Assessing Biofilm Dispersal in Murine Wounds. *J. Vis. Exp.* 174, e62136. doi: 10.3791/62136

Roberts A. E., Kragh K. N., Bjarnsholt T., Diggle S. P. (2015). The Limitations of *In Vitro* Experimentation in Understanding Biofilms and Chronic Infection. *J. Mol. Biol.* 427, 3646–3661. doi: 10.1016/j.jmb.2015.09.002

Rogers S. A., Huigens R. W.3rd, Cavanagh J., Melander C. (2010). Synergistic Effects Between Conventional Antibiotics and 2-Aminoimidazole-Derived Antibiofilm Agents. *Antimicrob. Agents Chemother.* 54, 2112–2118. doi: 10.1128/AAC.01418-09

Romling U., Balsalobre C. (2012). Biofilm Infections, Their Resilience to Therapy and Innovative Treatment Strategies. *J. Intern. Med.* 272, 541–561. doi: 10.1111/joim.12004

Rumbaugh K. P., Diggle S. P., Watters C. M., Ross-Gillespie A., Griffin A. S., West S. A. (2009). Quorum Sensing and the Social Evolution of Bacterial Virulence. *Curr. Biol.* 19, 341–345. doi: 10.1016/j.cub.2009.01.050

Rybtke M. T., Borlee B. R., Murakami K., Irie Y., Hentzer M., Nielsen T. E., et al. (2012a). Fluorescence-Based Reporter for Gauging Cyclic Di-GMP Levels in Pseudomonas Aeruginosa. *Appl. Environ. Microbiol.* 78, 5060–5069. doi: 10.1128/AEM.00414-12

Rybtke M. T., Borlee B. R., Murakami K., Irie Y., Hentzer M., Nielsen T. E., et al. (2012b). Fluorescence-Based Reporter for Gauging Cyclic Di-GMP Levels in Pseudomonas Aeruginosa. *Appl. Environ. Microbiol.* 78, 5060–5069. doi: 10.1128/AEM.00414-12

Ryder C., Byrd M., Wozniak D. J. (2007). Role of Polysaccharides in Pseudomonas Aeruginosa Biofilm Development. *Curr. Opin. Microbiol.* 10, 644–648. doi: 10.1016/j.mib.2007.09.010

Schindelin J., Arganda-Carreras I., Frise E., Kaynig V., Longair M., Pietzsch T., et al. (2012). Fiji: An Open-Source Platform for Biological-Image Analysis. *Nat. Methods* 9, 676–682. doi: 10.1038/nmeth.2019

Stanley N. R., Lazazzera B. A. (2004). Environmental Signals and Regulatory Pathways That Influence Biofilm Formation. *Mol. Microbiol.* 52, 917–924. doi: 10.1111/j.1365-2958.2004.04036.x

Starkey M., Hickman J. H., Ma L., Zhang N., De Long S., Hinz A., et al. (2009). Pseudomonas Aeruginosa Rugose Small-Colony Variants Have Adaptations That Likely Promote Persistence in the Cystic Fibrosis Lung. *J. Bacteriol.* 191, 3492–3503. doi: 10.1128/JB.00119-09

Thanabalasuriar A., Scott B. N. V., Peiseler M., Willson M. E., Zeng Z., Warrener P., et al. (2019). Neutrophil Extracellular Traps Confine Pseudomonas Aeruginosa Ocular Biofilms and Restrict Brain Invasion. *Cell Host Microbe* 25, 526–536.e4. doi: 10.1016/j.chom.2019.02.007

Tseng B. S., Zhang W., Harrison J. J., Quach T. P., Song J. L., Penterman J., et al. (2013). The Extracellular Matrix Protects Pseudomonas Aeruginosa Biofilms by Limiting the Penetration of Tobramycin. *Environ. Microbiol.* 15, 2865–2878. doi: 10.1111/1462-2920.12155

Watters C., DeLeon K., Trivedi U., Griswold J. A., Lyte M., Hampel K. J., et al. (2013). Pseudomonas Aeruginosa Biofilms Perturb Wound Resolution and Antibiotic Tolerance in Diabetic Mice. *Med. Microbiol. Immunol.* 202, 131–141. doi: 10.1007/s00430-012-0277-7

Wolcott R. D., Hanson J. D., Rees E. J., Koenig L. D., Phillips C. D., Wolcott R. A., et al. (2016). Analysis of the Chronic Wound Microbiota of 2,963 Patients by 16S rDNA Pyrosequencing. *Wound Repair Regener.* 24, 163–174. doi: 10.1111/wrr.12370

Wolcott R. D., Rumbaugh K. P., James G., Schultz G., Phillips P., Yang Q., et al. (2010). Biofilm Maturity Studies Indicate Sharp Debridement Opens a Time-

Dependent Therapeutic Window. *J. Wound Care* 19, 320–328. doi: 10.12968/jowc.2010.19.8.77709

Wozniak D. J., Wyckoff T. J. O., Starkey M., Keyser R., Azadi P., Toole G. A., et al. (2003). Alginate Is Not a Significant Component of the Extracellular Polysaccharide Matrix of PA14 and PAO1 Pseudomonas Aeruginosa Biofilms. *Proc. Natl. Acad. Sci.* 100, 7907. doi: 10.1073/pnas.1231792100

Yang L., Hu Y., Liu Y., Zhang J., Ulstrup J., Molin S. (2011). Distinct Roles of Extracellular Polymeric Substances in Pseudomonas Aeruginosa Biofilm Development. *Environ. Microbiol.* 13, 1705–1717. doi: 10.1111/j.1462-2920.2011.02503.x

Zhao G., Usui M. L., Lippman S. I., James G. A., Stewart P. S., Fleckman P., et al. (2013). Biofilms and Inflammation in Chronic Wounds. *Adv. Wound Care (New Rochelle)* 2, 389–399. doi: 10.1089/wound.2012.0381

Zindle J. K., Wolinsky E., Bogie K. M. (2021). A Review of Animal Models From 2015 to 2020 for Preclinical Chronic Wounds Relevant to Human Health. *J. Tissue Viability* 30, 291–300. doi: 10.1016/j.jtv.2021.05.006

Conflict of Interest: The authors declare that the research was conducted in the absence of any commercial or financial relationships that could be construed as a potential conflict of interest.

Publisher's Note: All claims expressed in this article are solely those of the authors and do not necessarily represent those of their affiliated organizations, or those of the publisher, the editors and the reviewers. Any product that may be evaluated in this article, or claim that may be made by its manufacturer, is not guaranteed or endorsed by the publisher.

frontiers | Frontiers in Cellular and Infection Microbiology

ORIGINAL RESEARCH
published: 11 May 2022
doi: 10.3389/fcimb.2022.884065

Phenol-Soluble Modulins From *Staphylococcus aureus* Biofilms Form Complexes With DNA to Drive Autoimmunity

Kaitlyn Grando[1‡], *Lauren K. Nicastro*[1‡†], *Sarah A. Tursi*[1‡†], *Jaime De Anda*[2], *Ernest Y. Lee*[2†], *Gerard C. L. Wong*[2] *and Çağla Tükel*[1*]

[1] Center for Microbiology and Immunology, Lewis Katz School of Medicine, Temple University, Philadelphia, PA, United States, [2] Department of Bioengineering, Department of Chemistry and Biochemistry, California Nano Systems Institute, University of California, Los Angeles, Los Angeles, CA, United States

The bacterial amyloid curli, produced by Enterobacteriales including *Salmonella* species and *Escherichia coli*, is implicated in the pathogenesis of several complex autoimmune diseases. Curli binds to extracellular DNA, and these complexes drive autoimmunity *via* production of anti-double-stranded DNA autoantibodies. Here, we investigated immune activation by phenol-soluble modulins (PSMs), the amyloid proteins expressed by *Staphylococcus* species. We confirmed the amyloid nature of PSMs expressed by *S. aureus* using a novel specific amyloid stain, (*E*,*E*)-1-fluoro-2,5-bis(3-hydroxycarbonyl-4-hydroxy) styrylbenzene (FSB). Direct interaction of one of the *S. aureus* PSMs, PSMα3, with oligonucleotides promotes fibrillization of PSM amyloids and complex formation with bacterial DNA. Finally, utilizing a mouse model with an implanted mesh-associated *S. aureus* biofilm, we demonstrated that exposure to *S. aureus* biofilms for six weeks caused anti-double-stranded DNA autoantibody production in a PSM-dependent manner. Taken together, these results highlight how the presence of PSM-DNA complexes in *S. aureus* biofilms can induce autoimmune responses, and suggest an explanation for how bacterial infections trigger autoimmunity.

Keywords: PSM, Phenol Soluble Modulins, *Staphycoccus aureus*, biofilm, mesh, autoimmune disease, SLE, curli

OPEN ACCESS

Edited by:
Lauren O Bakaletz, Nationwide Children's Hospital, United States

Reviewed by:
Meytal Landau, Technion Israel Institute of Technology, Israel
Hanne Ingmer, University of Copenhagen, Denmark

***Correspondence:**
Çağla Tükel
ctukel@temple.edu

***Present address:**
Lauren K. Nicastro, GlaxoSmithKline, Collegeville, PA, United States
Sarah A. Tursi, Janssen Research & Development, LLC, Spring House, PA, United States
Ernest Y. Lee, Department of Dermatology, University of California, San Francisco, San Francisco, CA, United states

‡*These authors have contributed equally to this work*

Specialty section:
This article was submitted to Biofilms, a section of the journal Frontiers in Cellular and Infection Microbiology

Received: *25 February 2022*
Accepted: *04 April 2022*
Published: *11 May 2022*

Citation:
Grando K, Nicastro LK, Tursi SA, De Anda J, Lee EY, Wong GCL and Tükel Ç (2022) Phenol-Soluble Modulins From Staphylococcus aureus Biofilms Form Complexes With DNA to Drive Autoimmunity. Front. Cell. Infect. Microbiol. 12:884065. doi: 10.3389/fcimb.2022.884065

INTRODUCTION

Biofilms are communities of bacterial cells embedded in an extracellular matrix. Many bacterial species form biofilms, and approximately 40% of bacterial species produce amyloids within their biofilms (Larsen et al., 2007). Curli, produced by Enterobacteriaceae, including *Salmonella* species and *Escherichia coli*, are the best-characterized bacterial amyloid. Curli fibers enshroud individual bacteria as part of an extracellular matrix (ECM) to aid in biofilm surface attachment, formation of the mature biofilm architecture, and protection of the biofilm from harsh environmental conditions (Costerton et al., 1995; Reisner et al., 2003; Kikuchi et al., 2005; McCrate et al., 2013). Curli form proteinaceous fibers ranging from 4 to 12 nm in width composed of β-sheet strands oriented

perpendicular to the axis of the fiber (Chapman et al., 2002; Chiti and Dobson, 2006; Schnabel, 2010), similar in structure to human amyloids like amyloid-β implicated in Alzheimer's disease (Michelitsch and Weissman, 2000; Ghosh et al., 2021). Curli forms complexes with extracellular DNA (eDNA) in biofilms of *Salmonella enterica* serovar Typhimurium and *E. coli*. The DNA is incorporated into curli fibers, accelerating amyloid polymerization and bolstering the biofilm structure (Gallo et al., 2015).

After infections resolve, some patients develop autoimmune responses including reactive arthritis (ReA) (Carter and Hudson, 2009; Nicastro and Tükel, 2019). Moreover, individuals who have a chronic autoimmune disease like systemic lupus erythematosus (SLE) often experience disease flares when they acquire a bacterial infection (Staples et al., 1974; Shahram et al., 1993; Petri, 1998; Pachucki et al., 2020). Previous work established that the conserved quaternary structure of amyloid curli activates the heterocomplex of Toll-like receptors TLR2 and TLR1 and initiates a pro-inflammatory response (Tükel et al., 2009; Tükel et al., 2010). Curli-eDNA complexes can internalize into TLR9-containing endosomes *via* TLR2 binding (Tursi et al., 2017). Subsequent recognition of the eDNA in the curli-eDNA complex by TLR9 can lead to the production of type I interferons (IFNs) and anti-double stranded DNA (dsDNA) autoantibodies (Tursi et al., 2017). *In vitro* and *in vivo* studies suggest that amyloid curli-eDNA complexes play a role in the pathogenesis of autoimmune diseases including ReA and SLE (Gallo et al., 2015). ReA develops in about 5% of patients who suffer from gastroenteritis due to infections with enteric pathogens such as *Salmonella, Campylobacter*, *Shigella*, or *Yersinia* (Carter and Hudson, 2009). Studies using *S.* Typhimurium as a model organism revealed that the joint inflammation and autoimmune sequalae observed following infection are driven by curli (Miller et al., 2020). Furthermore, it was recently demonstrated that exposure to curli is associated with disease flares in patients with SLE (Pachucki et al., 2020). At present, the mechanistic links between enteric infections and autoimmune outcomes are not well understood.

Persistent *Staphylococcus aureus* infections are often associated with the formation of a biofilm and are of particular interest as they are recalcitrant to immune responses and unresponsive to antibiotic therapies (Boles and Horswill, 2008). Persistent infections involving *S. aureus* biofilms can lead to osteomyelitis and endocarditis (Fernández Guerrero et al., 2009; Olson and Horswill, 2013), and *S. aureus* biofilm growth often occurs on medical implants (Kathju et al., 2015; Langbach et al., 2016). Studies have shown that *S. aureus* carriage is associated with certain autoimmune diseases such as granulamatosis with polyangiitis, psoriasis, and SLE (Conti et al., 2016; Totté et al., 2016; Salmela et al., 2017; Ceccarelli et al., 2019). Further, superantigen expression by *S. aureus* is critical for the activation of autoreactive T cells in mice (Tuffs et al., 2018).

S. aureus, a Gram-positive pathogen, produces amyloids known as phenol-soluble modulins (PSMs) that also form complexes with DNA (Schwartz et al., 2012; Schwartz et al., 2016). PSMs are essential for proper development and stabilization of biofilms formed by *S. aureus* but also serve a role in biofilm detachment and dispersal leading to systemic dissemination of the pathogen through mechanisms that are not well-understood (Wang et al., 2007; Periasamy et al., 2012; Schwartz et al., 2012; Zaman and Andreasen, 2020). PSMs are amphipathic alpha-helical proteins that range in size from 20 to 45 amino acids in length. *S. aureus* expresses nine types of PSMs that are classified further into α and β groups (α1 to 4 and β1 and 2) and δ-toxin (Wang et al., 2007; Peschel and Otto, 2013). Recently, research has indicated that eDNA forms complexes with PSMs and promotes PSM fibrillization (Schwartz et al., 2016). PSMα3 is of particular interest as the recently solved microcrystallographic structure of PSMα3 indicated that it forms cross-α amyloid fibrils that have structures similar to those of amyloid cross-β sheet structures, as seen in curli fibers (Tayeb-Fligelman et al., 2020). High levels of fluorescence are observed when either cross-α amyloid fibrils or cross-β sheet structures bind to Thioflavin T (Tayeb-Fligelman et al., 2017). Similar to curli and other human amyloids, PSM fibrils are agonists of TLR2 (Hajjar et al., 2001; Cheng et al., 2008; He et al., 2009; Tükel et al., 2009; Chen et al., 2014). Additionally, PSMs activate the human formyl peptide receptor 2 (FPR2/ALX), which has previously been implicated in endogenous inflammatory processes (Kretschmer et al., 2010; Rautenberg et al., 2011; Kretschmer et al., 2012). Of the PSMs, PSMα3 has the highest propensity for membrane permeation and DNA binding (Laabei et al., 2014; Schwartz et al., 2016; Towle et al., 2016), which can both lead to inflammation.

Here, we examined whether chronic infection with *S. aureus* biofilms would drive autoimmune responses *via* the production of PSM-eDNA complexes, similar to autoimmune responses triggered by curli-eDNA complexes. We found that intraperitoneal injection of synthetic PSMα3 fibrillized with CpG DNA into mice elicits a robust anti-dsDNA autoantibody response. To assess whether similar outcomes can be precipitated using an infection model, we showed that implantation of a mesh-associated *S. aureus* biofilm into a mouse directly leads to induction of anti-dsDNA autoantibodies, and importantly, does so in a TLR2 and TLR9 dependent manner. In contrast, intraperitoneal infection with *S. aureus* wildtype SH1000 or Δ*psm* mutant does not induce autoantibody production. These results indicate that both PSMα3 and DNA are involved in the induction of autoantibodies. Moreover, the mechanisms of entry and immune activation implicate both TLR2 and TLR9, which suggest that PSMα3-DNA complexes and curli-DNA complexes behavior similarly in immune activation. These results using either *S. aureus* biofilm infection or synthetic PSMs illustrate how bacterial biofilms can lead to infection-associated autoimmunity.

RESULTS

S. aureus Biofilms Contain PSMs

PSMs are secreted by *Staphylococcus* in high amounts in a quorum-sensing-controlled fashion (Kretschmer et al., 2012). The role of PSMs in the structuring and stabilizing of biofilms

due to their amyloid conformation had been controversial, but recently it was reported that PSMs are crucial for formation of *S. epidermidis* biofilms on indwelling devices (Le et al., 2019). *S. aureus* PSMs form fibrillar structures *in vitro* that resemble curli fibrils, and, like curli, PSMs bind DNA (Schwartz et al., 2016). To characterize PSM-containing biofilms, we first examined *S. aureus* SH1000 and its isogenic *psm* mutant that lacks all six PSMα- and β-encoding genes. We utilized a Congo red derivative (*E,E)*-1-fluoro-2,5-bis(3-hydroxycarbonyl-4-hydroxy) styrylbenzene (FSB) that specifically bind amyloids to study the biofilms formed by these strains. FSB was synthesized for specific detection of amyloid-β in Alzheimer's disease brain tissue with little background staining (Sato et al., 2004). When tested on *E. coli* UTI89, a uropathogenic clinical strain whose biofilm extracellular matrix is composed primarily of curli and cellulose, unlike Congo red, FSB stained curli but not the carbohydrate cellulose, supporting that FSB specifically stains amyloidogenic proteins (Reichhardt and Cegelski, 2018).

S. aureus SH1000 biofilms were grown in peptone-NaCl-glucose (PNG) media while UTI89 biofilms were grown in LB no salt as described previously, to compare amyloid staining between PSMs and curli (Schwartz et al., 2012; Tursi et al., 2020). *S. aureus* SH1000 biofilms were stained with the amyloid-specific FSB and with the nucleic-acid-specific Syto9 dye and examined with confocal microscopy. We found that FSB stained the *S. aureus* SH1000 biofilm (**Figure 1A**, left), while there was minimal visible FSB staining of the *Δpsm* mutant (**Figure 1A**, right). This small amount of staining may be due to the presence of other amyloidogenic proteins in the *S. aureus* extracellular matrix, such as additional PSMs, which were not deleted in our *Δpsm* mutant and has been shown to form amyloid fibrils *in vitro* (Zhou et al., 2021). Next *S. aureus* SH1000, its isogenic *psm* mutant, and UTI89, which expresses curli, were grown in sterile glass tubes and pellicles were stained by crystal violet. SH1000 and UTI89 formed visible pellicle biofilms, while SH1000 *Δpsm* did not (**Figure 1B**). Although SH1000 biofilms showed FSB staining throughout the biofilm (**Figure 1C**), when 3D images of SH1000 were compared to images of UTI89 biofilms, SH1000 biofilms were less compact (**Figure 1C**) and significantly thinner (**Figure 1D**), highlighting that *S. aureus* PSMs are an integral part of the biofilm structure. However, these results also suggested that although PSMs are expressed in the PNG limited media, it might not be the optimal *in vitro* conditions for PSM expression or biofilm formation.

Like curli-eDNA complexes, *S. aureus* PSMs have also been shown to bind DNA (Schwartz et al., 2016). However, unlike the net negatively charged β-sheet subunits of curli fibers, the α-helical PSMs (PSMα1-4) are amphiphiles with net positive charge (Peschel and Otto, 2013). For instance, the recently published crystal structure of the cross-α fibers formed by PSMα3 (Tayeb-Fligelman et al., 2020) indicate the positions of cationic charges along the fibrillation axis on the hydrophilic surface of the PSM fiber (**Figure 2A**). The existence of high local cationic charge densities suggest potential binding sites for dsDNA (Wong, 2006; Wong and Pollack, 2010). To visualize direct interaction of the two oppositely charged polyelectrolytes,

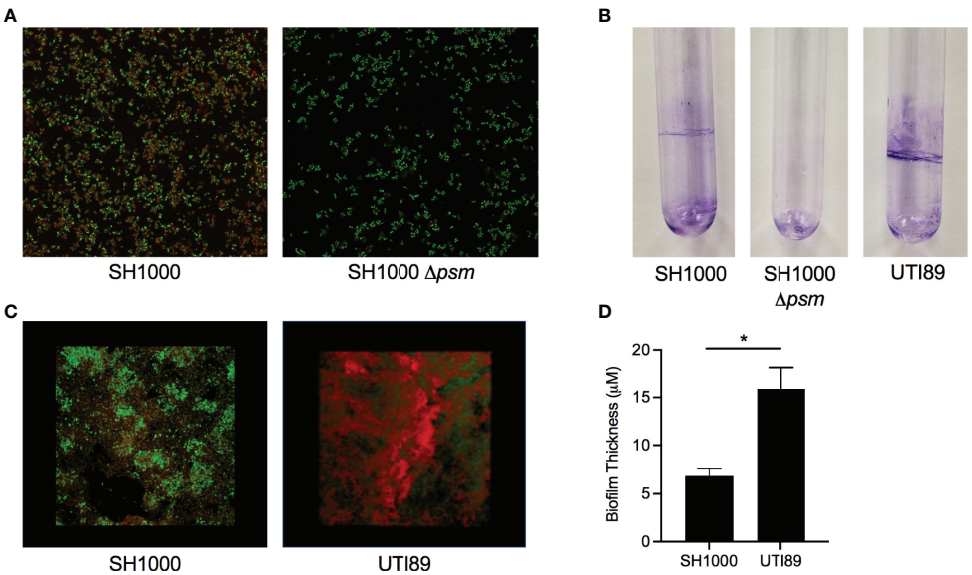

FIGURE 1 | *Staphylococcus aureus* biofilms contain amyloid that can be detected by an amyloid specific stain. **(A)** Confocal Laser Scanning Microscopy (CLSM) images of *in vitro* biofilms of *S. aureus* SH1000 (lab strain) and SH1000 phenol soluble modulin mutant (Δ*psm*) were stained with syto9 (green) and FSB (red) to determine the expression of PSM amyloids. **(B)** Crystal Violet staining of pellicle biofilms grown in glass tubes of SH1000, SH1000 Δ*psm*, and UTI89 (*E. coli* clinical isolate). **(C)** CLSM surface images of *in vitro* biofilms of *S. aureus* SH1000 and *E coli* UTI89 were stained with syto9 (green) and FSB (red). **(D)** Overall biofilm thickness of SH1000 and UTI89 biofilms as determined by Leica TCS imaging software. Mean and SEM graphed; significance was calculated using Unpaired t test (*, $P < 0.05$).

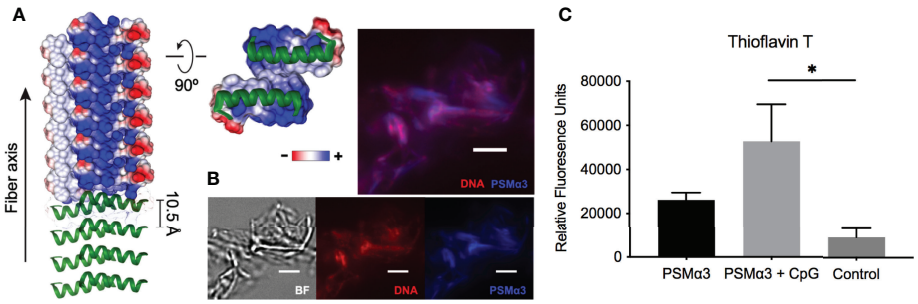

FIGURE 2 | DNA promotes PSM fibrillation *via* direct association. **(A)** Crystal structure of PSMα3 fiber (PDB: 5I55) with electric potentials of charge residues projected on surface model. The electric potentials were calculated using Chimera software. **(B)** Fluorescence staining of PSMα3-DNA complexes using nucleic acid dye BOBO-3 iodine (red) and Thioflavin T, which only binds to fibrillar amyloid structures. Scale bar: 3μm.**(C)** Fibrillization of synthetic PSMα3 with or without CpG DNA was monitored by Thioflavin T fluorescence and reported as relative fluorescent units (RFU). Mean and SEM graphed; significance was calculated using One-way ANOVA with Tukey's multiple comparisons test (*, $P < 0.05$).

we incubated synthetic PSMα3 with bacterial genomic DNA for 24 hours for fibrillation. At the end of the incubation period, the fluorescent dye Thioflavin T, which only binds to fibrillar amyloid structures, and the nucleic acid dye BOBO-3 iodide, were added to the solution for fluorescent imaging of the microscopic PSM-DNA complexes (**Figure 2B**). We observed fibrillar particles with overlapping fluorescent signal of DNA and PSM amyloid dyes that confirm their direct molecular interaction. To examine whether DNA can promote the formation of fibrillar structures (Towle et al., 2016), we incubated synthetic PSMα3 with or without CpG DNA, unmethylated oligonucleotides containing CpG motifs for TLR9 binding to simulate the unmethylated CpG-rich bacterial DNA (Bird, 1987), and monitored fibrillization by incubating with Thioflavin T. We found that PSMα3 polymerizes into a fibrillar amyloid structure to a greater extent in the presence of DNA compared to PSMα3 alone (**Figure 2C**). These results highlight the similarities of PSMs and curli: both are naturally produced in biofilm formation; both can be stained by amyloid-specific dyes; and both involve DNA in fibrilization processes.

Systemic Presence of Synthetic PSMα3-DNA Complexes Elicits an Autoantibody Response

Complexes of curli and eDNA induce anti-dsDNA and anti-chromatin autoantibody production in mouse models (Gallo et al., 2015). We therefore tested whether PSMα3 peptide, fibrillized with and without CpG DNA, would induce autoantibody responses in wild-type Balb/C or in autoimmune disease-prone NZBXW/F1 mice. Mice were injected intraperitoneally twice per week with PSMα3 alone, PSMα3 fibrillized with CpG DNA, or PBS as a negative control. Then anti-dsDNA autoantibodies were monitored in the serum compared to the highly autoimmune MRL/lpr mouse sera as a positive control. NZBXW/F1 mice treated with either PSMα3 or PSMα3-DNA showed increased production of autoantibodies compared to PBS-treated mice (**Figure 3A**). PSMα3-treated and PSMα3-DNA-treated mice produced autoantibodies as early as 1 week after the first injection (**Figure 3A**). Between weeks 4 and 5, autoantibody production appeared to plateau. The level of autoantibody production induced by PSMα3 fibrillized with

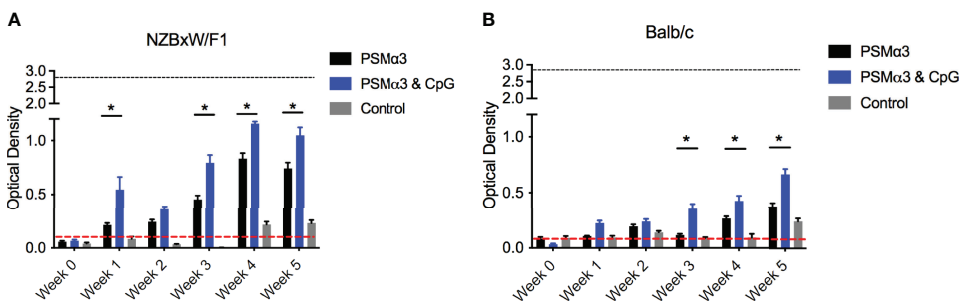

FIGURE 3 | Intraperitoneal injection of synthetic PSMα3 fibrillized with CpG DNA elicits an autoantibody response. **(A)** NZBxW/F1 or **(B)** Balb/c mice were injected bi-weekly with PSMα3 fibrillzed alone (black bar) or fibrillzed in the presence of CpG DNA (blue bar) or control mice were injected with sterile PBS (gray bar). Mice were tail bled weekly and the production of anti-dsDNA autoantibodies were detected (Optical density 650-405nm). Black dotted line represents the maximum anti-dsDNA autoantibody production of positive control sera and the red dotted line represent autoantibody detection in naïve serum. Mean and SEM graphed; significance was calculated using a 2-way ANOVA and Tukey's multiple comparisons tests (*, $P < 0.05$).

CpG DNA did not reach the level induced by MRL/lpr sera but was significantly higher than the amount produced by mice injected with PSMα3 alone. In Balb/C mice, we again observed significantly more autoantibody production upon treatment with the PSMα3-DNA complex than the mice treated with PSMα3 alone (**Figure 3B**). Although the autoantibody response in Balb/C mice was lower than in the autoimmune disease-prone mice, these data indicate that the PSMα3-DNA complex is more immunogenic than PSMα3 alone and has the capacity to elicit an autoantibody response both in wild-type mice and mice predisposed to developing autoimmunity.

S. aureus Colonized Mesh Implantation Induces Autoantibody Production

We next investigated the effect of biofilm-associated *S. aureus* infection of mice on autoantibody production. As *Staphylococcus* species can colonize surgical mesh and cause infections following surgeries in humans, we grew either *S. aureus* SH1000 or the Δ*psm* mutant under biofilm-inducing conditions on sterile surgical mesh (1x1 mm) for 48 hours at 37°C. Biofilms were stained either with amyloid specific dyes Congo red (**Figure 4A**) or FSB (**Figure 4B**). Amyloid staining was observed both with Congo red and FSB, but the *S. aureus* psm mutant did not show any staining, as expected (**Figure 4C**). To confirm that the mesh could be colonized with equal numbers of wild-type and mutant SH1000, the bacteria were recovered by sonication and enumerated on tryptic soy agar; bacterial numbers confirmed that *S. aureus* SH1000 and the Δ*psm* mutant can colonize the mesh and form biofilms that contain equal numbers of bacteria (**Figure 4F**), even though the robustness of biofilm is different due to their difference in ECM (**Figures 4A-C**).

Biofilm-associated mesh were then inserted into the back flanks of anesthetized mice similar to a catheter insertion surgery that we developed recently (Tursi et al., 2020). After implantation, sera samples were taken weekly or biweekly for 10 weeks, and anti-dsDNA autoantibodies and bacterial CFU were quantified. In NZBxW/F1 mice, implanted with the mesh carrying *S. aureus* SH1000 biofilm, autoantibodies were detected

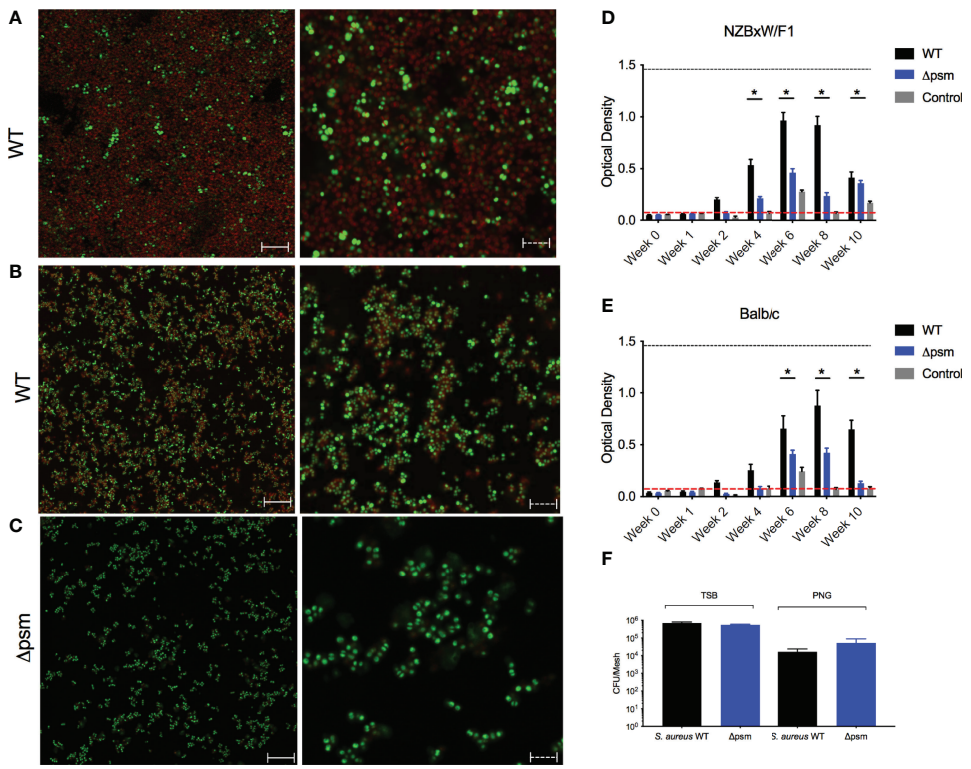

FIGURE 4 | *S. aureus*-colonized mesh implantation induces autoantibody production. To determine the expression of PSM amyloids, Confocal Laser Scanning Microscopy (CLSM) images of *in vitro* biofilms of *S. aureus* **(A)** SH1000 (WT) and **(C)** Δ*psm* SH1000 stained with syto9 (green) and Congo red (red); or **(B)** SH1000 (WT) stained with syto9 (green) and amyloid-specific dye 1-Fluoro-2,5-bis[(E)-3-carboxy-4-hydroxystyryl]benzene (FSB). Biofilms visualized at 100x, solid scale bar represents 50μM and dashed scale bar represents 5μM. *S. aureus* WT (black bars) or Δ*psm* (blue bars) biofilm-colonized mesh or control mesh was implanted subcutaneously into the back flanks of **(D)** NZBxW/F1 or **(E)** Balb/c mice. Blood was collected *via* tail bleeding every week and sampled for production of dsDNA autoantibodies (optical density 650-405nm). Black dotted line represents the maximum autoantibody production of positive control sera and the red dotted line represents autoantibody detection in naïve serum. Mean and SEM graphed; significance was calculated using a 2-way ANOVA and Tukey's multiple comparisons tests (*, $P < 0.05$). **(F)** Biofilms of *S. aureus* SH1000 wildtype (WT) (black bar) or Δ*psm* mutant (blue bars) were grown on mesh in either tryptic soy broth or peptone-based media (PNG) for 48 hours at 37°C. Biofilms were sonicated and the recovered bacteria were enumerated as colony forming units. Mean and SEM graphed; significance was calculated using a 1-way ANOVA and multiple comparisons tests. No statistical significance was determined.

at 4 weeks post-implantation (**Figure 4D**). Although anti-dsDNA antibodies were detected in NZBxW/F1 mice that had been implanted with mesh colonized with Δ*psm* (**Figure 4D**), the levels of antibodies were significantly lower, indicating the importance of the PSM component of the biofilm in production of anti-dsDNA autoantibodies. In the Balb/C mice, the response to the wild-type biofilm implant was slightly delayed relative to that in autoimmune disease-prone mice with only marginal production at 4 weeks, and the extent of anti-dsDNA antibody production was lower in mice with Δ*psm*-colonized mesh implants (**Figure 4E**). In both NZBxW/F1 and Balb/C mice, anti-dsDNA autoantibodies declined after week 8. Unlike humans, *S. aureus* cannot establish long-term infections in mice and are cleared. Analyses of blood taken from these mice showed that active infection was undetectable after 2 weeks (**Figure S1**). The results showing that anti-dsDNA autoantibodies persist in circulation, even after bacteria can no longer be detected, suggest that the immune system detects the PSM-DNA complexes on *S. aureus* biofilms and respond to the DNA.

Autoantibody Production Induced by *S. aureus*-Colonized Mesh Implants Are Dependent on TLRs

PSM-DNA complexes induced a TLR-dependent immune response *in vitro*. To confirm that the autoantibody production in response to biofilm-associated mesh depends on TLRs, we performed mesh implantation experiments in wild-type C57BL/6 mice and in mice lacking TLR2 or TLR9 or both. SH1000-colonized mesh and control sterile mesh were implanted subcutaneously in the back flanks of the mice. At week 6 after implantation with SH1000-colonized mesh, we observed significantly higher levels of autoantibodies in the wild-type mice compared to the TLR-deficient mice (**Figure 5A**). Little or no autoantibody production was detected in mice implanted with sterile mesh, and no significant differences were detected between wild-type and mutant mice at any time point (**Figure 5B**). Thus, the autoimmune responses are dependent on biofilm colonization of the mesh and are TLR-dependent.

Intraperitoneal Injection of *S. aureus* Does Not Induce Autoantibody Production

As acute staphylococcal infections are not associated with autoimmunity, we hypothesized that the longer exposure to PSM-containing *S. aureus* biofilm rather than the acute bacterial infection would drive the autoantibody response in mice. To test this, we injected Balb/C and NZBxW/F1 mice intraperitoneally with 10^7 colony-forming units (CFU) of *S. aureus* SH1000, the isogenic Δ*psm* mutant, or with PBS as a negative control, and tracked autoantibody production by analysis of mouse sera. Blood was sampled for evaluation of systemic bacteria by plating on tryptic soy agar plates. Overall bacterial numbers were low and below the detection limit in both mouse strains, indicating *S. aureus* clearance almost immediately after infection. In both Balb/C and NZBxW/F1 mice, the levels of anti-dsDNA autoantibodies were low upon injection of either strain of *S. aureus* and comparable to PBS injections (**Figures 6A, B**). Together, these data show that acute exposure to PSMs in not sufficient to generate an autoimmune response. Our previous data above showed that chronic exposure to synthetic PSMα3 in complex with DNA (**Figure 3**), or to PSM-containing *S. aureus* biofilm (**Figure 4**), induces autoantibody production, suggesting that chronic biofilm infections with *S. aureus* rather than acute bacterial infections may drive the autoantibody response in humans.

DISCUSSION

In this study, we demonstrated striking similarities between the PSMs of *S. aureus* and the well-characterized bacterial amyloid curli. Curli fibers are the major proteinaceous component of several enteric bacterial biofilms, including *E. coli* and *Salmonella*, and play a pivotal role in the three-dimensional structure of the ECM (Olsén et al., 1989; Costerton et al., 1995; Larsen et al., 2007; Hung et al., 2013; McCrate et al., 2013; Tursi and Tükel, 2018). Curli provides strength to the ECM mainly by its amyloid properties, such as resistance to enzymatic degradation and physical stress. Amyloid proteins are known

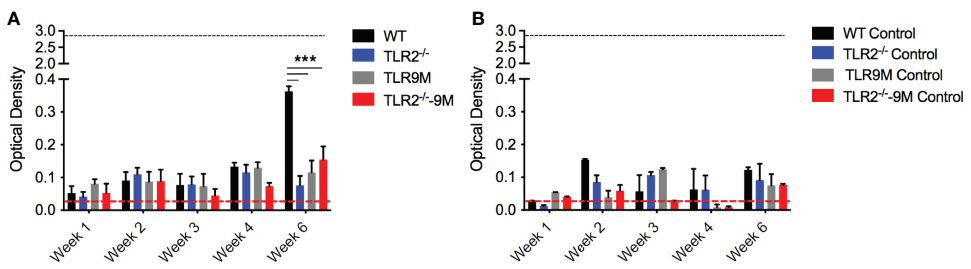

FIGURE 5 | *S. aureus*-colonized mesh implantation induces autoantibody production dependent on TLRs. **(A)** *S. aureus* WT colonized mesh or **(B)** control mesh was implanted subcutaneously into the back flanks of C57BL/6 wildtype (WT) (black bars), TLR2$^{-/-}$ (blue bars), TLR9 mutant (TLR9M) (gray bars), and TLR2$^{-/-}$-TLR9M (TLR2$^{-/-}$9M) (red bars) mice. Blood was collected *via* tail bleeding every week and sampled for production of anti-dsDNA autoantibodies (optical density 650-405nm). Black dotted line represents the maximum autoantibody production of positive control sera and the red dotted line represent autoantibody detection in naïve serum. Mean and SEM graphed; significance was calculated using a 2-way ANOVA and Tukey's multiple comparisons tests (***, $P < 0.001$).

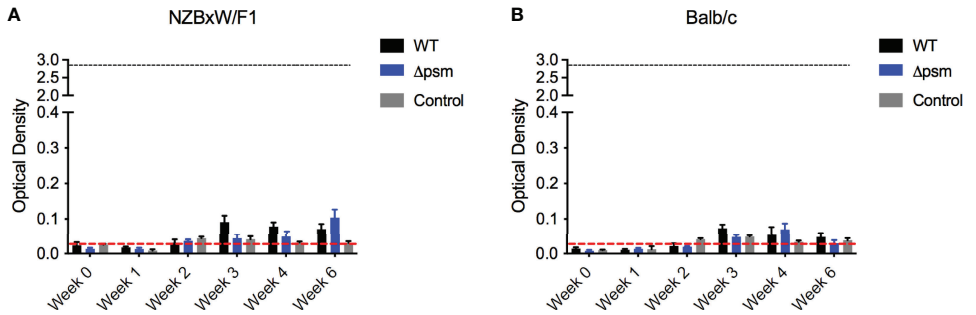

FIGURE 6 | Intraperitoneal infection with *S. aureus* wildtype SH1000 or Δ*psm* mutant does not induce autoantibody production. **(A)** NZBxW/F1 or **(B)** Balb/c mice were injected intraperitoneally with 10^7 *S. aureus* WT (black bars) or *psm* mutant (Δ*psm*) (blue bars) or PBS-injected control mice (gray bars). Serum was collected weekly to measure the levels of anti-dsDNA autoantibody production (optical density 650-405nm). Black dotted line represents the maximum autoantibody production of positive control sera and the red dotted line represent autoantibody detection in naïve serum. Mean and SEM graphed; significance was calculated using a 2-way ANOVA and Tukey's multiple comparisons tests. No statistical significance was determined.

to bind Congo red dye but recent studies have shown that other carbohydrates, like cellulose in the ECM, can also bind Congo red (Reichhardt and Cegelski, 2018). Therefore, we utilized the Congo red derivative, FSB stain, which specifically binds the amyloid component of the biofilms allowing studies on amyloids to be more specific (Sato et al., 2004; Reichhardt and Cegelski, 2018). Previous studies showed that PSMs produced by *S. aureus* form curli-like amyloid structures (Schwartz et al., 2012; Schwartz et al., 2016). However, the studies on PSMs have been controversial, as these proteins play multiple functions during the lifestyle of *Staphylococcus* species and within their biofilms. In this study, we determined that when, wild-type *S. aureus* SH1000 biofilms are grown in PNG media, unlike traditional biofilms formed by *S. aureus*, SH1000 formed visible pellicles at the air-liquid interphase, while the Δ*psm* mutant did not (**Figure 1B**). PSMs also stained with the amyloid-specific FSB stain, similar to the *E. coli* UTI89 strain that expresses curli (**Figures 1A, C**). However, the biofilms formed by *S. aureus* SH1000 were not as robust as *E. coli* UTI89, indicating differences in biofilm architecture between PSM-containing and curli-containing biofilms.

Both curli and PSMs bind DNA in the ECM (Gallo et al., 2015; Schwartz et al., 2016; Towle et al., 2016; Tayeb-Fligelman et al., 2017). The periodicity of cationic helical subunits along the PSMα3 cross-α amyloid fibers (Tayeb-Fligelman et al., 2020) present a cationic scaffold for interaction with the highly negatively charged DNA (**Figure 2A**), cognate to recent characterization of protofibrils formed by cationic amphiphilic antimicrobial peptides when complexed with DNA (Lee et al., 2020). Previous studies have determined that bacterial DNA promotes polymerization of curli. Consistent with these findings, synthetic PSMα3 formed increased fibrillar structures in the presence of DNA (**Figures 2B, C**). These results support the hypothesis that PSMs act as amyloids, with a critical role in biofilm formation and the extracellular matrix of *S. aureus* biofilms (Schwartz et al., 2012; Schwartz et al., 2016).

There is evidence that infectious agents can trigger gut or systemic autoimmune diseases as well as autoimmune disease flares. Although controversial, bacterial biofilms on implanted devices, such as surgical mesh, have been implicated in coercion of the immune system into breaking tolerance and inducing autoimmune diseases (Chughtai et al., 2017a; Chughtai et al., 2017b; Clancy et al., 2019; Strietzel et al., 2019). Many bacteria that colonize implanted devices have the capacity to produce amyloids (Nicastro and Tükel, 2019). Recent work showed the presence of multiple-species biofilms containing staphylococcal species on implanted mesh (Kathju et al., 2015; Langbach et al., 2016; Le et al., 2019). *In vivo* intraperitoneal injection of PSMα3, with and without DNA, or subcutaneous implantation of SH1000 *S. aureus* biofilms grown on mesh, and not the Δ*psm* mutant biofilms, induced a significant anti-dsDNA autoantibody response, especially in autoimmune-prone mice (**Figures 3**, **4**). This response was TLR-dependent, with WT mice producing a significant autoantibody response while there was no significant response in TLR2- and TLR9-deficient mice (**Figure 5**). Though we did not test TLR-dependence in autoimmune-prone mice, we would expect similarly accelerated autoantibody response to mesh implantation, which would be ameliorated in TLR-deficient mice, but this requires further testing to determine if TLRs are the only receptors responsible when other risk factors for autoimmunity are present. Meanwhile intraperitoneal injection of planktonic *S. aureus*, regardless of PSMs, did not provoke an autoantibody response (**Figure 6**), emphasizing that only chronic biofilm infections containing PSMs induce such a response.

For the first time, we have observed that even without DNA, fibrillar PSMα3 alone was able to induce low levels of anti-dsDNA autoantibodies. As it was previously reported that PSMα3 is cytotoxic to immune cells (Wang et al., 2007; Cheung et al., 2014; Laabei et al., 2014; Tayeb-Fligelman et al., 2017), the autoimmune response generated following systemic injections of mice with only PSMα3 could be due to the formation of complexes of PSMα3 with eukaryotic DNA released from the lysed cells. It is also plausible that PSMs form cytotoxic intermediate fibrils, like those of curli which were recently reported to occur during the early stages of biofilm

formation (Nicastro et al., 2019). At the same time, it is unlikely that the presence of CpG DNA alone induced the autoantibody response: previous studies have shown that BALB/C mice or C57BL/6-*lpr/lpr* mice immunized with CpG DNA alone did not produce anti-dsDNA autoantibodies, but instead CpG DNA worked as an adjuvant to enhance the immune response by stimulating TLR9 (Tran et al., 2003; Lartigue et al., 2006).

Overall, the anti-dsDNA autoantibody levels in these experiments were relatively low compared to what was observed in response to curli-DNA complexes (Gallo et al., 2015; Tursi et al., 2017; Miller et al., 2020). We noted the rapid clearing of *S. aureus* in our model (**Supplementary Figure 1**), which could lead to the observed decrease in anti-dsDNA autoantibodies. It is our expectation that chronic exposure to *Staphylococcus* species that can form robust biofilms, with high loads of PSMs and DNA in their ECM, could break tolerance and generate stronger and sustained autoimmune response. Together, these results corroborate studies suggesting a pro-inflammatory role of PSMs (Wang et al., 2007; Syed et al., 2015; Nakagawa et al., 2017), which appears to be TLR-dependent (Hajjar et al., 2001; Hanzelmann et al., 2016; Schlatterer et al., 2018), and similar to curli, associated with the generation of a type I IFN and autoimmune response (Gallo et al., 2015; Tursi et al., 2017), though the exact mechanism remains to be determined.

Despite the similarities observed between curli and PSMα3 in the *in vitro* and *in vivo* experiments performed in this study, it is important to note that literature remains controversial on the topic of whether the amyloidogenic properties of PSMs are indeed critical and play a multi-functional role in *S. aureus* biofilms. Several studies contest that rather than forming the structure of the extracellular matrix, like curli does for *E. coli*, PSMs are responsible for dispersal of the biofilm and dissemination to other areas (Kong et al., 2006; Otto, 2008; Dastgheyb et al., 2015). A role for PSM amyloids was also implicated in creating the characteristic channels in mature *S. aureus* biofilms that allow nutrient distribution to the deeper regions of the biofilm, and in regulating the dynamic waves of detachment and systemic spread from mature biofilms by acting as surfactants to break up the extracellular matrix (Periasamy et al., 2012; Le et al., 2014). One such study acknowledges the amyloidogenic properties of PSMs *in vitro*, but noted that there appears to be no correlation between the amyloidogenicity of PSMs and their role in biofilm extracellular matrix structure nor inflammatory response (Zheng et al., 2018). We find that this is not inconsistent with our expectations: given that DNA and PSMα3 self-assemble into an electrostatic complex, their structure and stability can be influenced by solution conditions, as will their downstream inflammatory capacity. This contention is echoed in studies by both groups (Schwartz et al., 2012; Schwartz et al., 2016; Zheng et al., 2018), where formation of PSM amyloids were highly condition-specific. What's more, it is already known that PSMs are significantly regulated by quorum-sensing (Kong et al., 2006; Boles and Horswill, 2008; Le et al., 2014), so it is possible that *in vivo* in different tissues or niches, PSMs serve multiple purposes, which may be regulated by both their expression level and structure as soluble peptides that act as surfactants or as amyloid aggregates which contribute to biofilm structure.

In summary, we have demonstrated a significant correlation between PSMs in *S. aureus* biofilms and anti-dsDNA autoantibody production, a marker of autoimmunity, in mice. *Staphylococcus epidermidis* is the most common implant-associated infection; this strain is a skin commensal, but becomes an opportunistic pathogen when introduced systemically *via* indwelling devices (Otto, 2009). PSMs have also been shown to play major roles in *S. epidermidis*, similar to that seen in *S. aureus*, including pro-inflammatory functions and biofilm dispersal and structure (Mehlin et al., 1999; Wang et al., 2011). One study suggests that PSMs in *S. epidermidis* do not form amyloid structures like those in *S. aureus* but remain important for overall biofilm maturation and architecture (Le et al., 2019). Future experiments are needed to determine if there are stages during *in vivo* biofilm formation with increased amyloid PSM-DNA complexes, that can subsequently induce autoantibody responses, to resolve the role of PSM amyloidogenicity in *Staphylococcus* biofilm-associated inflammation and autoimmune disease. Alternatively, PSMs dislodging from the biofilm could be sufficient to stimulate the immune cells to create an autoinflammatory environment. Further epidemiological studies on the association between different *Staphylococcus* strains, their PSM levels and structures, and autoimmune sequelae, are needed to fully elucidate the contribution of PSMs and their mechanism of pathogenicity. Should we find that PSMs function similar to curli as critical components of *S. aureus* and/or *S. epidermidis* biofilms, therapies targeting amyloids may be pursued in order to treat these notoriously antibiotic-resistant infections.

MATERIALS AND METHODS

Bacterial Strains and Culture Conditions

The *S. aureus* SH1000 and the Δ*psm* mutant strain were described previously (Schwartz et al., 2016). Uropathogenic *E. coli* UTI89 (isolated from a patient with an acute bladder infection) was kindly provided by Dr. Scott Hultgren from Washington University in St. Louis. Overnight cultures of SH1000 and the Δ*psm* mutant were grown in tryptic soy broth at 37°C with shaking at 200 rpm; *S.* Typhimurium IR715 *msbB* mutant was previously described (Raffatellu et al., 2005) and was grown in LB broth supplemented with 100 μg/mL kanamycin at 37°C with shaking at 200 rpm; and *E. coli* UTI89 was grown in LB broth at 37°C with shaking at 200 rpm.

Biofilm Growth Analysis by Confocal Microscopy

Biofilms of *S. aureus* SH1000, the isogenic Δ*psm* mutant, or *E. coli* UTI89 were grown on sterile glass circular coverslips or on medical mesh by diluting overnight cultures 1:100 in PNG media for *S. aureus* strains, or LB low salt media for UTI89, for 48 hours at 37°C (Schwartz et al., 2012; Tursi et al., 2020). To visualize

PSM in biofilms, coverslips were washed three times with sterile PBS and stained with 3 μg/mL Syto9 (ThermoFisher, S34854) for 10 minutes in the dark. Biofilms were then gently washed three times with sterile PBS and stained with 12.5 μM FSB (Millipore, 07602) or 10 ug/m Congo red (Sigma Aldrich, HT60-1KT) for an additional 10 minutes. Coverslips were placed upside down in 8-well Multi-test Slides (MP Biomedicals, 096040805E) with 3 μl Vectashield (Vector Labs, H-1000) between the coverslip and slide to prevent photo-bleaching. Syto9 was visualized with excitation at 483 nm and emission of 503 nm, FSB was visualized with excitation at 390 nm and emission of 511 nm, and Congo red was visualized with excitation at 561 nm and an emission of 650-750nm using a Leica TCS confocal imaging system at 63x magnification. Biofilm thickness was measured on Leica TCS imaging software.

Crystal Violet Staining of Biofilms

Pellicle biofilms were grown and stained with crystal violet as previously described (Schwartz et al., 2012). Briefly, overnight cultures of *S. aureus* SH1000, SH1000 Δ*psm* mutant, and *E. coli* UTI89 were diluted 1:100 into 3 mL of PNG media for *S. aureus* strains or LB low salt media for UTI89 and biofilms were grown in sterile glass tubes for 48 hours at 37°C with shaking at 200 rpm. Pellicle biofilms formed at the air-liquid interface and were washed with 10 mL ddH_2O with or without 1% SDS, vortexed briefly, and then stained with 0.1% crystal violet. Tubes were gently washed with ddH_2O and then photographed.

Isolation of Curli

Biofilms of *S.* Typhimurium were grown by diluting overnight cultures 1:100 in YESCA broth supplemented with 4% DMSO to enhance curli formation as previously described (Lim et al., 2012). Cultures were grown at 26°C for 72 hours with shaking at 200 rpm. Curli was isolated from biofilms as previously described (Collinson et al., 1999).

Calculation of Electrostatic Potentials on PSMα3 Fibrils

The cross-α crystal structure of PSMα3 amyloid fibril was downloaded from RCSB Protein Data Bank (PDB: 5I55). The electrostatic potential surface values were calculated using UCSF Chimera software (Pettersen et al., 2004). The values are calculated according to Coulomb's law with dielectric constant of 80 and a distance-dependent dielectric.

Fluorescence Visualization of PSM-DNA Complexes

Synthetic PSMα3 peptide (MEFVAKLFKFFKDLLGKFLGNN) was purchased from LifeTein. PSMα3 (10 mg/ml) was fibrillized in the presence of *Escherichia coli* genomic DNA (ThermoScientific, J14380.MA) at a charge ratio of 2:1 (5 mg/ml). The solution was incubated at room temperature overnight with shaking. After the incubation period, Thioflavin T (Sigma, T3516) and BOBO-3 Iodine (ThermoScientific, B3586) dyes were added to the solution for fiber amyloid and DNA staining, at final concentration of 10 μM and 6 μM respectively. The complexes were imaged using an Andor Neo sCMOS camera with Andor IQ software on an Olympus IX83 microscope equipped with a 100x oil objective and Zero Drift Correction 2 continuous autofocus system (pixel resolution of 0.065 μm/pixel). BOBO-3 Iodine DNA staining was visualized with Lambda LS (Sutter Instrument) xenon arc lamp and a red fluorescent protein (RFP) filter, excitation at 553 nm and emission at 574 nm, with an exposure of 500ms; Thioflavin T PSMα3 amyloid stain was visualized using a cyan fluorescent protein (CFP) filter, excitation at 433 nm and emission at 475 nm, with an exposure of 250ms.

Synthetic PSMα3 Fibrillization

Synthetic PSMα3 peptide (MEFVAKLFKFFKDLLGKFLGNN) was purchased from Biosynthesis. PSMα3 (2.5 μg/ml) was fibrillized in the presence or absence of CpG DNA (*In vivo*gen, ODN 1826) at a charge ratio of 20. Fibrillization was monitored in the presence of 10 μM Thioflavin T (Sigma, T3516) for 10 minutes protected from light. The relative fluorescent units (RFU) were detected (excitation 440 nm/emission 490 nm) using a BMG Labtech POLARstar Omega plater reader.

Intraperitoneal Injection of Mice With Amyloid or Bacteria

NZBWF1/J (Jackson Labs, stock no: 100008) or Balb/cJ (Jackson Labs, stock no: 000651) mice, 6-8 weeks of age, were injected intraperitoneally with 50 μg of synthetic PSMα3 or PSMα3-DNA complexes twice weekly. Alternatively, mice were injected with 10^7 *S. aureus* SH1000 or Δ*psm* mutant strains. Controls were injected intraperitoneally with 50 μL of sterile PBS. Blood was sampled weekly. Serum was collected by incubating blood for 30 minutes at 37°C and then centrifugation at 6000 rpm for 10 minutes. When applicable, 50 μl of blood was plated on tryptic soy agar to enumerate bacteria.

Quantification of Bacteria on *S. aureus*-Colonized Mesh

Biofilms of *S. aureus* SH1000 and the Δ*psm* mutant grown on mesh in either tryptic soy broth or PNG were washed three times with sterile PBS to remove planktonic bacteria. Mesh were then placed in a sterile tube containing 3 ml PBS and sonicated for three intervals of 30 seconds at 30% amplitude. Prior experiments ensured that this sonication procedure did not kill the bacteria. Serial dilutions were used to enumerate bacteria released from the mesh.

Mesh Insertion Into Mice

C57BL/6 wild-type or TLR-deficient mice were anesthetized with 2-4% isoflurane. The hair on the back flanks of the mice was removed. After sterilization of the site, a small incision was made using a scalpel. A 1 mm x 1 mm piece of mesh (sterile or colonized with biofilm) was inserted by creating a subcutaneous tunnel on the back flank. The incision was closed using a simple interrupted suture.

Anti-dsDNA Autoantibody ELISA

The ELISA to quantify anti-dsDNA antibodies was performed as previously described (Gallo et al., 2015). Briefly, a 96-well plate (Costar, 07-200-33) was coated with 0.01% poly-L-lysine (Sigma,

P8920) in PBS for 1 hour at room temperature. After coating, the plate was washed three times with distilled water. The plate was coated with 2.5 μg/mL calf thymus DNA (Invitrogen, 15633–019) in borate buffered saline (BBS; 17.5 g NaCl, 2.5 g H_3BO_3, 38.1 g sodium borate in 1 L H_2O) and stored overnight at 4°C. The plate was washed three times with BBS and blocked with BBS containing 3% BSA and 1% Tween20 for 2 hours at room temperature. After washing five times with BBS, the plate was incubated with serial dilutions of control serum, naïve serum, or serum samples overnight at 4°C. After washing, biotinylated goat anti-mouse IgG (Jackson ImmunoResearch, 115-065-071) was added, and samples were incubated at room temperature for 2 hours with gentle rocking, and then incubated with avidin-alkaline phosphate conjugate (Sigma, A7294) at room temperature for 2 hours. Finally, the plate was washed five times with BBS and then incubated with 4-nitrophenyl phosphate disodium salt hexahydrate (Sigma-Aldrich, N2765) at a concentration of 1 mg/mL at room temperature protected from light. Optical densities were read using ELISA plate reader at 650 nm and 405 nm using a Molecular Devices Microplate Reader. Serum of a 6-to 8-week-old C57BL/6 mouse with no evidence of autoimmunity was used as a negative control for autoantibody production. As a positive control, serum from an MRL/lpr lupus-prone mouse, previously shown to have high levels of autoantibodies, diluted 1:250 in BBS, was used. All the samples shown in each figure were tested in the same ELISA assay, and the result are shown as raw optical density (O.D.).

Statistical Analyses

Data were analyzed using GraphPad Prism software. One-way or two-way ANOVA with *post-hoc* Tukey multiple comparison tests were used as appropriate. The p values <0.05 were considered significant. *$p < 0.05$, ** $p < 0.01$, ***$p < 0.001$, and ****$p < 0.0001$ were marked in the figures.

DATA AVAILABILITY STATEMENT

The original contributions presented in the study are included in the article/**Supplementary Material**. Further inquiries can be directed to the corresponding author.

ETHICS STATEMENT

The animal study was reviewed and approved by Institutional Animal Care and Use Committee at Temple University Lewis Katz School of Medicine.

AUTHOR CONTRIBUTIONS

All authors listed have made a substantial, direct, and intellectual contribution to the work and approved it for publication.

FUNDING

CT is supported by NIH grants AI153325, AI151893, and AI148770. GW, JDA, EYL are supported by NSF DMR 1808459 and NIH R37 AI052453. JA is supported by NSF Graduate Research Fellowship Program DGE-1650604. EL acknowledges support from the Systems and Integrative Biology Training Program (NIH T32GM008185), the Medical Scientist Training Program (NIH T32GM008042) and the Dermatology Scientist Training Program (NIH T32AR071307) at the University of California, Los Angeles. EL also acknowledges an Early Career Research Grant from the National Psoriasis Foundation. Molecular graphics and analyses performed with UCSF Chimera, developed by the Resource for Biocomputing, Visualization, and Informatics at the University of California, San Francisco, with support from NIH P41-GM103311.

SUPPLEMENTARY MATERIAL

The Supplementary Material for this article can be found online at: https://www.frontiersin.org/articles/10.3389/fcimb.2022.884065/full#supplementary-material

Supplementary Figure 1 | Blood sampled from **(A)** NZBxW/F1 or **(B)** Balb/c mice implanted with *S. aureus* WT (black bars), Δ*psm* (blue bars) biofilm colonized mesh or control mesh (gray bars) was plated on tryptic soy agar and enumerated as colony forming units (CFU) per ml of blood. Mean and SEM graphed, two-way ANOVA using multiple comparisons used to determine significance. No statistical significance was determined.

REFERENCES

Bird, A. P. (1987). CpG Islands as Gene Markers in the Vertebrate Nucleus. *Trends Genet.* 3, 342–347. doi: 10.1016/0168-9525(87)90294-0

Boles, B. R., and Horswill, A. R. (2008). Agr-Mediated Dispersal of Staphylococcus Aureus Biofilms. *PloS Pathog.* 4, e1000052. doi: 10.1371/journal.ppat.1000052

Carter, J. D., and Hudson, A. P. (2009). Reactive Arthritis: Clinical Aspects and Medical Management. *Rheum. Dis. Clin. North Am.* 35, 21–44. doi: 10.1016/j.rdc.2009.03.010

Ceccarelli, F., Perricone, C., Olivieri, G., Cipriano, E., Spinelli, F. R., Valesini, G., et al. (2019). Staphylococcus Aureus Nasal Carriage and Autoimmune Diseases: From Pathogenic Mechanisms to Disease Susceptibility and Phenotype. *Int. J. Mol. Sci.* 20, E5624. doi: 10.3390/ijms20225624

Chapman, M. R., Robinson, L. S., Pinkner, J. S., Roth, R., Heuser, J., Hammar, M., et al. (2002). Role of Escherichia Coli Curli Operons in Directing Amyloid Fiber Formation. *Science* 295, 851–855. doi: 10.1126/science.1067484

Cheng, N., He, R., Tian, J., Ye, P. P., and Ye, R. D. (2008). Cutting Edge: TLR2 Is a Functional Receptor for Acute-Phase Serum Amyloid A. *J. Immunol.* 181, 22–26. doi: 10.4049/jimmunol.181.1.22

Chen, M., Zhou, H., Cheng, N., Qian, F., and Ye, R. D. (2014). Serum Amyloid A1 Isoforms Display Different Efficacy at Toll-Like Receptor 2 and Formyl Peptide Receptor 2. *Immunobiology* 219, 916–923. doi: 10.1016/j.imbio.2014.08.002

Cheung, G. Y. C., Kretschmer, D., Queck, S. Y., Joo, H.-S., Wang, R., Duong, A. C., et al. (2014). Insight Into Structure-Function Relationship in Phenol-Soluble Modulins Using an Alanine Screen of the Phenol-Soluble Modulin (PSM) α3 Peptide. *FASEB J.* 28, 153–161. doi: 10.1096/fj.13-232041

Chiti, F., and Dobson, C. M. (2006). Protein Misfolding, Functional Amyloid, and Human Disease. *Annu. Rev. Biochem.* 75, 333–366. doi: 10.1146/annurev.biochem.75.101304.123901

Chughtai, B., Sedrakyan, A., Mao, J., Eilber, K. S., Anger, J. T., and Clemens, J. Q. (2017a). Is Vaginal Mesh a Stimulus of Autoimmune Disease? *Am. J. Obstet. Gynecol.* 216, 495.e1–495.e7. doi: 10.1016/j.ajog.2016.12.021

Chughtai, B., Thomas, D., Mao, J., Eilber, K., Anger, J., Clemens, J. Q., et al. (2017b). Hernia Repair With Polypropylene Mesh Is Not Associated With an Increased Risk of Autoimmune Disease in Adult Men. *Hernia* 21, 637–642. doi: 10.1007/s10029-017-1591-1

Clancy, C., Jordan, P., and Ridgway, P. F. (2019). Polypropylene Mesh and Systemic Side Effects in Inguinal Hernia Repair: Current Evidence. *Ir. J. Med. Sci.* 188, 1349–1356. doi: 10.1007/s11845-019-02008-5

Collinson, S. K., Parker, J. M., Hodges, R. S., and Kay, W. W. (1999). Structural Predictions of AgfA, the Insoluble Fimbrial Subunit of Salmonella Thin Aggregative Fimbriae. *J. Mol. Biol.* 290, 741–756. doi: 10.1006/jmbi.1999.2882

Conti, F., Ceccarelli, F., Iaiani, G., Perricone, C., Giordano, A., Amori, L., et al. (2016). Association Between Staphylococcus Aureus Nasal Carriage and Disease Phenotype in Patients Affected by Systemic Lupus Erythematosus. *Arthritis Res. Ther.* 18, 177. doi: 10.1186/s13075-016-1079-x

Costerton, J. W., Lewandowski, Z., Caldwell, D. E., Korber, D. R., and Lappin-Scott, H. M. (1995). Microbial Biofilms. *Annu. Rev. Microbiol.* 49, 711–745. doi: 10.1146/annurev.mi.49.100195.003431

Dastgheyb, S. S., Villaruz, A. E., Le, K. Y., Tan, V. Y., Duong, A. C., Chatterjee, S. S., et al. (2015). Role of Phenol-Soluble Modulins in Formation of Staphylococcus Aureus Biofilms in Synovial Fluid. *Infect. Immun.* 83, 2966–2975. doi: 10.1128/IAI.00394-15

Fernández Guerrero, M. L., González López, J. J., Goyenechea, A., Fraile, J., and de Górgolas, M. (2009). Endocarditis Caused by Staphylococcus Aureus: A Reappraisal of the Epidemiologic, Clinical, and Pathologic Manifestations With Analysis of Factors Determining Outcome. *Med. (Baltimore)* 88, 1–22. doi: 10.1097/MD.0b013e318194da65

Gallo, P. M., Rapsinski, G. J., Wilson, R. P., Oppong, G. O., Sriram, U., Goulian, M., et al. (2015). Amyloid-DNA Composites of Bacterial Biofilms Stimulate Autoimmunity. *Immunity* 42, 1171–1184. doi: 10.1016/j.immuni.2015.06.002

Ghosh, U., Thurber, K. R., Yau, W.-M., and Tycko, R. (2021). Molecular Structure of a Prevalent Amyloid-β Fibril Polymorph From Alzheimer's Disease Brain Tissue. *Proc. Natl. Acad. Sci.* 118, e2023089118. doi: 10.1073/pnas.2023089118

Hajjar, A. M., O'Mahony, D. S., Ozinsky, A., Underhill, D. M., Aderem, A., Klebanoff, S. J., et al. (2001). Cutting Edge: Functional Interactions Between Toll-Like Receptor (TLR) 2 and TLR1 or TLR6 in Response to Phenol-Soluble Modulin. *J. Immunol.* 166, 15–19. doi: 10.4049/jimmunol.166.1.15

Hanzelmann, D., Joo, H.-S., Franz-Wachtel, M., Hertlein, T., Stevanovic, S., Macek, B., et al. (2016). Toll-Like Receptor 2 Activation Depends on Lipopeptide Shedding by Bacterial Surfactants. *Nat. Commun.* 7, 12304. doi: 10.1038/ncomms12304

He, R. L., Zhou, J., Hanson, C. Z., Chen, J., Cheng, N., and Ye, R. D. (2009). Serum Amyloid A Induces G-CSF Expression and Neutrophilia *via* Toll-Like Receptor 2. *Blood* 113, 429–437. doi: 10.1182/blood-2008-03-139923

Hung, C., Zhou, Y., Pinkner, J. S., Dodson, K. W., Crowley, J. R., Heuser, J., et al. (2013). Escherichia Coli Biofilms Have an Organized and Complex Extracellular Matrix Structure. *mBio* 4, e00645-00613. doi: 10.1128/mBio.00645-13

Kathju, S., Nistico, L., Melton-Kreft, R., Lasko, L.-A., and Stoodley, P. (2015). Direct Demonstration of Bacterial Biofilms on Prosthetic Mesh After Ventral Herniorrhaphy. *Surg. Infect. (Larchmt)* 16, 45–53. doi: 10.1089/sur.2014.026

Kikuchi, T., Mizunoe, Y., Takade, A., Naito, S., and Yoshida, S. (2005). Curli Fibers are Required for Development of Biofilm Architecture in Escherichia Coli K-12 and Enhance Bacterial Adherence to Human Uroepithelial Cells. *Microbiol. Immunol.* 49, 875–884. doi: 10.1111/j.1348-0421.2005.tb03678.x

Kong, K.-F., Vuong, C., and Otto, M. (2006). Staphylococcus Quorum Sensing in Biofilm Formation and Infection. *Int. J. Med. Microbiol.* 296, 133–139. doi: 10.1016/j.ijmm.2006.01.042

Kretschmer, D., Gleske, A.-K., Rautenberg, M., Wang, R., Köberle, M., Bohn, E., et al. (2010). Human Formyl Peptide Receptor 2 Senses Highly Pathogenic Staphylococcus Aureus. *Cell Host Microbe* 7, 463–473. doi: 10.1016/j.chom.2010.05.012

Kretschmer, D., Nikola, N., Dürr, M., Otto, M., and Peschel, A. (2012). The Virulence Regulator Agr Controls the Staphylococcal Capacity to Activate Human Neutrophils *via* the Formyl Peptide Receptor 2. *J. Innate Immun.* 4, 201–212. doi: 10.1159/000332142

Laabei, M., Jamieson, W. D., Yang, Y., van den Elsen, J., and Jenkins, A. T. A. (2014). Investigating the Lytic Activity and Structural Properties of Staphylococcus Aureus Phenol Soluble Modulin (PSM) Peptide Toxins. *Biochim. Biophys. Acta* 1838, 3153–3161. doi: 10.1016/j.bbamem.2014.08.026

Langbach, O., Kristoffersen, A. K., Abesha-Belay, E., Enersen, M., Røkke, O., and Olsen, I. (2016). Oral, Intestinal, and Skin Bacteria in Ventral Hernia Mesh Implants. *J. Oral. Microbiol.* 8, 31854. doi: 10.3402/jom.v8.31854

Larsen, P., Nielsen, J. L., Dueholm, M. S., Wetzel, R., Otzen, D., and Nielsen, P. H. (2007). Amyloid Adhesins Are Abundant in Natural Biofilms. *Environ. Microbiol.* 9, 3077–3090. doi: 10.1111/j.1462-2920.2007.01418.x

Lartigue, A., Courville, P., Auquit, I., François, A., Arnoult, C., Tron, F., et al. (2006). Role of TLR9 in Anti-Nucleosome and Anti-DNA Antibody Production in Lpr Mutation-Induced Murine Lupus. *J. Immunol.* 177, 1349–1354. doi: 10.4049/jimmunol.177.2.1349

Le, K. Y., Dastgheyb, S., Ho, T. V., and Otto, M. (2014). Molecular Determinants of Staphylococcal Biofilm Dispersal and Structuring. *Front. Cell Infect. Microbiol.* 4, 167. doi: 10.3389/fcimb.2014.00167

Lee, E. Y., Srinivasan, Y., de Anda, J., Nicastro, L. K., Tükel, Ç., and Wong, G. C. L. (2020). Functional Reciprocity of Amyloids and Antimicrobial Peptides: Rethinking the Role of Supramolecular Assembly in Host Defense, Immune Activation, and Inflammation. *Front. Immunol.* 11, 1629. doi: 10.3389/fimmu.2020.01629

Le, K. Y., Villaruz, A. E., Zheng, Y., He, L., Fisher, E. L., Nguyen, T. H., et al. (2019). Role of Phenol-Soluble Modulins in Staphylococcus Epidermidis Biofilm Formation and Infection of Indwelling Medical Devices. *J. Mol. Biol.* 431, 3015–3027. doi: 10.1016/j.jmb.2019.03.030

Lim, J. Y., May, J. M., and Cegelski, L. (2012). Dimethyl Sulfoxide and Ethanol Elicit Increased Amyloid Biogenesis and Amyloid-Integrated Biofilm Formation in Escherichia Coli. *Appl. Environ. Microbiol.* 78, 3369–3378. doi: 10.1128/AEM.07743-11

McCrate, O. A., Zhou, X., Reichhardt, C., and Cegelski, L. (2013). Sum of the Parts: Composition and Architecture of the Bacterial Extracellular Matrix. *J. Mol. Biol.* 425, 4286–4294. doi: 10.1016/j.jmb.2013.06.022

Mehlin, C., Headley, C. M., and Klebanoff, S. J. (1999). An Inflammatory Polypeptide Complex From Staphylococcus Epidermidis: Isolation and Characterization. *J. Exp. Med.* 189, 907–918. doi: 10.1084/jem.189.6.907

Michelitsch, M. D., and Weissman, J. S. (2000). A Census of Glutamine/Asparagine-Rich Regions: Implications for Their Conserved Function and the Prediction of Novel Prions. *Proc. Natl. Acad. Sci. U S A.* 97, 11910–11915. doi: 10.1073/pnas.97.22.11910

Miller, A. L., Pasternak, J. A., Medeiros, N. J., Nicastro, L. K., Tursi, S. A., Hansen, E. G., et al. (2020). *In Vivo* Synthesis of Bacterial Amyloid Curli Contributes to Joint Inflammation During S. Typhimurium Infection. *PloS Pathog.* 16, e1008591. doi: 10.1371/journal.ppat.1008591

Nakagawa, S., Matsumoto, M., Katayama, Y., Oguma, R., Wakabayashi, S., Nygaard, T., et al. (2017). Staphylococcus Aureus Virulent Psmα Peptides Induce Keratinocyte Alarmin Release to Orchestrate IL-17-Dependent Skin Inflammation. *Cell Host Microbe* 22, 667–677.e5. doi: 10.1016/j.chom.2017.10.008

Nicastro, L., and Tükel, Ç. (2019). Bacterial Amyloids: The Link Between Bacterial Infections and Autoimmunity. *Trends Microbiol.* 27, 954–963. doi: 10.1016/j.tim.2019.07.002

Nicastro, L. K., Tursi, S. A., Le, L. S., Miller, A. L., Efimov, A., Buttaro, B., et al. (2019). Cytotoxic Curli Intermediates Form During Salmonella Biofilm Development. *J. Bacteriol.* 201 (18), e00095–19. doi: 10.1128/JB.00095-19

Olsén, A., Jonsson, A., and Normark, S. (1989). Fibronectin Binding Mediated by a Novel Class of Surface Organelles on Escherichia Coli. *Nature* 338, 652–655. doi: 10.1038/338652a0

Olson, M. E., and Horswill, A. R. (2013). Staphylococcus Aureus Osteomyelitis: Bad to the Bone. *Cell Host Microbe* 13, 629–631. doi: 10.1016/j.chom.2013.05.015

Otto, M. (2008). Staphylococcal Biofilms. *Curr. Top. Microbiol. Immunol.* 322, 207–228. doi: 10.1007/978-3-540-75418-3_10

Otto, M. (2009). Staphylococcus Epidermidis – the "Accidental" Pathogen. *Nat. Rev. Microbiol.* 7, 555–567. doi: 10.1038/nrmicro2182

Pachucki, R. J., Corradetti, C., Kohler, L., Ghadiali, J., Gallo, P. M., Nicastro, L., et al. (2020). Persistent Bacteriuria and Antibodies Recognizing Curli/eDNA Complexes From Escherichia Coli Are Linked to Flares in Systemic Lupus Erythematosus. *Arthritis Rheumatol.* 72, 1872–1881. doi: 10.1002/art.41400

Periasamy, S., Joo, H.-S., Duong, A. C., Bach, T.-H. L., Tan, V. Y., Chatterjee, S. S., et al. (2012). How Staphylococcus Aureus Biofilms Develop Their Characteristic Structure. *Proc. Natl. Acad. Sci. U S A.* 109, 1281–1286. doi: 10.1073/pnas.1115006109

Peschel, A., and Otto, M. (2013). Phenol-Soluble Modulins and Staphylococcal Infection. *Nat. Rev. Microbiol.* 11, 667–673. doi: 10.1038/nrmicro3110

Petri, M. (1998). Infection in Systemic Lupus Erythematosus. *Rheum. Dis. Clin. North Am.* 24, 423–456. doi: 10.1016/s0889-857x(05)70016-8

Pettersen, E. F., Goddard, T. D., Huang, C. C., Couch, G. S., Greenblatt, D. M., Meng, E. C., et al. (2004). UCSF Chimera–A Visualization System for Exploratory Research and Analysis. *J. Comput. Chem.* 25, 1605–1612. doi: 10.1002/jcc.20084

Raffatellu, M., Chessa, D., Wilson, R. P., Dusold, R., Rubino, S., and Bäumler, A. J. (2005). The Vi Capsular Antigen of Salmonella Enterica Serotype Typhi Reduces Toll-Like Receptor-Dependent Interleukin-8 Expression in the Intestinal Mucosa. *Infect. Immun.* 73, 3367–3374. doi: 10.1128/IAI.73.6.3367-3374.2005

Rautenberg, M., Joo, H.-S., Otto, M., and Peschel, A. (2011). Neutrophil Responses to Staphylococcal Pathogens and Commensals *via* the Formyl Peptide Receptor 2 Relates to Phenol-Soluble Modulin Release and Virulence. *FASEB J.* 25, 1254–1263. doi: 10.1096/fj.10-175208

Reichhardt, C., and Cegelski, L. (2018). The Congo Red Derivative FSB Binds to Curli Amyloid Fibers and Specifically Stains Curliated E. Coli. *PloS One* 13, e0203226. doi: 10.1371/journal.pone.0203226

Reisner, A., Haagensen, J. A. J., Schembri, M. A., Zechner, E. L., and Molin, S. (2003). Development and Maturation of Escherichia Coli K-12 Biofilms. *Mol. Microbiol.* 48, 933–946. doi: 10.1046/j.1365-2958.2003.03490.x

Salmela, A., Rasmussen, N., Tervaert, J. W. C., Jayne, D. R. W., Ekstrand, A., European Vasculitis Study Group. (2017). Chronic Nasal Staphylococcus Aureus Carriage Identifies a Subset of Newly Diagnosed Granulomatosis With Polyangiitis Patients With High Relapse Rate. *Rheumatol. (Oxford)* 56, 965–972. doi: 10.1093/rheumatology/kex001

Sato, K., Higuchi, M., Iwata, N., Saido, T. C., and Sasamoto, K. (2004). Fluoro-Substituted and 13C-Labeled Styrylbenzene Derivatives for Detecting Brain Amyloid Plaques. *Eur. J. Med. Chem.* 39, 573–578. doi: 10.1016/j.ejmech.2004.02.013

Schlatterer, K., Beck, C., Hanzelmann, D., Lebtig, M., Fehrenbacher, B., Schaller, M., et al. (2018). The Mechanism Behind Bacterial Lipoprotein Release: Phenol-Soluble Modulins Mediate Toll-Like Receptor 2 Activation *via* Extracellular Vesicle Release From Staphylococcus Aureus. *mBio* 9, e01851-18. doi: 10.1128/mBio.01851-18

Schnabel, J. (2010). Protein Folding: The Dark Side of Proteins. *Nature* 464, 828–829. doi: 10.1038/464828a

Schwartz, K., Ganesan, M., Payne, D. E., Solomon, M. J., and Boles, B. R. (2016). Extracellular DNA Facilitates the Formation of Functional Amyloids in Staphylococcus Aureus Biofilms. *Mol. Microbiol.* 99, 123–134. doi: 10.1111/mmi.13219

Schwartz, K., Syed, A. K., Stephenson, R. E., Rickard, A. H., and Boles, B. R. (2012). Functional Amyloids Composed of Phenol Soluble Modulins Stabilize Staphylococcus Aureus Biofilms. *PloS Pathog.* 8, e1002744. doi: 10.1371/journal.ppat.1002744

Shahram, F., Akbarian, M., and Davatchi, F. (1993). Salmonella Infection in Systemic Lupus Erythematosus. *Lupus* 2, 55–59. doi: 10.1177/096120339300200110

Staples, P. J., Gerding, D. N., Decker, J. L., and Gordon, R. S. (1974). Incidence of Infection in Systemic Lupus Erythematosus. *Arthritis Rheum.* 17, 1–10. doi: 10.1002/art.1780170102

Strietzel, F.-P., Schmidt-Westhausen, A.-M., Neumann, K., Reichart, P.-A., and Jackowski, J. (2019). Implants in Patients With Oral Manifestations of Autoimmune or Muco-Cutaneous Diseases - A Systematic Review. *Med. Oral. Patol. Oral. Cir. Bucal.* 24, e217–e230. doi: 10.4317/medoral.22786

Syed, A. K., Reed, T. J., Clark, K. L., Boles, B. R., and Kahlenberg, J. M. (2015). Staphlyococcus Aureus Phenol-Soluble Modulins Stimulate the Release of Proinflammatory Cytokines From Keratinocytes and Are Required for Induction of Skin Inflammation. *Infect. Immun.* 83, 3428–3437. doi: 10.1128/IAI.00401-15

Tayeb-Fligelman, E., Salinas, N., Tabachnikov, O., and Landau, M. (2020). Staphylococcus Aureus Psmα3 Cross-α Fibril Polymorphism and Determinants of Cytotoxicity. *Structure* 28, 301–313.e6. doi: 10.1016/j.str.2019.12.006

Tayeb-Fligelman, E., Tabachnikov, O., Moshe, A., Goldshmidt-Tran, O., Sawaya, M. R., Coquelle, N., et al. (2017). The Cytotoxic Staphylococcus Aureus Psmα3 Reveals a Cross-α Amyloid-Like Fibril. *Science* 355, 831–833. doi: 10.1126/science.aaf4901

Totté, J. E. E., van der Feltz, W. T., Bode, L. G. M., van Belkum, A., van Zuuren, E. J., and Pasmans, S. G. M. A. (2016). A Systematic Review and Meta-Analysis on Staphylococcus Aureus Carriage in Psoriasis, Acne and Rosacea. *Eur. J. Clin. Microbiol. Infect. Dis.* 35, 1069–1077. doi: 10.1007/s10096-016-2647-3

Towle, K. M., Lohans, C. T., Miskolzie, M., Acedo, J. Z., van Belkum, M. J., and Vederas, J. C. (2016). Solution Structures of Phenol-Soluble Modulins α1, α3, and β2, Virulence Factors From Staphylococcus Aureus. *Biochemistry* 55, 4798–4806. doi: 10.1021/acs.biochem.6b00615

Tran, T. T., Reich, C. F., Alam, M., and Pisetsky, D. S. (2003). Specificity and Immunochemical Properties of Anti-DNA Antibodies Induced in Normal Mice by Immunization With Mammalian DNA With a CpG Oligonucleotide as Adjuvant. *Clin. Immunol.* 109, 278–287. doi: 10.1016/j.clim.2003.08.012

Tuffs, S. W., Haeryfar, S. M. M., and McCormick, J. K. (2018). Manipulation of Innate and Adaptive Immunity by Staphylococcal Superantigens. *Pathogens* 7, 53. doi: 10.3390/pathogens7020053

Tükel, C., Nishimori, J. H., Wilson, R. P., Winter, M. G., Keestra, A. M., van Putten, J. P. M., et al. (2010). Toll-Like Receptors 1 and 2 Cooperatively Mediate Immune Responses to Curli, a Common Amyloid From Enterobacterial Biofilms. *Cell Microbiol.* 12, 1495–1505. doi: 10.1111/j.1462-5822.2010.01485.x

Tükel, C., Wilson, R. P., Nishimori, J. H., Pezeshki, M., Chromy, B. A., and Bäumler, A. J. (2009). Responses to Amyloids of Microbial and Host Origin Are Mediated Through Toll-Like Receptor 2. *Cell Host Microbe* 6, 45–53. doi: 10.1016/j.chom.2009.05.020

Tursi, S. A., Lee, E. Y., Medeiros, N. J., Lee, M. H., Nicastro, L. K., Buttaro, B., et al. (2017). Bacterial Amyloid Curli Acts as a Carrier for DNA to Elicit an Autoimmune Response *via* TLR2 and TLR9. *PloS Pathog.* 13, e1006315. doi: 10.1371/journal.ppat.1006315

Tursi, S. A., Puligedda, R. D., Szabo, P., Nicastro, L. K., Miller, A. L. , Qiu, C., et al. (2020). Salmonella Typhimurium Biofilm Disruption by a Human Antibody That Binds a Pan-Amyloid Epitope on Curli. *Nat. Commun.* 11,1007. doi: 10.1038/s41467-020-14685-3

Tursi, S. A., and Tükel, Ç. (2018). Curli-Containing Enteric Biofilms Inside and Out: Matrix Composition, Immune Recognition, and Disease Implications. *Microbiol. Mol. Biol. Rev.* 82(4) e00028–18. doi: 10.1128/MMBR.00028-18

Wang, R., Braughton, K. R., Kretschmer, D., Bach, T.-H. L., Queck, S. Y., Li, M., et al. (2007). Identification of Novel Cytolytic Peptides as Key Virulence Determinants for Community-Associated MRSA. *Nat. Med.* 13, 1510–1514. doi: 10.1038/nm1656

Wang, R., Khan, B. A., Cheung, G. Y. C., Bach, T.-H. L., Jameson-Lee, M., Kong, K.-F., et al. (2011). Staphylococcus Epidermidis Surfactant Peptides Promote Biofilm Maturation and Dissemination of Biofilm-Associated Infection in Mice. *J. Clin. Invest.* 121, 238–248. doi: 10.1172/JCI42520

Wong, G. C. L. (2006). Electrostatics of Rigid Polyelectrolytes. *Curr. Opin. Colloid. Interface Sci.* 11, 310–315. doi: 10.1016/j.cocis.2006.12.003

Wong, G. C. L., and Pollack, L. (2010). Electrostatics of Strongly Charged Biological Polymers: Ion-Mediated Interactions and Self-Organization in Nucleic Acids and Proteins. *Annu. Rev. Phys. Chem.* 61, 171–189. doi: 10.1146/annurev.physchem.58.032806.104436

Zaman, M., and Andreasen, M. (2020). Cross-Talk Between Individual Phenol-Soluble Modulins in Staphylococcus Aureus Biofilm Enables Rapid and Efficient Amyloid Formation. *eLife* 9, e59776. doi: 10.7554/eLife.59776

Zheng, Y., Joo, H.-S., Nair, V., Le, K. Y., and Otto, M. (2018). Do Amyloid Structures Formed by Staphylococcus Aureus Phenol-Soluble Modulins Have a Biological Function? *Int. J. Med. Microbiol.* 308, 675–682. doi: 10.1016/j.ijmm.2017.08.010

Zhou, X., Zheng, Y., Lv, Q., Kong, D., Ji, B., Han, X., et al. (2021). Staphylococcus Aureus N-Terminus Formylated δ-Toxin Tends to Form Amyloid Fibrils, While the Deformylated δ-Toxin Tends to Form Functional Oligomer Complexes. *Virulence* 12, 1418–1437. doi: 10.1080/21505594.2021.1928395

Conflict of Interest: The authors declare that the research was conducted in the absence of any commercial or financial relationships that could be construed as a potential conflict of interest.

this article, or claim that may be made by its manufacturer, is not guaranteed or endorsed by the publisher.

frontiers | Frontiers in Cellular and Infection Microbiology

REVIEW
published: 28 June 2022
doi: 10.3389/fcimb.2022.863949

Next-Generation Probiotic Therapy to Protect the Intestines From Injury

Mecklin V. Ragan[1†], Samantha J. Wala[1†], Steven D. Goodman[2], Michael T. Bailey[2] and Gail E. Besner[1]*

[1] Center for Perinatal Research, Department of Pediatric Surgery, Columbus, OH, United States, [2] Nationwide Children's Hospital, The Ohio State University, Columbus, OH, United States

Probiotics are live microorganisms that, when administered in adequate amounts, provide health benefits to the host. Some strains of the probiotic *Lactobacillus reuteri* (*L. reuteri*) have both antimicrobial and anti-inflammatory properties that may be exploited for the treatment and prevention of different gastrointestinal diseases, including necrotizing enterocolitis (NEC) and *Clostridioides difficile* (*C. difficile*) infection. Our laboratory has developed a new delivery system for *L. reuteri* in which the probiotic is incubated with biocompatible, semipermeable, porous dextranomer microspheres (DM) that can be loaded with beneficial and diffusible cargo. *L. reuteri* can be induced to form a biofilm by incubating the bacteria on the surface of these microspheres, which enhances the efficacy of the probiotic. Loading the DM with sucrose or maltose induces *L. reuteri* to produce more biofilm, further increasing the efficacy of the probiotic. Using a rat model of NEC, *L. reuteri* administered in its biofilm state significantly increases animal survival, reduces the incidence of NEC, preserves gut barrier function, and decreases intestinal inflammation. In a murine model of *Clostridiodes difficile* infection, *L. reuteri* administered in its biofilm state decreases colitis when administered either before or after *C. difficile* induction, demonstrating both prophylactic and therapeutic efficacy. There are currently no FDA-approved probiotic preparations for human use. An FDA-approved phase I clinical trial of *L. reuteri* in its biofilm state in healthy adults is currently underway. The results of this trial will be used to support a phase 1 clinical trial in neonates, with the goal of utilizing *L. reuteri* in its biofilm state to prevent NEC in premature neonates in the future.

Keywords: ***Lactobacillus reuteri*, biofilm, probiotics, necrotizing enterocolitis, *Clostridioides difficile***

OPEN ACCESS

Edited by:
Diane McDougald, University of Technology Sydney, Australia

Reviewed by:
Troy Markel, Indiana University, United States
Scott Rice

***Correspondence:**
Gail E. Besner
gail.besner@nationwidechildrens.org

[†]These authors have contributed equally to this work and share first authorship

Specialty section:
This article was submitted to Biofilms, a section of the journal Frontiers in Cellular and Infection Microbiology

Received: *27 January 2022*
Accepted: *25 May 2022*
Published: *28 June 2022*

Citation:
Ragan MV, Wala SJ, Goodman SD, Bailey MT and Besner GE (2022) Next-Generation Probiotic Therapy to Protect the Intestines From Injury. Front. Cell. Infect. Microbiol. 12:863949. doi: 10.3389/fcimb.2022.863949

INTRODUCTION

Bacteria grow and adhere to almost every surface, and form complex, multicellular communities called biofilms. Biofilms facilitate successful colonization and maintenance of a bacterial population by protecting bacteria against environmental conditions (Branda et al., 2005). Probiotic bacteria are live microorganisms that can be beneficial to the host when administered in adequate amounts. However, when consumed orally, probiotics face numerous challenges, including the acidic environment of the stomach, effectors of the host immune system, and competition with commensal and pathogenic bacteria. These factors prevent probiotics from being sufficiently sustained within the host, thereby reducing their potential beneficial effects (Navarro et al.,

2017). There is extensive, ongoing research examining the use of probiotics for the treatment and prevention of intestinal diseases. In particular, our lab has been investigating the efficacy of the probiotic bacteria *Lactobacillus reuteri* (*L. reuteri*) administered in its biofilm vs. planktonic (free-living) state, to treat necrotizing enterocolitis and *Clostridioides difficile* (*C. difficile*) infections.

Lactobacillus reuteri is a Gram-positive bacterium originally isolated in 1962 by German microbiologist Gerhard Reuter. Using human fecal and intestinal samples from infants and adults, Reuter demonstrated that *L. reuteri* was the predominant autochthonous bacterium in both populations. He isolated multiple strains, including DSM20016 (Kandler et al., 1980; Reuter, 2001). In the years since, further genomic studies have demonstrated that human *L. reuteri* strains belong to two distinct multilocus sequence analysis (MLSA) clades, clades II and VI. While human strains in clade VI are more closely related to isolates from chickens, those in clade II are very specific to humans.

Certain rare strains, including DSM20016, are known to have multiple attributes beneficial to the host, including antimicrobial and anti-inflammatory properties (Spinler et al., 2014). The antimicrobial properties of *L. reuteri* are secondary to its ability to produce the antimicrobial compound 3-hydroxyproprionaldehyde (3-HPA), also known as reuterin (Jones and Versalovic, 2009). *L. reuteri* utilizes glycerol dehydratase to produce reuterin from glycerol. Reuterin inhibits the growth of multiple gastrointestinal pathogens, including *C. difficile*, by inducing oxidative stress (Engevik et al., 2020). *L. reuteri* also has extracellular glucosyltransferase (GTF) proteins that catalyze the formation of exopolysaccharides of glucose (glucans) from disaccharide sugars and possess glucan-binding domains that allow for strong binding to other glucans, important to biofilm formation. The anti-inflammatory abilities of *L. reuteri* are partially due to its ability to produce histamine *via* histidine decarboxylase. Histamine is a biologically active compound that modulates host mucosal immunity and suppresses proinflammatory tumor necrosis factor (TNF) production (Jones and Versalovic, 2009; C. M. Thomas et al., 2012). In addition, by metabolizing folate, *L. reuteri* can produce ethionine, which can use ethylation to modify human chromatin (Röth et al., 2019). There is also evidence that *L. reuteri* induces anti-inflammatory T-regulatory cells, suppresses T helper 1 (Th1) and Th2 cytokine responses, and alters dendritic cell activity; however, the mechanisms by which this occurs are poorly understood (Jones and Versalovic, 2009). Our studies use *L. reuteri* strain DSM20016—a strain that possesses both antimicrobial and anti-inflammatory properties.

Biofilms possess a community architecture, replete with a self-made extracellular matrix, and that is often facilitated by adherence to a surface. Biofilm formation enables bacteria to resist environmental conditions, resulting in successful colonization and maintenance of the bacterial population (Salas-Jara et al., 2016). *L. reuteri* grown in its biofilm state on the surface of biocompatible microspheres has an increased ability to survive in acidic environments such as that of the stomach and to adhere to intestinal epithelial cells. The biocompatible microspheres we use are composed of separation pharmacia dextran (Sephadex aka dextranomer microspheres or DM), which are beads of crosslinked dextran typically used for gel-filtration chromatography but also mimic the native glucans that *L. reuteri* makes. In addition, prebiotic nutrients beneficial to the probiotic bacteria can be loaded into the lumen of the Sephadex beads (Navarro et al., 2017). Harnessing the ability of *L. reuteri* to form a biofilm, we have developed a novel probiotic delivery system in which *L. reuteri* is induced to form a biofilm on the surface of DM (*L. reuteri* + DM), allowing for enhanced efficacy. Loading DM with maltose (DM-maltose, which is the substrate for GtfW) or sucrose (DM-sucrose, which is an inducer of *gtfW*) induces increased biofilm formation, enhancing the efficacy of the probiotic (Navarro et al., 2017).

Bacterial colonization of the intestine is essential for the development of a healthy gut microbiome (Harmsen et al., 2000). In contrast to that of term infants, the gut microbiome of premature infants has a notably smaller proportion of beneficial bacteria such as *Lactobacillus* and *Bifidobacteria* and higher numbers of pathogenic bacteria, likely secondary to frequent antibiotic use, exposure to the hospital environment, and artificial feeding. The intestinal dysbiosis that is present in premature infants is associated with the development of necrotizing enterocolitis (NEC) (Mshvildadze et al., 2008).

NEC is a devastating disease affecting premature infants, characterized by extensive intestinal inflammation that often progresses to tissue destruction, bacterial translocation, sepsis, and often death. Approximately 10% of infants born weighing less than 1,500 g will develop the disease, and mortality for affected infants is 20%–30%. Current treatment and preventive approaches for NEC remain suboptimal, with the mainstays of treatment being orogastric tube decompression, total parenteral nutrition (TPN), and administration of broad-spectrum antibiotics. Surgical resection is required when there is a failure of medical management and concern for bowel viability. For infants who survive, they continue to face numerous long-term complications, including gastrointestinal problems, failure to thrive, short gut syndrome, and neurodevelopmental delay (Neu and Walker, 2011).

C. difficile infection is also related to a disruption in the gut microbiome. *C. difficile* is one of the most common nosocomial infections. From a 2011 surveillance study in the United States, there were an estimated 453,000 *C. difficile* infections of which 29,300 led to death (Lessa et al., 2015). According to the American College of Gastroenterology, there was a 43% increase in *C. difficile* infection between 2001 and 2012, largely driven by recurrent infections which increased by 188% over the same timeframe (Ma et al., 2017; Kelly et al., 2021). This anaerobic, Gram-positive *Bacillus* is the primary culprit in antibiotic-driven pseudomembranous colitis, which is thought to be due to a disruption of healthy gut microbiota from a single dose or multiple doses of antibiotics. Risk factors that predispose to *C. difficile* infection include hospitalization, age over 65 years, and antibiotic use (Desai et al., 2016; Kelly et al., 2021). Colitis is driven by the release of toxins A and B, both of which are exotoxins that disrupt intestinal cell integrity. Treatment options

for patients with active *C. difficile* infection range from oral or intravenous antibiotics, fecal transplantation, and, in fulminant cases of toxic megacolon, emergent total colectomy. Approximately US$5.4 billion is spent annually to treat *C. difficile* infections in the United States (Desai et al., 2016). A prophylactic medication would be extraordinarily cost-effective. However, to date, there is insufficient data to support the use of prophylactic treatments (Kelly et al., 2021).

Given the role of intestinal dysbiosis in the development of NEC and *C. difficile* infections, probiotic administration has been studied as a preventive strategy. However, the multiple studies that have been performed have been met with conflicting results. The Probiotics in Preterm Infants (PiPs) Trial was a multicenter, double-blinded, randomized, placebo-controlled trial conducted from 2010 to 2013 that examined daily dosing of *Bifidobacterium breve BBG-001* in the prevention of NEC, late-onset sepsis, and death in preterm infants while monitoring for probiotic colonization of participants. They found no evidence that the use of *Bifidobacterium breve BBG-001* was protective against NEC, late-onset sepsis, or death in premature infants (Costeloe et al., 2016). However, when used in combination, the probiotics *Lactobacillus* and *Bifidobacterium* spp. have been shown to prevent NEC in very low birth weight (VLBW) infants (Denkel et al., 2016). This is supported by a meta-analysis that showed a reduction in NEC incidence from a combination of *Lactobacillus* and *Bifidobacterium* species among 1,623 VLBW neonates from 8 randomized control trials (Thomas et al., 2017). Another study used the NEO-KISS database, a German surveillance system for nosocomial infections in VLBW infants, to investigate the routine use of a dual-strain probiotic formulation containing *Lactobacillus acidophilus* and *Bifidobacterium* spp. called Infloran in German NICUs from 2004 to 2014. Interestingly, while there is no FDA-approved pharmaceutical-grade probiotic in the United States, Infloran is licensed by the Swiss Agency for Therapeutic Products of the Federal Office of Public Health in Switzerland as a drug for diarrhea, and thus it is available in a pharmaceutical-grade quality. They found that the use of Infloran significantly reduced the risk of NEC, overall mortality, and nosocomial bloodstream infections (Denkel et al., 2016). This is supported by a recent meta-analysis that showed greater NEC reduction with routine multistrain probiotic use compared to routine administration of a single strain (Deshmukh & Patole, 2021). While *Lactobacillus* and *Bifidobacterium* spp. have been shown to prevent NEC in VLBW infants, the positive effects of probiotic administration appear dependent upon repetitive administration (at least daily) (Braga et al., 2011). Although rare, there have been case reports of probiotic-induced sepsis in infants (Zbinden et al., 2015), raising some concern for daily probiotic administration in VLBW infants. A Cochrane review examining 54 studies with a total of 10,604 infants who were either very preterm (born earlier than 8 weeks) or VLBW found a significant reduction in NEC (RR, 0.54; 95% CI, 0.45 to 0.65). However, evidence was assessed as low certainty due to limitations in trial design and publication bias (Sharif et al., 2020).

Lactobacillus and *Bifidobacterium* spp. have also been investigated for protective effects against *C. difficile* infection. Although some studies have found beneficial effects, results have been mixed, leading the American Gastroenterology Association to recommend against the use of probiotics for the prevention of antibiotic-induced *C. difficile* (Kelly et al., 2021).

Given these concerns and shortcomings of probiotics in human studies, our lab set out to develop an improved method of probiotic administration that would increase probiotic efficacy with fewer doses. Here, we review the currently published literature and progression of our laboratories' work, which demonstrates the efficacy of a single dose of *L. reuteri* in its biofilm state in the treatment of NEC and *C. difficile* infections. This is not a general review of the field but a focused overview of our laboratories' contributions to applied probiotic use for these diseases. We also discuss the future implications of this probiotic formulation on the treatment of intestinal diseases (**Figure 1**).

L. REUTERI IN ITS BIOFILM STATE PROTECTS THE INTESTINES FROM EXPERIMENTAL NEC AND DECREASES NEURODEVELOPMENTAL IMPAIRMENT IN SURVIVORS OF NEC

Using a rat model of NEC, we have demonstrated that a single dose of *L. reuteri* grown on biocompatible microspheres significantly reduces the incidence and severity of NEC and preserves gut barrier function. In our rat NEC model, premature neonatal rat pups are delivered *via* cesarean section and exposed to repeated episodes of hypercaloric feeding, hypoxia, and hypothermia over a 96-h time period to induce NEC. The hypercaloric diet consisted of 5 daily gavage feedings of increasing volumes of formula each day, with the first feed including a dose of lipopolysaccharide (2 mg/kg) that activates toll-like receptor 4. The first 3 feeds each day were combined with 90-s episodes of hypoxia (<1.5% oxygen) followed by hypothermia (4°C × 10 min). Experimental groups received a single enteral dose of *L. reuteri* grown on unloaded microspheres (biofilm state) compared to *L. reuteri* administered in its planktonic (free-living) state. The intestinal injury was graded using a standardized histology injury scoring system, and intestinal permeability was quantified by measuring serum levels of enterally administered fluorescein isothiocyanate-labeled dextran. Pups treated with a single dose of *L. reuteri* in its biofilm state demonstrated a significant reduction in histologic injury with reduced intestinal permeability, indicating improved gut barrier function, whereas a single dose of planktonic *L. reuteri* had no effect (Olson et al., 2016).

Preloading DM with sucrose or maltose enhances *L. reuteri* biofilm formation, increases *L. reuteri* adherence to human intestinal epithelial cells, and prolongs *L. reuteri* survival in acidic pH (Navarro et al., 2017). With this in mind, we next sought to test the efficacy of *L. reuteri* induced to produce increased biofilm formation by preloading DM with sucrose or

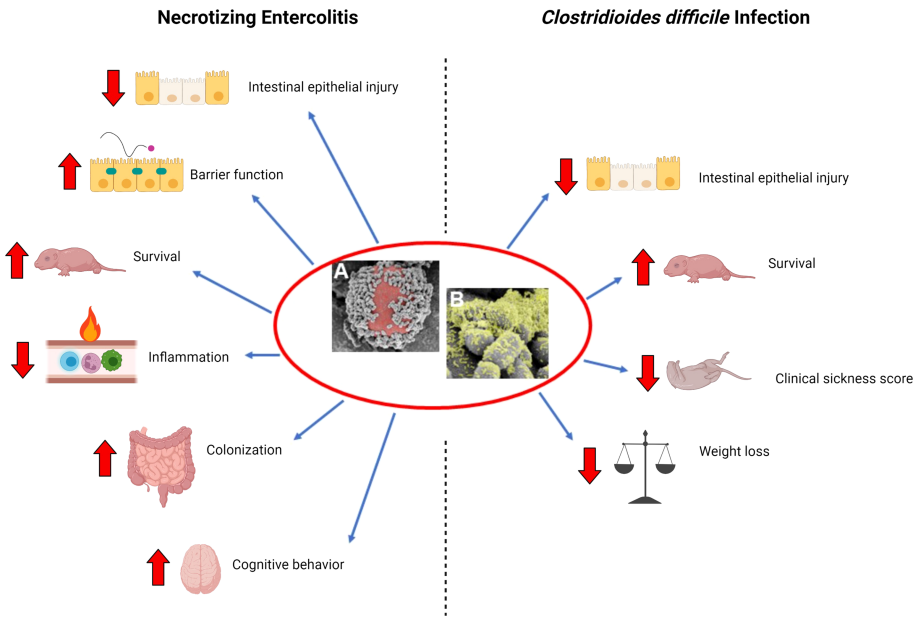

FIGURE 1 | Beneficial effects of *L. reuteri* in its biofilm state. **(A)** Scanning electron microscopy (SEM) image demonstrating multiple *L. reuteri* adherent to the surface of a DM (red); **(B)** upon adherence to DM, *L. reuteri* is induced to form a biofilm (green). Necrotizing Enterocolitis: *L. reuteri* in its biofilm state decreases intestinal epithelial injury, increases gut barrier integrity, increases survival, decreases inflammation, increases probiotic persistence in the gastrointestinal tract, and improves cognitive behavior in a rat model of necrotizing enterocolitis (NEC). *Clostridiodes difficile* infection: *L. reuteri* in its biofilm state decreases intestinal epithelial injury, increases survival, decreases clinical sickness score, and decreases weight loss when administered either as prophylaxis or treatment in a mouse model of *C. difficile* infection. Created with BioRender.com.

maltose, or by mutating the *L. reuteri gtfW* gene to reduce the ability of *L. reuteri* to produce a biofilm, in a rat model of NEC (Olson et al., 2018). GtfW is a strain-specific, cell-associated extracellular enzyme involved in *L. reuteri* biofilm formation (Navarro et al., 2017). Pups in experimental groups received a single enteral dose of *L. reuteri* + DM, *L. reuteri* + DM-sucrose, or *L. reuteri* + DM-maltose. The intestinal histologic injury was graded, intestinal permeability was determined by measuring serum levels of enterally administered fluorescein isothiocyanate-labeled dextran, inflammatory gene expression was determined by quantitative real-time PCR, and preservation of the gut microbiome was determined using DNA isolation and 16S rRNA sequencing. We found that administration of a single dose of *L. reuteri* induced to form increased amounts of biofilm by incubation with either maltose- or sucrose-loaded DM, had significantly improved animal survival, decreased incidence of NEC, reduced intestinal mucosal barrier breakdown, and decreased intestinal inflammation, compared to *L. reuteri* incubated with unloaded DM or *L. reuteri* in its planktonic state. Importantly, *L. reuteri* + DM-maltose led to increased *L. reuteri* persistence in the intestinal tract and caused the composition of the gut microbiome to more closely resemble that of breastfed uninjured animals. Finally, the administration of *L. reuteri* with a mutated *gtfW* gene (i.e., *L. reuteri* is unable to readily produce a biofilm) led to a loss of protection against NEC, highlighting the importance of biofilm formation in the protective effects of *L. reuteri* (Olson et al., 2018).

L. reuteri has antimicrobial properties due to its ability to produce reuterin *via* glycerol dehydratase and anti-inflammatory properties partially attributable to its ability to produce histamine *via* histidine decarboxylase. We next investigated the effects of the antimicrobial and anti-inflammatory properties of *L. reuteri* on protecting the intestines from NEC. Prior to the induction of NEC, rat pups received either native or mutant forms of *L. reuteri* in either its planktonic or biofilm states. The mutant forms of *L. reuteri* were either reuterin- or histamine-deficient, decreasing the antimicrobial or anti-inflammatory properties of the probiotic, respectively. The intestinal injury was graded using a standardized histologic injury scoring system (Caplan et al., 1994). As in our prior studies, rat pups that received a single dose of *L. reuteri* in its biofilm state had a significantly decreased incidence of NEC. Administration of reuterin-deficient or histamine-deficient forms of *L. reuteri*, in either the planktonic or biofilm state, resulted in a significant loss of efficacy. This demonstrates the importance of both reuterin and histamine production by *L. reuteri* in its ability to confer intestinal protection against NEC (Shelby et al., 2021). This also highlights both an infectious and an inflammatory etiology of the disease.

There is a growing body of evidence demonstrating a connection between gut microbiota and brain function *via* a bidirectional gut-brain axis, which regulates communication between the enteric nervous system (ENS) and the central nervous system (CNS) (Cryan and Dinan, 2012). Given the known predisposition for infants surviving NEC to have

neurodevelopmental delays and cognitive impairments (Neu and Walker, 2011), we next investigated whether our novel probiotic delivery system had neuroprotective effects on survivors of NEC. We induced NEC in rat pups using our standard rat NEC model, as described above. The incidence of death due to NEC in this model is approximately 65%. Surviving pups were placed with foster dams and subjected to daily developmental milestone testing for 23 days. These tests included daily weight, ear and eye opening, auditory startle, tests to measure labyrinthine, body righting, and coordination (air righting, cliff aversion, surface righting, and negative geotaxis), tests to measure strength (forelimb grasp), and tests to measure animal locomotion and the extinguishing of pivoting behavior (open field traversal). In addition, cognitive and memory tests were performed between 4 and 8 weeks of age. These tests included the Y-maze test to assess spatial learning and reference memory, the novel object recognition test to measure nonspatial working memory and recognition memory, the Barnes maze test to evaluate spatial learning and memory, and the elevated plus-maze test to look for anxiety-like behavior. Once collected at the end of the experiment, rat brain specimens were subjected to immunofluorescent staining, RNA isolation, and quantitative real-time PCR. We found that rat pups exposed to NEC reached developmental milestones significantly slower than breastfed pups, with mild improvement when treated with a single dose of *L. reuteri* in its biofilm state. While exposure to NEC was noted to have negative effects on cognitive behavior, these effects were prevented with the administration of a single dose of *L. reuteri* in its biofilm state. In addition, the behavioral effects of NEC were found to be associated with increased numbers of activated microglia, decreased myelin basic protein (MBP), and decreased neurotrophic gene expression. All these effects were prevented by the administration of a single dose of *L. reuteri* in its biofilm state (Wang et al., 2021).

L. REUTERI IN THE TREATMENT AND PREVENTION OF EXPERIMENTAL *CLOSTRIDIOIDES DIFFICILE* INFECTION

We have examined the use of *L. reuteri* as prophylaxis and treatment in a murine model of *C. difficile* infection, comparing *L. reuteri* in its biofilm state to its planktonic state (Shelby et al., 2020). To induce *C. difficile* infection, adult C57BL/6 mice received an oral antibiotic cocktail followed by an intraperitoneal injection of clindamycin two days later. Depending on whether the mouse was in the prophylactic or treatment arm of the study, animals received a single dose of saline, planktonic *L. reuteri*, or *L. reuteri* + DM-maltose before or after gastric gavage of 1.5 x 10^7 CFU of *C. difficile*, respectively, and clinical sickness scores (CSS) and histologic injury scores (HIS) consistent with *C. difficile* colitis were determined (Shelby et al., 2020). In the prophylactic experiment, mice that received a single dose of *L. reuteri* + DM-maltose had significantly decreased weight loss, decreased CSS, decreased HIS, and increased survival after 6 days compared to the control saline group. In addition, mice that received *L. reuteri* + DM-maltose had significantly increased survival after 6 days compared to those that received planktonic *L. reuteri*. In the treatment experiment, animals given *L. reuteri* + DM-maltose had significantly less weight loss, decreased HIS, and increased survival compared to the saline control group. There was a further improvement in CSS and decreased HIS in the *L. reuteri* + DM-maltose group compared to the *L. reuteri* + DM-water group. Therefore, there may be a role for both the prevention and treatment of *C. difficile* infection using *L. reuteri* in its biofilm state (Shelby et al., 2020).

L. reuteri has several characteristics that make it effective in the prevention and treatment of *C. difficile* infection. First, it is resistant to the antibiotics used to treat *C. difficile*, such as vancomycin, metronidazole, and fidaxomicin, therefore allowing it to be co-administered with these antibiotics (Spinler et al., 2017). *L. reuteri* is believed to induce reactive oxidative species within *C. difficile* through its production of reuterin, leading to altered metabolism, decreased toxin production, and increased susceptibility to vancomycin and metronidazole (Engevik et al., 2020). Although a randomized controlled trial using planktonic *L. reuteri* in children to prevent diarrhea and antibiotic-associated diarrhea did not show a significant effect when compared to a placebo, it is possible that there would be a clinical difference in the prevention and treatment of *C. difficile* in humans administered *L. reuteri* in its biofilm state (Kołodziej and Szajewska, 2019).

HUMAN CLINICAL TRIALS OF *L. REUTERI* IN ITS BIOFILM STATE

We have demonstrated that *L. reuteri* in its biofilm state can reduce the incidence of NEC and *C. difficile* infection in rodent models of disease. However, there are currently no FDA-approved probiotics for human administration despite the increasing use of probiotics in NICUs throughout the United States (Viswanathan et al., 2016). Published clinical trials of probiotics have all used probiotics administered in their planktonic state, with the administration of single or multiple doses daily. Two randomized controlled studies using daily doses of *L. reuteri* DSM17938 found a statistically significant decrease in feeding intolerance and duration of hospitalization for preterm infants weighing ≤1,500 g (Rojas et al., 2012; Oncel et al., 2014). In our animal models, we deliver our formulation of *L. reuteri* in its biofilm state, allowing us to deliver a single dose rather than multiple daily doses. This may help to decrease the risk of downstream bacteremia associated with probiotic administration and increase patient compliance and treatment cost-effectiveness.

In conjunction with Scioto Biosciences Inc., GMP-grade *L. reuteri* in its biofilm state (SB-121) has been produced, and its safety and tolerability are currently being investigated in a randomized, double-blind, crossover phase I clinical trial (NCTT04944901 (*28-Day Daily-Dose Crossover Study of the Safety and Tolerability of SB-121 (Lactobacillus Reuteri With*

Sephadex® and Maltose) in Subjects, Ages 15 to 45 Years, Diagnosed With Autistic Disorder, 2021). Autism spectrum disorder is a neurodevelopmental disorder that is characterized by deficits in social behavior and the presence of restricted, stereotyped interests and behaviors. These behaviors involve dysregulation of the gut-brain axis as well as neuroinflammation. In mice subjected to maternal separation, *L. reuteri* DSM 17938 has been shown to downregulate inflammatory gene expression in the brain and enhance pro-social behavior (Park et al., 2021). In addition to neuroinflammation, oxytocin also strongly affects social behavior. Children with autism spectrum disorder have low levels of oxytocin, and in animal models, the administration of *L. reuteri* significantly increases oxytocin and improves social behavior (Kong et al., 2020). These findings support the current phase 1 clinical trial of SB-121 in healthy adults with an autism spectrum disorder. In this trial, volunteers with autism are blindly receiving either daily SB-121 or placebo for 28 days. Those that received SB-121 will then switch to placebo, and those that received placebo will then switch to SB-121 for an additional 28 days. Primary outcome measures will include adverse events, the presence of SB-121 in the stool, and the incidence of symptomatic *L. reuteri* bacteremia. Secondary outcome measures include changes in cognition, attention, and behavior; stool biomarkers; and C-reactive protein and TNF-α levels (since *L. reuteri* can produce anti-inflammatory compounds). The results of this trial should provide reassurance for the safe administration of *L. reuteri* in its biofilm state to not only treat neurodevelopmental disorders like autism spectrum disorder but also to prevent and treat NEC in premature infants and *C. difficile* colitis in susceptible individuals.

DISCUSSION

L. reuteri is a beneficial Gram-positive probiotic bacterium, with strain DSM20016 possessing antimicrobial and anti-inflammatory properties. Importantly, *L. reuteri* can be grown in its biofilm state by using permeable biocompatible microspheres loaded with prebiotics, such as maltose and sucrose, which allows increased adherence to human intestinal epithelial cells and prolonged survival under acidic conditions in the stomach (Navarro et al., 2017). We have demonstrated the efficacy of a single dose of *L. reuteri* administered in its biofilm state in reducing the severity of NEC and *C. difficile* infections in a rat model of NEC and a murine model of *C. difficile*.

While using probiotics to treat intestinal disorders manifested by dysbiosis may seem logical, the reality is more complicated. There are multiple combinations of a variety of probiotics sold over the counter. However, there is currently no FDA-approved probiotic on the market. Still, there is a growing use of probiotics in NICUs in the United States. In 1997, almost no NICUs in the United States were using probiotics (Gray et al., 2020). By 2015, only approximately 14% of NICUs in the United States administered probiotics to VLBW preterm infants (Viswanathan et al., 2016). There are a number of concerns regarding probiotic administration in infants contributing to the difficulty with bringing a product of this nature to market, including probiotic-associated sepsis and contamination, as exemplified by 3 preterm infants who developed *Bifidobacterium longum* bacteremia after receiving the probiotic Infloran® containing viable *Bifidobacterium longum* (Zbinden et al., 2015). The highest profile case involved a preterm VLBW infant who succumbed to gastrointestinal mucormycosis from probiotic ABC Dophilus Powder due to mold contamination with *Rhizopus oryzae* (Vallabhaneni et al., 2015). Beyond concerns for probiotic-associated sepsis, there is also a concern regarding the quality of these probiotic formulations. The precise contents contained within the non-FDA-approved formulations available at present are largely unknown. As recently as 2016, a study was conducted to validate the identity of bifidobacterial species and subspecies in 16 different commercial probiotic products, with only 1 of the 16 probiotics perfectly matching its bifidobacterial label (Lewis et al., 2016). There have also been several recent recalls in the last 5 years of dietary supplement-grade probiotics due to contamination, including with *Salmonella*, *Pseudomonas aeruginosa*, *Rhizopus*, and *Penicillium* species (Liva Global, 2021). These reports highlight the importance of producing a GMP-grade probiotic preparation for human administration. To date, there is no published trial using probiotics to prevent NEC in preterm infants that have met the definition of a "probiotic drug" by the International Scientific Association for Probiotics and Prebiotics (Poindexter and Committee on Fetus and Newborn, 2021). Despite 56 randomized control trials and 30 observational trials, there remains uncertainty about the benefits of probiotics (Razak et al., 2021).

The use of probiotics in the NICU may be far more acceptable to neonatologists if an FDA-approved formulation was available. However, there are concrete reasons why an FDA-approved probiotic product is not currently available for use in the NICU. One of the main challenges is cost. The cost of producing a GMP-grade drug formulation and the effort needed to get it approved by the FDA are enormous. In addition, if the target patient population is newborns, an extra level of scrutiny is appropriately applied, requiring initial phase 1 studies in adults prior to phase 1 studies in newborns, doubling the cost. It would be very challenging to bring a new formulation to the market without the support of biopharma. This brings another level of complexity into the picture. Being an orphan disease, NEC affects a minute portion of the population compared to diseases such as cancer or cardiovascular disease. The impetus for a company to support the development of therapies for NEC is therefore diminished. It is imperative that biopharma understands the importance of cures for orphan diseases in addition to cures for more common diseases affecting humankind.

In our experimental models, a single dose of *L. reuteri* administered in its biofilm state has proven efficacious in reducing the severity of NEC and *C. difficile* infections, and the safety and tolerability of GMP-grade *L. reuteri* in its biofilm state (SB-121) are currently being investigated as part of a phase I clinical trial. Moving forward, further clinical trials will be needed to demonstrate the safety and efficacy of *L. reuteri* in its biofilm state in the prevention and treatment of NEC and *C. difficile* infection.

AUTHOR CONTRIBUTIONS

MR and SW have contributed equally to this work and share first authorship. All authors contributed to manuscript revision, read, and approved the submitted version.

FUNDING

This work was supported by NIH R01 GM123482 Tunable Native Probiotic Formulations for the Treatment of Necrotizing enterocolitis (GEB, SDG, MTB).

REFERENCES

Braga, T. D., da Silva, G. A. P., de Lira, P. I. C., and de Carvalho Lima, M. (2011). Efficacy of *Bifidobacterium breve* and *Lactobacillus casei* Oral Supplementation on Necrotizing Enterocolitis in Very-Low-Birth-Weight Preterm Infants: A Double-Blind, Randomized, Controlled Trial. *Am. J. Clin. Nutr.* 93 (1), 81–86. doi: 10.3945/ajcn.2010.29799

Branda, S. S., Vik, S., Friedman, L., and Kolter, R. (2005). Biofilms: The Matrix Revisited. *Trends Microbiol.* 13 (1), 20–26. doi: 10.1016/j.tim.2004.11.006

Caplan, M. S., Hedlund, E., Adler, L., and Hsueh, W. (1994). Role of Asphyxia and Feeding in a Neonatal Rat Model of Necrotizing Enterocolitis. *Pediatr. Pathol.* 14 (6), 1017–1028. doi: 10.3109/15513819409037698

Costeloe, K., Bowler, U., Brocklehurst, P., Hardy, P., Heal, P., Juszczak, E., et al. (2016). A Randomised Controlled Trial of the Probiotic *Bifidobacterium breve* BBG-001 in Preterm Babies to Prevent Sepsis, Necrotising Enterocolitis and Death: The Probiotics in Preterm infantS (PiPS) Trial. *Health Technol. Assess.* 20 (66), 1–194. doi: 10.3310/hta20660

Cryan, J. F., and Dinan, T. G. (2012). Mind-Altering Microorganisms: The Impact of the Gut Microbiota on Brain and Behaviour. *Nat. Rev. Neurosci.* 13 (10), 701–712. doi: 10.1038/nrn3346

Denkel, L. A., Schwab, F., Garten, L., Geffers, C., Gastmeier, P., and Piening, B. (2016). Protective Effect of Dual-Strain Probiotics in Preterm Infants: A Multi-Center Time Series Analysis. *PLoS One* 11 (6), e0158136. doi: 10.1371/journal.pone.0158136

Desai, K., Gupta, S. B., Dubberke, E. R., Prabhu, V. S., Browne, C., and Mast, T. C. (2016). Epidemiological and Economic Burden of *Clostridium difficile* in the United States: Estimates From a Modeling Approach. *BMC Infect. Dis.* 16, 303. doi: 10.1186/s12879-016-1610-3

Deshmukh, M., and Patole, S. (2021). Prophylactic Probiotic Supplementation for Preterm Neonates-A Systematic Review and Meta-Analysis of Nonrandomized Studies. *Adv. Nutr.* 12 (4), 1411–1423. doi: 10.1093/advances/nmaa164

Engevik, M. A., Danhof, H. A., Shrestha, R., Chang-Graham, A. L., Hyser, J. M., Haag, A. M., et al. (2020). Reuterin Disrupts *Clostridioides difficile* Metabolism and Pathogenicity Through Reactive Oxygen Species Generation. *Gut. Microbes* 12 (1), 1788898. doi: 10.1080/19490976.2020.1795388

Gray, K. D., Messina, J. A., Cortina, C., Owens, T., Fowler, M., Foster, M., et al. (2020). Probiotic Use and Safety in the Neonatal Intensive Care Unit: A Matched Cohort Study. *J. Pediatr.* 222, 59–64.e1. doi: 10.1016/j.jpeds.2020.03.051

Harmsen, H. J., Wildeboer-Veloo, A. C., Raangs, G. C., Wagendorp, A. A., Klijn, N., Bindels, J. G., et al. (2000). Analysis of Intestinal Flora Development in Breast-Fed and Formula-Fed Infants by Using Molecular Identification and Detection Methods. *J. Pediatr. Gastroenterol. Nutr.* 30 (1), 61–67. doi: 10.1097/00005176-200001000-00019

Jones, S. E., and Versalovic, J. (2009). Probiotic *Lactobacillus reuteri* Biofilms Produce Antimicrobial and Anti-Inflammatory Factors. *BMC Microbiol.* 9, 35. doi: 10.1186/1471-2180-9-35

Kandler, O., Stetter, K.-O., and Köhl, R. (1980). Lactobacillus reuteri Sp. Nov., a New Species of Heterofermentative Lactobacilli. *Zentralblatt. Für. Bakteriologie.: I. Abt. Originale. C.: Allgemeine. Angewandte. Und. Ökologische. Mikrobiologie.* 1 (3), 264–269. doi: 10.1016/S0172-5564(80)80007-8

Kelly, C. R., Fischer, M., Allegretti, J. R., LaPlante, K., Stewart, D. B., Limketkai, B. N., et al. (2021). ACG Clinical Guidelines: Prevention, Diagnosis, and Treatment of *Clostridioides difficile* Infections. *Am. J. Gastroenterol.* 116 (6), 1124–1147. doi: 10.14309/ajg.0000000000001278

Kołodziej, M., and Szajewska, H. (2019). *Lactobacillus reuteri* DSM 17938 in the Prevention of Antibiotic-Associated Diarrhoea in Children: A Randomized Clinical Trial. *Clin. Microbiol. Infection.* 25 (6), 699–704. doi: 10.1016/j.cmi.2018.08.017

Kong, X.-J., Liu, J., Li, J., Kwong, K., Koh, M., Sukijthamapan, P., et al. (2020). Probiotics and Oxytocin Nasal Spray as Neuro-Social-Behavioral Interventions for Patients With Autism Spectrum Disorders: A Pilot Randomized Controlled Trial Protocol. *Pilot. Feasibility. Stud.* 6 (1), 20. doi: 10.1186/s40814-020-0557-8

Lessa, F. C., Mu, Y., Bamberg, W. M., Beldavs, Z. G., Dumyati, G. K., Dunn, J. R., et al. (2015). Burden of *Clostridium difficile* Infection in the United States. *New Engl. J. Med.* 372 (9), 825–834. doi: 10.1056/NEJMoa1408913

Lewis, Z. T., Shani, G., Masarweh, C. F., Popovic, M., Frese, S. A., Sela, D. A., et al. (2016). Validating Bifidobacterial Species and Subspecies Identity in Commercial Probiotic Products. *Pediatr. Res.* 79 (3), 445–452. doi: 10.1038/pr.2015.244

Livia Global (2021). *Livia Global Announces Voluntary Recall of Two Lots of Its Liviaone Liquid Probiotics Because of The Potential for Contamination With Pseudomonas Aeruginosa*.

Ma, G. K., Brensinger, C. M., Wu, Q., and Lewis, J. D. (2017). Increasing Incidence of Multiply Recurrent Clostridium difficile Infection in the United States: A Cohort Study. *Ann. Internal Med.* 167 (3), 152–158. doi: 10.7326/M16-2733

Mshvildadze, M., Neu, J., and Mai, V. (2008). Intestinal Microbiota Development in the Premature Neonate: Establishment of a Lasting Commensal Relationship? *Nutr. Rev.* 66 (11), 658–663. doi: 10.1111/j.1753-4887.2008.00119.x

Navarro, J. B., Mashburn-Warren, L., Bakaletz, L. O., Bailey, M. T., and Goodman, S. D. (2017). Enhanced Probiotic Potential of *Lactobacillus reuteri* When Delivered as a Biofilm on Dextranomer Microspheres That Contain Beneficial Cargo. *Front. Microbiol.* 8. doi: 10.3389/fmicb.2017.00489

Neu, J., and Walker, W. A. (2011). Necrotizing Enterocolitis. *New Engl. J. Med.* 364 (3), 255–264. doi: 10.1056/NEJMra1005408

Olson, J. K., Navarro, J. B., Allen, J. M., McCulloh, C. J., Mashburn-Warren, L., Wang, Y., et al. (2018). An Enhanced *Lactobacillus reuteri* Biofilm Formulation That Increases Protection Against Experimental Necrotizing Enterocolitis. *Am. J. Physiol. Gastrointestinal. Liver. Physiol.* 315 (3), G408–G419. doi: 10.1152/ajpgi.00078.2018

Olson, J. K., Rager, T. M., Navarro, J. B., Mashburn-Warren, L., Goodman, S. D., and Besner, G. E. (2016). Harvesting the Benefits of Biofilms: A Novel Probiotic Delivery System for the Prevention of Necrotizing Enterocolitis. *J. Pediatr. Surg.* 51 (6), 936–941. doi: 10.1016/j.jpedsurg.2016.02.062

Oncel, M. Y., Sari, F. N., Arayici, S., Guzoglu, N., Erdeve, O., Uras, N., et al. (2014). *Lactobacillus reuteri* for the Prevention of Necrotising Enterocolitis in Very Low Birthweight Infants: A Randomised Controlled Trial. *Arch. Dis. Childhood. Fetal. Neonatal. Edition.* 99 (2), F110–F115. doi: 10.1136/archdischild-2013-304745

Park, E. S., Freeborn, J., Venna, V. R., Roos, S., Rhoads, J. M., and Liu, Y. (2021). *Lactobacillus reuteri* Effects on Maternal Separation Stress in Newborn Mice. *Pediatr. Res.* 90 (5), 980–988. doi: 10.1038/s41390-021-01374-0

Poindexter, B.COMMITTEE ON FETUS AND NEWBORN (2021). Use of Probiotics in Preterm Infants. *Pediatrics* 147 (6), 92–98. doi: 10.1542/peds.2021-051485

Razak, A., Patel, R. M., and Gautham, K. S. (2021). Use of Probiotics to Prevent Necrotizing Enterocolitis: Evidence to Clinical Practice. *JAMA Pediatr.* 175 (8), 773–774. doi: 10.1001/jamapediatrics.2021.1077

Reuter, G. (2001). The Lactobacillus and Bifidobacterium Microflora of the Human Intestine: Composition and Succession. *Curr. Issues Intestinal. Microbiol.* 2 (2), 43–53.

Rojas, M. A., Lozano, J. M., Rojas, M. X., Rodriguez, V. A., Rondon, M. A., Bastidas, J. A., et al. (2012). Prophylactic Probiotics to Prevent Death and Nosocomial Infection in Preterm Infants. *Pediatrics* 130 (5), e1113–e1120. doi: 10.1542/peds.2011-3584

Röth, D., Chiang, A. J., Hu, W., Gugiu, G. B., Morra, C. N., Versalovic, J., et al. (2019). Two-Carbon Folate Cycle of Commensal *Lactobacillus reuteri* 6475 Gives Rise to Immunomodulatory Ethionine, a Source for Histone Ethylation. *FASEB J.* 33 (3), 3536–3548. doi: 10.1096/fj.201801848R

Salas-Jara, M. J., Ilabaca, A., Vega, M., and García, A. (2016). Biofilm Forming Lactobacillus: New Challenges for the Development of Probiotics. *Microorganisms* 4 (3). doi: 10.3390/microorganisms4030035

Sharif, S., Meader, N., Oddie, S. J., Rojas-Reyes, M. X., and McGuire, W. (2020). Probiotics to Prevent Necrotising Enterocolitis in Very Preterm or Very Low Birth Weight Infants. *Cochrane Database Systematic. Rev.* 10, CD005496. doi: 10.1002/14651858.CD005496.pub5

Shelby, R. D., Janzow, G. E., Mashburn-Warren, L., Galley, J., Tengberg, N., Navarro, J., et al. (2020). A Novel Probiotic Therapeutic in a Murine Model of Clostridioides Difficile Colitis. *Gut. Microbes* 12 (1), 1814119. doi: 10.1080/19490976.2020.1814119

Shelby, R. D., Mar, P., Janzow, G. E., Mashburn-Warren, L., Tengberg, N., Navarro, J. B., et al. (2021). Antibacterial and Anti-Inflammatory Effects of *Lactobacillus reuteri* in its Biofilm State Contribute to its Beneficial Effects in a Rat Model of Experimental Necrotizing Enterocolitis. *J. Pediatr. Surg.* 57 (7), 1382-1390. doi: 10.1016/j.jpedsurg.2021.09.001

Shelby, R. D., Tengberg, N., Conces, M., Olson, J. K., Navarro, J. B., Bailey, M. T., et al. (2020). Development of a Standardized Scoring System to Assess a Murine Model of Clostridium difficile Colitis. *J. Invest. Surg.* 33 (10), 887–895. doi: 10.1080/08941939.2019.1571129

Spinler, J. K., Auchtung, J., Brown, A., Boonma, P., Oezguen, N., Ross, C. L., et al. (2017). Next-Generation Probiotics Targeting Clostridium difficile Through Precursor-Directed Antimicrobial Biosynthesis. *Infection. Immun.* 85 (10). doi: 10.1128/IAI.00303-17

Spinler, J. K., Sontakke, A., Hollister, E. B., Venable, S. F., Oh, P. L., Balderas, M. A., et al. (2014). From Prediction to Function Using Evolutionary Genomics: Human-Specific Ecotypes of *Lactobacillus reuteri* Have Diverse Probiotic Functions. *Genome Biol. Evol.* 6 (7), 1772–1789. doi: 10.1093/gbe/evu137

Thomas, C. M., Hong, T., van Pijkeren, J. P., Hemarajata, P., Trinh, D., Hu, W., et al. (2012). Histamine Derived From Probiotic *Lactobacillus reuteri* Suppresses TNF *via* Modulation of PKA and ERK Signaling. *PLoS One* 7 (2), e31951. doi: 10.1371/journal.pone.0031951

Thomas, J. P., Raine, T., Reddy, S., and Belteki, G. (2017). Probiotics for the Prevention of Necrotising Enterocolitis in Very Low-Birth-Weight Infants: A Meta-Analysis and Systematic Review. *Acta Paediatrica.* 106 (11), 1729–1741. doi: 10.1111/apa.13902

Vallabhaneni, S., Walker, T. A., Lockhart, S. R., Ng, D., Chiller, T., Melchreit, R., et al. (2015). Notes From the Field: Fatal Gastrointestinal Mucormycosis in a Premature Infant Associated With a Contaminated Dietary Supplement–Connecticut 2014. *MMWR. Morbidity. Mortality. Weekly. Rep.* 64 (6), 155–156.

Viswanathan, S., Lau, C., Akbari, H., Hoyen, C., and Walsh, M. C. (2016). Survey and Evidence Based Review of Probiotics Used in Very Low Birth Weight Preterm Infants Within the United States. *J. Perinatology.* 36 (12), 1106–1111. doi: 10.1038/jp.2016.144

Wang, Y., Jaggers, R. M., Mar, P., Galley, J. D., Shaffer, T., Rajab, A., et al. (2021). *Lactobacillus reuteri* in Its Biofilm State Promotes Neurodevelopment After Experimental Necrotizing Enterocolitis in Rats. *Brain. Behavior. Immun. - Health* 14. doi: 10.1016/j.bbih.2021.100256

Zbinden, A., Zbinden, R., Berger, C., and Arlettaz, R. (2015). Case Series of Bifidobacterium Longum Bacteremia in Three Preterm Infants on Probiotic Therapy. *Neonatology* 107 (1), 56–59. doi: 10.1159/000367985

Conflict of Interest: GB, SG, and MB have stock options in Scioto Biosciences, Inc.

The remaining authors declare that the research was conducted in the absence of any commercial or financial relationships that could be construed as a potential conflict of interest.

Publisher's Note: All claims expressed in this article are solely those of the authors and do not necessarily represent those of their affiliated organizations, or those of the publisher, the editors and the reviewers. Any product that may be evaluated in this article, or claim that may be made by its manufacturer, is not guaranteed or endorsed by the publisher.

Advantages of publishing in Frontiers

OPEN ACCESS
Articles are free to read for greatest visibility and readership

FAST PUBLICATION
Around 90 days from submission to decision

HIGH QUALITY PEER-REVIEW
Rigorous, collaborative, and constructive peer-review

TRANSPARENT PEER-REVIEW
Editors and reviewers acknowledged by name on published articles

Frontiers
Avenue du Tribunal-Fédéral 34
1005 Lausanne | Switzerland

Visit us: www.frontiersin.org
Contact us: frontiersin.org/about/contact

REPRODUCIBILITY OF RESEARCH
Support open data and methods to enhance research reproducibility

DIGITAL PUBLISHING
Articles designed for optimal readership across devices

FOLLOW US
@frontiersin

IMPACT METRICS
Advanced article metrics track visibility across digital media

EXTENSIVE PROMOTION
Marketing and promotion of impactful research

LOOP RESEARCH NETWORK
Our network increases your article's readership